Author:
Kemppinen, Lotta I M

Title:
Investigating the timing and nature of diamond-forming events through the study of diamond-hosted sulphide inclusions

Investigating the timing and nature of diamond-forming events through the study of diamond-hosted sulphide inclusions

Lotta I. M. Kemppinen

A dissertation submitted to the University of Bristol in accordance with the requirements for award of the degree of Doctor of Philosophy in the Faculty of Science

Department of Earth Sciences

23/09/19

Acknowledgements

First and foremost, I would like to acknowledge my wonderful supervisory team. Simon Kohn has been the greatest principal supervisor with his support, advice, enthusiasm for molybdenite and the science throughout. Ian Parkinson has been invaluable during the completion of this thesis, and I am particularly grateful for the lab work experience I acquired thanks to him. Galina Bulanova and Chris Smith have excelled at their supervisory role, going above and beyond to always help with PhD-related things or other. At the University of Bristol, I would like to thank Stuart Kearns and Ben Buse for their guidance and patience with me whenever I would return to conduct EPMA or SEM analyses, seeing as it was always a pleasure on my part. Richard Brooker has been a constant source of help for whatever was needed in the basement, which is very much appreciated. David Edwards, Jacob Wood and Laura Speich were great fellow "diamond students" and I would also like to thank all the friends and colleagues I have met at Bristol and through the Deep Volatiles programme for making the past four years all that much more enjoyable. To my family, friends and Luke, thank you for your constant love and support.

Contents

List of figures

List of tables

Abstract

The study of mineral inclusions in diamonds offers a unique opportunity to investigate the nature of different diamond-forming events and the conditions under which they took place. Sulphide inclusions are over-represented in many lithospheric diamond populations worldwide (e.g. Gurney et al., 1979; Stachel and Harris, 2008; Shirey et al., 2013; Harvey et al., 2016), but the reasons behind their abundance remain ambiguous. Sulphide inclusions could be genetically linked with their host diamonds providing an insight into diamond-forming reactions and related processes. Additionally, as the principal hosts of chalcophile (sulphur-loving) and siderophile (iron-loving) elements in the Earth's mantle, sulphide inclusions can be used in Re-Os dating of diamond growth events.

The different attributes of sulphide inclusions in diamonds from different localities worldwide have been investigated using a variety of non- and minimally destructive spectroscopic and analytical techniques. The first chapter provides a summary of the global sulphur cycle and presents an overview of what is known in literature about sulphide inclusions in diamonds. In the second chapter, diamond-forming reactions involving sulphur-bearing materials are explored; petrological observations of sulphide inclusions and their internal features are provided by means of Raman spectroscopy, computed x-ray microtomography (x-CT) and Fourier-transform infrared spectroscopy FT-IR spectroscopy, adding to the knowledge of what is known about the nature of the involvement of sulphides in diamond formation. The presence of molybdenite as a disseminated phase inside the body and rosette fractures of intact diamond-hosted sulphide inclusions from Mir (Yakutia) is reported in the third chapter, alongside the potential effects of its presence on Re-Os systematics within sulphide inclusions and implications for radiometric dating. Further observations on the pervasive occurrence of

molybdenite inside sulphide inclusions in diamonds from worldwide localities are presented in the fourth chapter; different reasons to explain the presence of molybdenite, and the origin of Mo, are considered. Preliminary stable sulphur isotope results for sulphide inclusions in diamonds from Mir, Dachine (French Guiana), Juina-5 and Collier-4 (Brazil) are then presented in the fifth chapter and an attempt is made at determining the origin of the sulphides included in the studied lithospheric and sublithospheric diamonds; the results reveal a recycled sulphur signature in the sulphide inclusions, and particularly when compared with published carbon isotope data for the diamond populations, show the promise of stable sulphur isotopes for future study.

The presence of sulphides in diamond-forming regions of the Earth's mantle may be inherently linked to diamond growth and therefore, detailed studies of natural diamond-hosted sulphide inclusion provide a unique means of investigating the conditions under which diamonds grew. Sulphides can provide interesting insights into the behaviour of trace elements such as Mo in the mantle, and as the principal hosts of siderophile elements, serve as time capsules due to their Re and Os compositions. Altogether, the work presented here aim to underline the importance of detailed studies of intact diamond-hosted inclusions, which can help provide an invaluable insight into timing of diamond-forming events, the involvement of sulphides in these and the global sulphur cycle.

1. Introduction

1.1. Overview

Sulphide inclusions in diamonds can provide a unique insight into the reactions taking place in different diamond-forming media. The chemical inertness of diamond allows it to transport to the surface pristine material that was captured within it during diamond growth, offering direct samples of the Earth's deep interior. Through their ability to reflect on subduction-related processes, diamonds potentially record some of the processes that make the Earth habitable (e.g. Taylor et al., 1998; Cartigny, 2005; Tappert et al., 2005; Shirey and Richardson, 2011; Walter et al., 2011). Similarly, diamond-hosted sulphide inclusions can provide a better understanding of chalcophile (sulphur-loving) and siderophile (iron-loving) element systematics in the mantle. These can be used to constrain various processes involved in the evolution of the crust and mantle over time, subduction processes and the formation of economically valuable ore deposits (e.g. Review by Harvey et al., 2016; Aulbach et al., 2012; Wilkinson, 2013). Furthermore, the presence of sulphur-bearing species in diamond-forming domains likely imposes strong controls on the prevailing redox conditions, resulting phase relations and mantle reactions involving volatiles. However, despite the common occurrence of sulphides as inclusions in diamonds, work is still required in order to establish their relationship with diamond, and their involvement in diamond-forming reactions.

This chapter provides an overview on the formation of diamonds, the main inclusions they host, and what these can tell us about the diamond-forming substrate. A review of what is known about the timing of diamond-forming events globally is provided, outlining different radiometric dating methods and focusing particularly Re-Os dating applied to sulphides. A summary of the global sulphur cycle and the behaviour of sulphides in the upper mantle source

regions where diamonds can form is then provided. The paragenesis and compositions of diamond-hosted sulphide inclusions are discussed, alongside their scientific uses. An additional section (1.7) outlines the characteristics of the studied diamonds and reasons for their selection.

The second chapter presents a detailed study of the internal structure and mineralogy of sulphide inclusions in diamonds and implications for the various diamond-forming scenarios involving sulphides. Observations made in sulphide inclusions hosted in natural diamonds from Udachnaya, Mir (Yakutia, Russia) and Juina-5 (Brazil) will be used to constrain some of the reactions involved in the formation of their host diamonds. A discussion will follow on the close associations of sulphide and silicate inclusions in diamonds, and possible links between sulphides derived from the mantle and deep volatile-rich phases.

A valuable scientific aspect of the study of diamond-hosted sulphides has involved their use in Re-Os dating of diamond-forming events and associated mantle processes. The third chapter reports on the common presence of molybdenite as a discrete, primary phase in sulphide inclusions in eclogitic diamonds from Mir, Argyle, Dachine (French Guiana), Damtshaa, Letlhakane, Orapa (Botswana), peridotitic diamonds from Diavik (Canada), Murowa (Zimbabwe) and one sub-lithospheric diamonds from Juina-5. With the exception of rheniite, molybdenite has the highest concentration of Re on Earth and therefore the work, which is published in Earth and Planetary Science Letters (Kemppinen et al., 2018), addresses the potential implications of molybdenite non-recovery and non-analysis during Re-Os dating on the ages of diamonds.

The presence of molybdenum (Mo) concentrations in diamond-forming mantle domains that are sufficiently high to precipitate molybdenite in sulphide inclusions is surprising and potential reasons for its abundance are explored in the fourth chapter. An overview of the global Mo cycle through time is provided, alongside further observations of molybdenite in diamonds

from different localities. Additionally, the Re-Os compositions and isochron and model ages of diamond-hosted sulphide inclusions reported in literature are discussed alongside exploring the effects of realistic amounts of Re loss on the ages of sulphide inclusions with natural Re-Os compositions.

In the fifth chapter, preliminary mass dependent and mass independent stable sulphur isotope results are presented for sulphide inclusions in eclogitic diamonds from Mir and Dachine, and sub-lithospheric diamonds from Juina-5 and Collier-4 (Juina area, Brazil). An interpretation of the results provides an insight into the origin of the studied sulphide inclusions, as well as supplying clues about the behaviour of sulphur-bearing materials undergoing subduction. The outcome of the work can help constrain the source and nature of sulphur-bearing materials and melts involved in the formation of diamonds of different age and originating at different depths, thereby abetting a better understanding the global sulphur cycle.

1.2. Diamond formation

Diamond is a unique metasomatic mineral which can form through a variety of processes occurring in the Earth's mantle typically at pressures and temperatures exceeding 5-6 GPa and 1200°C (e.g. Fig. 1.1.A; e.g. Shirey et al., 2013; Navon et al., 1999; Stachel and Harris, 2009). Diamonds can form from supercritical carbon-bearing fluids or melts percolating through the Earth's mantle; as a consequence of pH changes (Sverjensky and Huang, 2015) isobaric cooling and/or redox reactions involving fluids/melts which are mainly CO_2 or CH_4-dominated (Fig. 1.1.B) (e.g. Stachel and Luth, 2015 and references therein) as:

$$CO_2 = C + O_2$$

$$CH_4 + O_2 = C + 2H_2O$$

Sulphides have also been suggested to play a role in promoting diamond growth, the examples of which will be discussed in chapter 2. Diamond stability in the mantle is largely controlled by the oxygen fugacity (fO_2) of the system, which is typically established in reference to the fayalite-magnetite-quartz (FMQ) redox buffer (Δ log fO_2 (FMQ)). Diamonds form under relatively reducing conditions (log fO_2 (FMQ) = <-1.5), with the most oxidising conditions permitting diamond growth below the enstatite-magnetite-olivine-diamond (EMOD) buffer (Fig. 1.1.C). At low oxygen fugacities (log fO_2 (FMQ) < ~ -5; Fig. 1.1.C), the potential for crystallising diamonds is hampered by the stabilisation of metallic Fe and dissolution of carbon into the metal (e.g. Rohrbach et al., 2011; 2014; Smith and Kopylova, 2014; Luth and Stachel, 2014).

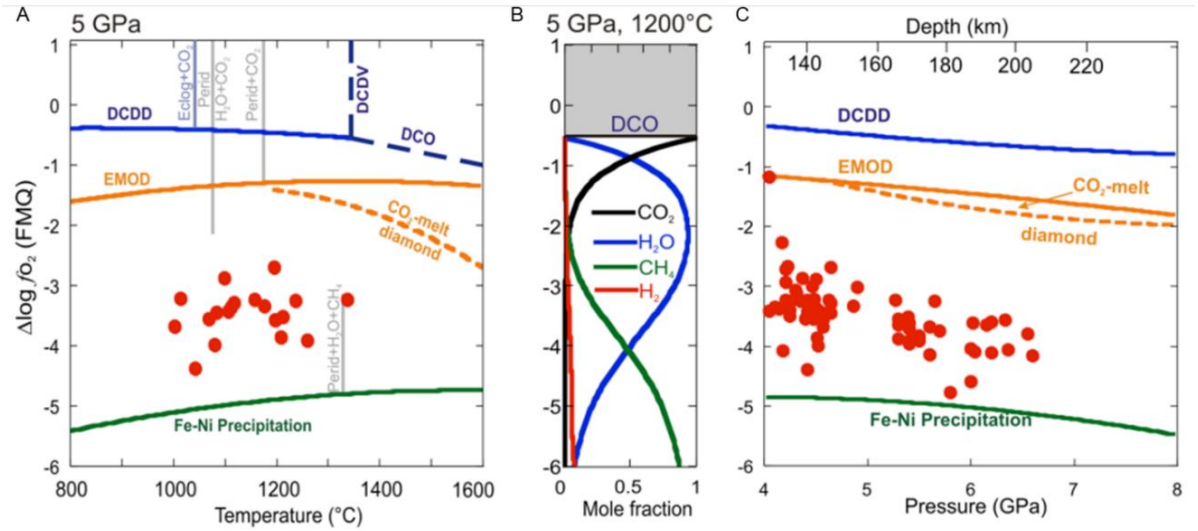

Figure 1.1. Plots showing the reactions which determine carbon speciation at conditions typical of cratonic diamond formation, relative to the oxygen fugacity of the system (fayalite-magnetite-quartz – FMQ – buffer) and as a function of its temperature (A), fluid composition (B) and pressure (C). The blue solid curves in A and C represent the dolomite-coesite-diopside-diamond (DCDD) buffer; the dashed blue lines in A correspond to the dolomite-coesite-diopside-CO_2 (DCDV) and diamond-carbon-oxygen (DCO) buffers. The orange curve (enstatite-magnesite-olivine-diamond – EMOD – buffer) represents the fO_2 at which diamond becomes stable over magnesite (solid line) or melt-hosted CO_2 (dashed line) in peridotitic mantle. The red circles represent the oxygen fugacities at which garnet peridotite xenoliths are stable around 5 GPa (with data obtained from calculations made by Gudmundsson and Wood, 1995). The green curves in A) and C) depict the low fO_2 conditions at which Fe-Ni metal will precipitate, reducing the stability of diamond (from Shirey et al., 2013)

The simple composition of diamond makes the interpretation of its formation environment difficult; therefore, the inclusions hosted in diamonds are essential for acquiring a better understanding of the diamond-forming medium. Most lithospheric gem-quality diamonds can be assigned either to an eclogitic or peridotitic paragenesis, depending on the silicate and oxide mineral inclusions they host, indicating growth in eclogite or peridotite. Diamonds containing silicate mineral inclusions of the eclogitic suite record growth on a subducted oceanic crust substrate (e.g. Kesson and Ringwood, 1989; Richardson et al., 1990; Richardson et al., 2001). Peridotitic diamonds, on the other hand, are interpreted as sampling growth in the "normal" mantle. Eclogitic and peridotitic diamonds have also been distinguished by their carbon and oxygen isotope compositions (e.g. Cartigny et al., 2005 review), eclogitic diamonds often exhibiting, recycled non-mantle-like (i.e. $\neq$ -5 ‰) signatures.

The involvement of sulphur in diamond-forming reactions has received less attention, despite being inherently associated with oxygen and carbon. Owing to the large time span sampled by diamonds (section 1.4.1), sulphide inclusions in diamonds can potentially track the cycling of sulphur at depth through time. Determining the nature and origin of sulphur-bearing materials enclosed in diamonds also requires an understanding of the behaviour of sulphur at the surface as well as in the Earth's interior. Because of the potential for recycling surface materials into the mantle, the next section therefore reviews the global sulphur cycle.

1.3. The global sulphur cycle

Sulphur is the 10th most abundant element in the solar system and 5th on Earth (Croswell, 1996; Morgan and Anders, 1980). As a moderately siderophile element, the behaviour of sulphur during the core-forming event early in Earth's history has long been a subject of considerable debate (e.g. Anderson et al., 1971; Suer et al., 2017). Much of the Earth's sulphur is thought to reside in its core, where it may have contributed to the physical and geochemical properties of

the core; for example, it has recently been suggested that iron sulphide melts exsolving from a Hadean silicate magma ocean, are likely to have segregated highly siderophile elements into the core during Earth's cooling and crystallisation, resulting in their depletion in the bulk silicate Earth (BSE) (Rubie et al., 2016; Laurenz et al., 2016). However, sulphur – along with hydrogen, oxygen and carbon – is a major magmatic volatile in the Earth's mantle and crust.

Sulphur is a redox-sensitive element which can exist in its reduced form (as S^{2-} or S^{0}) in sulphides, sulphide melts and reduced fluids, in intermediate form (as S^{4+}) in volcanically erupted SO_2, or in its oxidised form (as S^{6+}), typically occurring in sulphates, oxidised fluids and/or dissolved in molten silicates (Alard et al., 2011; Delpech et al., 2012; Evans and Powell, 2015; Zajacz, 2015; Kitayama et al., 2017; Bataleva et al., 2018). The three principal processes controlling the output of sulphur from the mantle to the surface can be recognised as volcanic or hydrothermal degassing, and weathering of basaltic crust (e.g. Canfield, 2004) (e.g. Fig. 2). Sulphide can then be fixed in oceanic crust through hydrothermal reduction of sulphate, and the subduction of sedimentary sulphides is therefore thought to represent an important return pathway of sulphur into the mantle. The importance of the pathways in influencing the nature and size of different sulphur reservoirs has been related to the chemistry (oxygen concentrations in particular) of oceans and atmosphere through time. Three stages are outlined here (modified from Holland, 2006 and Canfield, 2004):

I. In the Archean and early Proterozoic (>2.45 Ga), the global sulphur cycle was driven by the burial and subduction of sulphide that had been hydrothermally or volcanically outgassed into an Fe-rich ocean in an oxygen-poor/missing atmosphere (Fig; 1.2.A).
II. After the first Great Oxidation event (GOE-I, ~2.45 Ga) in the Proterozoic, weathering of sulphide minerals on continents began, providing an additional source of sulphur to oceans, which evolved to become sulphidic (Fig. 1.2.B).

III. With the onset of a second rise in atmospheric oxygen concentrations (sometimes termed the second Great Oxidation event – GOE-II; e.g. Campbell and Squire, 2010; Mingxiang, 2016) ~0.66 ma, the formation of sulphate (SO_4) was made possible under oxygenated atmospheric and oceanic conditions, and its burial and subduction became the principal driver in the recycling of sulphur globally, with the subduction of sulphide becoming unimportant (Fig. 1.2.C).

Since only 15-30 % of sulphur recycled into the mantle is released into the atmosphere as SO_2 through magmatic degassing (Evans, 2012), most of the sulphur is likely retained within the subducting slab, either interacting with the surrounded upper mantle, or being transported deeper into the mantle. Acquiring a better understanding of the behaviour of sulphur in surface reservoirs is important for constraining its fate during subduction and its introduction into and interactions within diamond-forming regions. The nature and behaviour of sulphur at the surface of the Earth, in subduction zones and in the mantle are outlined in the following section.

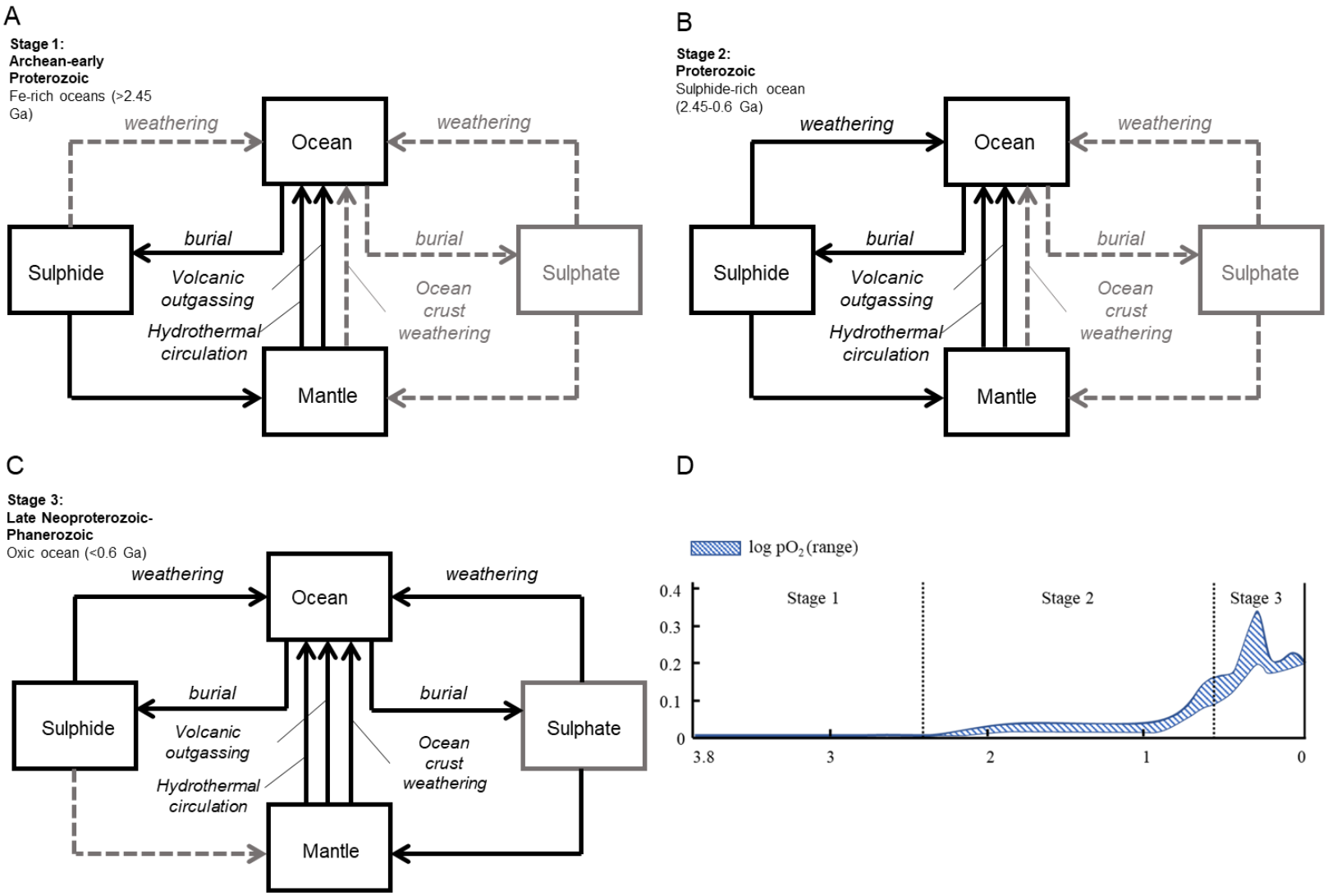

Figure 1.2. Schematic diagrams (A-C) outlining the pathways for the recycling of sulphur through time. Adapted from Canfield, 2004 (A-C) and Holland (2006) (D). Solid lines depict pathways which were active at a given time and dashed lines indicate that such pathways were not active.

1.3.1. Sulphur reservoirs at the Earth's surface

Sulphur is recognised as being an essential element for the evolution and sustenance of complex life, and an important source of sulphur to surface reservoirs has derived from (oxidative) weathering of oceanic crust, which has relatively high bulk sulphur concentrations (260-520 ppm) (e.g. Canfield et al. 2004). In modern ocean, sulphur (dissolved as SO_4^{2-}) is the second most abundant anion following Cl^- (e.g. Tomkins and Evans, 2015) with typical seawater concentrations of ~2.65 mg/L (Thompson, Johnston and Wirth, 1931).

Principally, sulphur can precipitate as sulphate, or alternatively is reduced to an Fe-S compound (e.g. Fig. 1.3). Sulphate reduction by microbial or thermochemical agents is a particularly important mechanism which contributes to around half of carbon re-mineralisation in marine sediments (Jørgensen, 1982; Canfield, 1993). The formation of sedimentary pyrite, and its weathering and burial in surface environments also impose strong controls on atmospheric oxygen contents (e.g. Berner, 1984; 1999; Raiswell and Berner, 1986).

Oceanic crust can become enriched with sulphur through seawater infiltration and hydrothermal alteration. Different sulphur-bearing minerals will be distributed as a function of depth, based on the extent of seawater infiltration and the temperature of the system (e.g. Tomkins and Evans, 2015). Alteration-driven iron oxidation is also associated with higher $Fe^{3+}/\Sigma Fe$ contents of oceanic crust and the formation of hematite (Barker et al., 2010). Further infiltration of seawater reacts to precipitate anhydrite ($CaSO_4$) up to temperatures ~408°C (Alt et al., 2010, Hannington et al., 2005), leading to a zonation pattern where the uppermost alteration zones are oxidised and anhydrite-dominated, occurring on top of zones where more reduced alteration has produced pyrite, which progressively become pyrrhotite-dominated at greater depths and reducing conditions (Alt et al., 1995; Tomkins and Evans, 2015).

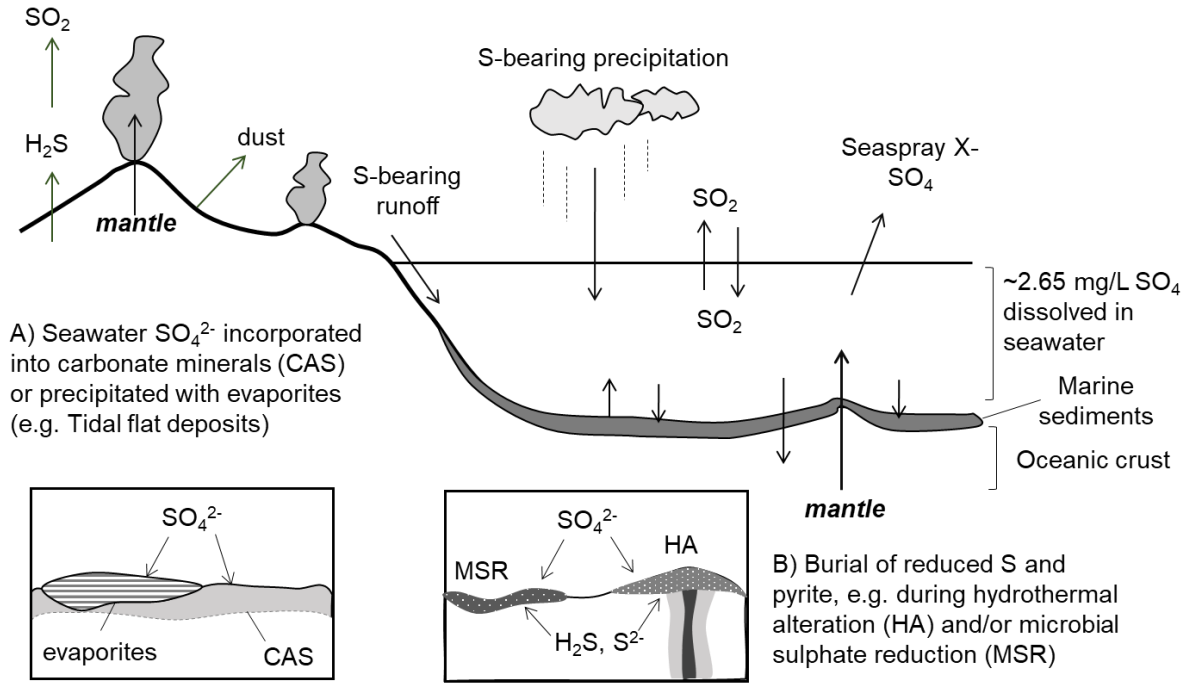

Figure 1.3. Simplified schematic diagram outlining possible pathways for sulphur cycling between the Earth's mantle and surface reservoirs. Sulphur can be outgassed directly into oceans or become concentrated in it as sulphate (SO_4^{2-}), as a result of weathering on land for example. Sulphate dissolved in seawater can then become incorporated in evaporites or carbonate-associated sulphides (CAS) under oxidising conditions or get reduced to sulphide through hydrothermal alteration (HA) or microbial sulphate reduction (MSR) on the seafloor.

1.3.2. Sulphur in subduction zones

Subduction of hydrated lithosphere plays a major role in the transport of water, ferric iron (Fe^{3+}), oxidised carbon and sulphur to depth and is a key process in controlling the global sulphur cycle (e.g. Evans and Powell, 2015; Bataleva et al. 2018). As well as being intricately associated with diamond formation, subduction processes are closely linked to the formation of economically important arc-related sulphide ore deposits and control the temporal evolution of the mantle's redox state (Evans and Powell, 2015; Alt et al., 1993; Evans, 2012; Jégo and Dasgupta, 2014; Tomkins and Evans, 2015).

Despite only constituting a minor component in subducting slabs, sulphur has a strong oxidation potential (e.g. Klimm et al., 2012a, 2012b; Tomkins and Evans, 2015; Debret et al.,

2016; Pons et al., 2016; Bénard et al., 2018) following the reaction: $SO_4^{2-} + 8FeO = S^{2-} + 4Fe_2O_3$. Due to the heterogeneous nature of the Earth's mantle, the redox- and compositional contrasts between a subducting slab and surrounding lithospheric mantle rocks control the different scenarios of sulphur behaviour during subduction (e.g; Smithies et al. 2003). The speciation of sulphur and its behaviour in silicate melts is strongly dependent on the oxygen fugacity (fO_2) of the system (e.g. Métriche and Mandeville, 2010; Canil and Fellows, 2017) (Fig. 1.4): under oxidising conditions, sulphur dissolves in melt as sulphate, whilst in reduced environments, sulphide species dominate (e.g. Fincham and Richardson, 1954; Canil and Fellows, 2017).

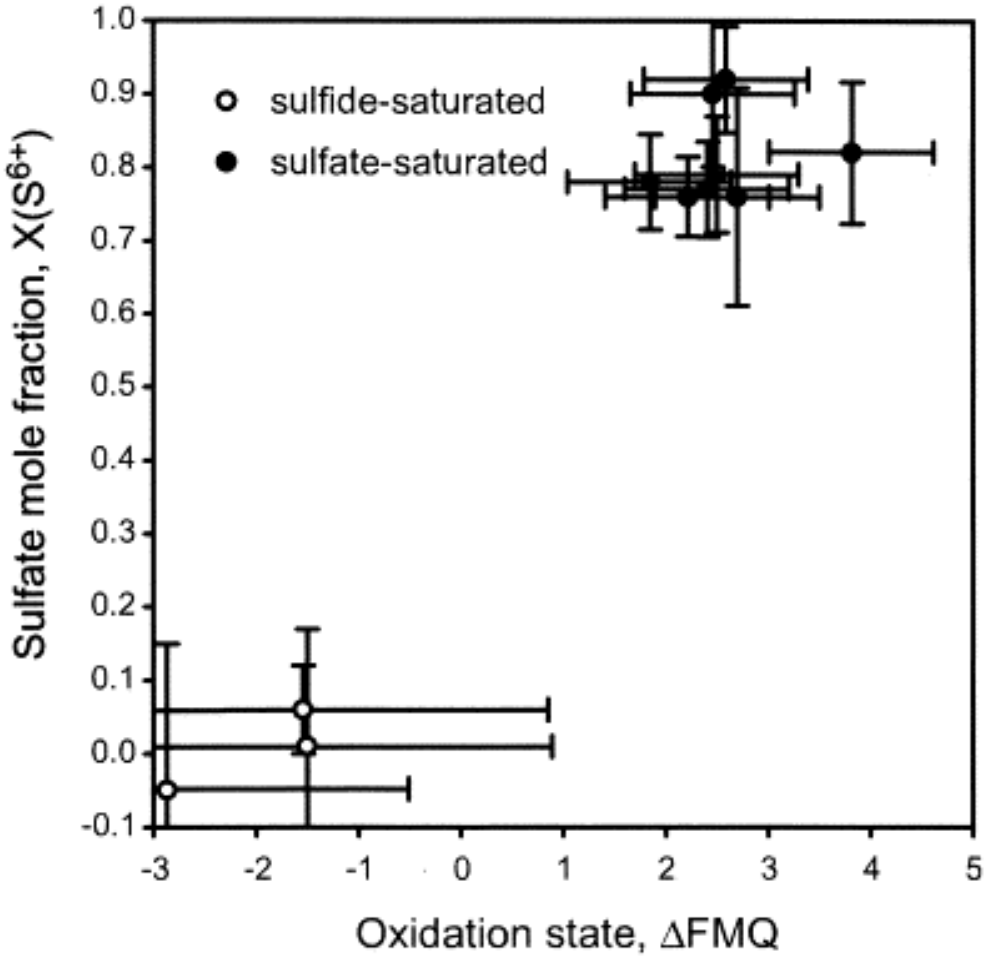

Figure 1.4. Sulphur speciation (S^{6+} or S^{2-}) and mole fraction of sulphate as a function of oxidation state (from Jugo et al., 2015)

Since oxidation state exerts a strong influence on the nature of the compounds sulphur can form, it also controls the mobility of chalcophile metals in subduction zones, their transport and deposition. In fact, it has been shown that the speciation of sulphur as sulphate or sulphide controls the retention or release of chalcophile and siderophile elements such as Zn, Pb, Mo, As, Cu and Sb in arc-related magmatic settings (e.g. Evans and Tomkins, 2015; Canil and Fellows, 2017).

Tomkins and Evans (2015) investigated the relative stabilities of the key sulphur-bearing minerals anhydrite and pyrite in basaltic oceanic crust undergoing subduction to constrain some of the processes controlling sulphur release in subduction zones. Whilst anhydrite was shown to break down at the blueschist-eclogite facies transition around 450-650 °C, the authors showed evidence for the stability of pyrite to up to 750 °C and ~4 GPa at least into the lower eclogite facies (Tomkins and Evans, 2015). It was suggested that sulphur release from a subducting slab could occur in two separate stages (Fig. 1.5): 1) anhydrite breakdown releases SO_2, $HSO_4^-$and H_2S at the blueschist–eclogite facies transition, and 2) pyrite breakdown releases H_2S across the transition into the eclogite facies (Fig. 1.5) (Tomkins and Evans, 2015). The remainder of slab-hosted sulphur is expected to be subducted deeper into the mantle as pyrrhotite if pressure and temperature increase and sulphur fugacity (fS_2) decreases or remain constant (e.g. Tomkins and Evans, 2015; reviews by Fleet, 2006 and Vaughan, 2006).

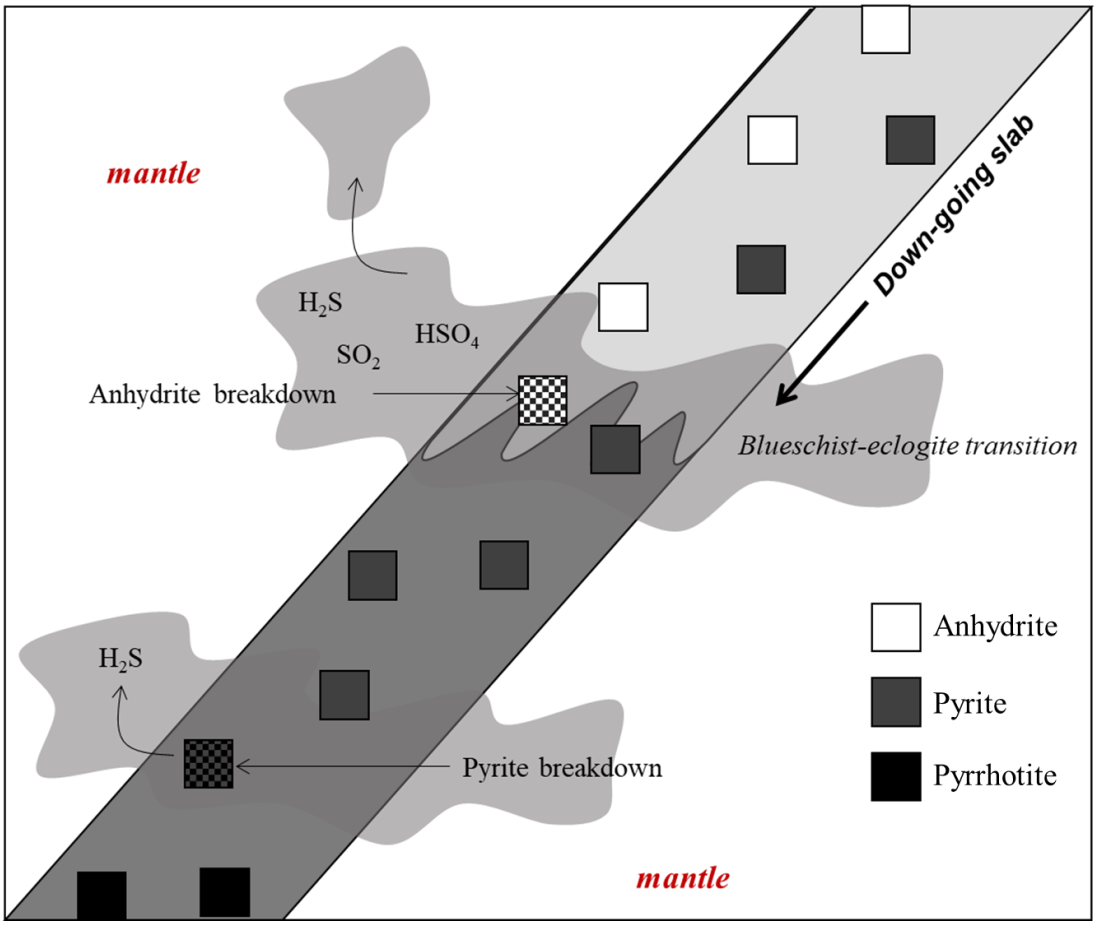

Figure 1.5. Schematic diagram (not to scale) showing two separate stages during which sulphur is released from a surface-derived slab during its subduction from blueschist into eclogite facies. Anhydrite breakdown at the blueschist-eclogite transition is accompanied by the release of H_2S, SO_2 and HSO_4 from the slab, while pyrite can remain stable well into the eclogite facies before breaking down to pyrrhotite and releasing H_2S in the process (e.g. Tomkins and Evans, 2015)

As well as being controlled by the chemical composition of the slab, the volatile content of a subducting slab is dependent on its thermal properties and angle of subduction (e.g. Fig. 1.6). The Archean mantle was hot (e.g. Nisbet et al., 1993), and consequently, plate tectonics were dominated by smaller, thicker and more buoyant oceanic lithosphere being flatly subducted into a more vigorously convecting mantle (e.g. Smithies et al. 2003). Indeed, early Archean (> 3.3 Ga) continental crust may have formed directly through melting of mafic crust (Smithies et al., 2003) Subduction-induced enrichment of ancient (>~3.1-3.3 Ga) mantle source regions has generally not been observed in Archean rocks (Smithies et al., 2003). However, low-angle subduction of oceanic crust may have enhanced crustal growth prior to 2.5 Ga, as suggested by

the preservation of both slab and mantle wedge components in many late Archean terrains (~3-2.5 Ga) (Smithies et al. 2003). Modern processes of crustal growth are predominantly driven by the subduction of "old and cold" oceanic lithosphere. Indeed, in modern convergent margins, cooler oceanic crust is commonly subducted at a steep angle (≥30◦; e.g. Gutscher et al., 2000a), and in some cases with acute inclinations (up to 70◦) (e.g. Vanuatu; Peate et al., 1997).

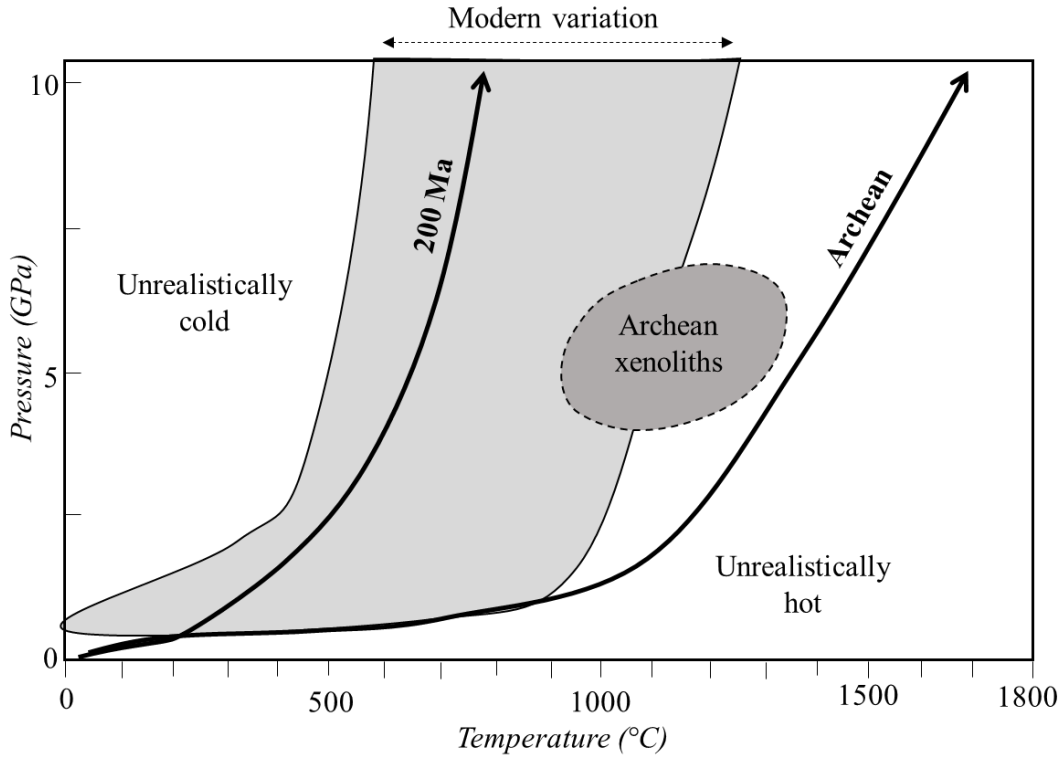

Figure 1.6. Plot of the pressure-temperature conditions of eclogitic mantle xenoliths which underwent subduction along a hot and shallow geotherm in the Archean and ones which were formed relatively recently (~200 Ma) through cold and steep subduction. Simplified from Santosh et al. (2010)

1.3.3. Sulphur in the mantle

Sulphur is only a minor element in the mantle, with relatively low average concentrations ranging from ~200 ppm in primitive mantle to ~150 ppm in depleted mantle (Dasgupta and Hirschmann, 2006). Unaltered mid ocean ridge basalts (MORB) commonly contain higher sulphur contents (~950-1440 ppm; Jenner et al., 2010), where sulphur predominantly occurs in

reduced magmatic sulphide minerals (pyrrhotite, chalcopyrite and pentlandite) (Tomkins and Evans, 2015). These, and other pristine mantle-derived sulphides can be studied when hosted in inclusions in silicate minerals from xenoliths (e.g. Andersen et al., 1987; Chaussidon et al., 1989; Alard et al., 2000; Burton et al., 2000; Aulbach et al., 2004; Harvey et al., 2006; 2011; 2016) and in diamond-hosted inclusions (e.g. Bulanova et al., 1996; Pearson et al., 1998; Westerlund et al., 2004; 2006; Taylor and Liu, 2009; Aulbach et al., 2012; Wiggers de Vries et al., 2013a; Harvey et al., 2016).

Sulphide is likely to reside as a homogeneous Fe ± Ni ± Cu-rich sulphide melt or monosulphide solid solution (MSS) in most regions of the Earth's mantle (e.g. Zhang et al., 2015; 2016), occurring as sulphide melts/liquids or as a monosulphide solid solution (MSS) (Chapter 3, section 1). Generally, sulphides co-exist immiscibly with silicate melts at the pressures and temperatures prevailing in much of the mantle (e.g. Fleet et al., 1977; Pedersen, 1979; Keays, 1987; Shushkanova et al., 2008a, b; Du et al., 2014). The physical properties of sulphide melts differ greatly from those of silicates; they have a higher density and electrical conductivity and lower melting point and viscosities (Bockrath et al. 2004; Mungall and Su 2005; Helffrich et al. 2011; Dobson et al., 2000), and as such have been interpreted as being responsible for geophysical anomalies in the mantle, for example the seismic anomalies at ~100 km depth beneath continental cratons (Helffrich et al., 2011; Zhang and Hirschmann, 2016), or perhaps explaining some of the properties observed in large low shear velocity provinces (e.g. Zhang et al., 2016).

Given the renowned immiscibility of sulphides and co-existing mantle phases, much work has been directed at investigating the solubility and behaviour of sulphur in silicate melts, often termed in reference to the sulphur content at sulphide saturation (SCSS) (e.g. Haughton et al., 1974; Shima and Naldrett, 1975; Carroll and Rutherford, 1985; Poulson and Ohmoto, 1990;

Mavrogenes and O'Neill, 1999; Moretti and Ottonello, 2005; Liu et al., 2007; Klimm and Botcharnikov, 2010; Botcharnikov et al. 2011; Klimm et al., 2012a; 2012b; Wykes et al., 2015; Fortin et al., 2015; Smythe et al., 2017; Bénard et al., 2018; Nash et al., 2019) or sulphur content at anhydrite saturation (SCAS) (e.g. Li and Ripley, 2009; Jugo 2009; Jugo et al., 2010; Masotta and Keppler, 2015). Early experiments which were run at 1 atm. pressures (e.g. Haughton et al., 1974; Shima and Naldrett, 1975) or relatively low pressures (<0.3 GPa. E.g. Carroll and Rutherford, 1985) soon revealed that there was a significant relation between fO_2 and sulphur solubility in silicate melts. Since then, a considerable body of work has been carried out investigating the relative importance of chemical composition, temperature, fO_2, fS_2 and pressure on the behaviour of sulphur.

There is a well-established relationship between the sulphur and FeO content of a silicate melt (e.g. O'Neill and Mavrogenes, 2002). Jugo et al. (2005) also found that in a basaltic system at 1-1.6 GPa and 1300-1355 °C, the sulphur content increased with increasing oxidation state, with the transition from sulphide to sulphate occurring at FMQ -1 to FMQ +2. Jugo et al. (2010) also investigated the sulphur speciation in natural and synthetic basaltic glasses and observed that only reduced magmas (i.e. MORB) were dominated by sulphide species. Furthermore, the behaviour of sulphur, particularly the SCSS, in all other environments could vary significantly with minor variations in fO_2 (> FMQ +1) (Jugo et al., 2009; 2010).

Tsujimura and Kitakaze (2005) determined the solubility of sulphur in silicate melts, particularly reduced melts with low FeO content, coexisting with graphite. It was shown that at high FeO (>10 mol %) sulphur solubility is strongly dependent on FeO content. However, in a system with moderate FeO contents (~1-10 mol %), the solubility of sulphur is independent of FeO and instead, increases with the addition of other components (e.g. CaO) to the system and occurs primarily as sulphate. Liu et al. (2006; 2007) investigated the SCSS of rhyolitic to

basaltic melts saturated with an Fe-S melt between 1250-1450°C and 0.5-1 GPa. Both temperature and oxygen fugacity were shown to be positively correlated with sulphur solubility, as in previous works, but the effect of pressure was seen to be negligible.

Most experiments had involved investigating SCSS in a variety of silicate melt compositions using a simple Fe-S phase. More recently, Smythe et al. (2017) conducted a series of experiments measuring the SCSS of silicate melts with the addition of a Fe-Ni-Cu component, at pressures and temperatures ranging between 1.5-24 GPa and 1400-2160°C. It was suggested that at constant temperatures, pressures and silicate melt chemistry, the composition of the sulphide phase imposed an effect on sulphur solubility; SCSS was positively dependent on the mole fraction of FeS in the sulphide liquid (or Fe/(Fe+Ni+Cu)) (Smythe et al., 2017). However, a strong correlation between SCSS and temperature was observed, whilst pressure was shown to decrease the sulphur solubility (Smythe et al., 2017; Fortin et al., 2015).

Similar pressure and temperature effects were observed by Fortin et al. (2015) who also reported that the addition of volatiles, such as H_2O can increase the SCSS in mafic melts (Fortin et al., 2015). Indeed, oxidised and hydrous basaltic magmas have been shown to carry large amounts of sulphur dissolved as sulphate (up to 1.5 wt. %) to relatively low pressures (1 GPa) at least (Jugo et al. 2005). Sulphur saturation in reduced basaltic melts on the other hand, is controlled by the presence and concentration of an immiscible Fe-S-O liquid; S^{2-} content largely depends on Fe content of a melt and its temperature (e.g. O'Neill and Mavrogenes, 2002; Liu et al., 2007).

Jorgenson (2017) found that sulphur is more soluble in carbonatite melts than in silicate melts, comparing their results with those which were experimentally determined by Liu et al. (2007) (up to ~0.5 wt. % vs. ~0.14 wt. % respectively). Carbonatites do not likely host more than 3% of the mantle's bulk sulphur (Jorgenson, 2017), however, due to their involvement in diamond-

forming processes (e.g. Shrauder and Navon, 1994; Walter et al., 2008; 2011; Klein-BenDavid et al., 2009; Bulanova et al., 2010; Kopylova et al., 2010; Ryabchikov and Kaminsky, 2013; Burnham et al., 2015; 2016; Thomson et al., 2016a; 2016b; Burnham et al., 2016), carbonatite melts could potentially provide some or all the sulphur into sulphide inclusions in diamonds. Furthermore, Woodland et al. (2019) recently investigated the solubilities of sulphate and sulphide in silicate-carbonate melts at pressures between 5-10 GPa and found the SCSS at 0.02-0.1 wt. % sulphur. However, more oxidised silicate-carbonate melts were found to host up to 2-3 wt. % S, dominated by S^{6+} in sulphate (Woodland et al., 2019). In fact, recent experiments by Chowdhury and Dasgupta (2019) investigating sulphate solubility and SCAS in hydrous basalts showed that sulphur content was seen to increase with temperature as well as CaO content and decrease with SiO_2. It was highlighted that sulphur as SO_4^{2-} can be a major component in sulphur-bearing silicate melts, with SCAS reaching ~2 wt. % S (Klimm et al., 2012a; 2012b; Chowdhury and Dasgupta, 2019).

The processes transferring and modifying sulphur-bearing phases upon their introduction into the mantle are likely complex. The means and extent of enrichment of sulphur and associated elements in certain diamond-forming regions require further investigation. Additionally, the behaviour of sulphur and its involvement in the reactions that produce diamond may have varied significantly over geological time, and with depth of formation. Understanding the nature of sulphide inclusions enclosed in diamond can therefore help constrain some of the processes involved in diamond formation, possibly disclosing more information on prevailing mantle conditions and the global cycling of sulphur.

1.4. Sulphide inclusions in diamonds

Sulphide inclusions in diamonds commonly resemble “normal” primary mantle sulphides in terms of their compositions and consist of an assemblage of Fe-Ni-Cu sulphides (pyrrhotite ±

pentlandite ± chalcopyrite) which have unmixed from an original liquid/melt or MSS (see introduction of chapter 3). Figure 1.7 shows the relative abundance of sulphide-bearing inclusions in diamonds of different parageneses, with data obtained from literature. Most lithospheric diamonds available for study have a peridotitic affinity (Fig. 1.7.A), however, sulphide inclusions are much more common in eclogitic diamonds (Fig. 1.7.B).

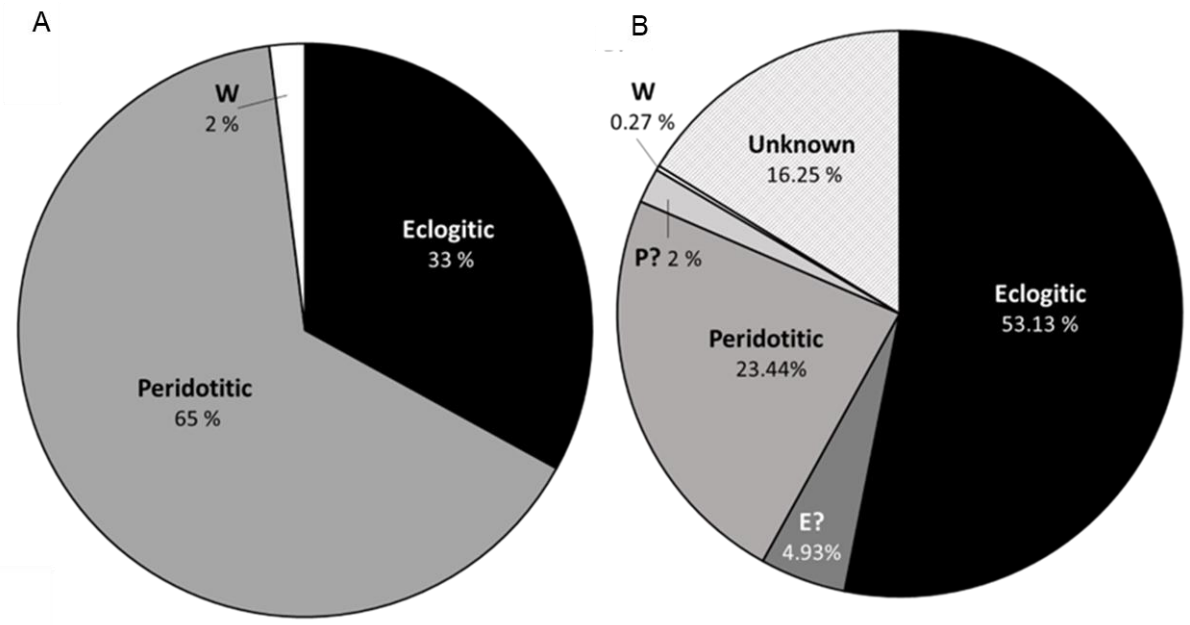

Figure 1.7. A) proportions of eclogitic, peridotitic and wehrlitic (W) diamonds reported worldwide from the inclusions they host (adapted from Stachel and Harris, 2009); B) proportions of sulphide inclusions belonging to different parageneses from reports made in literature. E? and P? signify that the authors inferred an eclogitic or peridotitic paragenesis from the Ni contents of the inclusions. Unknown denotes diamonds that contain sulphide inclusions only and which could not be attributed to an eclogitic, peridotitic or wehrlitic paragenesis.

Significant differences have been observed between sulphides included in peridotitic or eclogitic diamonds. E- type sulphides are comparatively poorer in Ni (> ~8-12 %) and Cr than sulphides hosted in P-type diamonds (Fig. 1.8), owing to the compatibility of both elements in peridotite during mantle melting and metasomatism.

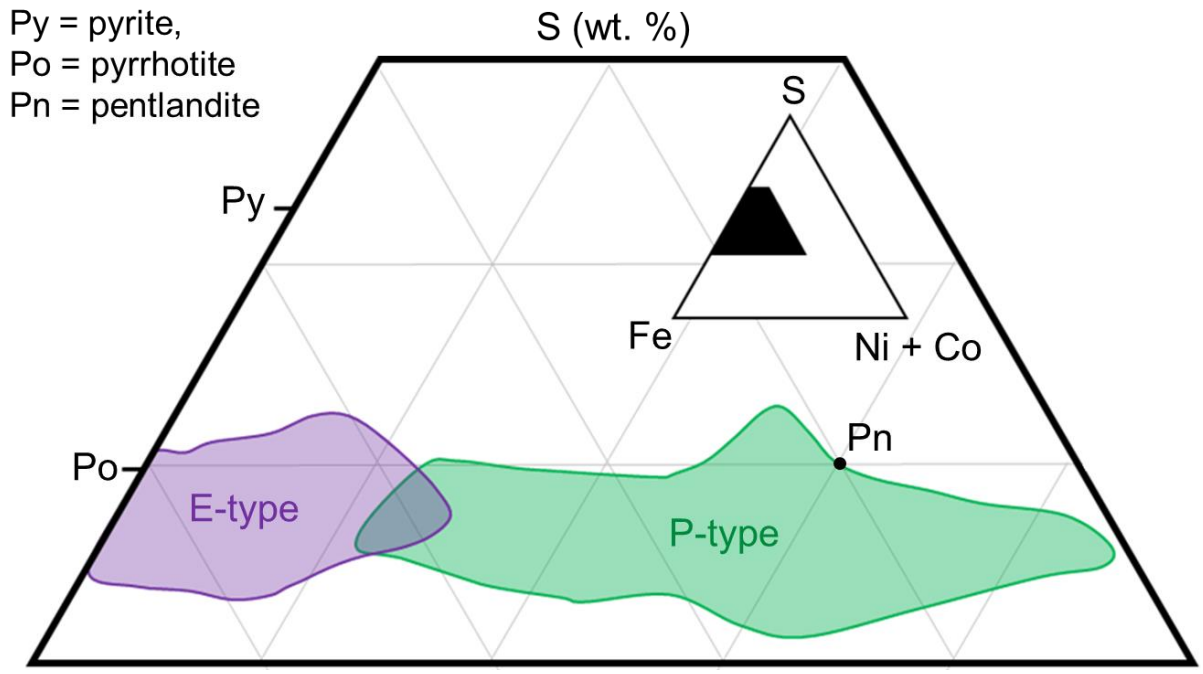

Figure 1.8. Fe, Ni+Co and S compositions of eclogitic (E-type) and peridotitic (P-type) diamond-hosted sulphide inclusions. Adapted and modified from Gréau et al., 2013.

It has also been suggested that sulphide-bearing diamonds may consist of a paragenesis of their own, and indeed, Deines and Harris (1995) argued that the assignment of Ni-rich sulphides to a peridotitic paragenesis was unclear in the absence of coexisting silicate inclusions. Titkov et al., (1998) proposed that some diamonds forming from carbon dissolved in sulphide melt would retain certain characteristics, such as Ni-induced defects in natural crystals. Furthermore, Thomassot et al. (2009), proposed that some sulphide inclusion-hosting diamonds may define a distinct population of their own. The authors showed that C and N compositions of sulphide-bearing diamonds from Jwaneng (Botswana) differed from Jwaneng diamonds of E- and P-type parageneses (Thomassot et al., 2009). The most reliable indicator of either E- or P-type sulphides is therefore the presence of co-existing silicate inclusions.

1.5. The ages of diamonds

Diamonds have formed throughout most of the Earth's history (since the Paleoarchean to the Mesozoic at least; Fig. 1.9), and the inclusions they host therefore hold valuable clues to the evolution of the planet (e.g. Gurney et al., 2010; Shirey and Richardson, 2011; Stachel and Luth, 2015).

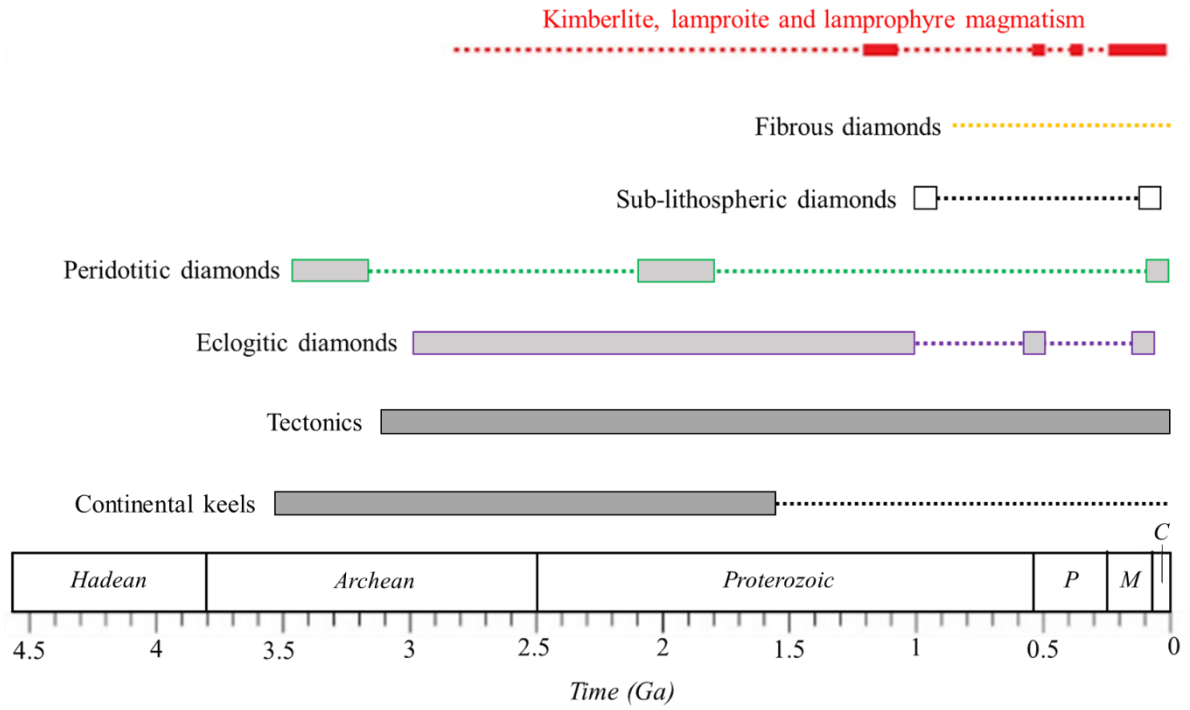

Figure 1.9. Published ages of eclogitic, peridotitic, sub-lithospheric and fibrous diamonds with relation to the ages of continental keel formation periods, tectonics and kimberlite, lamproite and lamprophyre magmatism over time. Modified and adapted from Gurney et al. (2010) and with age data for eclogitic and peridotitic diamonds adapted from Timmerman et al. (2017); P = Paleocene, M = Mesozoic, C = Cenozoic.

Valuable information has been gained from the study of radiometric isotopes in garnet, clinopyroxene and sulphide inclusions in diamonds, including information about Archean tectonics, the timing and mechanisms of continental lithosphere growth and the onset of modern-style plate tectonics (e.g. Helmstaedt and Schulze, 1989; Shirey et al., 2002; Aulbach et al., 2004; Shirey and Richardson, 2011). To date, various ages have been assigned to diamonds from different localities, using a variety of radiometric techniques (Table 1.1)

Table 1.1. Radiometric ages assigned to diamonds from literature

Location	Dating method	Archean (Ga)		Proterozoic (Ga)		Paleozoic - Mesoic (Ga)		Host (Ga)
Siberia		P-type	E-type	P-type	E-type	P-type	E-type	
23rd PC	Re-Os			2.1, 1.3	2.1, 1			
Mir	Re-Os				2.1, 1, 0.9, 0.6			0.36
	TE diffusion					0.36		
	U-Pb					0.37		
Udachnaya	Re-Os	3.1-3.5		1.8				0.36
	Pb isotopes			2				
	Sm-Nd			2				
	Ar/Ar				1.1			
Ural Mountains	Re-Os				1.28			
NE Siberia	U-Pb						0.334	
Aikhal	Re-Os	3.4						
N America								
Diavik	Re-Os	3.3-3.5			1.8-2.1			0.055
Panda	Re-Os	3.5						0.053
Victor	Re-Os			0.718				0.18-0.155
Africa								
Finsch	Sm-Nd	3.2	1.58					0.118
Jagersfontein	Re-Os				1.7, 1.1			0.086
Jwaneng	Re-Os		2.91		1.5			0.235
	Sm-Nd				1.54			
	Ar-Ar				1.886			
Kimberley	Re-Os		2.9					0.085
	Sm-Nd	3.2-3.3						
Koffiefontein	Re-Os		2.6, 1		1.1-2.9	0.069		0.09
Murowa	Re-Os	3.2						0.538
Premier	Sm-Nd		1.9		1.15			1.179
Orapa	Re-Os		1-2.9					0.093
	Sm-Nd				0.99			
	Ar-Ar				0.9-1			
Venetia	Re-Os	2						0.52
De Beers pool	Re-Os	3.2	2.9					
Zimmi					0.65			Alluvial
Australia								
Argyle	Sm-Nd				1.58			1.177
	Ar-Ar				1.16-1.54			
Ellendale	Re-Os			1.4-3				Alluvial
Sublithospheric								
Kalimantan	Re-Os	3.1						Alluvial
Collier-4	U-Pb						0.101	0.931

Published radiometric age data for diamonds from worldwide localities. Re-Os *data obtained from – Aulbach et al. (2009a, b; 2018), Laiginhas et al. (2009), Smith et al. (2009a, b; 2016), Pearson et al. (1998a, b; 1999; 2000), Pearson and Harris (2004), Richardson et al. (2001)* *(Continued on next page)*

(Continued) Richardson and Shirey (2008), Shirey et al. (2008), Smit et al. (2010), Westerlund et al. (2006), Wiggers de Vries et al. (2013a); Sm-Nd – *Koornneef et al. (2017), Richardson et al. (1984; 1990; 1993; 1998; 2004; 2009), Richardson (1986), Richardson and Harris (1997), Richardson and Shirey (2008), Timmerman et al. (2017) ;* U-Pb – *Afanasyev et al. (2009), Bulanova et al. (2010), Rudnick et al. (1993), Schmitt et al. (2019);* Ar-Ar – *Burgess et al. (1992, 2004);* Trace element (TE) diffusion patterns – *Shimizu and Sobolev (1995);* kimberlite emplacement ages – *Carlson et al. (1999), Davis (1977), Davis et al. (1980), Graham et al. (1999), Heaman et al. (1998; 2004), Kinny et al. (1989), Kong et al. (1999), Phillips et al. (1999), Pidgeon et al. (1989), Rickard et al. (1989), Smith et al. (1983; 1985; 2004)*

1.5.1. Silicate inclusions (Sm-Nd, Rb-Sr, Ar-Ar)

Early pioneering work aimed at dating individual inclusions in diamonds was performed using the Ar-Ar method, which yielded a wide range of ages (e.g. Phillips et al., 1989; Burgess et al., 1992; 1994). However, it was discovered that radiogenic Ar which migrated and was retained at the diamond-inclusion interface, would be lost during the inclusion's extraction from the diamond for analysis (e.g. Burgess et al., 1992). Richardson et al. (1990) then contemporaneously employed the Sm-Nd and Rb-Sr systems to date eclogitic garnet and clinopyroxene inclusions in diamonds, overcoming some of the problems of Ar-Ar dating. Early work employing the Sm-Nd and Rb-Sr systems required sufficient material to allow the isotope compositions of inclusions to be measured and much of this involved pooling together inclusions based on their Ca, Cr, Ti and Na contents (e.g. Richardson et al., 1990; 1993; Richardson and Harris, 1997).

Recent advances in analytical capabilities and sampling methods have since allowed for single silicate inclusions in diamonds to be dated (e.g. Richardson et al., 2009; Koornneef et al., 2017; Timmerman et al., 2017), reducing some of the uncertainties arising from and risks of the pooling methods – namely the need for large quantities of material, and the uncertainties about inclusion cogenecity. Indeed, it has become common practise to conduct a preliminary detailed study of the inclusions' position within the diamond, the stable isotope compositions and

nitrogen isotope systematics of diamonds belonging to a given population (e.g. Timmerman et al., 2017, 2018; Gress et al., 2018).

1.5.2. Sulphide inclusions (Re-Os)

Pearson et al. (1998) first applied the Re-Os isotope system to determine the ages of single sulphide inclusions in diamonds. The Re-Os system has since become a popular method used in radiometric dating of inclusions in diamonds (e.g. Pearson et al. 1998a; 1998b; 1999; 2000; Richardson et al., 2001; Pearson and Harris, 2004; Westerlund et al., 2006; Richardson and Shirey, 2008; Shirey et al., 2008; Aulbach et al. 2009a; b; 2018, Laiginhas et al., 2009; Smith et al., 2009a; b; 2016; Smit et al., 2010; Wiggers de Vries et al., 2013a; Harvey et al., 2016; Smit and Shirey, 2019), and indeed, yields a wealth of information about the mantle's evolution, partial melting events and continental crust evolution (e.g. Shirey and Walker, 1998).

Re-Os dating is based on the long-lived transition by decay of ^{187}Re to ^{187}Os (half-life = 41.6 $\times 10^9$ years). The age of a sulphide is calculated from an isochron based on the isotope ratios of parent and daughter isotopes to stable and relatively abundant ^{188}Os (Fig. 1.10A). Model ages (T_{MA}) (Fig. 1.10B) of diamond-hosted inclusions calculated in reference to a chondritic value have also been published in literature, and sometimes yield geologically valuable information (e.g. Westerlund et al., 2004; 2006; Wiggers de Vries et al., 2013a). However, due to the uncertainties associated with model ages, isochron age calculations are preferred (Richardson et al., 2004; Aulbach et al., 2009). Brief explanatory diagrams for the calculation of isochron ages and different types of model ages are provided in figure 1.10).

During melting of bulk peridotite, Os behaves compatibly and remains in the solid mantle residue, whilst Re is incompatible, entering a melt phase and becoming moderately enriched in

basaltic melts. The contrasting behaviour of Re and Os cause the high $^{187}Re/^{188}Os$ ratios observed in basaltic oceanic crust, and low ones in "normal" peridotite mantle. Indeed, metasomatism and mantle refertilisation processes generally do not significantly modify the Os isotope ratios of residual mantle rocks which have consistent high Os contents. The Re-Os isotope system is therefore regarded as the most favourable for the study of the geochemical evolution of the mantle, although geochronological uncertainties on T_{MA} and isochron ages can be relatively large (up to 300 Ma) as a result of mantle heterogeneities and/or limited characterisation of the mantle as a reference reservoir (Carlson 2005; Rudnick and Walker 2009).

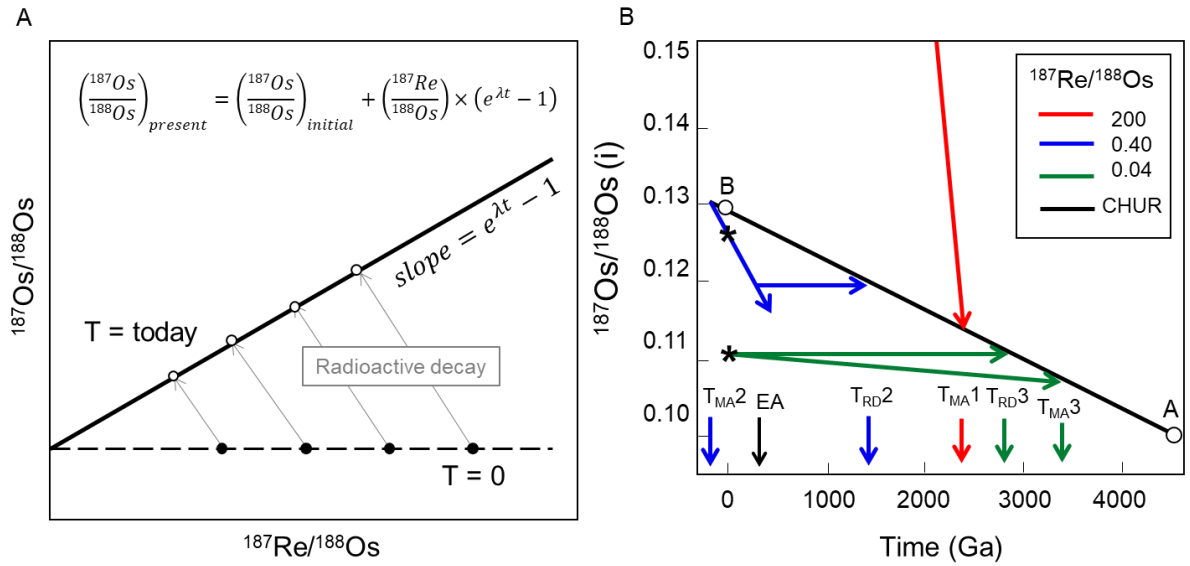

Figure 1.10. A) Simple representation of the isochron method, where four inclusions at the initial time of their encapsulation (closed circles) have the same $^{187}Re/^{188}Os$ ratio reflecting on their same age. As radioactive decay of ^{187}Re to ^{188}Os occurs over time, the inclusions evolve to in their composition and are expected to fall along a given slope (open circles) if they are cogenetic. The slope of the isochron ($e^{\lambda t}-1$) is used to calculate the age of the inclusions using the equation at the top of figure A. B) Figure modified from Shirey and Walker (1998) which outlined the different scenarios for model ages being calculated; red) a rock with a relatively high (200) initial $^{187}Re/^{188}Os$ ratio (e.g. an eclogite) has a model age ($T_{MA}1$) of ~2.4 Gy; blue) a peridotite that is depleted in Re has had Re added to it at its time of eruption 0.3 Ga. A time of Re depletion ($T_{RD}2$) age can be back calculated by subtracting the ^{187}Os produced by the recently added Re from the age calculation, but the T_{RD} will always generally underestimate the true age, nonetheless providing a minimum age. However, T_{MA} ages are meaningless, representing future ages (e.g. $T_{MA}2$). In green) a Re-depleted peridotite with no or negligible amounts of Re added to it at its time of eruption will have similar (in this case, old) T_{RD} and T_{MA} ages ($T_{RD}3$ and $T_{MA}3$), with the former underestimating the latter. CHUR refers to the Uniform Chondritic Reservoir evolution line and Asterisks show time 0 Ga.

1.5.3. Inclusion encapsulation and syngenecity

Understanding the mode of capture of inclusions in diamonds is important for their use in radiometric dating of diamond-forming events. Three terms for diamond-hosted inclusions have been distinguished by Nestola et al. (2014) as protogenetic (formed earlier than diamond, and not altered to the point of being isotopically reset/reaching isotopic equilibrium with the diamond-forming melt), syngenetic (formed simultaneously with diamond) and synchronous (a pre-existing mineral phase encapsulated in diamond at a time of chemical equilibrium and isotopic resetting). An example of synchronicity was proposed by the authors as the capture of sulphides as a melt/liquid or MSS. Since sulphides are immiscible with their surrounding mantle rocks, and likely form a single, homogeneous phase in most regions of the Earth's mantle, their enclosure in diamond should start their isotopic systems at time zero (e.g. Nestola et al., 2017; Aulbach et al., 2018).

However, Thomassot et al. (2009) discovered a sulphur mass-independent fractionation (S-MIF) signal indicative of an Archean atmospheric component, in various sulphide inclusions in diamonds from Jwaneng (Botswana) (referred to in Chapter 5). The inclusions were interpreted as having been trapped in diamonds as MSS during a later diamond-forming event, and yet the authors demonstrated that the sulphides' Archean pre-history was retained during their incorporation in diamond, providing an explanation for the observed highly radiogenic Os isotope compositions (Thomassot et al., 2009). Moreover, other workers have since shown that some silicate (Milani et al., 2016; Nestola et al., 2017; Nimis et al., 2019) and sulphide inclusions in diamonds could pre-date their host diamond (Smit et al., 2016; Smit and Shirey, 2019).

1.6. Aim of the study

Understanding the nature of entrapment of sulphide inclusions in diamonds is paramount for deciphering the information they convey about the chemical nature and dynamics of the Earth's interior. Indeed, it is important not only for accurately interpreting the radiometric ages assigned to diamonds, but also important for investigating the possible reactions involving sulphides and diamond. Detailed and minimally destructive studies of diamond-hosted sulphide inclusions can therefore convey valuable information about the nature of their involvement with their hosts, and the significance of their study.

1.7. Selection of diamonds

Spectroscopic and chemical information on sulphide inclusions in diamonds from worldwide localities (Fig. 1.11) has been compiled. The reasons for selecting the studied samples, how these were acquired, and the extent of their study are presented in section 1.7.1. In addition to the samples that were available for study, mentions of diamond populations from other localities that were not studied here are made in different chapters; literature data for each locality is also summarised (section 1.7.2.).

1.7.1. Studied diamonds

Samples from Mir, Udachnaya (Yakutia), Argyle (Australia), Murowa (Zimbabwe), Dachine (French Guiana), Juina-5, Collier-4 and Machado River (Brazil), Diavik (Canada), Jwaneng, Orapa, Damtshaa and Letlhakane (Botswana) have been studied (Fig. 1.11), each to varying degrees depending on the purpose. Samples were studied to different extents depending on:

Figure 2.11. World map showing the locations of diamond populations studied or referred to in the thesis; red symbols denote the localities from which diamonds were studied (Argyle, Collier-4, Dachine, Damtshaa, Diavik, Juina-5, Jwaneng, Letlhakane, Machado River, Mir, Murowa, Orapa and Udachnaya) and white symbols represent the source locations of diamonds that are referred to in the text (23rd Party Congress, Bingara, Bultfontein, Kankan, Klipspringer, Koffiefontein, Panda (also known as Ekati) and Zimmi).

- Whether the inclusions were exposed or not; only one inclusion was exposed in this study (inclusion 3 in Mir diamond 1584-r), and the rest of the inclusions were kept as they were
- The purpose of the analysis - e.g. x-ray microtomography (x-CT), scanning electron microscopy (SEM) and/or electron microprobe analyses (EPMA)
- The number of samples that could be analysed by certain methods due to time restrictions (e.g. synchrotron-based x-CT and SIMS)

Table 1.2. summarises the characteristics of the diamonds (paragenesis, host and original diamond size), their provenance and whether the samples have been previously published about in literature or not.

Table 1.2. Source, paragenesis and size of studied diamonds from Bristol collection

Locality	Diamond	Host	Type	Size	Source	Collection	Previous studies
Mir	1584	kimberlite	E	7	Diamond and Precious Metal Institute	Pre-existing	*Bulanova et al. (1995)*
	1591		E	6.2			*Bulanova et al. (1995), Wiggers de Vries et al. (2013)*
	1607		E	6.6			*Bulanova et al. (1996)*
	1700		E	7.5			*n/a*
	1702		E	7.7			*n/a*
	1703		E	6.8			*Wiggers de Vries et al. (2013), Bulanova et al. (2014)*
	1704		E	5.8			*n/a*
Udachnaya	3648	kimberlite	P	8		Pre-existing	*Rudnick et al. (1993), Taylor et al. (1995), Bulanova et al. (1995; 1996; 2003), Pearson et al. (1998; 1999), Hauri et al. (1998) and Palot et al. (2013).*
Murowa	V-10 D13	kimberlite	P	2.6	Rio Tinto	Pre-existing	*n/a*
	V10 - D16		P	2.8			
	V10 - D27		P	2.6			
Argyle	Arg 02	lamproite	E?	3	Rio Tinto	Pre-existing Selected (Antwerp)	*n/a*
	Arg60		E?	3.5			
	Arg 104		E?	2.8			
	L1		E	4.2			
	L11		E	4.5			
	L13		E	5			
	L16		E	5.5			
	L17		P?	5.5			
	L18		E	4.8			
	L26		E	4			
	L30		E?	5			
	L35		E?	6			
	L38		E	6			
	L40		P?	5.8			
	L45		E	4.6			
	L52		P?	5.5			
	L56		E?	5.5			
	L59		E	4.6			
	L61		P?	5			
	L75		E	6.5			
Diavik	DDM-B9	kimberlite	P?	5.5	Rio Tinto	Selected (Antwerp)	*n/a*
	DDM-B11		P?	5.8			
Dachine	Dac-BS-4A1	komatiite-boninite	E	1.9	Rio Tinto	Pre-existing	*Smith et al. (2016)*
	Dac-BS-4A3		E	2			
	Dac-BS-4A5		E	1.7			
	Dac-BS-4A7		E	1.6			
	Dac-BS-4A8		E	1.4			
	Dac-BS-4B2		E	1.3			
	Dac-BS-4B3		E	1.7			
	Dac-BS-4B4		E	1.8			
	Dac-BS-4B6		E	2.1			
	Dac-BS-4B7		E	1.8			
	Dac-BS-4B9		E	1.4			
	Dac-BS-4B10		E	1.1			
	45-1		E	1			

Juina-5	Ju5-03		UD	2.6			
	Ju5-13		UD	2.4			
	Ju5-21		UD	1.2			
	Ju5-53		UD	2.2			*Thomson (2014), Thomson et al. (2014)*
	Ju5-54		UD	1.5			
	Ju5-64	kimberlite	UD	2			
	Ju5-76		UD	1.2			
	Ju5-77		UD	1.8	Debora Araujo (Rio Tinto)	Pre-existing	*n/a*
	Ju5-97		UD	2			*Thomson (2014), Thomson et al. (2014)*
	Ju5-120		UD	2			*n/a*
Collier-4	ColN-2		UD	4.2			*n/a*
	ColN-9		UD	2.6			
	J6		UD	1.8			
	J12	kimberlite	UD	2.8			*Bulanova et al. (2010)*
	J15		UD	2.8			
	J16		UD	3.2			
	TR1-15		UD?	1.5			*n/a*
Machado River	P5		UD?	2.2			
	P6	Alluvial	UD	2	Rio Tinto	Pre-existing	*Burnham et al. (2016)*
	P15		UD?	2.5			
	P16		UD?	1.8			

Table 1.2. Summary of the paragenesis, provenance and previous studies relating to the studied diamonds from Mir, Udachnaya, Murowa, Argyle, Diavik, Dachine and Brazilian localities. E, P and UD indicate that inclusions typical of eclogitic, peridotitic or sublithospheric substrates occur inside the diamonds (? Indicates a suspected paragenesis based on other attributes of the diamond such as surface resorption features or diamond morphology). Size is expressed in mm. n/a indicates that the individual diamonds have not previously been published about.

1.7.1.1. Yakutian diamonds

Seven Mir samples and one Udachnaya diamond were studied most extensively by Raman spectroscopy and other methods because of the presence within them of multiple (>5), often large (>80 μm) and zonally distributed sulphide inclusions. The samples were provided to Galina Bulanova by the Diamond and Precious Metal Institute (Yakutsk, Russia) prior to the start of the PhD, as part of a collection which was previously studied (e.g. Bulanova et al., 1995; 1996; Pearson et al., 1999; Wiggers de Vries, 2013a, b; Bulanova et al., 2014).

1.7.1.2. Brazilian diamonds

A previously studied collection of sulphide inclusion-bearing diamonds from Juina-5, Collier-4 and Machado River (Juina area, Brazil) was used in this study. The samples were given to Galina Bulanova and Chris Smith by Debora Araujo (Rio Tinto) and Steven Shirey (Carnegie Institute) prior to the start of the PhD. The majority of the Juina-5 samples were previously studied by Andy Thomson during the completion of his, and one Collier-4 diamond which was studied in Chapter 5 has been reported on by Bulanova et al. (2010).

1.7.1.3. Argyle diamonds

A donation of 78 diamonds from Argyle was provided by Rio Tinto at the beginning of the PhD. A week was spent sorting through a large batch of rough diamonds (~16000 stones) at the Rio Tinto diamond sales and marketing headquarters in Antwerp (Belgium) and samples were selected based on the presence within them of inclusions surrounded by visible dark fractures. The Argyle diamonds were laser-cut into two or three pieces and the cut surfaces were polished mechanically to allow for Raman analyses. However, only few (<20) inclusions were characterised as sulphides according to Raman and as a result, 11 Argyle diamonds from a pre-existing collection were also obtained for Raman analysis, of which 7 contained sulphide inclusions or inclusions resembling sulphide.

1.7.1.4. Diavik diamonds

Alongside the Argyle diamonds selected in Antwerp, 10 diamonds from Diavik were selected due to their peridotitic nature and the interest in dating them. Because the diamonds were kept as whole stones, only 2 diamonds contained inclusions from which a Raman signal could be obtained, and therefore the samples were not studied further.

1.7.1.5. Dachine diamonds

The Dachine samples belong a previously studied collection obtained by Galina Bulanova and Chris Smith (from Rio Tinto). The diamonds and the inclusions studied here have been published about in Smith et al. (2016). The samples were provided for study because of the abundance within them of exposed and unexposed sulphide inclusions, despite the small size of the diamonds and the inclusions.

1.7.1.6. Murowa diamonds

Nine Murowa diamond off-cuts from a pre-existing collection provided to Chris Smith and Galina Bulanova by Rio Tinto and Murowa Diamonds Pty. Ltd. were acquired at the beginning of the PhD. The inclusions in these were only were only studied by Raman in order to determine if they consisted of sulphide, based on the presence of Raman-active chalcopyrite or molybdenite (five in three diamonds being detected).

1.7.1.7. Diamonds from Botswana

Diamonds from Damtshaa, Jwaneng, Letlhakane and Orapa were lent by Michael Gress (Vrije Universiteit Amsterdam), during a week-long visit to Bristol. Raman spectroscopy was employed simply to determine the presence or absence of molybdenite in the sulphide inclusions, but the diamonds were not studied further.

Table 1.3. summarises the methods of study employed to study those diamonds that contain sulphide inclusions and whether the inclusions are exposed or unexposed.

Table 1.3. Summary of techniques used on studied diamonds and references to data

Locality	Diamond		Inclusions	Techniques						Text		Appendix	
	Name	Sample	Exposed	Raman	x-CT	FTIR	SEM	EPMA	SIMS	Figures	Tables	Figures	Tables
Mir	1584-i	Plate (int)	-	X	X		X		X	2.5, 2.6, 3.2, 3.6, 4.12	2.2, 2.3	A1, A2	A1, A2
	1584-r	Plate (rim)	1	X	X		X	X		3.4, 3.5, 5.7, 5.8	-	A1, A2, B3	A1, A2, B1, B2
	1591	Central plate	-	X	X	X				2.5, 2.6, 3.1, 3.6	2.2, 2.3	A1, A2	A1, A2
	1607	Central plate	5	X	X	X	X		X	2.5, 4.12, 5.7, 5.8	2.2, 2.3	A1, A2, B3	A1, A2, B1, B2
	1700	Thick central plate	2	X			X	X	X	5.7, 5.8	-	A1, A2, B3	A1, A2, B1, B2
	1702	Off-cut	-	X	X					3.2	-	A1, A2, A3	A1, A2
	1703	Off-cut	-	X						2.1	-	A1, A2	A1, A2
	1704	Off-cut	-	X	X					3.2, 3.3	-	A1, A2	A1, A2
Udachnaya	3648 - 1	Central plate (core)	3	X	X	X				2.7, 2.8, 2.9, 2.10, 4.7	2.2	-	-
	3648 - 2	Central plate (int)	-	X		X				4.7	-	-	-
	3648 - 3	Central plate (rim)	-	X		X				-	-	-	-
Murowa	V-10 D13	Off-cut	1	X						4.11	-	-	-
	V10 - D16	Off-cut	1	X						-	-	-	-
	V10 - D27	Off-cut	1	X						-	-	-	-
Argyle	Arg 02	Central plate	-	X						-	-	-	-
	Arg60 - 1	Central plate	-	X						-	-	-	-
	Arg60 - 2	Off-cut	-	X						-	-	-	-
	Arg 104	Central plate	1	X			X			2.1, 4.8	-	-	-
	L1 - 1	Off-cut	-	X						-	-	-	-
	L11 - 1	Off-cut	-	x						-	-	-	-
	L13 - 1	Off-cut	-	X						-	-	-	-
	L16 - 1	Off-cut	-	X						-	-	-	-
	L17 - 1	Off-cut	-	X						-	-	-	-
	L17 - C	Central plate	-	X						2.1, 4.9	-	-	-
	L18 - 2	Off-cut	-	X						-	-	-	-
	L26 - 1	Off-cut	-	X						4.9	-	-	-
	L26 - 2	Off-cut	-	X						-	-	-	-
	L29 - 1	Off-cut	-	X						-	-	-	-
	L30 - 1	Off-cut	-	X						-	-	-	-
	L30 - 2	Off-cut	-	X						-	-	-	-
	L35 - 1	Off-cut	-	X						-	-	-	-
	L38 - C	Off-cut	-	X						4.8	-	-	-

	L40 - 1	Off-cut	-	X				4.8	-	-	-
	L45 - 1	Off-cut	-	X				4.8	-	-	-
	L45 - 2	Off-cut	-	X				4.8	-	-	-
	L52 - 2	Off-cut	-	X				-	-	-	-
	L56 - 2	Off-cut	-	X				-	-	-	-
	L59 - 1	Off-cut	-	X				-	-	-	-
	L61 - 1	Off-cut	-	X				-	-	-	-
	L75 - 1	Off-cut	-	X				-	-	-	-
Diavik	DDM-B9	Whole stone	-	X				-	-	-	-
	DDM-B11	Whole stone	-	X				-	-	-	-
Dachine	Dac-BS-4A-1	Polished windows	2	X		X	X	5.7, 5.8	-	B1	B1, B2
	Dac-BS-4A-3	Thick plate	3	X				-	-	-	-
	Dac-BS-4A-5	Polished windows	1	X				4.10	-	-	-
	Dac-BS-4A-7	Polished windows	1	X		X		-	-	-	-
	Dac-BS-4A-8	Polished windows	2	X		X	X	5.7, 5.8	-	B1	B1, B2
	Dac-BS-4B-3	Off-cut	2	X				-	-	-	-
	Dac-BS-4B-4	Polished windows	1	X		X		-	-	-	-
	Dac-BS-4B-6	Off-cut	1	X		X	X	5.7, 5.8	-	B1	B1, B2
	Dac-BS-4B-7	Polished Windows	1	X				-	-	-	-
	Dac-BS-4B-9	Polished windows	1	X		X	X	5.7, 5.8	-	-	-
	Dac-BS-4B-10	Off-cut	1	X		X	X	5.7, 5.8	-	B1	B1, B2
	45-1	Polished windows	1	X		X		-	-	-	-
Juina-5	Ju5-03	Off-cut	1	X	X	X	X	2.11, 2.12, 2.13, 5.7, 5.8	2.2	B2	B1, B2
	Ju5-21	Polished windows	1	X				-	2.2	-	-
	Ju5-53	Off-cut	1	X		X	X	5.7, 5.8	-	B2	-
	Ju5-54	Polished windows	1	X	X	X	X	2.13, 5.7, 5.8	2.2	B2	B1, B2
	Ju5-64	Polished windows	1	X	X	X		-	-	-	B1, B2
	Ju5-76	Polished windows	1	X				-	-	-	-
	Ju5-77	Polished windows	1	X	X	X		2.13	2.2	-	-
	Ju5-97	Polished windows	1	X	X	X		2.13	2.2	-	-
	Ju5-120	Off-cut	1	X		X	X	5.7, 5.8	-	B2	B1, B2
Collier-4	J6	Thick central plate	1	X	X	X	X	5.7, 5.8	-	B2	B1, B2
	J15	Off-cut	3	X		X		-	-	-	-
	J16	Off-cut	1	X	X	X		-	-	-	-
	Col-N9	Off-cut	1	X	X	X		-	-	-	-

Table 1.3. (previous page) Techniques employed on inclusions in the studied diamonds from Mir, Udachnaya, Argyle, Diavik, Dachine, Juina-5 and Collier-4, indicated by X symbols. x-CT = x-ray microtomography; FTIR = Fourier-transform infrared spectroscopy; SEM = scanning electron microscopy; EPMA = electron microprobe analysis; SIMS = secondary ion mass spectrometry. Provided are also the recorded number of exposed inclusions in each of the studied diamonds. The samples studied consist of off-cuts, laser-cut and polished plates or whole stones with polished windows (PW), except for two Diavik diamonds which were kept intact. The numbers of the figures and tables referring to the samples in the text and appendix are also provided.

1.7.2. Other diamond localities

References are made in the text to diamonds from the 23rd Party Congress kimberlite (Yakutia, Russia), Bingara (New South Wales, Australia), Bultfontein (South Africa), Kankan (Guina), Klipspringer, Koffiefontein (South Africa), Panda (Canada), Premier (South Africa) and Zimmi (Sierra Leone) which were not studied here. Table 1.4. summarises some of the literature available for each of the mentioned (other) diamond localities.

Table 1.4. Examples of literature available for each of the studied or mentioned (other) diamond populations

Locality		Studies	Chapters	Figures	Tables	Appendix
Studied diamonds						
Argyle	Western Australia	*Jaques et al. (1986; 1990), Richardson (1986), Richardson et al. (1990), Liu et al. (1990), Burgess et al. (1992), Honda et al. (2012)*	2-4	2.1; 4.8; 4.9	1.1; 4.1	
Collier-4	Juina area, Brazil	*Bulanova et al. (2008; 2010), Walter et al. (2008; 2011), Kaminsky et al. (2009; 2010), Smith et al. (2010), Araujo et al. (2013), Burnham et al. (2015)*	2-5	5.7; 5.8	1.1; 4.1	B
Dachine	French Guiana	*Capdevila et al. (1999), Cartigny et al. (2010), Smith et al. (2016)*	3-5	4.10; 5.7; 5.8	4.1	B
Damtshaa	Botswana	*Deines et al. (2009), Ickert et al. (2013), Gress et al. (2017), Nimis et al. (2019)*	3, 4		4.1	
Diavik	NW Territories, Canada	*Klein-BenDavid et al. (2004; 2007), Tomlinson et al. (2006), Donnelly et al. (2007), Araujo et al. (2009), Aulbach et al. (2009), Van Rythoven et al. (2009), Miller et al. (2014)*	2, 4	2.2; 4.6; 4.13; 4.16	1.1; 4.1	
Juina-5	Juina area, Brazil	*Harte et al. (1999), Kaminsky et al. (2001; 2009), Hutchison et al. (2001), Hayman et al. (2005), Brenker et al. (2007), Walter et al. (2008; 2011), Bulanova et al. (2010), Araujo et al. (2013), Zedgenizov et al. (2014), Thomson (2014), Thomson et al. (2014; 2016) Burnham et al. (2015; 2016)*	2-5	2.11-2.14; 5.7; 5.8	4.1	B
Jwaneng	Botswana	*Burgess et al. (1992), Schrauder et al. (1994; 1996), Gurney et al. (1995), Deines et al. (1997), Cartigny et al. (1998), Richardson et al. (1998; 2004), Shirey et al. (2002), Stachel et al. (2004), Honda et al. (2004; 2011), Thomassot et al. (2009; 2017), Gress et al. (2018), Davies et al. (2018)*	3-5	5.5; 5.7; 5.8	1.1; 4.1	
Letlhakane	Botswana	*Shirey et al. (2002; 2003), Deines and Harris (2004), Deines et al. (2009), Timmerman et al. (2017), Gress et al. (2017)*	3, 4		4.1	
Machado River	NW Brazil	*Bulanova et al. (2008), Longo et al. (2009; 2010), Schmitz et al. (2012), Burnham et al. (2015; 2016), Kohn et al, (2016), Borges et al. (2016)*	4		4.1	
Mir	Yakutia, Russia	*Bulanova and Pavlova (1987), Bulanova et al. (1988; 1995; 1996; 1998; 2002; 2014), Garanin et al. (1990), Sobolev et al. (1991; 1998; 2004; 2016), Rudnick et al. (1993), Griffin et al. (1993), Shimizu et al. (1994), Shimizu and Sobolev (1995), Taylor et al. (1998), Reutskii et al. (1999), Yuryeva et al. (2017), Schmitt et al. (2019)*	2-5	2.5; 2.6; 3.1-3.6; 4.12; 4.16; 5.7; 5.8	1.1; 4.1	A, B
Murowa	Zimbabwe	*Smith et al. (2004; 2009), Klein-BenDavid et al. (2009), Bulanova et al. (2012), Gaillu et al. (2012), Moss et al. (2013), Kohn et al. (2016)*	3, 4	4.11	4.1	

Orapa	Botswana	*Gurney et al. (1984), Chaussidon et al. (1987), Deines et al. (1991; 1993; 1995; 2004); Burgess et al. (1992; 2004), Cartigny et al. (1999), Farquhar et al. (2002), Shirey et al. (2002; 2008), Phillips et al. (2004; 2008), Stachel et al. (2004), Timmerman et al. (2017; 2018); Thomassot et al. (2017)*	3, 4	5.5; 5.7	1.1; 4.1	
Udachnaya (3648)	Yakutia, Russia	*Rudnick et al. (1993), Taylor et al. (1995), Bulanova et al. (1995; 1996; 2003), Pearson et al. (1998; 1999), Hauri et al. (1998) and Palot et al. (2013).*	2-4	2.7-2.10; 4.6; 4.7; 4.13; 4.16	1.1; 4.1	
Other						
23rd Party Congress	Yakutia, Russia	Rudnick et al. (1993), Bulanova et al. (1995; 1996); Wiggers de Vries et al. (2013a)	4.4.4.1; 5.1.2.4; 5.4.1	4.16	1.1	
Bingara	New South Wales	Meyer et al. (1995), Barron et al. (2008), Davies et al. (1998a; 1998b; 1999; 2002; 2003)	3.3.4; 4.1.3; 4.5			
Bultfontein	South Africa	Richardson et al. (1984), Wilding et al. (1991; 1994), Giuliani et al. (2016), Nimis et al. (2016)	2.1.1	5.5; 5.7		
Kankan	Guinea	Stachel et al. (2000a; b; 2002; 2005), McCammon et al. (2004), Weiss et al. (2009; 2014), Palot et al. (2012; 2014)	2.1.1	2.2		
Klipspringer	South Africa	Westerlund et al. (2000; 2004), McCarthy et al. (2007), Kidane et al. (2015; 2017)	5.1.2.4	5.6		
Koffiefontein	South Africa	Rickard et al. (1989), Deines et al. (1991), Deines and Harris (1995), Pearson et al. (1998b), Izraeli et al. (2001; 2004), Navon et al. (2003), Pearson and Harris (2004), Nimis et al. (2016), Timmerman et al. (2018a)	2.1.1	2.2; 2.3	1.1	
Panda	NW Territories, Canada	Stachel et al. (2003), Gurney et al. (2004), Tappert et al. (2005), Westerlund et al. (2006), Tomlinson et al. (2006; 2009), Burgess et al. (2009), Cartigny et al. (2009), Fedortchouk et al. (2010), Melton et al. (2013)	2.1.1; 5.4	2.2; 5.5; 5.7; 5.8	1.1	
Zimmi	Sierra Leone	Smit et al. (2016; 2017; 2018; 2019)	4.4.4.1; 5.1.2.3; 5.1.2.4	4.16; 5.5-5.7	1.1	

Table 1.4. Examples of literature sources available for diamonds from the studied localities, and ones which are referred to elsewhere in the text (Other). Summarised are also the figures, tables and sections in the text or appendix that refer to diamonds from each locality.

Chapter 2. Diamond-forming reactions involving sulphides: observations of natural sulphide inclusions

2.1. Introduction

The abundance of sulphide inclusions in diamonds relative to expected mantle sulphide contents implies that sulphides may play an important role in promoting the growth of certain diamonds. Indeed, their potential role in diamond-formation has long been recognised (e.g. Sharp, 1966; Harris, 1968; 1972; Marx, 1972; Langford et al., 1974; Fesq et al., 1975; Gurney et al., 1982; Haggerty, 1986; Eldridge et al., 1991; Deines and Harris, 1995). Marx (1972) and Langford (1974) first suggested diamond nucleation mechanisms involving the reduction of CO_2 by sulphide for at least some diamond populations worldwide: $2FeS + CO_2 = 2FeO + S_2 + C$ (diamond) (Marx, 1972). Haggerty et al. (1986) also underlined the importance of sulphur (present as C-O-S, $C\text{-}S_2$ or as immiscible sulphide liquids) in acting as a catalyst to reduce mantle carbon, by forming various compounds with surrounding components. It has additionally been suggested that significant amounts of sulphides may have remained in the upper mantle during the formation of sub-continental lithosphere, promoting diamond growth by helping maintain a reduced environment (e.g. Haggerty et al., 1986).

Several workers have since experimentally investigated the involvement of sulphides with diamond formation (Table 2.1). Diamond was first synthesised in a sulphide-carbon medium by Litvin et al (2002). Later, Litvin et al. (2005) reported direct diamond crystallisation from a carbon-saturated sulphide (pyrrhotite) melt at 7.5-8.9 GPa and between 1800-2100 °C. Experiments conducted by Pal'yanov et al. (2006); Shushkanova and Litvin (2008a) and

Spivak et al. (2008) also revealed spontaneous diamond-growth in a carbon-saturated pyrrhotite medium at mantle-like pressures and temperatures (Table 2.1.). Shushkhanova and Litvin (2008b) then demonstrated that carbon could be dissolved in miscible carbonate-silicate (aragonite-pyrope) and co-existing immiscible sulphide (pyrrhotite) melts in sufficiently high concentrations to promote spontaneous diamond growth at 7 GPa and between 1130-1925 °C. There is nonetheless a consensus that, due to the immiscibility of sulphide melts and silicate phases, and the presence of syngenetic silicate and sulphide inclusions in diamonds (e.g. Litvin et al., 2005), natural upper mantle sulphide melts are unlikely to serve as efficient growth media for natural diamonds.

Table 2.1. Experimental diamond-forming media involving sulphur

Authors	System	T °C	GPa
Litvin et al. (2005)	C + Fe-Ni-Cu-S melt	1400-1850	7.5-8.9
Spivak et al. (2008)	C + FeS melt	1660	6.7
Shushkanova and Litvin (2008[a])	C + FeS melt	1500-1700	6-7.1
Shushkanova and Litvin (2008[b])	CaCO3-pyrope-FeS	1130-1925	7
Zhimulev et al. (2012)	Fe-Ni- & Fe-Co-S melt + C (14 wt. % S)	1300	5.5
Zhimulev et al. (2016)	Fe-C + S (0.8-3.2 wt. % S)	1300-1370	5.3-5.5
Pal'yanov et al. (2006)	$(Fe,Ni)_9S_8$ & Fe-S melt + graphite	>1600	>7.5
Chepurnov et al. (2009)	Fe-Co-S-C	1300	5.5

List of conditions (compositions, pressures and temperatures of a system) used to successfully form diamond experimentally, derived from known literature.

However, Zhimulev et al. (2012), have advocated for a close genetic relationship between diamond and carbon- and/or metal-bearing sulphide systems, and showed that diamond could crystallise from carbon dissolved in pre-eutectic Fe-Ni and Fe-Co-sulphide melts (<14 wt. %

sulphur) at 5.5 GPa and 1300 °C (Table 2.1). Subsequently, Zhimulev et al. (2016) synthesised diamond from Fe-S-C melts which contained only 0.8-3.2 wt. % S. The authors pointed out that pressure was an important factor in promoting diamond formation in the Fe-S-C system, as well as the presence of Ni, Cu and Co, which are present in natural systems and would lower the melting temperatures of the sulphide-bearing melt (Zhimulev et al., 2012; 2016).

It has also been shown that sulphides, both in molten or solid form, can act as reducing agents, acting on oxidising, subducted-slab derived melts/fluids, in order to promote diamond formation in the system $MgCO_3$–SiO_2–Al_2O_3–FeS at 6.3 GPa and between 1250-1800 °C (Palyanov et al., 2007). The diamonds were grown as octahedra, and their formation involved the reduction of carbonate by a sulphide with a pyrrhotite-pyrite composition, revealing the role of sulphide in reducing CO_2-bearing fluids formed by decarbonation (Palyanov et al., 2007; Marx, 1972). In some of their experiments, the initial pyrrhotite would change in composition with increasing temperature from a stoichiometric FeS, to $Fe_{0.89}S$ at 1250 °C and $Fe_{0.85}S$ at 1450 °C, and at even higher temperatures, pyrite and pyrrhotite would form as exsolution products during cooling (Palyanov et al., 2007).

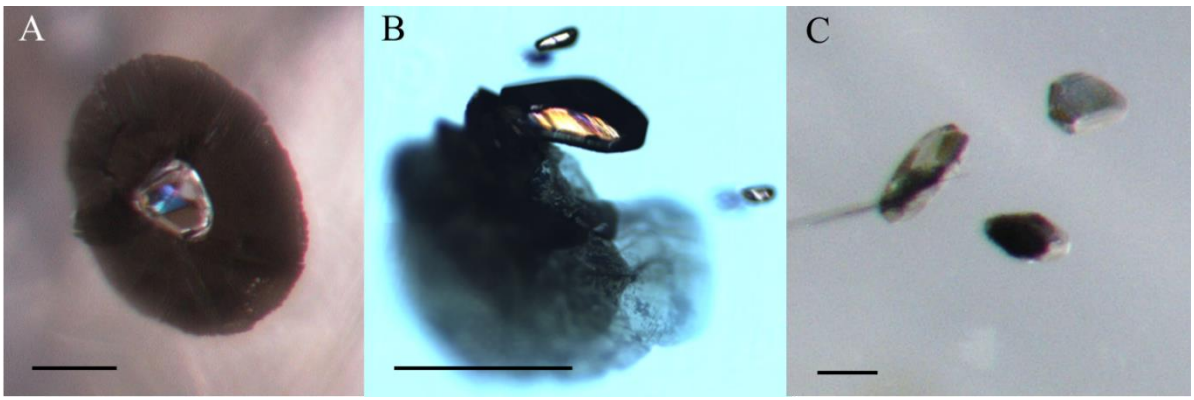

Figure 2.1. Raman optical micrographs of diamond-hosted sulphide inclusions from Mir, Yakutia (A) and Argyle, Australia (B and C); A) a euhedral to sub-rounded inclusion is surrounded by a dark flat fracture system. B) two sub-rounded sulphide microinclusions occur in proximity of an elongated euhedral sulphide inclusion which has dark fractures extending from one end of its body. Two intact sulphide inclusions and one pre-exposed one (white line delineates the exposed surface of the inclusion) are free of rosette fractures. Scales = 100 µm

Other factors, such as oxygen fugacity and the compositions of the diamond growth substrate and diamond-forming fluids, may strongly influence the nature of the diamond-forming reactions involving sulphides. In fact, the different shapes, sizes and presence or lack of decompression fractures around sulphide inclusions in diamonds (e.g. Fig. 2.1) could also reflect on differences in their internal composition and/or mode of capture. A better understanding of the behaviour of sulphides during a diamond-forming event can be gained from the study of sulphide inclusions in natural diamonds. Furthermore, due to the seemingly close genetic association of diamonds and sulphides, the possibility of evolving typical diamond-forming fluids from a sulphide-dominated growth medium requires further investigation.

2.1.1. Diamond-forming fluids

The frequent association of diamonds with fractures and veins in xenoliths and xenolith-hosted alteration zones (Schulze et al., 1996, Taylor et al., 2000, Taylor and Anand, 2004), other metasomatic minerals (phlogopite, apatite, chlorite…) (Meyer, 1987, Anand et al., 2004, Bulanova et al., 2004), as well as their growth patterns and morphology (e.g. Sunagawa, 1981; 1984; Davies et al., 1999) suggest that diamond formation is closely associated with the presence of fluids in the Earth's mantle (e.g. Weiss et al.,2009). The chemical inertness of diamond allows it to preserve pristine fluids that were captured during its growth in the Earth's mantle and transport them to the surface. These fluid inclusions provide important clues about the composition of the fluids and co-existing phases involved in diamond formation.

A wide range of chemistries have been observed in diamond-hosted fluid inclusions, which are most abundant in rapidly grown fibrous diamonds (e.g., Boyd et al., 1987, Navon et al., 1988; Schrauder et al., 1994; Burgess et al., 2002, Zedgenizov et al., 2007; Klein-BenDavid et al., 2004; 2007; 2014), cuboid (e.g. Zedgenizov et al., 2009) or cloudy diamonds (e.g. Israeli et al.,

2001) and sometimes observed in monocrystalline diamonds (Giardini and Melton, 1975; Logvinova et al., 2011; Weiss et al., 2014; Smith et al., 2015; Jablon and Navon, 2016). The fluids typically consist of high-density fluids with compositions that have commonly been associated with one of three main endmembers: silicic, saline or carbonatitic (Fig. 2.3) (e.g. Klein Ben-David et al., 2009; Weiss et al., 2009).

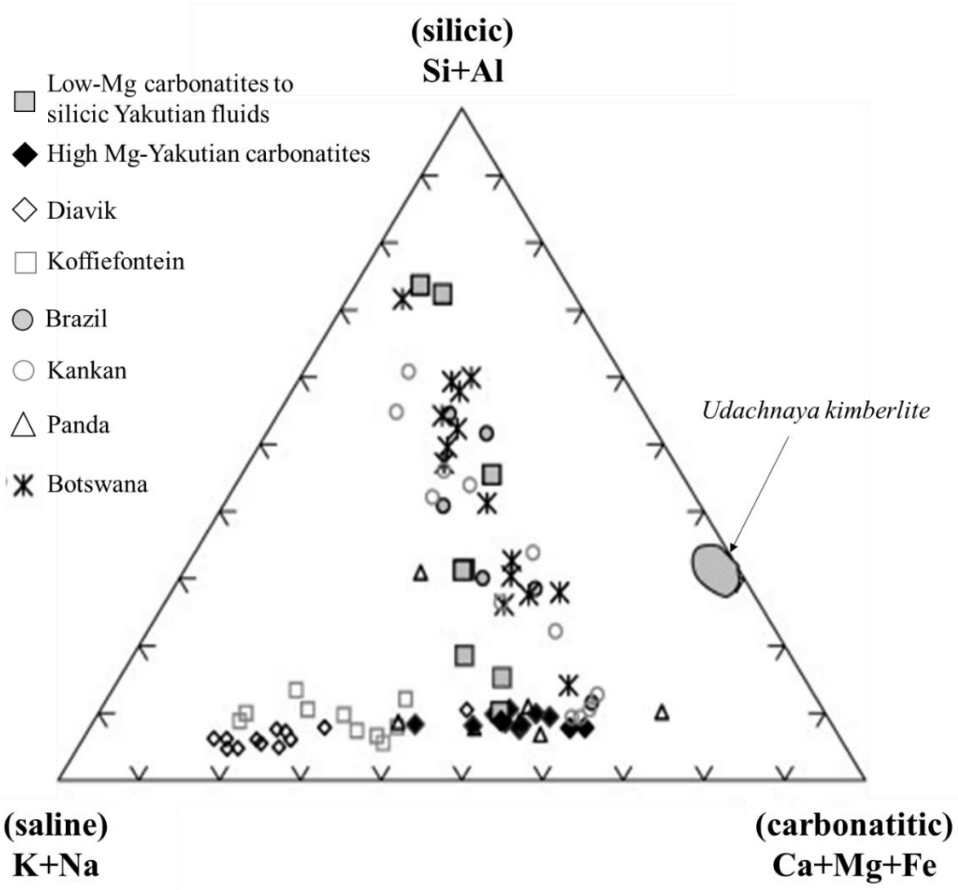

Figure 2.2. Compositions of fluid inclusions in diamonds from different localities worldwide plotted to show their distribution across the three endmembers (saline, silicic and carbonatitic) (modified from Klein-BenDavid et al., 2009).

An example of co-existing silicate inclusions and fluid microinclusions has also previously been reported in fibrous diamonds the Panda kimberlite in Canada (e.g. Tomlinson et al., 2006; 2009), where the fluids were dominated by H_2O, and varying amounts of KCl and Fe-Ca-Mg carbonate. It was suggested that both solid and fluid inclusions were relics of the metasomatic event which formed the diamond encapsulating them (Tomlinson et al., 2006; 2009). Later,

Jablon and Navon (2016) also identified carbonate-bearing high-density fluids (HDF) in microinclusions on twinning planes in monocrystalline gem quality diamonds from Venetia and Voorspoed (South Africa), indicating that they grew from a similar HDF to the one forming fibrous diamonds.

Monocrystalline diamonds generally do not host as much water in their matrix (in the form of fluid micro or nano-inclusions) as fibrous, cloudy or coated diamonds (e.g. Chrenko et al., 1967; Navon et al., 1988; Zedgenizov et al., 2006; Bureau et al., 2012; Weiss et al., 2014). However, Nimis et al. (2016) recently identified a thin (< 1.5 μm), hydrous silicic film around syngenetic silicate and oxide mineral inclusions in gem-quality eclogitic and peridotitic diamonds from the Siberian (Udachnaya) and Kaapvaal cratons (Premier, Bultfontein and Koffiefontein) (Fig. 2.3). The feature, which was imaged by x-ray computed microtomography (X-CT) and analysed by Raman spectroscopy was interpreted as sampling some of the diamond-forming fluid (Nimis et al., 2016).

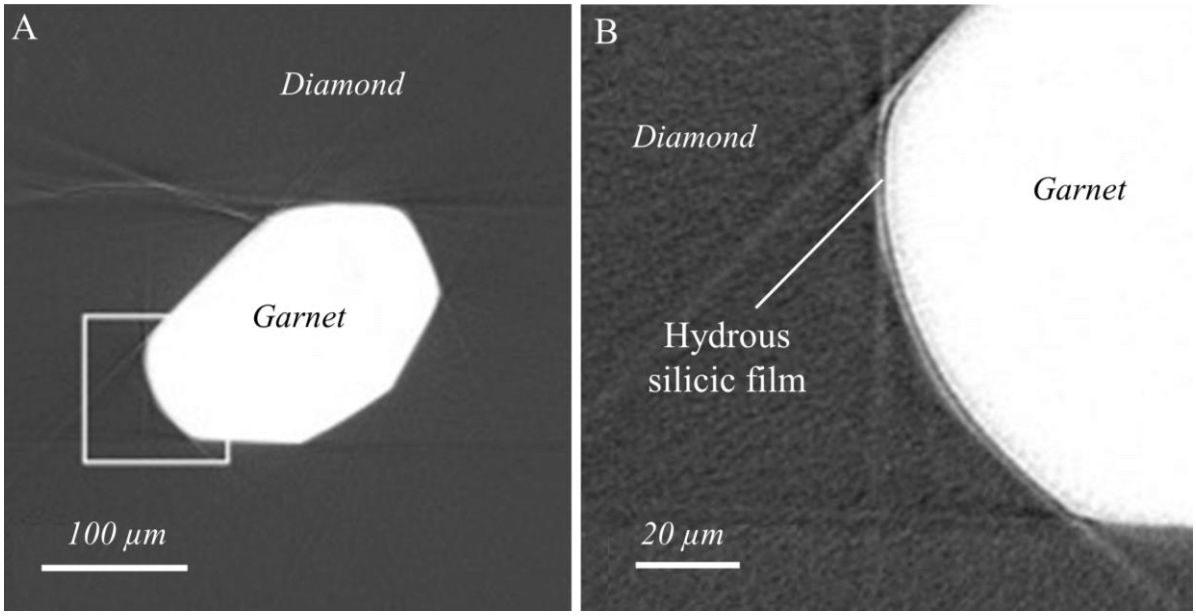

Figure 2.3. Computed x-ray microtomography (X-CT) images from Nimis et al., (2016) showing an E-type garnet inclusion (higher density = white) in diamond (lower density background = grey; A). B) reveals the presence of a low-density (dark) rim at the interface between the inclusion and the diamond, which consist of a hydrous silicic fluid.

2.1.2. The solubility of C, H and O in sulphide melts

Sulphides are anhydrous minerals which typically do not incorporate volatile elements such as C, H and O into their structure, and therefore, very little work has been published investigating the solubility of these elements in sulphide minerals. Relatively little research has been directed at studying the volatile element and silica contents of natural sulphide melts. The existing work on C, H and O solubility in sulphide melts has largely been conducted experimentally, with some corroborating observations of natural features. Examining the features associated with sulphides derived from mantle-depths can potentially provide information on their original composition, their potential ability to store phases normally not observed in solid sulphide minerals and phases coexisting with sulphides and carbon.

2.1.2.1. Carbon

Sulphide melts are potentially important reservoirs of carbon in the mantle, particularly in its reduced, metal-saturated domains (Dasgupta et al., 2009; Tsuno and Dasgupta, 2015; Zhang et al., 2015; 2018). In the reduced, mid- to deep-upper mantle, carbon should principally be hosted in diamond and/or graphite but owing to the enhanced solubility of carbon in Fe-Ni alloy melts, diamonds may also become destabilised. Tsuno and Dasgupta (2015) observed that the presence of sulphur could significantly lower the temperature of Fe-Ni-C alloy liquid stability (e.g. suggested also by Chepurov et al., 1988). While carbon solubility in the metallic alloy-enriched melts was shown to decrease with increasing sulphur contents (irrespective of temperature), it was demonstrated that sulphur could be an important agent in promoting diamond stability in relatively carbon-poor (5-20 ppm C), depleted oceanic mantle, through diminishing the solubility of C in the metal-enriched melts providing a possible explanation for the abundance of sulphide inclusions in diamonds relative to rarer alloy or carbide inclusions (Tsuno and Dasgupta, 2015).

Subsequent experiments conducted by Zhang et al. (2015) investigated the solubility of carbon in crystalline monosulphide solid solution (<0.2 wt. %) and in sulphide melt (0.1-0.3 wt. %). The composition investigated ($Fe_{0.69}Ni_{0.23}Cu_{0.01}S_{1.00}$) was characterised by a relatively low metal/sulphur (M/S) ratio, and the possibility of growing diamond directly from a sulphide melt parental medium was dismissed because of the low solubility of carbon in the sulphide melt (Zhang et al., 2015). However, it was suggested that sulphide melts with higher M/S ratios and Ni contents would be stable over a more extensive stability field, encompassing that of diamonds; indeed, while natural monosulphide melts would be capable of hosting up to half of all available carbon in enriched lower upper mantle domains, the total carbon available in a depleted lower upper mantle setting could be hosted in sulphide melts (Zhang et al., 2015).

Most recently, Zhang et al. (2018) experimentally determined the solubility of carbon in Fe-Ni-S melts with various metal/metal and metal/sulphur ratios and demonstrated that up to 4-6 wt. % C could be hosted in metal-rich sulphide melts, with solubility decreasing with increasing sulphur content. Indeed, Ni-rich (>~18 wt. %) sulphide melts were shown to exhibit miscibility with C-rich melts, and it was determined that under the reduced conditions which prevail in the deeper (>250 km) mantle, carbon could primarily be hosted in metal-rich sulphide melts, with the remaining carbon being present as diamond, or solid C alloy (Zhang et al., 2018).

In natural magmatic systems, sulphur and CO_2 have been shown to share similar characteristics in terms of their degassing behaviour, relative to H_2O, F, Cl and Br (e.g. Kendrick et al., 2014). Andersen et al. (1987) studied mantle-derived clinopyroxene megacrysts from San Carlos (Arizona) and identified primary sulphide melt inclusions coexisting with CO_2-rich inclusions. The authors observed decrepitation features surrounding some of the sulphide inclusions (Fig. 2.4) and proposed that a volatile phase could have been expelled from an original sulphide melt trapped in clinopyroxene at mantle depths. The finding implied that sulphide melts can coexist

immiscibly with silicate melt and CO_2-rich fluids (up to 10 wt. % CO_2) at least in some parts of the upper mantle (~1-1.5 GPa and 1000-1200 °C; Andersen et al., 1987).

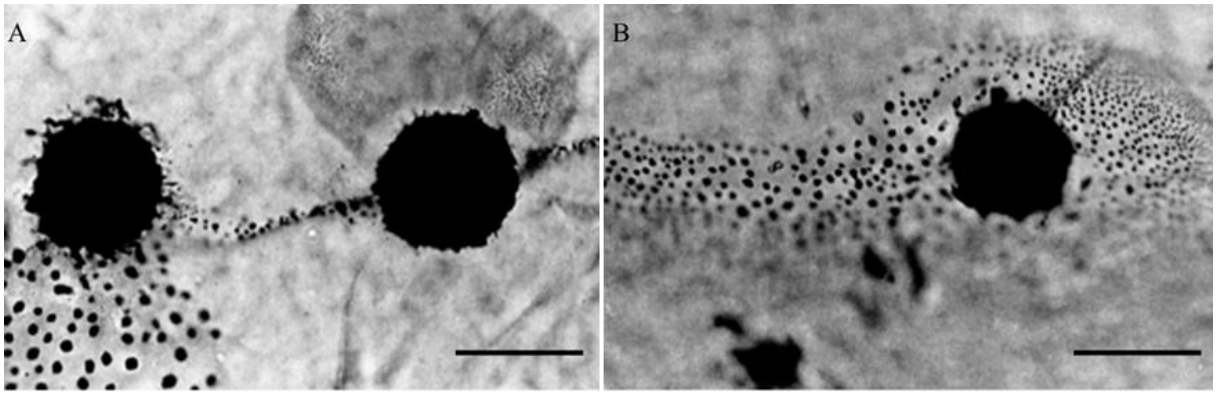

Figure 2.4. Photomicrographs of decrepitation halos (e.g. A) and CO2-filled vesicles (e.g. B) surrounding decrepitated sulphide inclusions in clinopyroxene megacrysts from San Carlos (Arizona) (from Andersen et al., 1987). Scales = 100 µm

2.1.2.2. Hydrogen

Difficulties with experimentally investigating the solubility of H-compounds in mantle-like sulphide melt have mainly been attributed to uncertainties regarding the relationship between pressure and sulphide melting temperatures, the use of metal capsules (e.g. Au) and the diffusion of H_2 from the sample (Wykes and Mavrogenes, 2005). Wykes and Mavrogenes (2005) investigated the effect of water on sulphide melting temperatures in a FeS-PbS-ZnS system at ~1.5 GPa and between 900 and 865°C. The authors showed that in the absence of a parental silicate melt component, anatectic sulphide melts (partial melts of pre-existing sulphides) could potentially hold some water (present as a hydrosaline fluid) although the content could not be determined (Wykes and Mavrogenes, 2005).

There have also been reports in literature attesting to the solubility of H_2O in natural sulphide melts (e.g. Fraser mine, Sudbury Igneous Complex, Canada). Li et al. (1992) suggested that quartz-sulphide veinlets and surrounding epidote and chlorite alteration zones were formed

through the exsolution of an aqueous Cl-rich fluid from a cooling sulphide melt (or residual Cu-rich liquid). Elevated halogen concentrations have also been measured in such alteration zones associated with sulphide deposits (e.g. Jago et al., 1994; McCormick et al., 2002; Mungall and Brenan, 2003). Mungall and Brenan (2003) showed experimentally that increased halogen contents were associated with the exsolution of a saline, most likely anhydrous fluid from a sulphide melt.

2.1.2.3. Oxygen fugacity

Oxygen fugacity imposes the strongest controls on the composition, properties and behaviour of sulphide melts in the mantle. The oxygen fugacity of a system controls sulphur speciation (present as sulphide S^{2-} or sulphate S^{6+}), as well as influencing the metal concentration of the sulphide melt (Ballhaus, 2001), which in turn controls the ability of chalcophile elements other than Fe to be substituted into the MSS/sulphide melt (Ballhaus and Ulmer, 1995). While natural MSS does not contain significant oxygen (e.g. Mungall, 2007), sulphide melts are however highly susceptible to oxidation.

Gaetani and Grove (1999) investigated the wetting properties of sulphide melts on typical mantle olivine grains as a function of their oxygen and sulphur fugacity. It was shown that near the IW oxygen buffer, oxygen could dissolve in sulphide melts in trace amounts (0.09 wt. %), whilst almost 9 wt. % oxygen could be concentrated in sulphide melts near at FMQ buffer conditions (Gaetani and Grove, 1999). It was shown that the presence of O in sulphide melts (Fe-Ni-Cu-S-O) – which have relatively low melting temperatures – plays a role in controlling the dihedral angle between olivine and sulphide, it was confirmed that sulphides are potentially mobile under typical upper mantle conditions (Gaetani and Grove, 1999). Sulphide melts are therefore likely to act as important metasomatic agents in the mantle, explaining the chalcophile element fractionation patterns observed in peridotites having undergone partial

melting (e.g. Peach et al., 1990; 1993; Hattori and Hart, 1991; Martin, 1991; Gaetani and Grove, 1999; Hart and Gaetani, 2006; Kiseeva et al., 2017)

It has been determined that while oxygen fugacity at the FMQ buffer is generally so high that in an Fe-S-O system O present in sufficient concentrations will place the composition of a melt on the magnetite side of the magnetite-MSS cotectic, the presence of Ni and Cu would lower O solubility in a sulphide liquid (Naldrett, 2004; Yoshiki-Gravelsins and Toguri, 1993; Kress, 2007; Mungall, 2007; Fonseca et al., 2008). The speciation of O in sulphide melts is not well known but is generally expected to be hosted as FeO (wüstite) (e.g. Shima and Naldrett, 1975). Magnetite (Fe_2O_3) however, is the most common Fe oxide mineral associated with sulphide minerals in natural magmatic environments (e.g. Naldrett, 1969), typically formed as a result of desulphurisation (e.g. Maier and Barnes, 1996; Li and Ripley, 2006).

2.1.3. Chapter aims

Sulphide minerals are commonly encountered as inclusions in natural diamonds, and therefore aspect of their study revolves around investigating their involvement in the reactions that can form diamond in nature. In this chapter, different diamond-forming reactions involving sulphides are discussed based on miscellaneous observations made by Raman spectroscopy, x-ray microtomography, fourier-transform infrared spectroscopy, scanning electron microscopy and electron microprobe analyses in sulphide inclusion-bearing diamonds from various localities worldwide.

2.2. Samples and methods

Observations have been made on three eclogitic diamonds from Mir (Yakutia, Russia), one peridotitic diamond (3648) from Udachnaya (Yakutia, Russia) and five sub-lithospheric diamonds from Juina-5 (Brazil) (Table 2.2). Synchrotron-radiation x-ray microtomography (X-CT) scans of selected Mir samples were acquired by Simon C. Kohn and Dan Howell at the Swiss Light Source, with voxel sizes of 0.163 µm. Additional X-CT analyses were performed at the University of Bristol (using a Nikon XTH 225ST X-ray tomography scanner) with voxel sizes ranging between ~3.3-3.8 µm. Raman spectroscopy, using a Thermo Scientific DXRxi Raman imaging microscope, was carried out on all the samples using a blue 455 nm laser at 6 mW and a green 532 nm laser at 10 mW, using various count numbers and maximum exposure times of 30 seconds. Fourier-transform infrared spectroscopy (FTIR) point measurements (Thermo Nicolet iN10MX) were made to analyse the forsterite-bearing (i.e. peridotitic) diamond from Udachnaya (using a 100 x 100 µm beam area). Scanning electron microscopy (SEM) maps (Hitachi S-3500N) and electron microprobe analyses (Cameca SX100) were performed on previously exposed inclusions in the Brazilian diamonds (table 2.2).

Table 2.2. Summary of methods employed on the studied inclusions

Diamond	Locality	State of inclusions	Raman	X-CT	F-TIR	SEM	EPMA	Total of inclusions
1584-int	Mir	Unexposed	Y	Y (s)	Attempted	Y		10+
1591		Unexposed	Y	Y (s)	Attempted	Y		10+
1607		Unexposed	Y	Y (s)	Attempted	Y		10+
3648	Udachnaya	Unexposed	Y	Y (ih)	Y	Y		10+
Ju5-03	Juina-5	Exposed and unexposed	Y			Y	Y	10+
Ju5-21		Exposed	Y			Y		1
Ju5-54		Exposed	Y	Y (ih)		Y		1
Ju5-77		Exposed	Y	Y (ih)		Y		1
Ju5-97		Exposed	Y	Y (ih)		Y	Y	1

Summary of the inclusions analysed in this chapter by technique (X-CT = x-ray microtomography; s = synchrotron-based; ih = in-house; FTIR = Fourier-transform infrared spectroscopy; SEM = scanning electron microscopy; EPMA = electron probe microanalysis).

2.3. Results

2.3.1. Mir diamonds

2.3.1.1. Raman spectroscopy

Sulphide inclusions are dominant features in Mir diamonds 1584-i, 1591 and 1607, and characteristically consist of pyrrhotite, molybdenite ± chalcopyrite ± pentlandite (see Chapter 3). Raman reveals that the central inclusions in diamonds 1584 and 1607 consist of rutile, and co-existing sulphide and anatase, respectively (Appendix A). Diamond 1584 contains a coesite-sulphide inclusion in its outer-intermediate zone (Appendix A), and three bimineralic inclusions of omphacite and sulphide are hosted in the intermediate growth zone of diamond 1607 (Appendix A).

2.3.1.2. X-ray microtomography (X-CT)

A low-density rim occurs at the edges of 33 out of 36 sulphide inclusions in Mir diamonds 1584-i, 1591 and 1607 which were scanned using X-CT (e.g. Fig. 2.5). The contacts between the low-density phase and higher density sulphide appear irregular in places (Fig. 2.5.A). The low-density phase forms an irregularly distributed film often at opposite ends of elongated inclusions (e.g. Fig. 2.5.B and 2.5.C). Minute (~0.8 µm) vesicle-like features can also be observed within the sulphide, close to its interface with diamond (Fig. 2.6.A). High-density sulphide is also frequently seen within thin rosette fractures radiating from the bodies of the inclusions, where the fractures are presumably thick enough to be observed by X-CT (i.e > 0.163 µm).

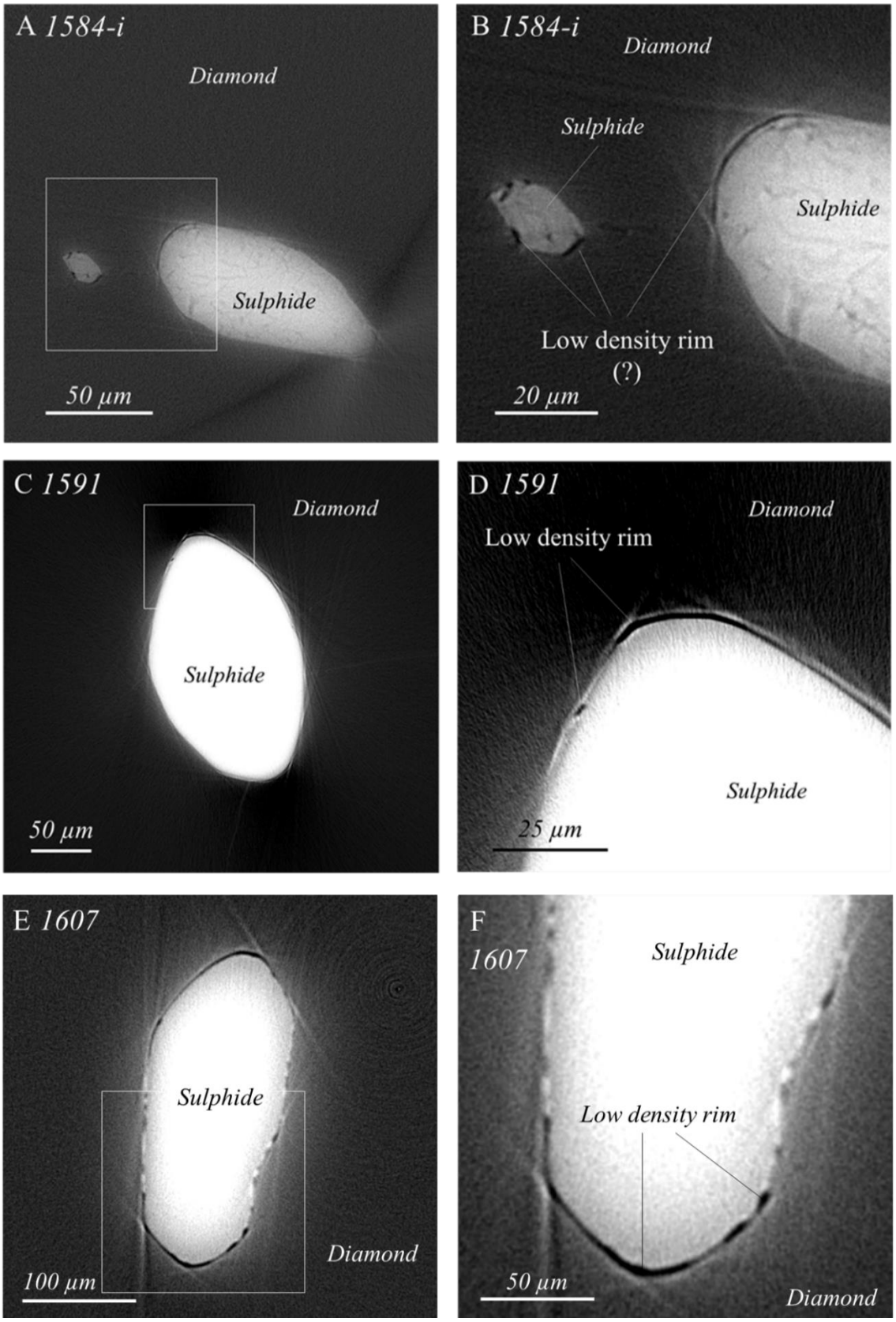

Figure 2.5. X-ray microtomography images of intact, high density (bright) sulphide inclusions in lower density (darker) Mir diamonds 1584 (A, B), 1591 (C, D) and 1607 (E, F); an irregular, 0.8-1.2 μm thick low-density (darkest) rim is observed at the far ends of the inclusions. Voxel size = 0.163 μm

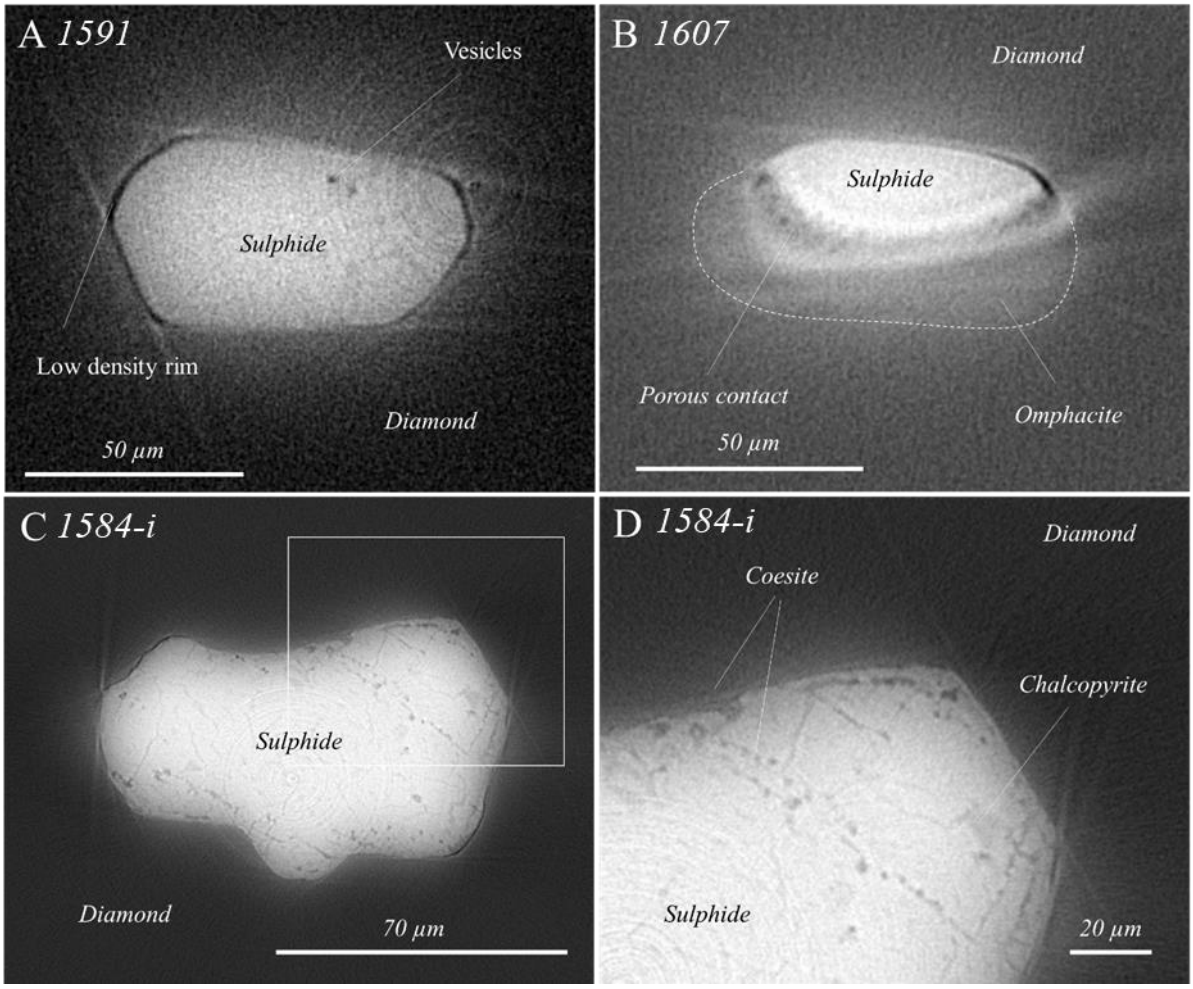

Figure 2.6. X-ray microtomography slice images of intact sulphide-bearing inclusions in Mir diamonds; A) two sub-micron (<0.8 µm) sized low-density vesicles occur within sulphide near the elongated end of an inclusion in diamond 1591. B) sulphide and omphacite occur adjacent to one another in a bimineralic inclusion in diamond 1607, where the two are separated by an apparently vesiculated contact. C) a single coesite-bearing sulphide inclusion occurs in diamond 1584-rim, the close-up of which in D) reveals that low-density coesite forms discrete pockets in the rim of sulphide inclusions as well as being present as straight and narrow veinlets cross-cutting chalcopyrite exsolution features. Voxel size = 0.163 µm

X-CT data of the omphacite-sulphide inclusion 1607-6 reveals that the two minerals occur adjacent to one another and are separated by a porous region (Fig. 2.6.B). Omphacite dominates only slightly by volume (~51.87 %), with sulphide (~48 %) and a low-density rim (~0.12 %) accounting for the remainder of the inclusion (table 2.3). The bimineralic coesite-sulphide inclusion in diamond 1584-rim was also analysed by X-CT (Fig. 2.6.C and 2.6.D). Coesite is seen as a low-density phase occurring as veinlets and discrete pockets within and near the edges

of the inclusion. Meandering chalcopyrite veinlets can also be observed in figure 2.6.D, whereas the coesite veinlets are relatively sharp and straight and crystallographically oriented with the inclusion and relative to diamond. With the X-CT technique, it was not possible to estimate the proportions of coesite and sulphide, due to the small size of the exsolution features and similar enough densities of diamond (3.51 g/cm3) and coesite (2.93 g/cm3) or chalcopyrite (4.19 g/cm3) which made reconstructing the volumes of the latter phases difficult with the Avizo software, but sulphide predominates by volume (~ > 90 %).Volume reconstructions of X-CT data of eight sulphide inclusions in the three Mir diamonds reveal varying proportions of the low-density rim around the higher density sulphide inclusions body (Table 2.3). The lowest average volume (0.12 %) was constructed from bimineralic sulphide-omphacite inclusion 1607-6, but there is no discernible relationship between the volume of the low-density phase and the size of the inclusion.

Table 2.3. Volume estimates of phases in sulphide inclusions observed by x-ray microtomography

Inclusion	Shape	Low-density rim	Error	Sulphide	Omphacite
1584-T1	Euhedral, elongated	0.234	0.003	99.766	
1584-T2	Euhedral, elongated	0.193	0.001	99.807	
1591-T1	Elongated	0.146	0.0007	99.854	
1591-T2	Elongated	1.152	0.012	98.848	
1591-T3	Elongated	0.776	0.003	99.224	
1591-T4	Elongated	0.823	0.008	99.177	
1607-6	Euhedral, elongated	0.121	0.003	48.008 ± 0.47	51.87 ± 0.47
1607-T2	Euhedral, elongated	0.165	0.004	99.835	

Proportional averaged (n = >3) volume estimates of sulphide inclusions (sulphide) and surrounding low density films (rim) in Mir diamonds (all values in %). Inclusion 1607-6 is a bimineralic sulphide-omphacite inclusion for which the proportions of each are also reported.

2.3.2. Udachnaya diamond 3648

2.3.2.1. Raman and FTIR

Optical and Raman microscopy show that the seed inclusion cluster of Udachnaya diamond 3648 consists of variety of different sized (~ <5-80 µm) and shaped inclusions (Fig. 2.7). Notably, Raman indicates that the central inclusion cluster consists mainly of larger sulphide and olivine inclusions. Closely associated with these are microinclusions of graphite, enstatite and a phase exhibiting two broad peaks centred around 600-650 and 750-800 cm^{-1} and a broad band around 3600 cm^{-1} (Fig. 2.8.A). Raman maps reveal that the three bands for the latter phase are often observed at the edges of opaque sulphide inclusions and in microinclusions (<5 µm) and inclusions trails (Fig. 2.8.B and 2.8.C) distributed across the width, breadth and length of the central seed inclusion area.

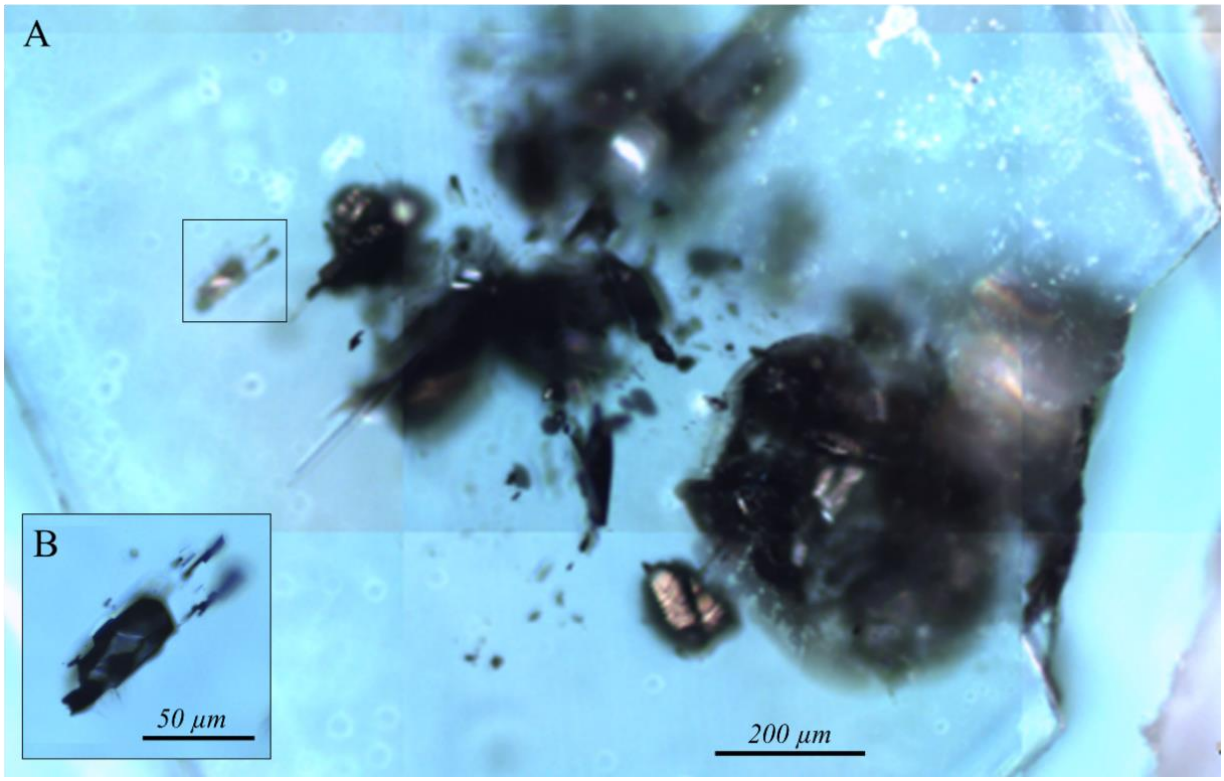

Figure 2.7. A) Raman optical microscope image of the central inclusion cluster of Udachnaya diamond 3648 (a euhedral olivine inclusion is seen inset in B).

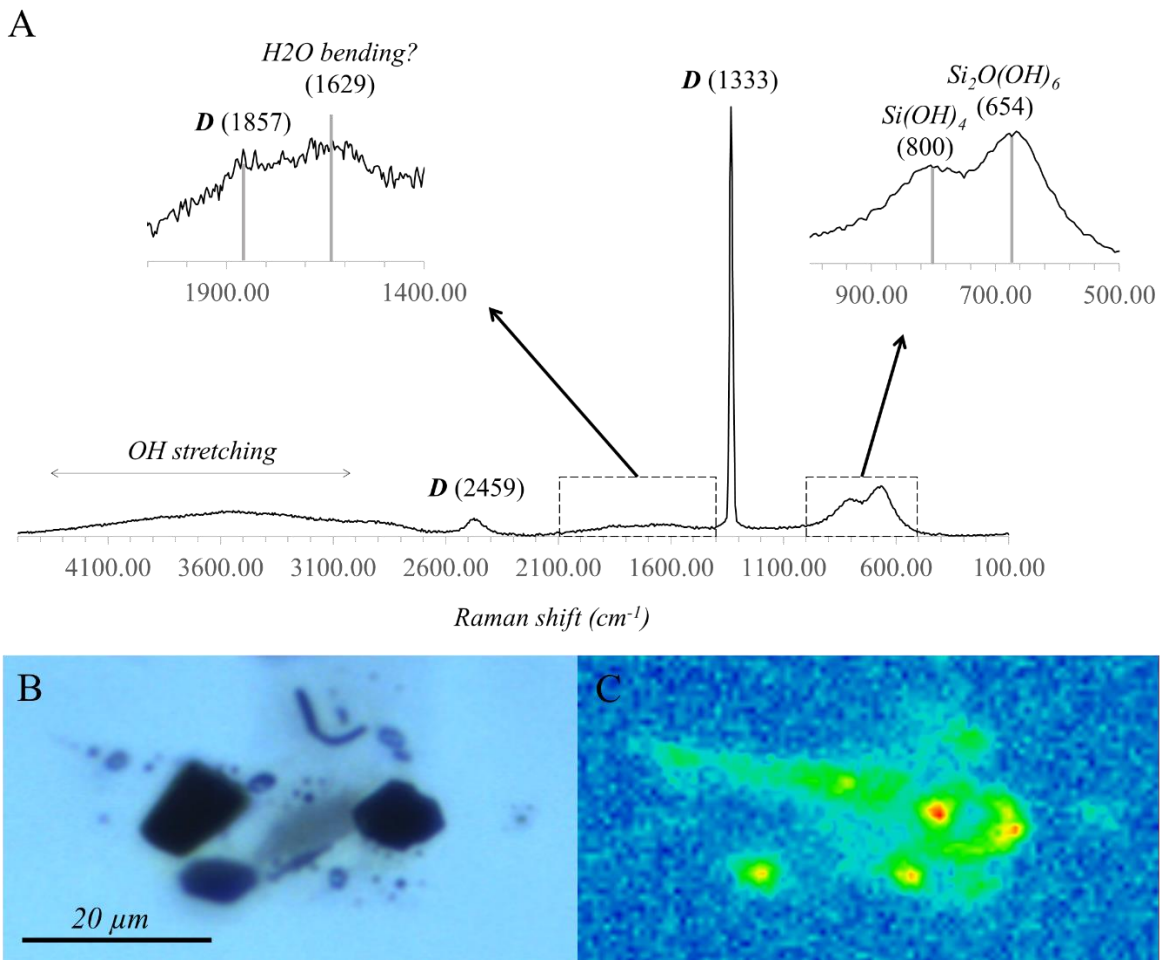

Figure 2.8. A) Raman spectrum of a hydrous silicic phase occurring amidst sulphide (s), graphite (g) e.g. B) and olivine inclusions in Udachnaya diamond 3648. C) A Raman map of the inclusion cluster shown in B reveals that the hydrous silicic phase forms microinclusions surrounding sulphide inclusions and also occurs at their rim.

Fourier-transform infrared spectroscopy (F-TIR) point measurements in the area surrounding visibly opaque sulphide inclusions and their fractures, reveal a phase corresponding to a carbonate with four main IR peak at 1427, 1088 and 877-840 cm^{-1} (Fig. 2.9). No features associated with water (in 4000-3000 cm^{-1} regions) were observed in the point measurements, which were acquiring a signal with a 100 x 100 µm spot size. A broad shoulder band is seen between 1600 and 1500 cm^{-1}, perhaps corresponding to a N-related species (e.g. N=O).

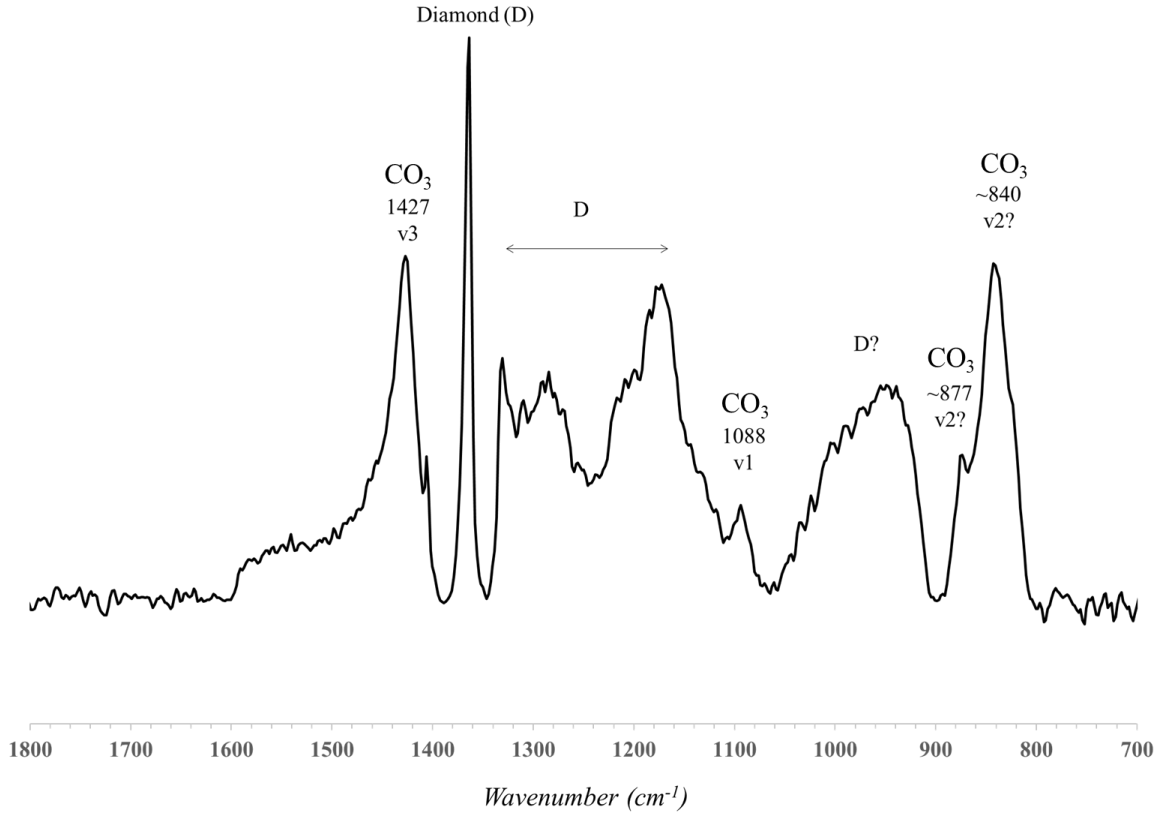

Figure 2.9. The F-TIR spectrum of a point measurement made in the central region of the inclusion cluster in the core of Udachnaya diamond 3648 is likely to be that of a carbonate phase. No features associated with water (around 3600 cm^{-1}) were observed by F-TIR, and therefore this region is not shown here. v1, v2 and v3 denote the characteristic symmetric (v1) and asymmetric (v3) stretching and symmetric bending (v2) peaks for CO_3 in carbonate minerals.

2.3.2.2. X-ray microtomography (x-CT)

The central inclusion cloud of Udachnaya diamond 3648 was scanned by x-ray microtomography (x-CT) and reveals that the central inclusion cluster consists of high-density sulphide accompanied by at least two phases with densities less than diamond (Fig. 2.10.A-2.10.D). One of the low-density phases is present as elongated and relatively flat inclusions, whilst the other is only observed <3 times in x-CT and forms as small rounded inclusions (Fig. 2.10.E and 2.10.F). Some of the micro-inclusions observed by Raman microscopy are likely too small (<5 µm) to be analysed by X-CT or FTIR.

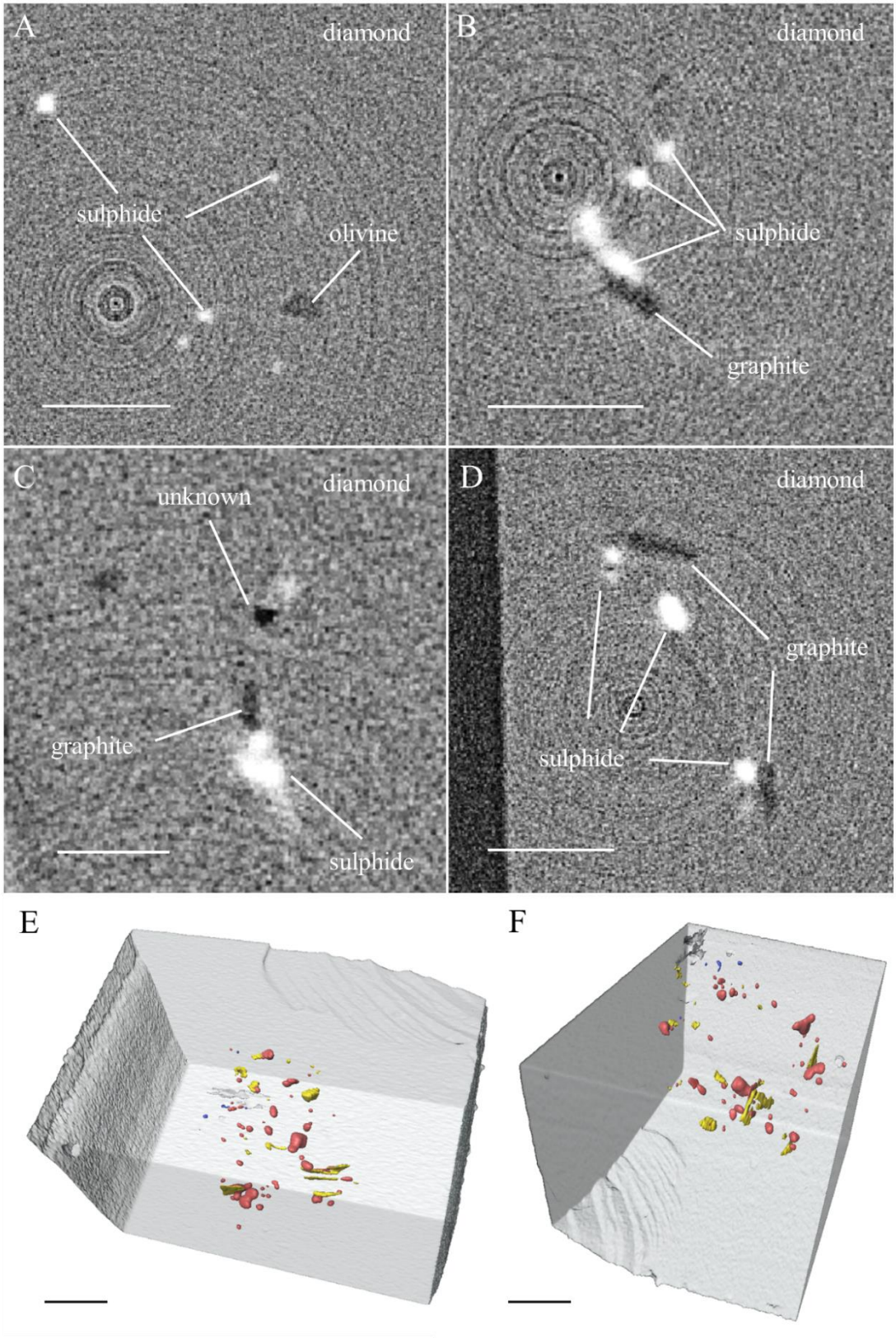

Figure 2.10. A-D) x-ray microtomography (X-CT) scans taken at different depths through the core region of Udachnaya diamond 3648 reveal the close spatial relationship between several phases of different density including sulphides, graphite, olivine and at least one unknown low-density phase. E and F) 3D X-CT reconstruction of the central core region of diamond 3648 showing the close association of sulphides (red), elongated graphite (yellow) and the low-density phase (blue). Scales in A-D= 100 µm, scales in E and F = 200 µm

2.3.3. Sublithospheric diamonds

2.3.3.1. Raman and scanning electron microscopy (SEM)

Juina diamond Ju5-03 contains more than 10 sulphide inclusions which are possibly distributed across different growth zones of the diamonds. The inclusions are relatively small and angular in shape (e.g. Fig. 2.11.B and 2.11.C) and according to Raman, consist of pyrite (Fig. 2.11.A and 2.12.C).

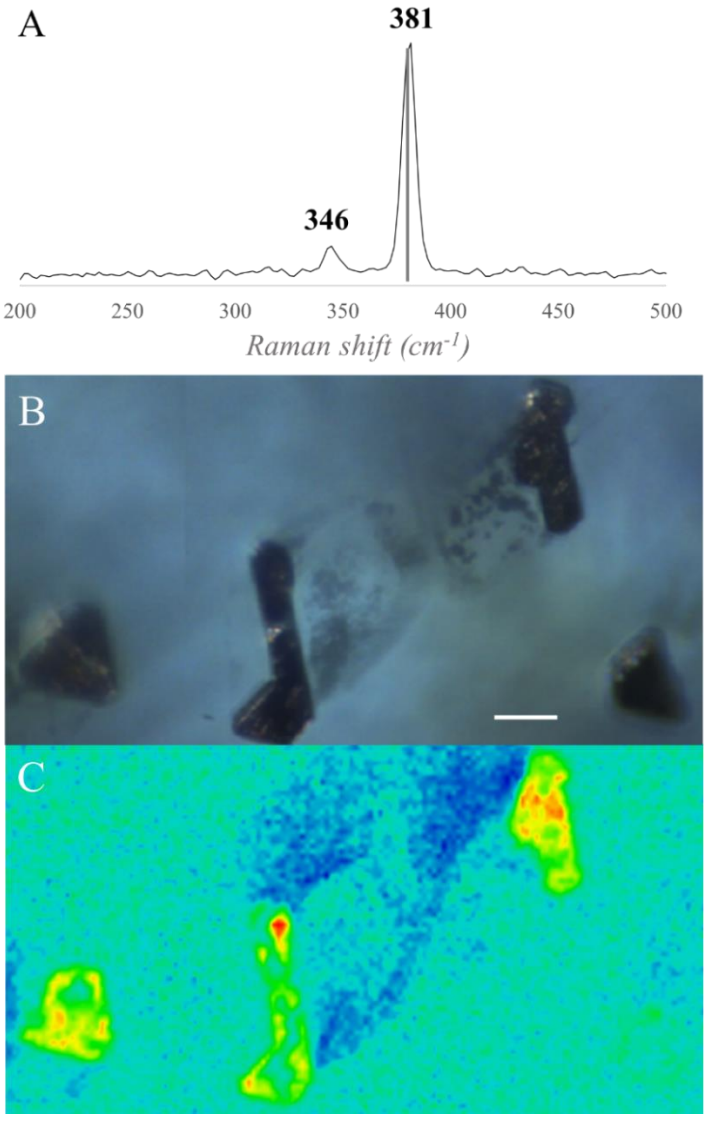

Figure 2.11. A) Raman optical microscope image of a group of angular opaque inclusions in sub-lithospheric Juina-5 diamond Ju5-03. B) Raman peak height maps reveal that the inclusions consist of pyrite (FeS_2), where red and yellow colours indicate where at the given focus level, the signal for pyrite is most intense. Scale = 10 µm

No clear fractures were observed between the inclusions and the exterior surface of the diamond. In the same diamond occur an inclusion consisting of walstromite and titanate as well as a single inclusion of calcite (Fig. 2.12).

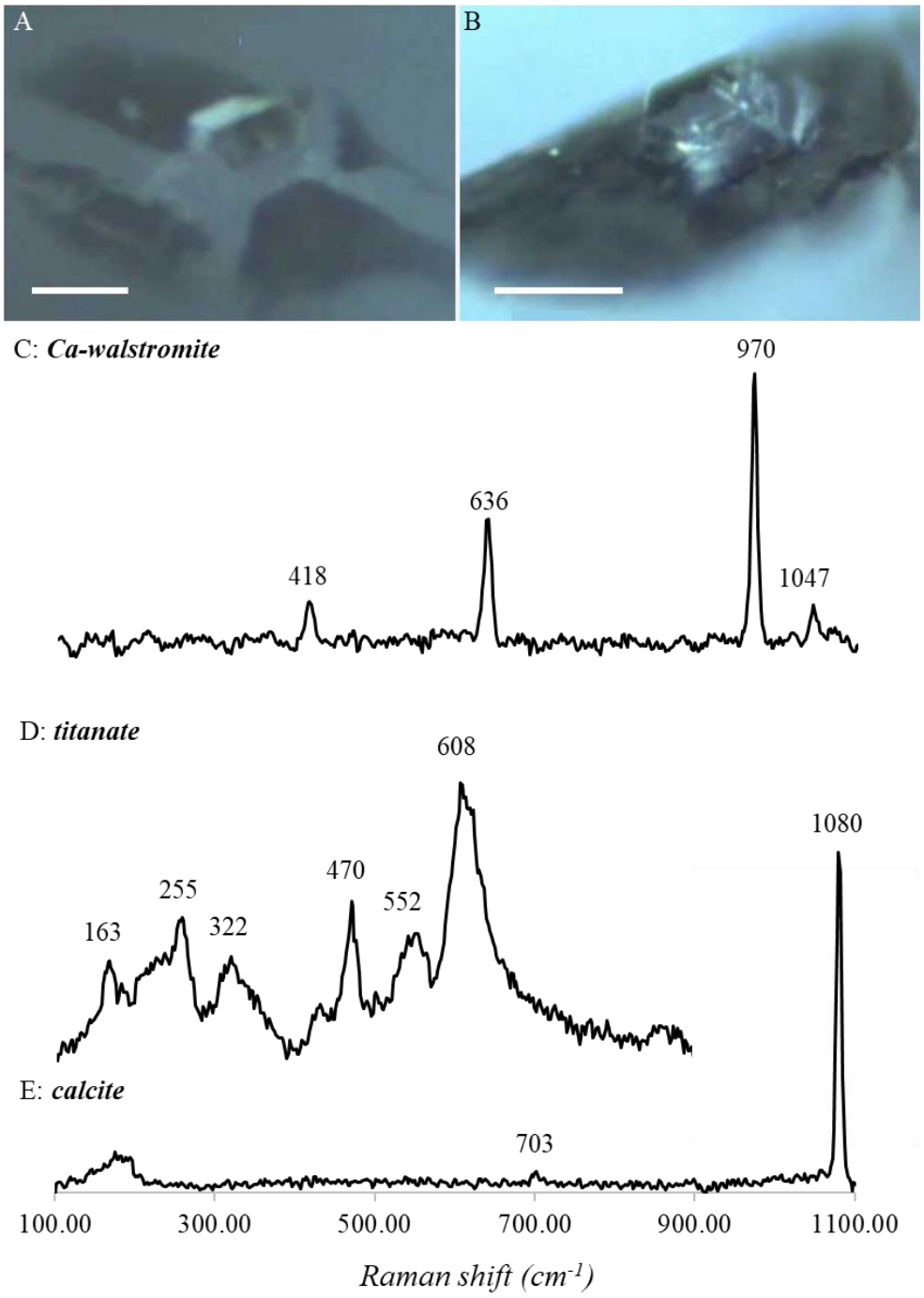

Figure 2.12. A and B) Raman optical images of a former Ca-perovskite inclusion (A) and an inclusion of calcite (B) in Juina-5 diamond Ju5-03. C-E) Raman spectra obtained with a blue laser of co-existing Ca-walstromite and titanate in the inclusion shown in A) and calcite (shown in B). Scales = 20 µm

Electron dispersive spectroscopy (EDS) point measurements using scanning electron microscopy (SEM) confirm that some of the previously exposed inclusions in Juina-5 diamonds consist of pyrite (e.g. Ju5-54 and Ju5-97; Fig. 2.13.A and 2.13.C). In Ju5-03, the single exposed sulphide inclusion consists of an assemblage of pyrrhotite, pentlandite and chalcopyrite (or former MSS; Fig. 2.13.D-F). Out of the five Juina-5 diamonds with pre-exposed sulphide inclusions, two pyrite inclusions were identified, while the remaining inclusions consist of pyrrhotite ± pentlandite ± chalcopyrite (e.g. Ju5-77). Both pyrite and former MSS inclusions can exhibit different shapes from angular to rounded.

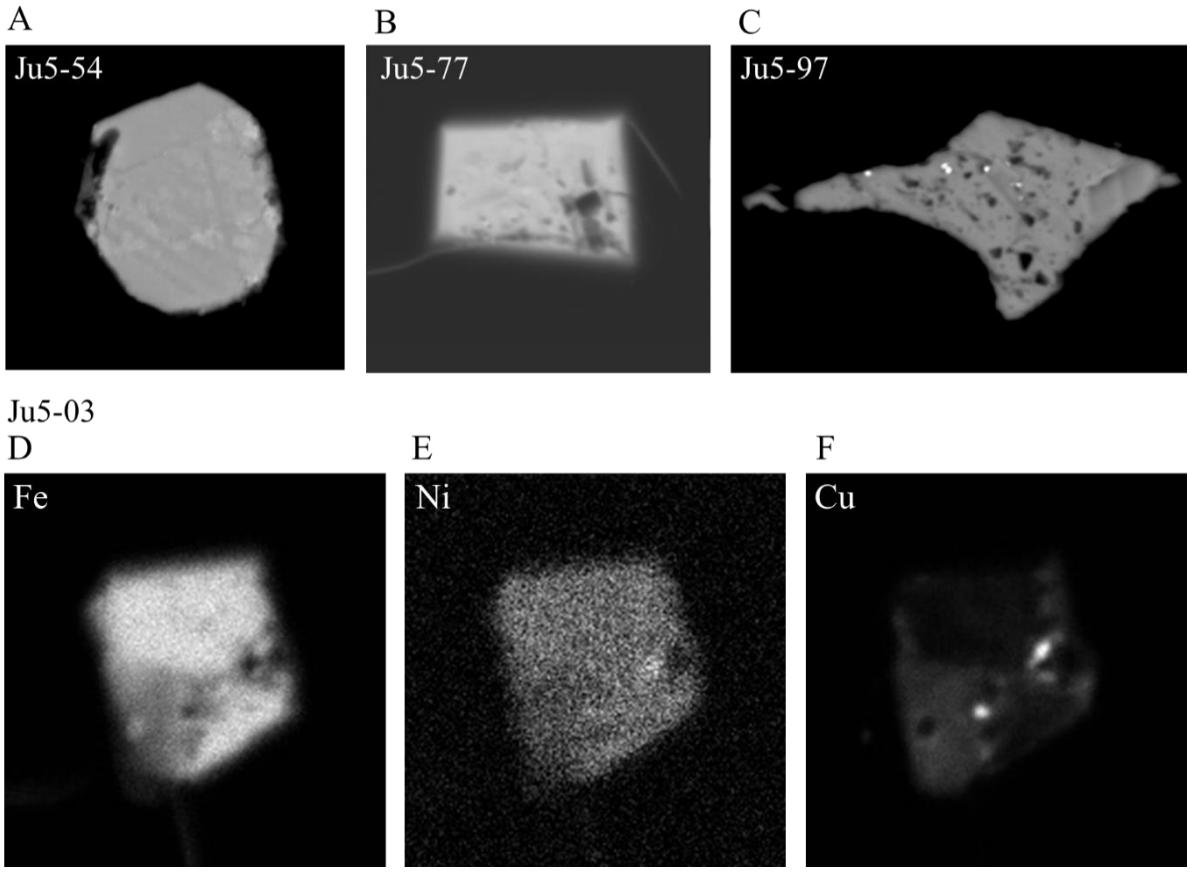

Figure 2.13. A-C) Scanning electon microscope (SEM) backscattered electron (BSE) images of exposed sulphide inclusions in sublithospheric diamonds from Juina-5, consisting of pyrite (rounded inclusion in A and angular inclusion in B) or pyrrhotite ± pentlandite ± chalcopyrite. D-F) electron microprobe (EPMA) x-ray maps showing the distribution of Fe, Ni and Cu in an exposed former MSS sulphide inclusion in Juina diamond Ju5-03.

2.4. Discussion

2.4.1 Mir diamonds

2.4.1.1. Low-density rim

An interfacial, low-density phase has been observed with X-CT around at least 33 out of 36 intact sulphide inclusions in 3 eclogitic diamonds from Mir (Fig. 2.5). The observed features are not interpreted as consisting of a void for several reasons. The thermal decompression properties of sulphides differ significantly from those of their host diamond; sulphides have higher expansion coefficients and isothermal compressibilities than diamond (e.g. 7.4-8.5 10^{-5} K^{-1} for Fe sulphides, up to 13.5 10^{-5} K^{-1} for pentlandite vs. 0.003 10^{-5} K^{-1} and 0.185 10^{-6} bar^{-1} for diamond), meaning that sulphides respond more strongly to changes in temperature and pressure (e.g. Tenailleau, 2005; Sugake and Kitakazi, 1997; Atkins and De Paula, 2010). This is thought to explain the presence of sulphide in thermal decompression fractures (e.g. Fig. 2.5.E.). Low density vesicles are also observed in one of the Mir sulphide inclusions, and potentially provide stronger evidence for the potential expulsion or degassing of a low-density phase from an original sulphide melt/liquid. Finally, the presence of anomalous birefringence halos surrounding the studied Mir sulphide inclusions (Appendix A.4) indicates that the inclusions are likely to be under high pressure; indeed, such features are commonly formed as a result of residual strain (e.g. Barron et al., 2008; Howell et al., 2010; Howell, 2012).

The low-density features resemble closely the films which were observed by Nimis et al. (2016) surrounding silicate and oxide inclusions in diamonds (e.g. Fig. 2.4), although the composition of the phase has not been determined. The exposure times used by Nimis et al. (2016) during their Raman analyses were much longer (120 to 240 s) than the ones attainable here (<30 s), likely allowing the acquisition of a signal from a weakly Raman-active phase whilst fluorescence from the diamond could also sometimes obscure a faint Raman signal.

Fluorescence was not found to be an issue, and therefore the lower acquisition times could explain why no clear diagnostic peaks were resolved at the edges of the studied Mir samples.

However, an interesting thing to note is the comparatively large size of the sulphide inclusions in Mir diamonds, and the fact that the same Raman settings (including acquisition time) were used to detect a hydrous silicic phase in Udachnaya diamond 3648. Indeed, no features associated with liquid water were found at the edges of the Mir sulphide inclusions, perhaps implying that the rim phase in these inclusions is anhydrous. Additionally, no clear signals attributed to CH species were found, making a CO_2-bearing phase one potential candidate since it will likely not be observed by Raman because of the dominating signal of diamond.

It is feasible that the low-density rim is in fact a trapped sample of the fluid which formed the Mir diamonds, such as the finding reported by Nimis et al. (2016). Alternatively, as the irregular nature of the contact between the low-density phase and sulphide (e.g. Fig. 2.5F), and the presence of low-density sub-micron-sized vesicles near the outer portions of some of the inclusions (e.g. Fig. 2.6.A) perhaps suggest that (at least some of) the low-density phase may have originally been hosted in a sulphide melt or MSS. Further work is needed to determine whether the observed phase samples water-rich fluids, which have been linked to the formation of large, gem-quality diamonds (e.g. Nimis et al., 2016), or if the fluid is anhydrous, as suggested by Mungall and Brenan (2003) for example.

2.4.1.2. Silicates associated with sulphides

Three inclusions in the intermediate growth zone of Mir diamond 1607 consist of omphacite and sulphide. It has been suggested that the Mir diamonds crystallised on a sulphide ± iron matrix, on an omphacite and sulphide-rich substrate (e.g. Bulanova et al., 1998). From the textural relationship between sulphide and omphacite shown by X-CT in figure 2.6.B, it can be

inferred that the two phases were captured contemporaneously in diamond, and may represent a snapshot of a metasomatic event which facilitated the formation of diamonds at Mir (e.g. Bulanova et al., 1995; Anand et al., 2004; Wiggers de Vries et al., 2013a). The inclusions are all located within the same growth zone of the diamond (e.g. Appendix A), and therefore possibly reflect on the episodic nature of the diamond-forming fluid-rock interactions (e.g. Wiggers de Vries et al., 2013a; 2013b; Bulanova et al., 2014) and/or the availability of sulphide.

Sulphide and coesite (SiO_2) are seen to be intergrown (Fig. 2.6.D and E) in one inclusion in Mir diamond 1584-rim, where higher density sulphide predominates by volume (Table 2.3). The internal features of the inclusion suggest SiO_2 exsolution from an original sulphide melt, and the crystallographic orientation of the SiO_2 veinlets may indicate their unmixing at a different time than chalcopyrite was formed. The proximity of the SiO_2 veinlets to the edges of the inclusions and their straight nature perhaps suggest a late exsolution event (possibly exsolved from the residual Cu-rich liquid; Chapter 3, Section 3.1.).

Despite the considerable interest in the solubility of sulphur in silicate melts, the solubility of SiO_2 in sulphide melts has received little attention. In early experiments by Maclean and Shimazaki (1976) and Shimazaki and MacLean (1976), several wt. % SiO_2 was measured in sulphide in a FeS-FeO-SiO_2 system, but the bulk composition, fO_2 and fS_2 conditions were not representative of natural systems, and the addition of other components to the silicate melt would be expected to drop SiO_2 solubility in sulphide significantly (D. Smythe, personal communication).

It has however been suggested that the solubility of SiO_2 could be more extensive in sulphide melts than is currently thought (e.g. Wykes and Mavrogenes, 2005). It was recently shown by Guntoro et al. (2018) that the presence of SiO_2 in a FeS-FeO-SiO_2 system could create a

miscibility gap between sulphide and oxide melts at 1200 °C and atm. pressures, with moderate FeS concentrations (~40-68 wt. % FeS). Kalinowski (2002) identified Mn-silicates in experiments investigating the melting of Mn-bearing sulphides. Furthermore, an Fe-Si-Cl phase was quenched from a Cl-bearing sulphide melt by Mungall and Brenan (2003). Wykes and Mavrogenes (2005) hypothesised that the addition to a sulphide melt of non-chalcophile elements such as Mn or Cl could increase SiO_2 solubility in sulphide, in a similar way that Cl can enhance the solubility of sulphur in silicate melts (e.g. Botcharnikov et al., 2004). Alternatively, other factors, such as changes in oxygen fugacity could play a role in allowing Si-bearing compounds to form within a sulphide melt, particularly in a sulphide-dominated and Si-poor system.

2.4.2. Udachnaya diamond 3648

The single Udachnaya diamond plate examined in this study (diamond plate 3648) has been previously studied in literature by Rudnick et al. (1993), Taylor et al. (1995), Bulanova et al. (1995; 1996; 2003), Pearson et al. (1998; 1999), Hauri et al. (1998) and Palot et al. (2013). The sample hosts sulphide inclusions from core to rim, as well as preserving the central seed inclusion cluster of the diamond (Fig. 2.7), providing a wealth of information about the conditions which promoted diamond growth. Although it is likely that diamond 3648 grew during multiple temporally distinct diamond-forming episodes (Rudnick et al., 1993, Bulanova et al., 1996; Pearson et al., 1999; Palot et al., 2013), only possible reactions which began forming the diamond will be explored here.

Bulanova et al. (1998) showed that peridotitic diamonds at Udachnaya grew in a forsterite- and Ni-rich sulphide-dominated environment, in a graphite, iron and wüstite-bearing medium. Indeed, it was shown then that the diamonds were formed under reducing conditions (near the IW buffer) in the presence of a fluid which was accompanied by immiscible sulphides and a

carbonate-rich fluid (Bulanova et al., 1998). Later studies of fluid microinclusions in fibrous and cuboid Udachnaya diamonds revealed the involvement in diamond formation of Mg- and/or Ca-rich carbonate-bearing fluids formed as a result of mantle metasomatism through carbonatitic and hydrous melts, or partial melting of carbon-rich eclogite and/or peridotite (Zedgenizov et al., 2007). Indeed, studies of diamondiferous eclogite xenoliths from Udachnaya have revealed that some diamonds crystallised through the interaction of high-density fluids with compositions intermediate between carbonatitic and hydrous-silicic endmembers with an eclogitic substrate, also involving reactions between mantle peridotite and K and LREE-rich melts (e.g. Shatsky et al., 2008). It was also shown that Mg-rich olivine-bearing diamonds at Udachnaya were formed through a single metasomatic process that involved crustally-derived fluids/melts (Logvinova et al., 2015).

In addition to sulphide, graphite, olivine ± enstatite inclusions, Raman indicates the presence of a non-crystalline phase with two broad bands around 600-650 and 750-800 cm^{-1} in Udachnaya diamond 3648 (Fig. 2.8). The peak shapes and positions are similar to those reported by Nimis et al. (2016), in which case they correspond to $Si_2O(OH)_6$ and $Si(OH)_4$ within an aqueous fluid (indicated by the broad O-H stretching band around 3600 cm^{-1}). The close observed association in the central inclusion cluster of the above-mentioned phases (e.g. Fig. 2.10) and carbonate revealed by FTIR (Fig. 2.9) can inform about the materials that were involved in the diamond-forming reaction. An inclusion of wüstite was also previously identified by Bulanova et al., (1995) in the core region of diamond 3648.

It was not possible to confidently determine which of the inclusion-hosted phases with densities significantly lower than diamond observed by X-CT correspond to graphite (2.266 g/cm^3), carbonate (~2.7-3 g/cm^3), and/or the silicic hydrous fluid (density unknown). However, the low-density phase is most likely to consist of graphite, according to the elongated shape of the

inclusions (Fig. 2.10). The apparent small size of the silicic fluid-bearing micro inclusions (smaller than the X-CT voxel size > 3.3 µm) likely makes them unobservable with conventional microscopy, although some inclusions may be large enough (<20 µm) and therefore visible as dark, rounded features (Fig. 2.10.C, E and F). No carbonate was detected by Raman spectroscopy, nor were any carbonate-resembling inclusions observed by Raman microscopy. However, the pervasive presence of graphite throughout the inclusion cluster may restrict the visibility of certain inclusions, such as inclusions of carbonate which were analysed by FTIR but not by Raman and may also be coated in graphite. Nonetheless, based on the close association of the phases observed by Raman and FTIR, and their textural relationships determined by X-CT one possible way of forming at least some of the Udachnaya diamonds could involve the reaction between carbonate, sulphide and enstatite to form sulphate, wüstite, olivine and diamond:

$$4MgCO_3 + 2FeS + FeSiO_3 = 2MgSO_4 + 3FeO + Mg_2SiO_4 + C$$

The olivine inclusions analysed in Udachnaya diamond 3648 are Mg-rich (e.g. Rudnick et al., 1993; Hauri et al., 1998; Pearson et al., 1999). Magnesite (or alternatively, calcite) may have interacted with sulphide melts in an upper mantle, enstatite-bearing substrate to form diamond, wüstite, olivine and Mg-sulphate. Sulphate is not observed as an inclusion in this diamond, possibly owing to the high solubility of sulphate in oxidising fluids (Schrauder and Navon, 1994; Schrauder et al., 1994; Debret and Sverjensky, 2017), and its subsequent reduction to sulphide following migration elsewhere into a reduced mantle. Enstatite is only rarely observed as micro inclusions within the cluster, perhaps suggesting its presence as a minor unreacted product.

Relatively little variation in carbon isotope compositions has been observed across the growth zones of diamond 3648, with the compositions plotting close to mantle range ($\delta^{13}C$ = -8.9 ‰

to -4.6 ‰) (Hauri et al., 1998). Contributions of carbon to the diamond-forming medium from both subducted and mantle sources are plausible, and because of the reducing conditions that diamond 3648 grew in (near IW buffer), it is also conceivable that some carbon was dissolved in the original sulphide melt (e.g. Zhang et al., 2015; 2018). Most significantly however, the central core portion of the diamond provides evidence for the close genetic relationship between the diamond and co-existing immiscible sulphide, silicate and carbonate melts/fluids.

2.4.3. Sublithospheric diamonds

2.4.3.1. Polyphase inclusions

Silicate mineral inclusions in sub-lithospheric diamonds generally consist of two or more coexisting phases since the components of most of these have unmixed from a homogeneous phase that is only stable at lower mantle pressures and temperatures. Generally, sub-lithospheric diamond-hosted inclusions have been classified as belonging to one of three suites, each evidencing their formation in the Earth's Transition Zone or possibly in the lower mantle, and in the presence of a recycled component (e.g. Thomson et al., 2014); Basic (majoritic garnet) and ultrabasic (Mg-perovskite + ferropericlase) inclusion populations have been identified, alongside a Ca-rich suite of inclusions, which are characterised by carbonates, Ca-Si-Ti-bearing minerals and/or some aluminous material (Harte and Richardson, 2012 and references therein). Indeed, this group is most commonly distinguished by the occurrence of $CaSiO_3$ (walstromite) inclusions co-existing with $CaTiO_3$ (normal perovskite) and $CaTiSiO_5$ (titanite) phases, where carbonates are sometimes also present (Harte and Richardson, 2012). The walstromite is likely the inversion product of a higher pressure CaSi-perovskite. In the studied sulphide inclusion-bearing Juina-5 diamonds, only carbonate and walstromite inclusions have been identified by Raman (e.g. Fig. 2.12). However, ferropericlase inclusions

have also been associated with sulphides in diamonds from Diavik with a possible sublithospheric origin (e.g. Donnelly et al., 2007).

Whilst the diamonds hosting basic or ultrabasic inclusions are thought to have formed from water-rich fluids and/or melts released from a dehydrating slab, the formation of the Ca-rich suite-bearing diamonds is likely linked to the formation of carbonatite melts, formed by the melting of deeply subducted carbonated materials (Walter et al., 2008; Bulanova et al., 2010; Harte and Richardson, 2012)

2.4.3.2. Sulphide inclusions

The sulphide inclusions in sublithospheric diamonds from Juina-5 exhibit a variety of compositions. Primary sulphide inclusions studied in lithospheric diamonds from localities worldwide have generally been reported as consisting of pyrrhotite ± pentlandite ± chalcopyrite ± bornite ± cubanite ± heazlewoodite (Deines and Harris, 1995; Taylor and Liu, 2009; Harvey et al., 2016). Several earlier reports have also been made about pyrite sometimes being present as a single phase or as a primary exsolution product in sulphide inclusions in diamonds from Southern Africa (e.g. Eldridge et al., 1991; Deines and Harris, 1995), Arkansas (Pantaleo et al., 1979), as well as co-existing with ferropericlase in a diamond from Diavik with a possible sublithospheric origin (Donnelly et al., 2007). While the occurrences of pyrite in literature are relatively rare, Thomson (2014) reported on 7 inclusions of pyrite – which were exposed for scanning electron microscopy – in 7 sub-lithospheric diamonds from Juina-5.

The frequent occurrence of pyrite (FeS_2) as single-phase inclusions in sublithospheric diamonds from Juina-5 is unusual considering the typical low temperature and pressure affinity of pyrite. However, the euhedral shape of the pyrite inclusions in Juina diamond Ju5-03 (Fig. 2.12) and the overall lack of fractures connecting the studied pyrite inclusions to the exterior

of their host diamonds suggest that these inclusions are likely syngenetic. It is therefore possible that the pyrite phase was through a reaction which accompanied diamond formation. One explanation for the occurrence of pyrite in sub-lithospheric diamonds could be that appreciable amounts of sulphur were added alongside oxidised carbonatite (C-O-H-S) melts or fluids into an otherwise reduced, metal or carbide-bearing mantle (e.g. Burnham et al. 2016). In fact, it has been demonstrated that sulphur (dissolved as S^{6+} in sulphate SO_4) is relatively soluble in oxidised melts, such as the ones emanating from the cold carbonated slab which provided material to the formation environment of the Juina diamonds. It is possible that FeS_2 was formed alongside diamond and simultaneously trapped within it, for example through the reactions:

$$6MgSO_4 + 7Fe_3C = 3FeS_2 + C + 6MgO + 18FeO$$

Or

$$2MgSO_4 + 7Fe = FeS_2 + 2MgO + 6FeO$$

A young (~101 my) U-Pb age has been assigned to a CaSiTi-perovskite inclusion in a sublithospheric diamond from Collier-4 (Juina area, Brazil) (Bulanova et al., 2010), and indeed, a Mesozoic subduction-related diamond-forming event has been suggested for the Juina diamonds (e.g. Harte and Richardson, 2012). The global sulphur cycle and availability of sulphur in oceans has varied over time (Chapter 1, Fig. 1.2) (Canfield, 2004; Holland, 2006); the second Great Oxidation event (GOE-II ca. 600 Ma) in particular, saw an appreciable rise in sulphur (occurring primarily sulphate) levels in the Earth's oceans. If the origin of the sulphur in pyrite is subducted sulphur (according to scenario above), the addition of excess sulphur into the deeper reduced mantle would have a significant effect on its redox state (Klimm et al., 2012a; 2012b, Bénard et al., 2018) by oxidising Fe^{2+} (e.g. in stoichiometric Fe

sulphide) to Fe^{3+} (e.g. in Fe_2O_3) (see above equation). Alternative explanations for the presence of primary pyrite inclusions in sublithospheric diamonds include that a) pyrite is in fact stable in some parts of the deeper mantle and has been captured as a primary mantle phase, b) pyrite has remained inert with the surrounding mantle during its subduction in the diamond-forming region or c) the pyrite inclusions have been captured in diamonds at shallower depths, under equally oxidising conditions.

2.5. Conclusions

Sulphide inclusions in diamonds possess many interesting features, which can be studied using a variety of analytical techniques. Sulphides included in diamonds typically vary among populations in their compositions and appearance; detailed studies of the inclusions are needed in order to gain an understanding of whether the inclusions represent diamond-forming reaction products, agents or simply surrounding mantle sulphides that are trapped in diamond at random. The nature of sulphide inclusions in diamonds and their mode of entrapment in turn dictates their viability in radiometric dating and provides further clues to the conditions which were prevailing during the growth of a diamond population.

Chapter 3. Identification of molybdenite in diamond-hosted sulphide inclusions: Implications for Re–Os radiometric dating

Lotta I. Kemppinen, Simon C. Kohn, Ian J. Parkinson, Galina P. Bulanova, Dan Howell and Chris B. Smith (2018) Earth and Planetary Science Letters 495, 101-111*

* In this paper, I.J. Parkinson and S.C. Kohn made very significant contributions to the science and writing of the manuscript. I.J.P. modelled and wrote figure 3.8 and section 3.4.2.1. S.C.K. contributed to scientific ideas and writing. G.P. Bulanova and C.B. Smith provided helpful discussions during the writing of the manuscript. D. Howell and S.C. Kohn acquired the X-CT scans of diamond-hosted sulphide inclusions.

Only the figure numbering, x-ray computed tomography abbreviation and appendix terminology have been altered to conform with the rest of the thesis.

ABSTRACT

Sulphide inclusions are common features of natural diamonds. They can provide an insight into the nature of diamond-forming reactions and are especially important for Re–Os dating of diamond formation. A discrete molybdenite (MoS_2) phase has been identified for the first time by Raman spectroscopy in 73 out of 80 syngenetic sulphide inclusions in 7 eclogitic diamonds from the Mir kimberlite (Yakutia, Russia). The sulphide inclusions were chemically and texturally characterised by electron probe microanalyses (EPMA), focused ion-beam scanning electron microscopy (FIB-SEM) and synchrotron-based X-ray tomographic microscopy (X-CT). Our observations suggest the molybdenite has unmixed from an original sulphide melt or

monosulphide solid solution. It occurs as sub-micron sized grains, commonly in association with the chalcopyrite rims of the inclusions and sometimes, within surrounding decompression cracks. Molybdenite has also been identified by Raman spectroscopy in at least 50% of sulphide inclusions in preliminary studies of eclogitic diamonds from Argyle (NW Australia), Orapa, Letlhakane, Damtshaa (Botswana) and Dachine (French Guiana), and peridotitic diamond-hosted inclusions from Udachnaya (Yakutia, Russia) and Murowa (Zimbabwe). We have modelled the effects that different amounts of Re loss – through its segregation into an unrecovered molybdenite phase – could have on the radiometric ages of diamonds dated using the Re–Os system. In general, Re loss through this process will lead to isochron ages older than the true age, and variable degrees of Re loss will lead to increased scatter around the apparent isochron. For model age calculations, the effects would depend on the $^{187}Re/^{188}Os$ ratio of the inclusions (if their compositions evolved above or below that of the chondritic mantle evolution curve) but Re loss could generate unrealistically old or future ages, particularly in eclogitic inclusions.

3.1. Introduction

Diamond-hosted sulphide inclusions can offer an insight into the processes responsible for diamond formation. Their compositions record mantle melting processes, subduction input and the cycling of volatiles through Earth's interior (e.g. Stachel and Harris, 2008, Walter et al., 2011). Diamond is an ideal container material and can shield mineral inclusions from subsequent alteration and recrystallization events. Therefore, syngenetic inclusions, which grew at the same time as the host diamond, can yield valuable information on the geochemical state of their mantle source region.

Diamonds commonly form by different redox reactions (e.g. Haggerty, 1986, Stachel and Harris, 2009) or isobaric cooling of hydrous fluids containing both CH4 and CO2 (Stachel and Luth, 2015). Several workers have proposed that sulphides act as reducing agents interacting with oxidised components to promote diamond growth (Bulanova et al., 1998, Palyanov et al., 2007) and, depending on their metal-sulphur ratios, sulphide melts can store significant amounts of carbon at depth (Zhang et al., 2015). Although sulphides are often the most common phase in inclusion-bearing diamonds (e.g. Taylor and Liu, 2009), their overabundance relative to the expected abundance of mantle sulphide remains enigmatic. Diamond-hosted sulphide inclusions are also particularly important because they can be used to date diamond-forming events using the Re–Os chronometer (Pearson et al., 1998, Harvey et al., 2016).

Sulphides typically exist as Fe–Ni–Cu sulphide melts in the deeper parts of continental lithospheric mantle, where most diamonds form (Zhang and Hirschmann, 2016). Upon sub-solidus cooling inside diamond, a Fe-rich monosulphide solid solution (MSS) can crystallise from such melts at around ~1200 °C, leaving a residual Cu- and/or Ni-enriched sulphide liquid. At ~1000 °C the MSS field can accommodate more Cu and Ni-rich compositions, and an intermediate solid solution (ISS) can progressively form below ~950 °C (Barton, 1973, Ebel

and Naldrett, 1997, Harvey et al., 2016). Depending on their initial composition and pressure-temperature-time history, originally homogeneous sulphide inclusions within the diamonds will unmix into assemblages of pyrrhotite ± pentlandite ± chalcopyrite (Taylor and Liu, 2009, Harvey et al., 2016). During cooling and exhumation, many inclusions develop characteristic rosette-shaped or disc-shaped decompression fractures (Harris, 1972) because of the different equations of state of diamond and sulphide. These fractures may be lined with sulphides (Richardson et al., 2004, Wiggers de Vries et al., 2013a, Harvey et al., 2016) extending outwards from the main sulphide body.

Lithospheric diamonds usually belong to two parageneses: the eclogite (E-type) or peridotite (P-type) suite. These parageneses are distinguished by the silicate or oxide inclusions they contain, indicating whether their main growth substrate was an eclogite or peridotite (Harris, 1968, Shirey et al., 2013). Sulphides in P-type are richer in Ni (>∼12 wt.%; Bulanova et al., 1999) compared to those included within E-type diamonds (Harvey et al., 2016). Eclogitic diamonds frequently contain a component derived from subducted oceanic crust (Schulze et al., 2013).

The majority of samples studied here are eclogitic diamonds from the Mir kimberlite pipe (Yakutia, Russia). They have complex crystallisation histories interpreted in terms of growth under different conditions in a reducing upper mantle environment beneath the Siberian craton (Bulanova et al., 1998). Diamond growth is thought to have occurred in the presence of a fluid which was accompanied by immiscible Fe–Ni–Cu sulphide melts, and their variable inclusion compositions are thought to reflect their source region's changing chemistry (Bulanova et al., 1996, Bulanova et al., 1998, Bulanova et al., 2014, Wiggers de Vries et al., 2013a).

The Re–Os geochronology of inclusions in peridotitic diamonds and eclogite xenoliths from the Udachnaya kimberlite gives an Archean age for the Siberian lithosphere (Pearson et al.,

1995, Richardson and Harris, 1997). The Mir diamonds are reported to have formed in the Proterozoic in two separate events at ~2.1 and between 0.9–1.1 Ga (Wiggers de Vries et al., 2013a; 2013b). Rudnick et al. (1993) had also inferred a 1 Ga difference in ages for the core and rim-located sulphides in one Udachnaya peridotitic diamond. Overall, it has been demonstrated that some Yakutian diamonds were formed episodically at <200 Ma intervals through multiple interactions with different evolving metasomatic fluids (Taylor et al., 1998, Wiggers de Vries et al., 2013a; 2013b, Bulanova et al., 2014).

The complex exsolution observed in sulphide inclusions in diamonds has the potential to cause problems with Re–Os age determinations if the whole inclusion is not extracted and dissolved. Chalcopyrite-rich rims have been observed previously (e.g. Bulanova et al., 1996, Anand et al., 2004) and even low abundances of other phases, especially if they are enriched in Re or Os, could lead to significant heterogeneity in platinum group element distribution within the inclusion. Similar issues have been discussed in the literature concerning the validity of using Laser Ablation ICPMS to obtain Re–Os data for sulphides in mantle xenoliths. As well as technical issues surrounding Re corrections (Pearson and Wittig, 2008) several authors have pointed out the importance of sampling the whole inclusion (e.g. Harvey et al., 2016), which is impossible if the inclusion is exposed by polishing. Therefore, laser ablation analyses of sulphides should be avoided for radiometric dating of sulphide inclusions.

In this study we have performed detailed high-resolution Raman spectroscopic mapping of sulphide inclusions and discovered that molybdenite is a relatively widespread, if low in abundance, exsolved phase in many sulphide inclusions in diamonds. The implications of molybdenite unmixing and segregation for Re–Os dating are explored.

3.2. Materials and methods

3.2.1. Samples

Seven previously studied macrodiamonds from the Mir kimberlite pipe were used in this study (Fig. A1 Appendix A). The characteristics of the samples are described in table A1 (Appendix A); the diamonds are colourless, ranging in size from 3 to 6 mm, and define shapes from well-defined to distorted octahedra. Most diamonds display step-layered octahedral faces and minor dissolution features at their edges. Cathodoluminescence (CL) imagery has shown the complex growth history and occasional features of internal resorption of some of the diamonds (Bulanova et al., 1999, Bulanova et al., 2014, Wiggers de Vries et al., 2013a) (Fig. A2, Appendix A). All diamonds are eclogitic based on the presence of inclusions of eclogitic affinity and their carbon isotopic composition (C) (Table A1, Appendix A). The Mir samples were previously selected, cut and polished for sulphide inclusion study at the Diamond and Precious Metal Institute (Siberian Branch RAS, Russia) but still contain abundant unexposed sulphide and some silicate inclusions (including omphacite, pyrope–almandine garnet and coesite, consistent with the findings of Bulanova et al., 1999). The sulphide inclusions have varying shapes, sizes and fractures associated with them. Some of them exhibit typical rosette-shaped fracture systems around the central sulphide inclusion and others have more discrete and relatively straight cracks surrounding them. All Mir sulphide inclusions examined have a euhedral to sub-euhedral body (in a negative diamond crystal shape), and range in size from 2 to 100 μm.

In addition, a few sulphide inclusions in one diamond from Udachnaya (Yakutia), three from Murowa (Zimbabwe), two from Argyle (Australia), two from Dachine (French Guiana), two from Orapa, three from Letlhakane, two from Damtshaa, five from Jwaneng (Botswana)

three from Collier-4 and four from Juina-5 (Brazil) were studied, and the presence or absence of molybdenite in these samples will also be reported here.

3.2.2. Sample preparation

The Mir diamonds were sawn and polished on dodecahedron planes into 1–3 mm thickness plates at the Institute of Geology of Diamond and Precious Metals (Yakutsk, Russia). All the studied inclusions were below the polished surface of the diamond (i.e. were completely encapsulated) before and during Raman measurements. Based on CL imaging and optical microscopy, there appear to be no cracks or healed cracks leading from the inclusions to the diamond surface. All mechanical polishing procedures for exposing inclusions to the surface were completed using an industrial diamond wheel. Molybdenum disulphide was not used at any stage in the preparation of the studied diamonds

3.2.3. Analytical methods

3.2.3.1. Raman spectroscopy

A Thermo Scientific DXRxi Raman imaging microscope was used with blue (455 nm) and green (532 nm) lasers. Laser power of 10 mW was used throughout, with 50 μm or 25 μm confocal pinholes. Long working distance objectives were used throughout (10× and 50×). Exposure times ranged up to 8 s with a maximum of 1000 scans. The blue laser provided better results because of the smaller excitation volume and less interference from diamond luminescence. The spectra were processed with the Raman OMNICxi software. A diamond signal at 1332 cm^{-1} was present in virtually every measurement.

3.2.3.2. Electron probe microanalysis (EPMA)

For one sample, an inclusion was exposed by polishing. Wavelength-dispersive spectroscopy (WDS) was undertaken at 30 kV using a Cameca SX100 microprobe with a slightly defocused (~3 μm size) beam to increase the analytical volume.

3.2.3.3. Focused ion beam SEM (FIB-SEM)

The FIB procedure was undertaken at the Interface Analysis Centre (School of Physics, University of Bristol) using a FEI Helios NanoLab 600 with three-axis micromanipulator, Oxford Inst X-Max50 energy dispersive system (EDS) with 7 nm resolution, platinum deposition and force measurement. During the FIB operation, a maximum beam current of 20 nA and a beam energy of 30 kV were used. EDS measurements were made at 20 and 30 kV. EDS element maps were acquired at 30 kV.

3.2.3.4. Synchrotron-radiation X-ray tomographic microscopy (SRXTM)

Three of the Mir diamonds were analysed at the TOMCAT beamline at the Swiss Light Source, Paul Scherrer Institut, Villigen, Switzerland. Absorption-Contrast Imaging (ACI) computed microtomography was performed using a 1 μm wide monochromatic beam in conjunction with a 20× objective, producing a voxel (3D pixel) of 0.325 μm, and a 40× objective, producing a voxel size of 0.163 μm.

3.3. Results

3.3.1. Raman spectroscopy

Molybdenite has a clear diagnostic Raman spectrum (Mernagh and Trudu, 1993) which has been observed in 73 out of 80 Mir sulphide inclusions (Fig. 3.1). Molybdenite has two first-order peaks at 408 and 392 cm−1, as well as small second order peaks at ~450, 596 and 757 cm−1 (Chen and Wang, 1974). Pyrrhotite (po), which is presumed to be the most abundant sulphide mineral is only weakly Raman active due to its crystal structure and was usually unobservable.

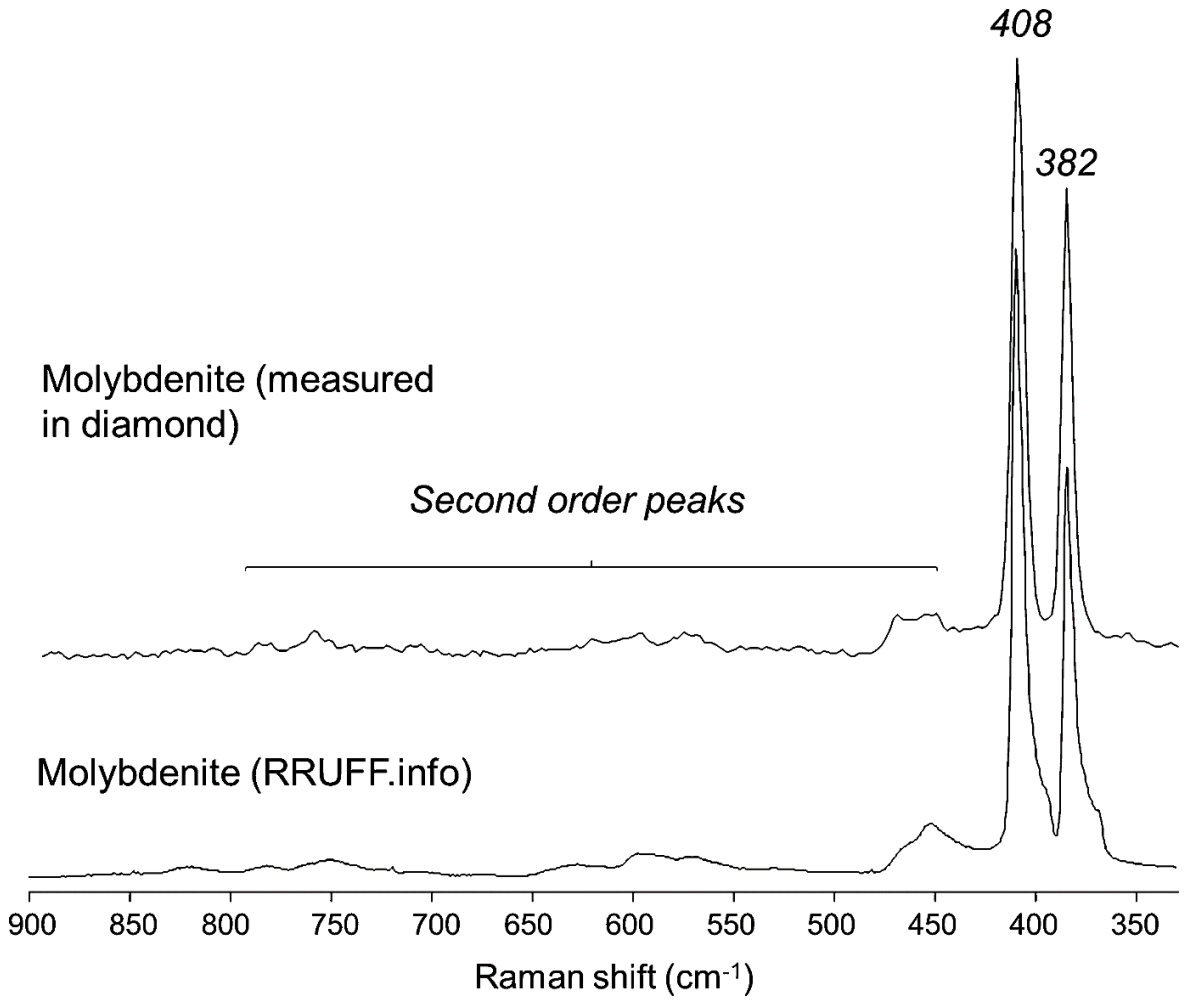

Figure 3.1. Comparison of the depolarised 532 nm laser Raman spectra of molybdenite (382, 408 cm^{-1}) measured with a blue 455 nm laser in a sulphide inclusion in Mir eclogitic diamond 1591 and a spectrum available on The University of Arizona's online RRUFF mineral spectra database (Lafuente et al., 2015).

The characteristics of some inclusions in Mir diamonds from which a molybdenite Raman signal was obtained are listed in Table A2 (Appendix A). Many of the diamonds contain several sulphide inclusions that are distributed from the core to rim zones. There is no discernible correlation between the position of the inclusion within the diamond and the presence or absence of molybdenite. Maps of the 408 cm^{-1} peak intensity for various inclusions with spatial resolutions of 0.6–0.8 μm were produced, with examples shown in Fig. 3.2. The maps show the distribution of molybdenite (red areas show where its Raman signal is most intense) but cannot be used to quantitatively assess the volume fraction of molybdenite in the inclusion because of potential scattering of the laser light, absorption of the laser by opaque phases and focusing limitations. Nonetheless, the data show unambiguously that molybdenite is widespread in the inclusions. It appears to form small (typically around 1 μm) and unevenly distributed grains, often seen near the edges of the sulphide inclusions. Molybdenite is commonly manifested as an irregular film near the inclusion walls (e.g. Fig. 3.2.A).

In 61 out of 80 inclusions, molybdenite is found closely associated with chalcopyrite, possibly in an intergrowth relationship (e.g. Fig. 3.2.B). Chalcopyrite is also commonly seen inside the decompression cracks surrounding an inclusion, where the material present can exhibit patchy or weave-like textures. Diamond 1702 hosts a cluster of molybdenite-bearing sulphide inclusions in its core (Fig. A1, Appendix A). A Raman signal for pyrrhotite (Fig. A3, Appendix A) was obtained in the fractures surrounding most of these, where chalcopyrite and molybdenite are also present. Fig. 3.2.C shows an inclusion in the rim zone of diamond 1702, which hosts molybdenite within its body while the cracks contain chalcopyrite.

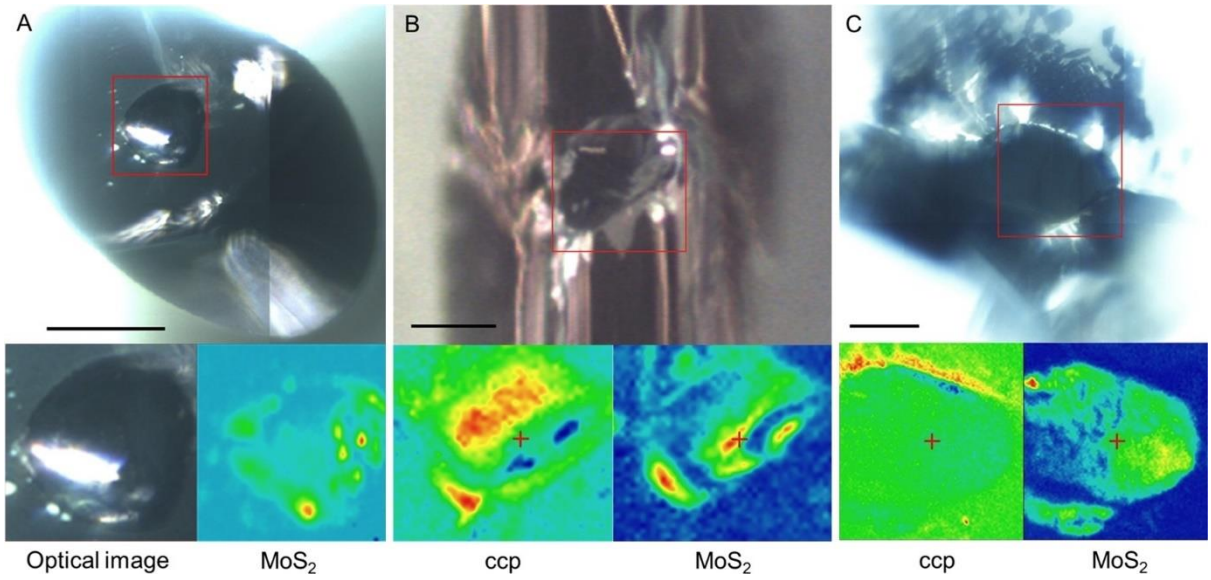

Figure 3.2. Optical images and Raman maps of molybdenite-bearing sulphide inclusions. The Raman maps are based on the baseline-corrected peak heights at 408 cm^{-1} peak for molybdenite and 293 cm^{-1} for chalcopyrite. The colour scaling was chosen to best represent the distribution of each phase; otherwise the colour scales are arbitrary and not comparable between images. Red indicates where the signal for the mapped phase is most intense. Yellow and green colours show areas where the signal is present, but weaker and/or barely detected). A) In diamond 1584-i, the body of an inclusion contains molybdenite (MoS_2) forming irregular disseminations at its edge. Scale = 50 µm. B) In inclusion 1704-2, chalcopyrite (ccp) and molybdenite appear to be intergrown. Scale = 30 µm. C) An inclusion in diamond 1702 is surrounded by rosette fractures lined with patchy intergrowths of dark material presumed to be sulphide and/or graphite. Raman peak height maps show the occurrence of molybdenite at the edge of the inclusion body while chalcopyrite is found in the decompression fractures. Scale = 50 µm. (For interpretation of the colours in the figure(s), the reader is referred to the web version of this article.)

An inclusion located in the intermediate zone of diamond 1703 (inclusion 1) contains omphacite adjacent to a non-Raman-active sulphide, but no molybdenite was detected. The inclusion is partially exposed, having lost some of its rim portions. Molybdenite is, however, found inside the sulphide inclusions that occur in the outer intermediate zone (zone of resorption and regrowth) of this diamond (Fig. A1, A2, Appendix A).

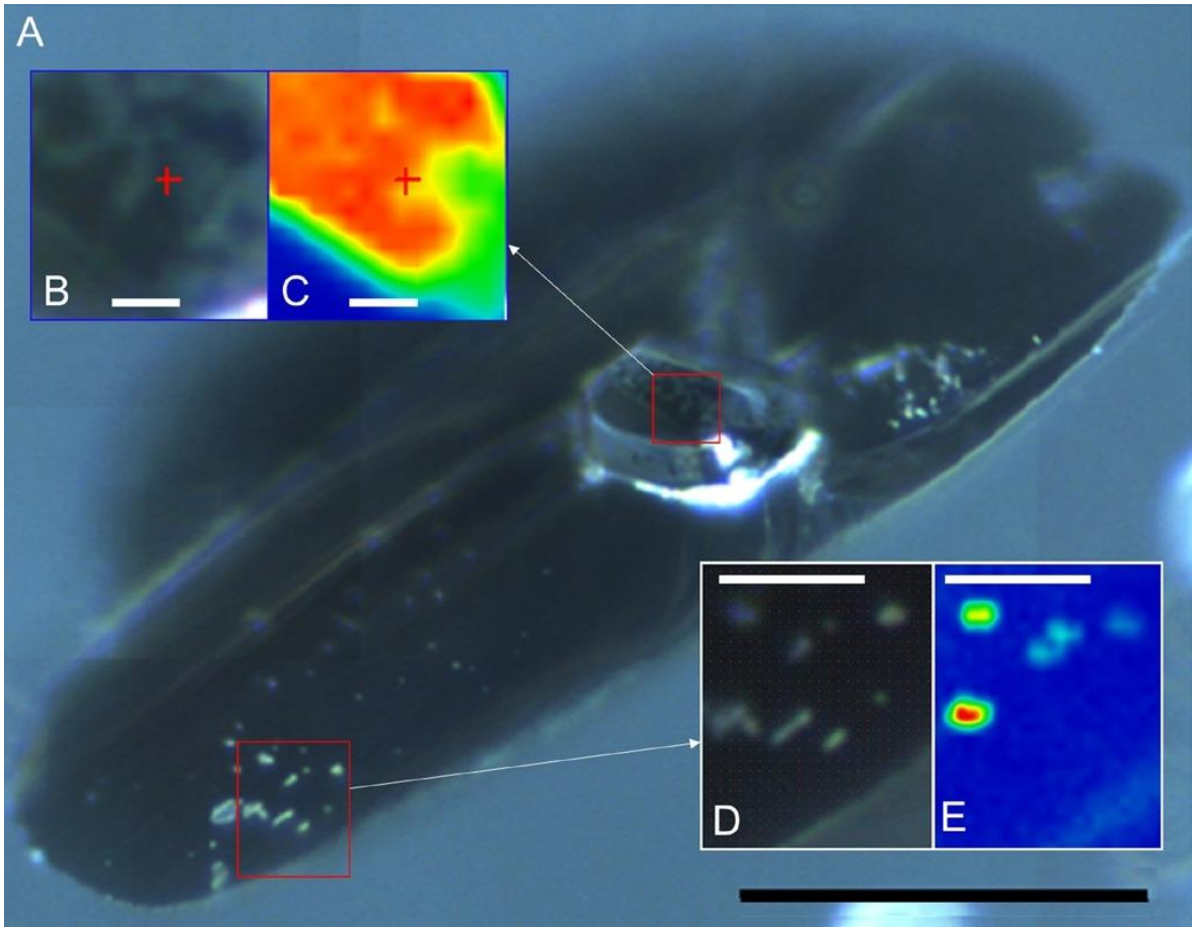

Figure 3.3. A) Optical microscope image of inclusion 1704-2. The hexagonal body of the inclusion exhibits dark patches on its surface, a higher magnification view of which (B) and corresponding Raman map of molybdenite distribution (C) are provided; molybdenite is distributed in the area where the dark mottled phase occurs. The inclusion is surrounded by planar decompression fractures, speckled with pale yellow grains (magnified in D). The corresponding Raman map in E shows molybdenite forming in points within the decompression fractures (Scale bars: A = 50 μm; B, C = 5 μm; D, E = 10 μm). The significance of the colours in the Raman maps is explained in the caption to Fig. 3.2.

Fig. 3.3.A shows sulphide inclusion 1704-2 oriented to the Raman optical microscope light in such a way that a dark phase with a mottled appearance can be seen on the surface of a hexagonal inclusion body (Fig. 3.3.B). Although the typically rhombohedral crystal shape of molybdenite cannot be discerned, Raman peak height maps show its presence is restricted to this surface (Fig. 3.3.C). Molybdenite (that seems to be in the form of plates with a maximum diameter of 3 μm) is also found within the rosette fractures surrounding this inclusion: the distribution of molybdenite in the inclusion's cracks, as shown by Raman peak height maps (Fig. 3.3.E), coincides with the pale-coloured points visible in transmitted light (Fig. 3.3.D).

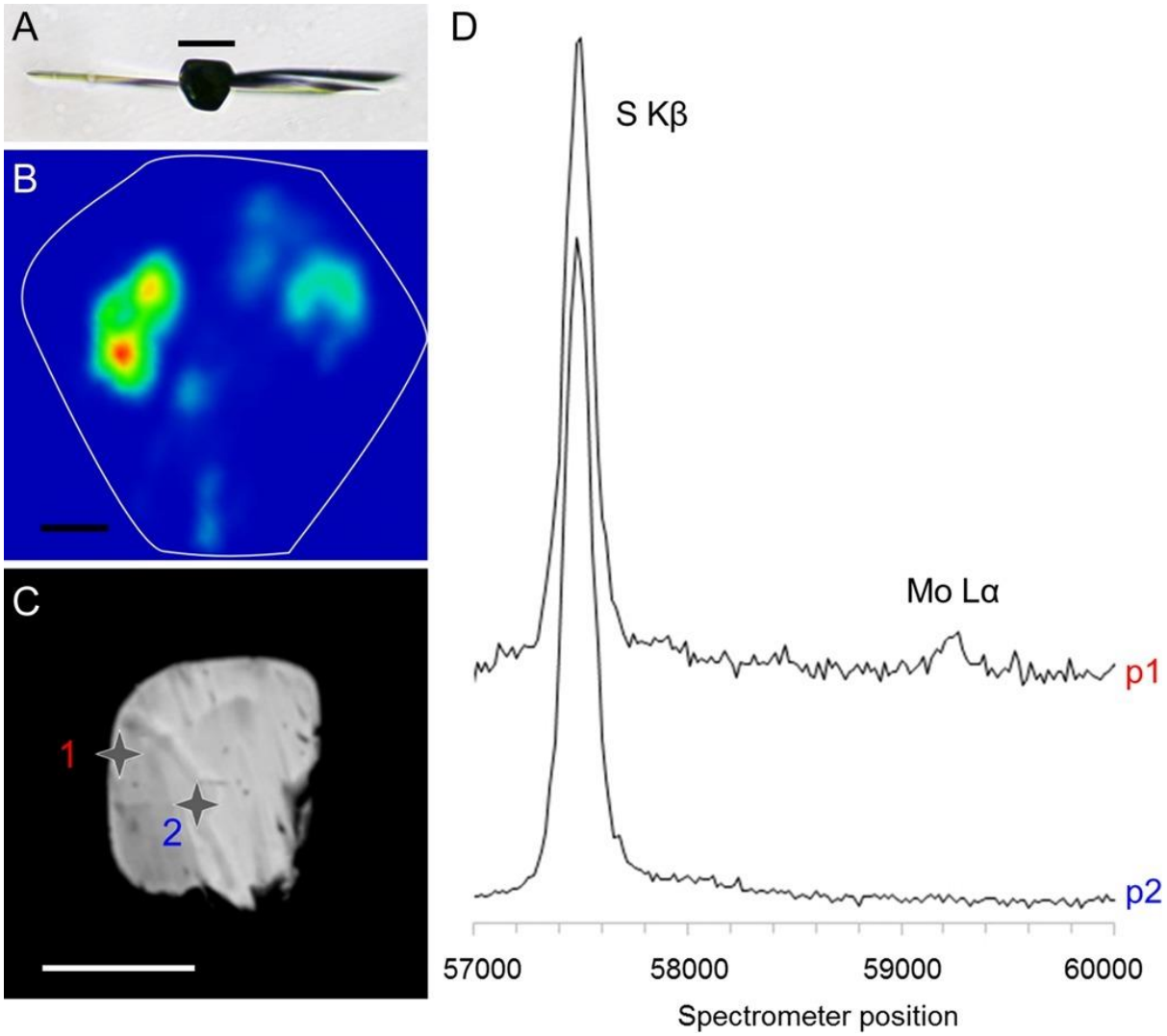

Figure 3.4. A) Optical plane-polarised image of unexposed inclusion 1584-r-3 shows a hexagonal inclusion body connected to disc-shaped decompression fractures. B) The Raman map shows the location of molybdenite inside the unexposed inclusion (the outline of which is drawn in white). The molybdenite is at the top surface of the inclusion in this projection. All the Raman signal originates from the surface of the inclusion as the laser light does not penetrate a significant depth into the opaque sulphide inclusion. C) Back-scattered electron (BSE) image of exposed inclusion 1584-r-3 showing the location of WDS point measurements 1 and 2 (grey crosses). Scales are 30, 5 and 10 μm in A, B and C respectively. D) WDS spectrum from point 1 (red) shows Molybdenum (Mo) enrichment relative to point 2 (blue). The y axis of the spectrum at point 2 has been scaled down by ~3.5, to make the sulphur K-beta (S Kβ) peaks in both spectra the same height. Less sulphur was measured at point 1 because of its proximity to the edge of the inclusion and presence of diamond.

Fig. 3.4.A shows sulphide inclusion 1584r-3 which exhibits a negative diamond shaped-body connected to relatively straight disc-shaped decompression cracks. A Raman peak height map in Fig. 3.4.B indicates that molybdenite is present. As the penetration depth of the blue laser light into the opaque sulphide inclusion is low, the observation of molybdenite peaks indicates

that molybdenite is located at the surface of the inclusion. Molybdenite could also be present inside the inclusion body but would be unobservable. In this example, no material was found inside the inclusion's fractures. In addition to molybdenite, the inclusion also contains chalcopyrite (Table A2, Appendix A). The diamond was polished in an attempt to expose the molybdenite for further analyses. Subsequent Raman peak height maps showed that the molybdenite was still present in some of the unexposed portions of the inclusion, very close to the edge of the exposed surface. However, no molybdenite was observed at the polished surface, possibly because it is so soft that it is removed as soon as it is exposed.

In summary, we have studied 80 sulphide inclusions in 7 diamonds from the Mir pipe using Raman, and of these, 73 inclusions clearly contained molybdenite. This is a minimum number, because it is possible that in other inclusions molybdenite was present, but undetected because it was obscured by other opaque sulphides. So, at least 90% of studied Mir sulphide inclusions contain molybdenite, hence it cannot be considered to be a mineralogical oddity; this observation has major implications for the analytical techniques used in the study of trace element abundances and Re–Os geochronology of sulphide inclusions in diamond. Additional techniques were therefore applied in order to obtain a better understanding of the molybdenite distribution.

3.3.2. EPMA and FIB-SEM

Exposed inclusion 1584-r-3 was studied by electron probe microanalysis (EPMA), but no features attributed to molybdenite were observed by back-scattered electron (BSE) (Fig. 3.4.C) or X-ray imaging of the exposed inclusion surface. The sulphur Kα peak overlaps with that of molybdenum L-lines so energy dispersive spectroscopy (EDS) cannot be used. Wavelength-dispersive spectra (WDS) were therefore obtained from near the edge of the inclusion wall (point 1) and the centre of the inclusion (point 2) (the locations are shown Fig. 3.4.C). WDS

spectra in Fig. 3.4.D show that Mo is concentrated near the edge of the inclusion, although pure MoS_2 could not be identified presumably because the MoS_2 particles are much smaller than the analysed volume (~3 μm).

Fig. 3.5.A shows the ~20 μm wide FIB-SEM section that was produced to study the diamond/sulphide interface of inclusion 1584-r-3. The inclusion was polished by focused-ion beam milling to achieve a cleaner surface (Fig. 3.5.B and 3.5.C). The FIB cross-section was imaged by EDS X-ray mapping (Fig. 3.5.D, 5.E and 5.F), but no MoS_2 was observed in the Mo element maps at 30 kV, again suggesting that the abundance is very low. It should be noted however, that molybdenite is a particularly soft sulphide, and could have been sputtered away during FIB-polishing. EDS X-ray maps were also acquired parallel to the polished surface (Fig. 3.5.G, 5.H and 5.I). Maps of both FIB-polished surfaces reveal an iron and nickel-enriched matrix with exsolved Cu-rich lamellae; these very clearly show the exsolution of chalcopyrite in veins and, crucially, at the rim of the inclusion.

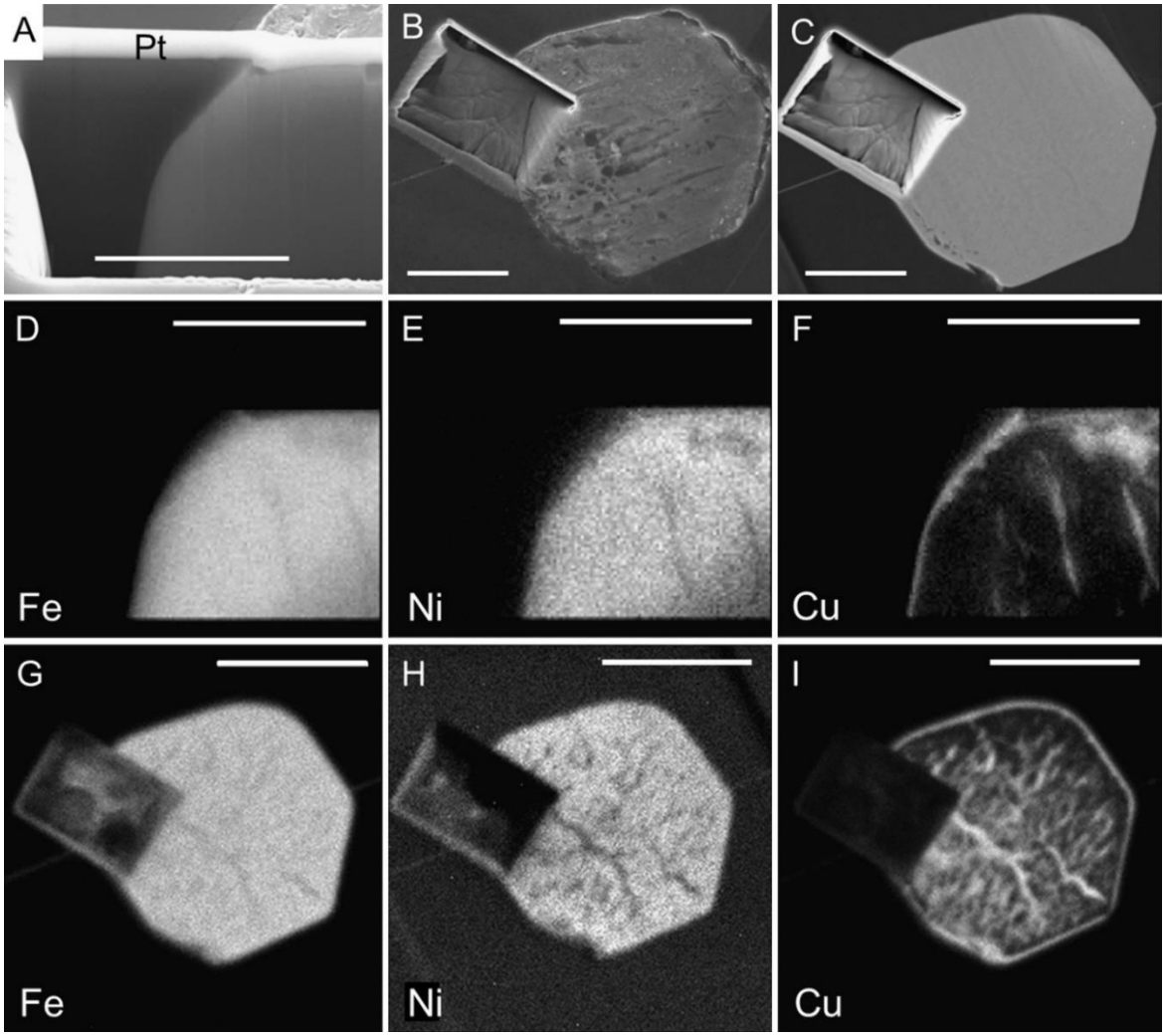

Figure 3.5. A) Back-scattered electron image of a Focused-Ion Beam (FIB) cross-section of exposed inclusion 1584-r-3 (Pt refers to the line of platinum deposition). Back-scattered electron images are also provided to show the surface of inclusion before (B) and after (C) FIB cleaning. The rectangular feature in B and C is the FIB trench, the wall of which is shown in A. EDS X-ray element maps (at 30 kV) show the distribution of Fe, Ni and Cu in sulphide inclusion 1584-r-3, parallel to the FIB-trench wall (D–F) and parallel to the polished exposed surface (G–I). X-ray maps show a Cu-rich rim and lamellae in a seemingly homogeneous Fe–Ni sulphide matrix. The scales = 8 (A, D, E and F), 15 (B and C) and 20 μm (G, H and I)

.

3.3.3. X-CT (x-ray tomography)

A total of 32 unexposed molybdenite-bearing sulphide inclusions within diamonds 1584-r, 1591 and 1607 were analysed by synchrotron-based X-ray microtomography. Absorption Contrast Imaging (ACI) results presented in Fig. 3.6 show a complex network of cracks radiating from the body of 29 of these inclusions (e.g. Fig. 3.6.A and 3.6.B). The

decompression fractures surrounding the inclusions contain high-density (bright) sulphide. Most of the inclusions also exhibit features resembling exsolution of a lower-density (darker) material within the sulphide body (Fig. 3.6.C). In two cases, the sulphides contain fractures that do not extend into diamond. Most of the sulphide inclusions analysed in diamonds 1591 and 1607 exhibit relatively uniform textures, with discrete lower density exsolution features near the inclusion walls. Although molybdenite could not be positively identified by X-CT, the data clearly show the complex unmixing and extrusion of sulphide material along cracks.

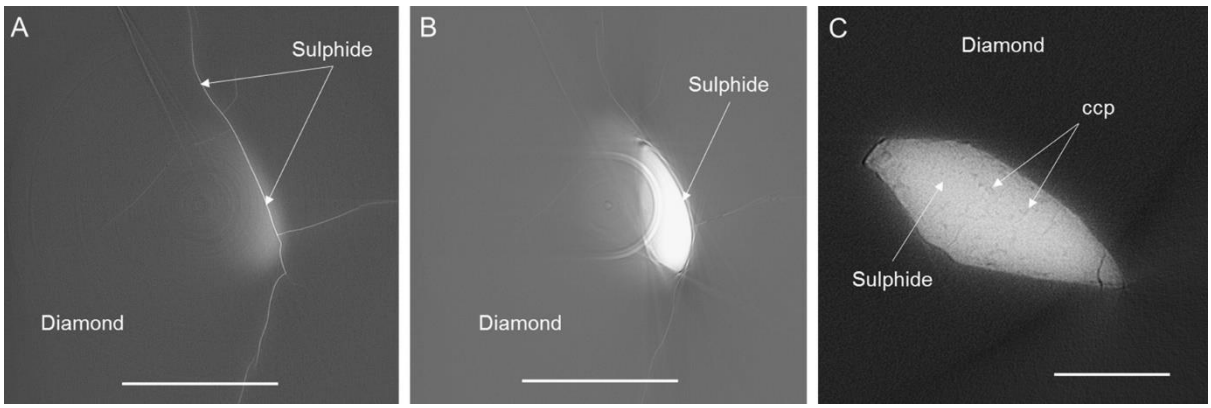

Figure 3.6. Synchrotron-based X-ray tomographic microscopy (X-CT) images through molybdenite-bearing sulphide inclusions in diamond (original pixel size = 0.163 μm). Absorption Contrast Imaging (ACI) detects density differences between different higher-density (bright) sulphide and lower-density (darker) diamond. A) Sulphide infills the rosette fractures radiating from the body of an inclusion in diamond 1591 (the main body of the inclusion is not seen in this slice of the 3-D image). B) A slice taken 10 μm from (A) showing the body of the sulphide inclusion. C) A sulphide inclusion in diamond 1584-i contains meandering lamellae of a darker, lower-density sulphide (chalcopyrite, ccp) within a brighter, higher density matrix (presumed Fe–Ni sulphide). The scales = 20 μm.

3.3.4. Occurrence of molybdenite in different types of diamonds

The common occurrence of molybdenite in Mir diamonds (>90% of inclusions) raises important questions about previous interpretations of sulphide inclusion compositions in diamonds. We have found one previous report of molybdenite in diamond; Davies et al. (2002) discovered molybdenite included in a grossular garnet inclusion from a New South Wales alluvial diamond from Bingara. To assess whether molybdenite is a ubiquitous phase, or unique

to the eclogitic paragenesis, a total of 35 inclusions in 27 samples from 10 other suites, including both eclogitic and peridotitic diamonds, were studied. So far, we have identified molybdenite in 3 out of 3 sulphide inclusions and an inclusion cloud in 1 peridotitic diamond from Udachnaya, 3 out of 3 inclusions in 3 peridotitic diamonds from Murowa (Zimbabwe), 2 out of 2 inclusions in 2 eclogitic diamonds from Dachine (French Guiana), 3 out 7 inclusions in 3 eclogitic diamonds from Argyle (Australia), 2 out of 3 inclusions in 2 diamonds from Orapa (Botswana), 2 out of 2 inclusions in 3 diamonds from Letlhakane (Botswana) and 2 out of 3 inclusions in 2 diamonds from Damtshaa (Botswana). However, molybdenite has not yet been seen in any of 7 inclusions in 5 diamonds from Jwaneng (Botswana) or in 7 studied sulphide inclusions from sub-lithospheric diamonds from Collier 4 and Juina-5 (Juina kimberlite field, Brazil). The reasons for the presence or absence of molybdenite is not yet clear. The presence of molybdenite in inclusions from both peridotitic and eclogitic diamonds implies that enrichment of Mo in sulphides to a level that causes molybdenite exsolution is not related to any specific paragenesis. Factors such as different sources of materials for sulphide and silicate inclusions or variations in oxygen fugacity may instead play a role.

3.4. Discussion

3.4.1. Unmixing from a sulphide melt

Sulphides mainly exist in molten form at the formation pressures and temperatures of lithospheric diamond formation, although under cooler conditions crystalline monosulphide solid solutions could also occur (Sobolev, 1974, Li and Audétat, 2012, Zhang and Hirschmann, 2016). The composition of mantle sulphide liquids would be significantly different from MSS (particularly in terms of Cu concentration), therefore if a sulphide liquid is trapped in diamond there are two possible scenarios for the period between diamond growth and exhumation depending on the prevailing conditions: (i) the inclusion consists of a sulphide liquid only; (ii)

the liquid partially crystallises to MSS and Cu-rich residual liquid. It is likely that further changes in sulphide mineralogy only occur during exhumation of the diamond to the surface by kimberlite transportation, and subsequent cooling. Raman data (Fig. 3.2, Fig. 3.3) and x-ray element maps (Fig. 3.5) of molybdenite-bearing sulphide inclusion 1584-r-3 are consistent with unmixing from an original Fe–Ni–Cu–Mo sulphide melt. In this section we will describe the likely changes occurring if sulphide inclusions are trapped as liquids, although the unmixing pathway would be similar if the trapped sulphide is MSS.

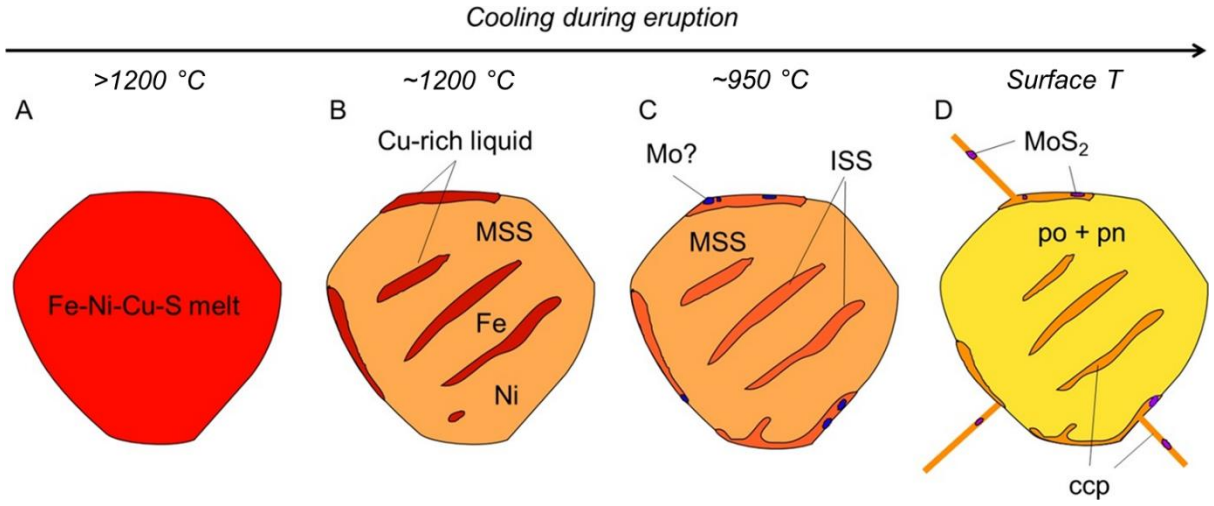

Figure 3.7. Simplified model of sulphide exsolution within molybdenite-bearing inclusion 1584-r-3. (A) The inclusion is trapped as melt before (B) exsolving into different phases, including a Cu-enriched liquid and monosulphide solid solution (MSS). Upon further cooling (C) the residual melt crystallises to intermediate solid solution (ISS) and possibly a Mo-bearing phase. On final cooling to room temperature (D) further unmixing produces a pyrrhotite (po) groundmass, closely associated with a discrete Ni-phase (e.g. pentlandite, pn), chalcopyrite (ccp) veinlets and rim and peripheral molybdenite (MoS_2) some of which is extruded along fractures (in D). For simplicity, the represented volumes of Cu-rich liquid, ISS and ccp are almost the same in (B), (C) and (D) respectively, although the small differences in composition between the phases will lead to some changes in relative mineralogical modes. Most of the steps in this scheme (including crystallisation of molybdenite) are thought to occur upon ascent of the diamond during kimberlite eruption.

The proposed post-entrapment crystallisation sequence is illustrated in Fig. 3.7. Following the trapping of sulphide liquid (Fig. 3.7.A) a Fe-rich MSS is the first solid to crystallise from melt at about 1200 °C, leaving a residual Cu-enriched sulphide liquid (Barton, 1973; Ebel and Naldrett, 1997) (Fig. 3.7.B). Upon further cooling below ~950 °C, a Cu-rich intermediate solid solution (ISS) may develop (Ebel and Naldrett, 1997). Either Mo is partitioning into the Cu-

rich phase, or a separate Mo-rich phase crystallises around the same time (Moh, 1978). It is not clear which of these processes is dominant, but ultimately the Mo is segregated into molybdenite at the edge of the inclusion.

The textures observed in the X-CT data of molybdenite and chalcopyrite-bearing inclusions (Fig. 3.6) show that some sulphide inclusions in diamond (e.g. 1584 in Fig. 3.6.C) have a higher proportion of chalcopyrite than others, perhaps reflecting a different source or simply trapping as sulphide melt rather than Fe-rich MSS. The details of the exsolution pathway are uncertain, because the phase equilibria of sulphide systems at high pressure are not well known. Moh (1978) showed that the liquid eutectic of the Cu–Mo–S system at 1 bar occurs at 1063 °C and phases in the Fe–Cu–Mo–S sulphide system can begin to crystallise around 1000 °C (Moh, 1978). There are no data on the analogous system including Ni. Finally, the system of fractures develops around the inclusions. Molybdenite and chalcopyrite are disproportionately sequestered into the cracks because they occur at the edges of the inclusions (Fig. 3.7.D). Perhaps the ductility of molybdenite (Anthony et al., 2003) also plays a role in the injection of molybdenite deep into the narrow fractures.

The range of formation temperatures established for Siberian eclogitic diamonds spans the range of coexistence of sulphide melts and MSS crystals (e.g. Sobolev, 1974) and variable fluid compositions could also influence sulphide solidii. As shown by the CL zonation of many of the Mir diamonds, the different diamond zones may have grown under distinct thermal or chemical conditions, thus in the same Mir diamond population it is possible that some inclusions were captured as Fe-rich MSS and others as sulphide melt. It is tempting to speculate that sulphide trapped as melt may contain more Mo than sulphide trapped as MSS, but more work would be required to confirm this idea.

3.4.2. The potential effect of molybdenite on Re–Os systematics

There is a distinct possibility that the molybdenite inside fractures in particular, will not be recovered for dissolution and analysis. The recognition that molybdenite is commonly associated with sulphide inclusions in diamonds has important implications for Re–Os dating of the inclusions, because Re will be strongly partitioned into molybdenite relative to the rest of the sulphide inclusion, whereas Os will be retained in the inclusion. When the diamond is 'cracked open' to retrieve the inclusion for Re–Os dating, there is a distinct possibility that the molybdenite inside fractures in particular, will not be recovered for analysis. Any molybdenite would be modally insignificant and may be invisible under a microscope. Here we will explore the implications of not recovering the molybdenite for Re–Os dating of sulphide inclusions.

The decay of ^{187}Re to ^{187}Os has been used to date inclusions in diamond based on their measured ratios of parent ^{187}Re and daughter ^{187}Os to non-radiogenic ^{188}Os. These compositions can be plotted and a best fit regression can then be derived to determine an isochron age; alternatively model ages (T_{MA} or T_{RD}) can be calculated with reference to chondritic $^{187}Re/^{188}Os$ and $^{187}Os/^{188}Os$ ratios (Harvey et al., 2016).

Because Re partitions strongly into molybdenite relative to Os (e.g. Stein et al., 2003), ^{187}Os and ^{188}Os would both remain in the sampled part of the inclusion, but a disproportionate amount of parent Re would potentially be lost from the sampled inclusion. Re-loss could potentially lead to incorrect dates being calculated, because the measured Re contents, contributing to the measured radiogenic Os would be lower than in the parental sulphide, so the $^{187}Os/^{188}Os$ ratio would be unsupported by the measured $^{187}Re/^{188}Os$ ratio. However, the details of how dates would be affected depend on many factors:

i) The modal abundance of molybdenite in the inclusions (controlled by the bulk Mo concentration of the inclusion and the solubility of Mo in the non-molybdenite phases).

ii) The proportion of molybdenite missed when extracting the inclusion.

iii) The bulk Re and $^{187}Re/^{188}Os$ ratio of the inclusion.

iv) The partition-coefficient of Re between molybdenite, chalcopyrite and the residual sulphide inclusion.

v) The timing of molybdenite exsolution relative to the age of formation of diamond (i.e. shortly after trapping of the inclusion, or during diamond exhumation by kimberlite).

vi) The method of age determination (Re/Os isochron age versus Re/Os model age).

3.4.2.1. Modelling the partitioning of Re into Mo-bearing sulphide

To model the potential distribution of Re between molybdenite and the coexisting sulphides, we have estimated how much molybdenite could form from sulphide melt trapped inside diamond. We consider the scenario of sulphide inclusions trapped as a homogeneous Fe–Ni–Cu–Mo sulphide melt ultimately forming molybdenite upon eruption and unmixing. The reported Mo concentration in sulphide inclusions in diamonds is around 10–700 ppm, (Bulanova et al., 1996; Wiggers de Vries et al., 2013a; Aulbach et al., 2012). If 120 ppm Mo (the mean of the reported values) were exsolved as MoS_2, this would correspond to 0.02 wt.% MoS_2.

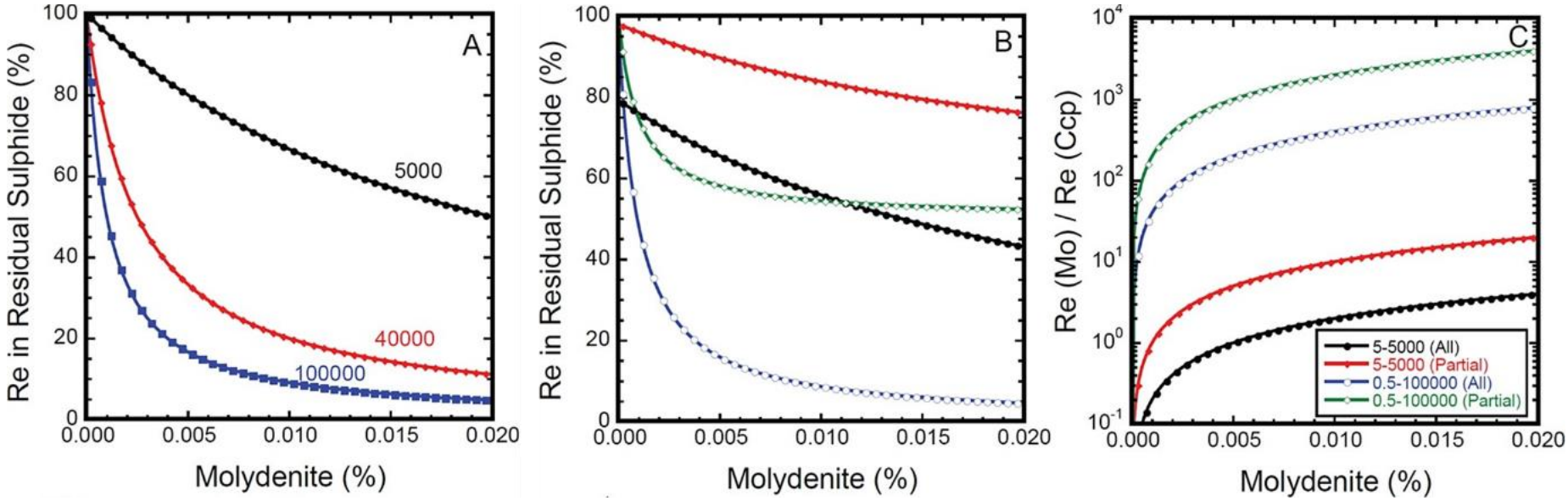

Figure 3.8.A) Model defining the relationship between the amount of molybdenite in a sulphide inclusion and the proportion of Re remaining in residual sulphide (MSS + chalcopyrite + pentlandite etc.) for different partition coefficients, Dmo/MSSRe (5000, 40000 and 100000) worked out from literature (see section 4.2.1). (B) and (C) consider partitioning of Re between three coexisting phases, molybdenite, chalcopyrite and pyrrhotite, where the mode of chalcopyrite is set to 5%. (B) shows the percentage of Re in the residual pyrrhotite (po) (i.e. excluding the Re hosted in unrecovered MoS_2 and ccp) and (C) shows the relative importance of MoS_2 and ccp for hosting Re. In (B) and (C) two scenarios are modelled, either all the Re in MoS_2 and ccp is lost from subsequent analysis (labelled "All" in the legend and considered to be an extreme assumption that is unlikely to be true) or 10% of the ccp and 50% of the MoS_2 are lost (labelled "Partial" in the legend and a more realistic possibility). For both cases two extreme combinations of partitioning are used in the model, either a high value of $D^{ccp/po}Re$ (5) and a low value of $D^{mo/po}Re$ (5000) or a low value of $^{Dccp/po}Re$ (0.5) and a high value of $D^{mo/po}Re$ (100000). The legend in (C) also applies to (B).

Due to the similar geochemical properties of Re^{4+} and Mo^{4+}, molybdenite hosts Re in higher concentrations relative to other sulphides. Published concentrations of Re in molybdenite relative to coexisting iron and copper sulphides (e.g. Mathur et al., 2002, Barra et al., 2003, Zu et al., 2015) were used to approximate the partition coefficients used in our model. The derived Re partition-coefficient for molybdenite relative to chalcopyrite and pyrrhotite is in the range 5000–190000. Fig. 3.8.A shows the percentage of Re that remains in the residual sulphide (po, ccp etc.) as a function of the modal percentage of molybdenite, modelled with partition coefficients between 5000 and 100000. For realistic parameters as much as 95% of the Re could be sequestered in molybdenite (although not all of it need be lost during extraction of the inclusion).

Further calculations have been performed to explore the relative importance of molybdenite and chalcopyrite in hosting Re (Fig. 3.8.C). Surprisingly the Re partition-coefficient for chalcopyrite/pyrrhotite is rather poorly known. Studies of coexisting chalcopyrite and pyrrhotite in mineral deposits (Barnes et al., 2006; O'Driscoll et al., 2009; Piña et al., 2012, Piña et al., 2016; Wang et al., 2015) suggest that Re has a small preference for pyrrhotite, with partition coefficients $DRe^{po/ccp} = \sim 1.5–56$. This contrasts with literature concerning unmixed sulphide inclusions in diamonds, which always states that Re is enriched in chalcopyrite relative to pyrrhotite. The latter idea originates from the study of Richardson et al. (2001) which measured the Re concentrations in a Cu-rich fragment from the edge of a sulphide inclusion and a Cu-poor part of the same inclusion. It was found that the Re concentration was higher in the Cu-rich part and it was therefore assumed that Re partitions into chalcopyrite. Our calculations using the Richardson et al. (2001) data and assuming that both fragments of inclusion DP9 contained only pyrrhotite and chalcopyrite suggest a value of $D^{ccp/po}Re \approx 2$. Furthermore, the time-resolved laser-ablation data of McDonald et al. (2017) suggest that Re is enriched at the Cu-rich edges of unmixed inclusions. However, the results of our study could

suggest that in fact the higher Re concentration in both studies resulted from the incorporation of small amounts of Re-rich molybdenite along with Re-poor chalcopyrite from the edge of the inclusion. Bearing in mind these considerations we have modelled the partitioning of Re between the three main phases with 5% chalcopyrite and values of $D^{ccp/po}Re$ in the range 0.5–5 and $D^{mo/MSS}Re$ = 5000–100000 (Fig. 3.8.B and 3.8.C). In these figures we consider the extreme case that all the MoS_2 and ccp is lost from the inclusion during the extraction process and the more realistic scenario that 10% of the ccp and 50% of the MoS_2 are lost during extraction. Obviously less Re is lost in the latter case, but even with conservative assumptions about partition coefficients and the mode of lost MoS_2 and ccp, the Re loss could be very significant (Fig. 3.8.B). The relative importance of MoS_2 and ccp for Re loss is explored in Fig. 3.8.C. For all the scenarios modelled here, MoS_2 is more important for Re loss than ccp with any MoS_2 mode above 0.005%. For the reasonable values of 0.02% MoS_2 in the inclusion, 10% loss of ccp and 50% loss of MoS_2 with partition coefficients of $D^{ccp/po}Re$ = 0.5 and Dmo/poRe = 100000, MoS_2 is 4000 times more effective than ccp in causing Re loss from the analysed part of the inclusion.

One final complication would pertain if the crystallisation and unmixing occurred faster than the rate of reequilibration. In that case the key process would be the partitioning of Re between MSS and a Cu-enriched liquid. Experimental data and observations on natural samples (Brenan, 2002, Barnes et al., 2008) imply that Re is compatible in MSS ($D^{MSS/liquid}Re \approx 2.5–9$) and this would lead to higher Re in pyrrhotite (crystallised from MSS) than chalcopyrite (crystallised from ISS, which itself would have crystallised from the liquid).

3.4.2.2. Modelling the effects of Re-loss on radiometric ages

Dating of sulphide inclusions can be accomplished by producing an isochron, from co-genetic inclusions. Alternatively, ages can also be derived using the model age equation by making assumptions about the initial isotope composition (usually a chondritic mantle). While the isochron method is preferable, much published dating of individual sulphide inclusions in diamonds has by necessity also used the model age method. Our work suggests that the molybdenite is formed at the time that the kimberlite host for the diamond/inclusion is erupted. In most cases this eruption is significantly later than the putative age of the diamond. Therefore, it is worthwhile undertaking some simple calculations to illustrate the effects of Re-loss on isochron and model age determinations.

Any form of open system behaviour will compromise an isochron and detection of this behaviour is assessed by the quality of fit of the isochron (mean square weighted deviate; MSWD). Taking the simplest possible effect of Re-loss, which is that the proportion of Re-loss is equal for each sulphide, will maintain both the quality of fit and value of the intercept of the isochron (see Fig. 3.9.A).

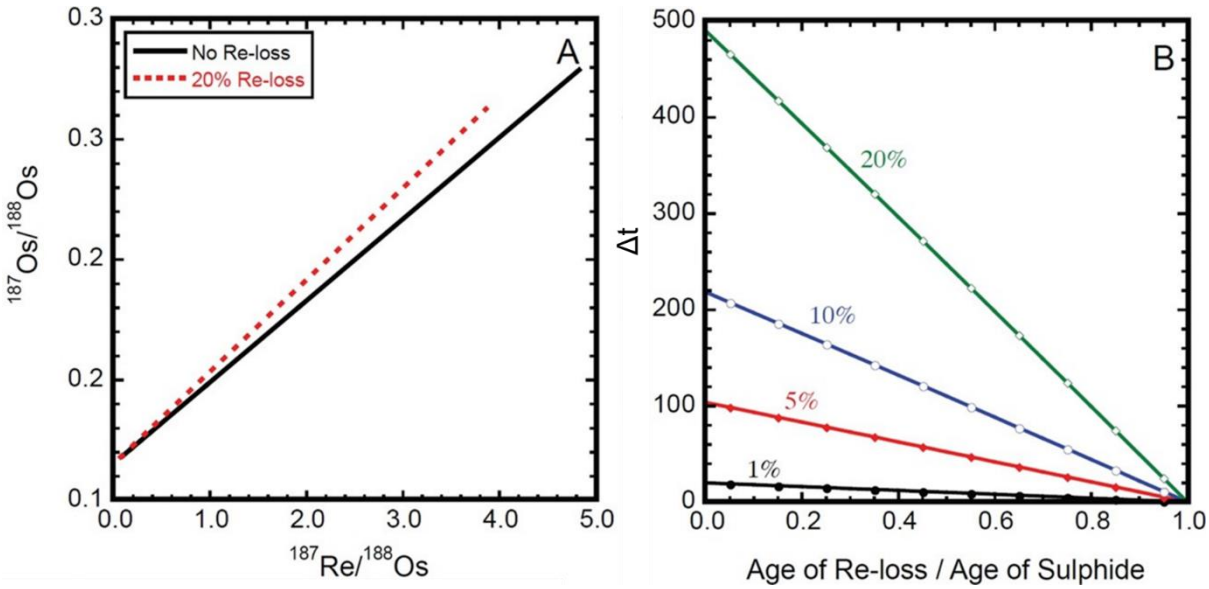

Figure 3.9. A) Isochron plot illustrating the effect of Re-loss, which is to increase the slope and therefore calculated age. B) Plot of the difference in isochron age from the true age (Δt) as a function of the timing of the Re-loss relative to the true age of the sulphide. In this calculation the true age of the sulphide was 2000 Ma, but Δt scales linearly with true age (i.e., for the same model parameters, if the true age was 1000 Ma, Δt would be half the value plotted in the figure). The four lines correspond to four different degrees of Re loss, 1, 5, 10 and 20%.

However, the isochron will give an age greater than the true age as Re-loss rotates the isochron anti-clockwise (steepens the slope). This increase in isochron age occurs irrespective of whether the points have Re/Os ratios greater or less than chondritic mantle (see discussion below). Fig. 3.9.B illustrates the effect of variable amounts of Re-loss on the isochron age by parameterising the ratio of when the Re-loss occurred relative to the true age of the sulphides. The calculations indicate the isochron age will increase with both increasing Re-loss and increasing time of Re-loss relative to the initial formation age of the sulphide. In nature, it is highly unlikely that each sulphide would lose proportionally the same amount of Re (or the recovery of molybdenite is equally efficient). The effect of variable Re-loss is to reduce the quality of the fit of the isochron and can produce an incorrect initial $^{187}Os/^{188}Os$ ratio. Modelling (not shown here) suggests that as little as 5% relative variability in the Re-loss of sulphides would produce isochrons with MSWDs significantly greater than 2.5. This may

explain why many published isochrons for sulphide inclusions from diamonds have MSWDs with values greater than 10.

The effect of Re loss on Re–Os model ages depends on whether the sulphide inclusion evolved with a Re/Os greater or less than the chondritic mantle. If the included sulphides evolve with a Re/Os ratio less than chondritic mantle, the evolution curve has a shallower slope than the mantle evolution curve. If Re loss occurs at some time after the formation of the sulphide it will then evolve along an even shallower slope. The resultant model age (T_{MA}) must always be younger than the true age of the sulphide (see Fig. 3.10.A). By contrast, when a sulphide has a Re/Os ratio greater than chondritic mantle, the sulphide will initially evolve on a steeper curve than the primitive mantle. Loss of Re at some point after formation of the inclusion will produce model ages with a greater age than the true age of the sulphide. However, there is a critical amount of Re loss whereby the model age will exceed that of the age of the Earth. Increasing loss will produce unrealistic ages until the model age line comes into parallelism with the mantle evolution curve and there is no solution. Further Re loss then produces future ages (Fig. 3.10.B).

In a similar manner to the isochron calculation we have calculated the deviation in the model age from the true age as a function of the timing of Re-loss, but also the initial $^{187}Re/^{188}Os$ ratio. Some representative calculations are illustrated in Fig. 3.10.C, with $^{187}Re/^{188}Os$ ratios from 0.3–10. Increasing the Re-loss will increase the disparity in the age as will increasing the time between Re-loss and the true age. A key part of the calculations is that sulphides that are slightly super-chondritic (e.g. $^{187}Re/^{188}Os$ ratio of 0.5 in Fig. 3.10.C) are highly sensitive to Re-loss and will readily generate unrealistically old ages or even future ages.

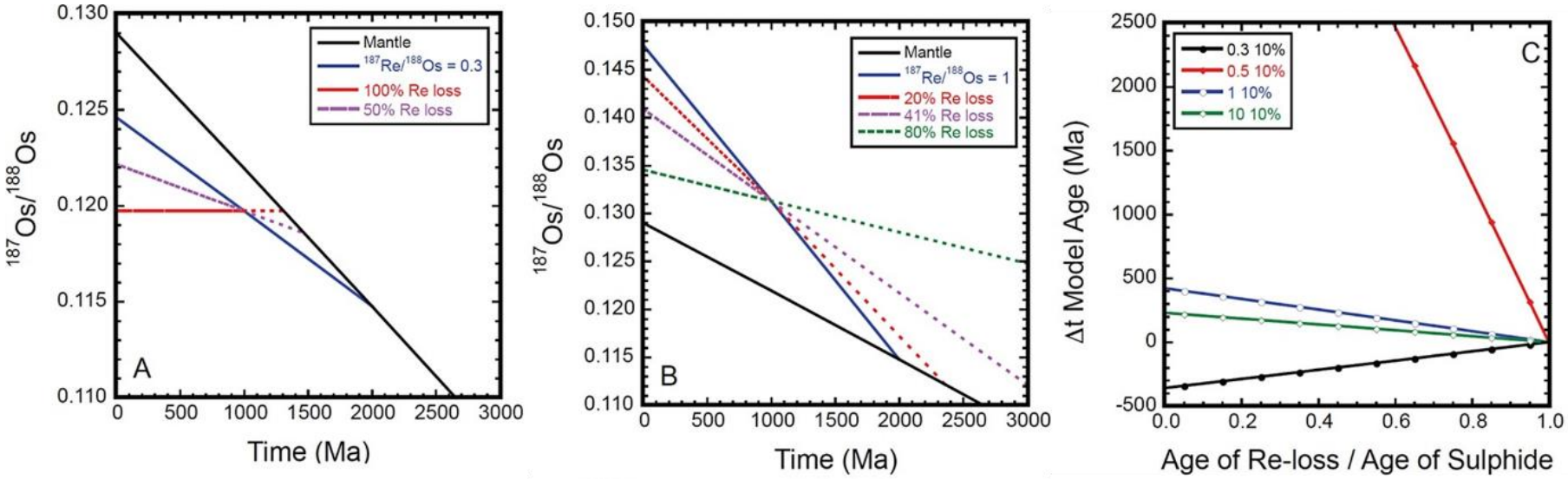

Figure 3.10. A) Plot illustrating the effect of Re-loss on the Os isotopic evolution of a sub-chondritic sulphide ($^{187}Re/^{188}Os$ = 0.3). In this example the sulphide was formed at 2000 Ma, but suffered Re-loss at 1000 Ma. The extreme case of 100% Re-loss will give a minimum model age of ~1300 Ma (T_{RD} =T_{MA}). The case of 50% Re-loss gives an older T_{MA} of ~1500 Ma, but in all cases Re-loss will give model ages younger than the true age. B) Plot illustrating the effect of Re-loss on the Os isotopic evolution of a supra-chondritic sulphide ($^{187}Re/^{188}Os$ = 1) with the same age and timing of Re-loss as above. Small amounts of Re-loss (e.g., 15%) result in a model age greater than the age of the sulphide. Increasing loss will give progressively greater ages up to the age of the Earth (in this case 41% loss). Further loss will yield ages older than the Earth and ultimately future ages (e.g. 80% loss). C) Plot of the difference in model age from the true age (Δt) as a function of the timing of the Re-loss relative to the true age of the sulphide and $^{187}Re/^{188}Os$ ratios of the sulphides, so 0.3 10% represents an initial $^{187}Re/^{188}Os$ of 0.3 and 10% Re-loss. In this case the true age of the sulphide was 2000 Ma so a Δt of 2500 Ma is essentially the age of the Earth. Again Δt scales linearly with true age.

By contrast, sulphides with highly super-chondritic ratios (e.g. $^{187}Re/^{188}Os$ ratio >10), such as those commonly found in eclogitic sulphide inclusions, are much less sensitive to Re-loss and are not included in Fig. 3.10.C for clarity. This predictive aspect of the model can be tested, but we have not assessed the literature data in detail because we do not know whether molybdenite was lost. However, unrealistically old or future age T_{MA} are not uncommon in the literature and it is interesting to note that many of the sulphides that give spurious ages have $^{187}Re/^{188}Os$ ratios that are slightly super-chondritic (<5) or could have started with a slightly super-chondritic $^{187}Re/^{188}Os$ ratio. However, we should make it clear that both robust and spurious model ages have been found for sulphides from a wide range of $^{187}Re/^{188}Os$ ratios. Robust ages may simply reflect a lack of molybdenite loss (or formation) and spurious ages could be explained by an incorrect choice of initial $^{187}Os/^{188}Os$ ratio or a multi-stage history. Clearly, isochron ages are far the best method for dating sulphide inclusions in diamonds, but we note that differential loss of molybdenite can impact on both the age and the initial $^{187}Os/^{188}Os$ ratio derived from the isochron.

We conclude that while the formation of molybdenite and subsequent non-recovery of molybdenite during analyses might not be the only reason for disturbing Re–Os ages, the presence of molybdenite around many sulphide inclusions makes Re-loss a distinct possibility. Our clear recommendation for future work is that Raman investigation of unexposed sulphide inclusions should be an essential precursor to breaking out inclusions for analysis. Raman would show whether molybdenite was present or not and would be the best way to assess whether molybdenite extrusion along cracks had occurred. We note that identification of molybdenite by standard electron beam-based x-ray analysis is surprisingly challenging because Mo K lines are not excited by standard operating conditions (15 kV accelerating voltage) and Mo Lα lines overlay S Kα lines are too close to resolve from by EDS. The use of higher accelerating voltages could also be problematical for thin layers of molybdenite because

of the increased penetration depth of the electron beam. A further test of the presence of molybdenite after careful extraction of the inclusion would be to leach any remaining material from the walls of the diamond and from fractures, and to measure Re in the resulting solution.

3.5. Conclusions

Molybdenite was identified by Raman spectroscopy in 73 out of 80 syngenetic sulphide inclusions in Mir eclogitic diamonds. Molybdenite most commonly occurs as sub-micron-sized grains near the walls of the inclusions and is interpreted as exsolved from originally homogeneous sulphide melts (or MSS) that were encapsulated in diamond over a range of trapping temperatures. Molybdenite often accompanies chalcopyrite, and both are commonly seen inside the decompression fractures surrounding an inclusion, therefore these phases may not be quantitatively recovered during extraction of the sulphide inclusion for Re–Os dating. However, mass balance calculations indicate that molybdenite has a larger inventory of Re relative to chalcopyrite and the non-recovery of molybdenite dominates the budget of Re that is potentially lost from the analyses of the inclusion. This Re-loss may have significant effects on the resultant model ages and potentially induce significant scatter on the isochron ages of the sulphides and host diamonds.

We have modelled the potential effect of molybdenite loss on the Re–Os age systematics of diamond-hosted sulphide inclusions. For ages calculated with the isochron method, different proportions of Re loss from the inclusions would affect the quality of fit of the isochron. Re-loss could lead to unrealistically old or even future model ages being calculated, in particular if the $^{187}Re/^{188}Os$ of the sulphide is slightly super-chondritic.

The presence of molybdenite in diamond-hosted sulphide inclusions is not unique to the Mir eclogitic diamonds. Raman indicates that several other eclogitic and peridotitic diamond-

hosted sulphide inclusions from Argyle, Dachine, Udachnaya, Murowa, Orapa, Letlhakane and Damtshaa also contain molybdenite. In order to militate against the problems identified in this study, we suggest that Raman investigations should precede sulphide extraction for Re–Os dating, in order to identify the presence of any molybdenite and its location within an inclusion in diamond.

.

Chapter 4. The significance of molybdenite in diamond-hosted sulphide inclusions

4.1. Introduction

Molybdenite (MoS_2) is a soft, black sulphide mineral resembling graphite, which was recently shown to be a frequently occurring phase in diamond-hosted sulphide inclusions from different localities (Kemppinen et al., 2018). As the main source of molybdenum (Mo) and rhenium (Re) in nature, molybdenite has been a mineral of scientific interest throughout the 20th century and until present (e.g. Crook, 1904; Dickinson and Pauling, 1923; Hiskey and Meloche, 1940; Hintenberger et al., 1954; Frondel et al., 1970; Padilla et al., 1997) and more recently, for its use in Re-Os dating (e.g. Luck and Allegre, 1982; Suzuki and Masuda, 1990; Stein et al., 1997; 2001; Markey et al., 2007; Wang et al., 2018). The presence of molybdenite can have significant implications for the Re and Os distributions within a sulphide system. Mo is a complex element which can behave as siderophile (iron-loving), chalcophile (sulphur-loving) or lithophile (silicate-loving) element depending on the composition and indirectly, the pressure-temperature conditions of a system (e.g. Lodders and Palme, 1991; Greaney et al., 2018 and references therein). However, molybdenite is a nominally crustal mineral, and therefore, understanding the reasons behind its unexpected occurrence in diamond-hosted inclusions can help constrain some of the controls on the global Mo cycle.

4.1.1. Molybdenum at the Earth's surface

Molybdenum (Mo) has an abundance of ~1.1 ppm by weight in the Earth's crust (Wedepohl, 1995), where it is commonly hosted in molybdenite which can form in a variety of geological hosts including skarn deposits hydrothermal replacement and porphyry copper deposits and granitic pegmatites (e.g. Frondel and Wickman, 1970). As well as being an economically valuable metal, Mo is a biologically essential trace element which plays an important role in nitrogen fixation and the sustenance of complex life (e.g. Egami 1974; Anbar, 2008). Trace element concentrations of sedimentary pyrites have shown variations in Mo concentrations in oceans over time; Large et al. (2014) observed Mo enrichment in oceans c. 0.66 Ga and c. 2.5 Ga, intermittent with marked depletions in marine Mo concentrations (Fig. 4.1). In fact, the appearance of a sedimentary Mo signal in the Proterozoic rock record is broadly associated with the increase in atmospheric oxygen after the first Great Oxidation event (GOE-I; ~2.45 Ga Farquhar et al., 2000; Anbar et al., 2007; Canfield et al., 2013) (Fig. 4.1).

Mo is geochemically versatile; it can form various chemical compounds and can exist in eight different oxidation states (-2 to +6), although the higher oxidation states (+4 and +6) are prevalent in terrestrial settings. Molybdenite is the only significant host of Mo at the surface of the Earth, where oxidation–reduction cycles are the major processes concentrating Mo (e.g. Wang, 2012). Indeed, Mo in organic-rich marine sediments are commonly used as a proxy for the paleo-redox conditions of oceans.

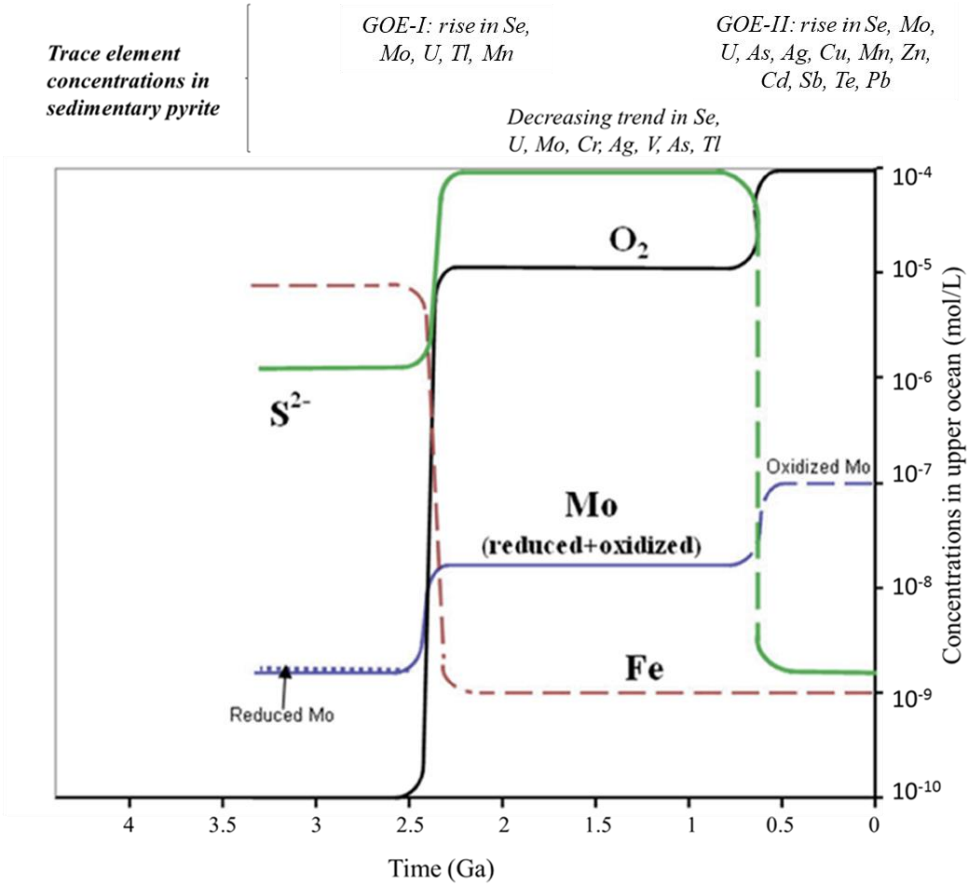

Figure 4.1. Diagram showing the evolution of Mo, S^{2-}, Fe and O_2 concentration in the upper ocean over time, modified from Wang (2012) and the trends in trace element concentrations measured by Large et al. (2014) in a variety of sedimentary pyrites. The appearance of Mo is correlated with that of O_2. GOE-I and GOE-II refer to first and second "Great Oxidation events" at ~2.45 Ga and ~0.66 Ga, respectively.

Figure 4.2 (next page) depicts some of the processes that can mobilise and concentrate Mo in the Earth's surface reservoirs. Oxidative weathering of continental crust (which has been operating since the end of the Archean) supplies Mo to continental margin sediments and into oceans, where it is highly soluble in oxidised fluids as a dissolved molybdate ($Mo^{6+}O_4^{2-}$) species (e.g. Candela and Holland, 1984, Keppler & Wyllie 1991). Owing to its enhanced solubility in oceans under the oxygenated conditions prevailing at the surface of the Earth today, Mo is the most concentrated trace metal dissolved in modern oceans, where it has an 800-million-year residence time (Morris, 1975). Up to 70% of the Mo in modern oceans (Bertine and Turekian, 1973; Morford and Emerson, 1999; Siebert et al., 2006) can be removed

and scavenged into oxic sediments along with metal oxides (McManus et al., 2006); Mo can be adsorbed onto Mn and Fe oxides and oxyhydroxides (e.g. Bertine and Turekian 1973; Manheim 1974; Canfield et al., 2013). MoO_4^{2-} initially dissolved in oxic seawater then undergoes a speciation change to particle reactive MoO_3 (Tossell, 2005).

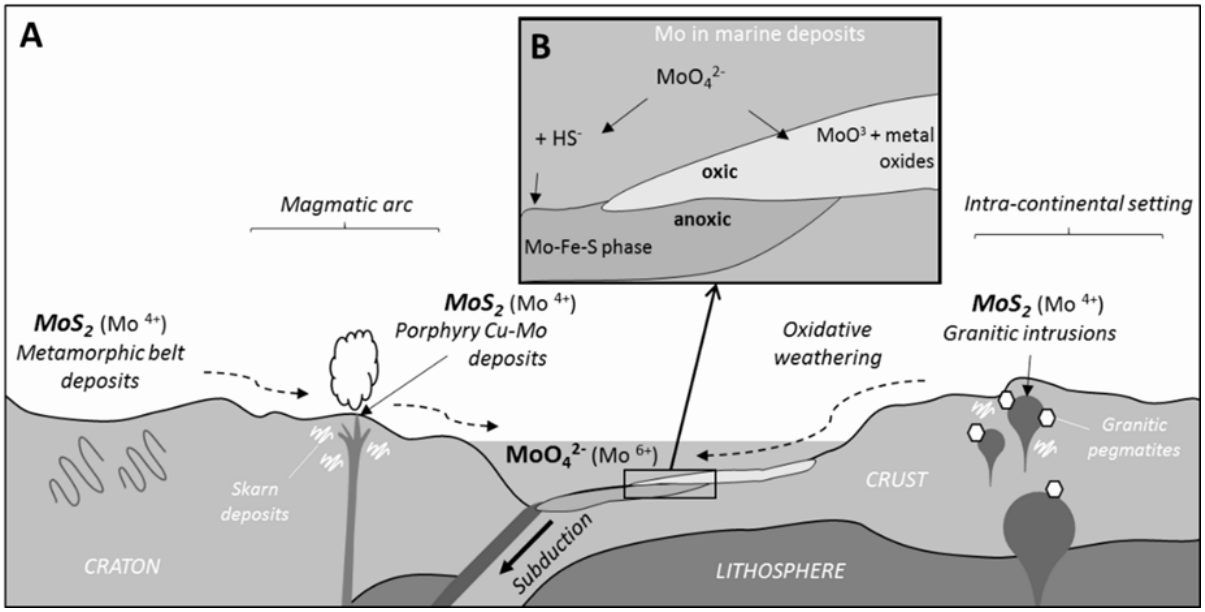

Figure 4.2. Schematic diagram depicting the transport of molybdenum (Mo) from continents to oceans, through oxidative weathering of molybdenite from its crustal sources (e.g. hydrothermal ore deposits). B. Upon release into oceans, sea water-soluble MoO_4^{2-} can be scavenged into oxic or anoxic marine sediments to form MoO_3 associated with Fe-Mn oxides, or metal-Mo-sulphide phases respectively (see text for explanation of process).

Various authors have shown that the availability of sulphur plays a major role in controlling the mobility of Mo, deposition of Mo-sulphides and accompanying reduction of Mo^{6+} to Mo^{4+} in anoxic marine settings. Under such conditions, Mo can also be incorporated into reducing organic-rich sediments in the presence of HS^- (e.g., Bertine, 1972, Berrang and Grill, 1974, Shimmield and Price, 1986, Emerson and Huested, 1991, Calvert and Pedersen, 1993). Under these conditions, soluble MoO_4^{2-} is converted to a thiomolybdate or oxothiomolybdate species (e.g., $MoO_xS_{4-x}^{2-}$ or $MoO_{4-x}S_x^{2-}$; Helz et al., 1996, Erickson and Helz, 2000, Zheng et al., 2000, Vorlicek et al., 2004; Barling et al., 2001), that can be removed from solution by sulphur-

bearing organic material (e.g., Tribovillard et al., 2004) or captured as Mo by Fe-sulphide phases (e.g., Helz et al., 1996, Erickson and Helz, 2000). In fact, in anoxic marine environments, Mo-Fe-S clusters on pyrite (FeS_2) could be an important sink of Mo (Bostick et al., 2003). Furthermore, fluids derived from hydrothermal vents are typically depleted in Mo, likely resulting from its removal from solution as a sulphide (e.g. Trefry et al., 1994).

Mo however is relatively insoluble under the reducing conditions that exist in most marginal or oceanic basins (e.g. Emerson and Huested, 1991; Helz et al., 1996; Morford and Emerson, 1999). Indeed, high Mo concentrations (20 to 160 ppm) relative to crustal abundances levels (~1.1 ppm) have been observed in a variety of anoxic basin sediments (e.g. Francois 1988, Emerson and Huested 1991, Ravizza et al 1991, Crusius et al 1996), implying that Mo is relatively enriched in sediments deposited under oxygen-deficient conditions (e.g. Pilipchuk and Volkov, 1974; Tribovillard et al., 2004). Mo enrichment in ancient pelagic clays and organic-rich sediments (e.g. Zheng et al., 2000, Tribovillard et al., 2004; Poulson et al., 2006) required significant atmospheric oxygen to mobilise Mo, but little to no oxygen in a sulphur-rich deposition environment (e.g. Tribovillard et al., 2004). Such conditions likely started at the end of the Archean, prevailed during Proterozoic times and became rarer at the beginning of the Phanerozoic (Fig. 4.1).

Recently, Li et al. (2019) compared the mineralogy and Mo concentrations of glacial diamictites of different ages to investigate the Mo budget of the upper continental crust (UCC) through time. The authors revealed that sulphides were unlikely to act as the principal hosts of Mo in the UCC prior to the first Great Oxidation event (GOE-I ~2.45 Ga), and that Archean Mo-enriched sedimentary sulphides were instead likely to have formed as a result of isolated episodes of oxidative weathering (brought on by transient increases in atmospheric oxygen) (Li et al., 2019), consistent with previous suggestions (e.g. Anbar et al., 2007; Large et al.,

2014; Lyons et al., 2014; Gregory et al., 2015). Since sulphides typically break down in the presence of oxygen (Williamson and Rimstidt, 1994, Johnson et al., 2019), and Mo-rich sulphides are relatively rare in the pre-GOE1 rock record (e.g. Helz and Vorlicek, 2019), the delivery of Mo to ocean basins is unlikely to have been significant with oxygen-poor atmospheric conditions (Li et al., 2019 and references therein).

4.1.2. Molybdenum in subduction zones

An important source of molybdenum today can be found in subduction-related porphyry Cu-Mo deposits, which supply 95 % of the world's Mo (John and Taylor, 2016). The composition of the material undergoing melting during subduction determines its ability to retain or release Mo (e.g. Casalini et al., 2019). Indeed, much attention has been directed at studying the mobility and behaviour of Mo in subduction zones, in order to better understand the global Mo cycle.

Mo oxides (e.g. MoO_2, MoO_3 or $HMoO_4^-$) can be highly mobile in oxidized, aqueous fluids that are characteristically derived from subducting slabs (e.g. Candela and Holland, 1984, Rusk et al., 2008), where Mo solubility in aqueous fluids is strongly dependent on oxygen fugacity, as well as the salinity of the fluid (e.g. Bali et al., 2012). Ulrich and Mavrogenes (2008) demonstrated that between 500 and 800 °C and at moderate pressures (150-300 MPa), Mo solubility in a fluid was positively correlated with higher temperatures and fluid salinities. Indeed, higher degrees of fluid salinity have been shown to be important for porphyry-type Cu-Mo mineralisation (Rusk et al., 2004). The pH of a fluid has also been shown to control how soluble Mo can be within it; at higher pH, Mo is more soluble (Manheim et al., 1978; Barling et al., 2001).

Under the early oxidising conditions pertaining to porphyry Cu-Mo systems, significant amounts of Mo reside in Ti-magnetite, titanite and biotite (e.g. Piccoli et al. 2000). Bali et al. (2012) observed that Mo then behaves incompatibly with major eclogitic minerals such as garnet and clinopyroxene during subsequent breakdown and/or re-equilibration of Ti-bearing phases and exsolution of an aqueous fluid but would become mostly incorporated in high-temperature residual rutile instead (<14.2 wt.% MoO_3 in rutile) (Bali et al., 2012). Mo^{6+} cannot directly be incorporated into the rutile structure by replacing Ti^{4+} but Mo can behave like other high field-strength elements (HFSE) (e.g., Fitton 1995; O'Neill and Eggins 2002) and replace Ti^{4+} though coupled substitutions as Fe^{2+} Mo^{6+}-Ti^{4+}_{-2} (Candela and Bouton, 1990; Rabbia et al., 2009). The mobility of Mo in subduction zones is likely to be strongly controlled by the presence or absence of rutile in eclogite (Bali et al., 2012) (Fig. 4.3).

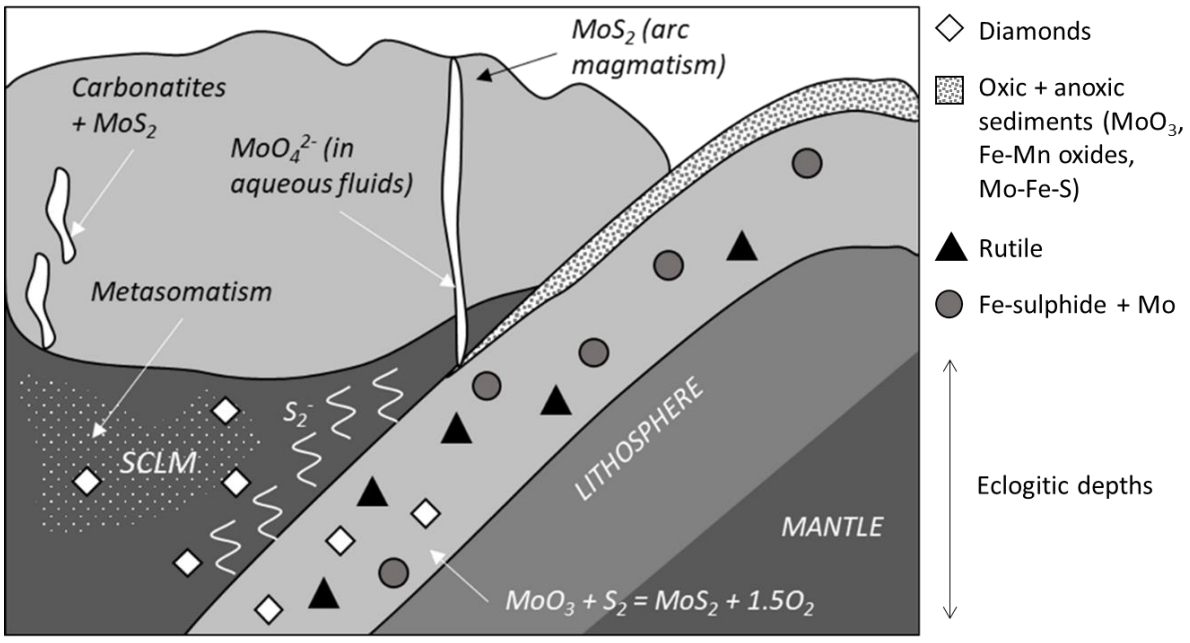

Figure 4.3. Simplified schematic diagram showing the possible pathways for Mo undergoing subduction within rutile-bearing oceanic lithosphere (not to scale). SCLM = sub-continental lithospheric mantle.

It has been commonly proposed that lithospheric mantle having undergone extensive pre-enrichment in Mo, could act as a source of Mo in arc magmatic settings (e.g. Wilkinson 2013). Indeed, König et al. (2008) also observed that Mo and W behaved differently and proposed that some phase (eclogitic rutile or sulphides) capable of selectively retaining Mo could be present in the subducting slab (e.g. Noll et al., 1996; Zack et al., 2002). The Mo stable isotope system provides a powerful tool for tracing surface-derived material entering Earth's interior. The Mo isotope compositions of subduction-related igneous rocks have provided evidence of the selective transfer of isotopically light Mo into the mantle at subduction zones, through its uptake into a fluid phase that is released from the subducting slab (e.g. Freymuth et al., 2015, König et al., 2016, Casalini et al., 2019).

Large variations in Mo concentrations have also been measured in the silicate and oxide phase assemblages in different types of igneous rocks. *High* Mo concentrations have been found in ocean island basalts (OIBs) (in nephelinite samples in particular; average = 4.95 ppm), with lower values reported for mid-ocean ridge basalts (average 0.48 ppm) (Liang et al., 2017). In contrast to MORBs, OIBs have a source enriched in incompatible trace elements, which are indicative of long-term recycling of lithospheric mantle (Galer and O'Nions, 1986) and a subducted oceanic crust material component (Hofmann and White, 1982).

Molybdenite has additionally been observed as a common primary phase in carbonatitic magmas (e.g. Xu et al., 2010; Song et al., 2016). Indeed, high Mo concentrations have been measured in carbonatites and in calcite-hosted fluid inclusions in carbonatitic magmas (<87 ppm and ~17 ppm respectively), implying that Mo enrichment was a primary feature in their formation (e.g. Song et al., 2016). The samples analysed had also been formed in a mantle source which had become enriched through recycled sediment contribution (Song et al., 2016).

Indeed, it was shown that primary carbonatite melts can form through melting of deeply subducted oceanic crust (e.g. Walter et al., 2008; Thomson et al. 2016).

4.1.3. The behaviour of Mo in the mantle

Mo shows geochemical similarities to the light rare-earth elements and is thought to be incompatible during mantle melting (e.g. Newsom and Palme, 1984; Adam and Green, 2006; Willbold and Elliott, 2017), thereby resulting in its relatively high crustal abundance (~1.1 ppm; Wedepohl, 1995). It has been proposed that the Earth's mantle is the major (>80%) repository for Mo in the bulk silicate Earth (BSE), while around 10% is thought to reside in continental crust (Sims et al., 1990; Liang et al. 2017). By volume however, Mo is relatively depleted in the mantle; average abundances of 39-47 ppb (Palme and O'Neill, 2003; Greber et al., 2015) for the primitive mantle, 25-<30 ppb for the depleted mantle (Salters and Stracke, 2004; Wang and Becker, 2018) and 23 ± 7 ppb for the BSE (Greber et al., 2015) have been reported.

4.1.3.1. Redox speciation of Mo

Mo is a highly redox sensitive element and its tetravalent (Mo^{4+}) and hexavalent (Mo^{6+}) oxidation states are the dominant species in igneous settings, although a stable Mo^{5+} valence has also been reported (e.g. Farges et al., 2006). The oxygen fugacity (fO_2) of natural mantle samples is commonly determined in reference to the FMQ (Fayalite-magnetite-quartz) buffer reaction: $\Delta \log fO_2$ (FMQ) = log fO_2 (sample) − log fO_2 (FMQ). At the top of the upper mantle, the oxygen fugacity has been shown to vary between +2 and -3 log. units from the FMQ buffer (e.g. Frost and McCammon, 2008, Stagno et al., 2013). Most lithospheric diamonds have formed above 250 km depth and at oxygen fugacities less than FMQ-1. Under lithospheric diamond-forming conditions, fO_2 typically ranges between FMQ -2 and -4 (e.g. Luth and

Stachel, 2014). Oxygen fugacity then decreases with depth as the mantle becomes metal-saturated (~ >250 km depths; e.g. Shirey et al., 2013). At ~250 km depth (or 8 GPa), fO_2 should be around 5. log units below FMQ (e.g. Frost and McCammon, 2008; Kaminsky et al., 2015). In the lowermost upper mantle (~14 GPa) fO_2 is expected to extend to around 0.8 log units below the iron–wüstite (IW) buffer and decrease with depth. Large variations in oxygen fugacity and unexpectedly high oxidation conditions have however been reported for the lower mantle region of many sub-lithospheric diamonds (Δlog fO_2 above IW buffer e.g. Kaminsky, 2017)

4.1.3.2. The lithophile nature of Mo

It has been shown that the lithophile behaviour of Mo is strongly dependent on oxygen fugacity (e.g. Fig. 4.4). Indeed, over an investigated fO_2 range of Δlog fO_2 (FMQ) -3.1 – +1 under upper mantle conditions, the partitioning of Mo between sulphide (liquid or melt) and silicate melt was found to vary significantly (Li and Audétat, 2012). At high oxygen fugacities (FMQ +1), the partitioning coefficient of Mo between sulphide and silicate doesn't exceed 0.2 (Li and Audétat, 2012).

Previous solubility studies of Mo (occurring as MoO_3) in silicate melts, investigating the effect of oxygen fugacity on the metal-silicate melt partitioning of Mo, determined that the valence state of Mo changes from 6+ (in melt) to 4+ (in minerals) at approximately 1 log unit below the IW buffer (Holzheid et al., 1994, O'Neill and Eggins, 2002; Farges et al., 2006). Mo^{4+} is the dominant species in silicate melts under the conditions at which metallic iron occurs (Holzheid et al., 1994; O'Neill and Eggins, 2002; Wade et al., 2012; Hin et al., 2019). Hillgren et al. (1993) also reported that Mo^{4+} was the stable species in FeO-bearing silicate melts over fO_2 values between IW-1 to IW + 3.5. Farges et al. (2006) observed that at similar oxygen fugacities (between IW and IW–1, at ~10–10.5 atm at 1350°C and 1 bar), Mo^{5+} can also be the

most commonly occurring redox state, in the apparent absence of an important FeO component. Finally, Mo could also exist as metallic Mo (Mo^0) at IW -1 to -5 in the deeper metal-saturated regions of the mantle (e.g. Walter 1995).

The effect of pressure on the behaviour of MoO_3 in silicate melts has been less well studied but is likely to be negligible (Burkemper et al. 2010). In their experiments, Burkemper et al. (2010) measured the MoO_3 content of a basaltic and peridotitic silicate melts at 1800 °C and 2.5 GPa and 2100 °C and 2.5 GPa respectively and found no temperature effect on MoO_3 solubility in silicate melts. Even if temperature a negligible direct effect on the behaviour of Mo in silicate melts, it would partly determine the composition of the melts/fluids, which in turn would affect Mo solubility.

Liang et al. (2017) measured the Mo abundance and isotope composition of 42 mafic and 15 ultramafic samples from a variety of magmatic settings. Mo has been observed to behave incompatibly during differentiation of intraplate basalt magmas (Yang et al., 2015, Greaney et al., 2017) and can dissolve in large quantities in silicate glasses (>5 wt. %) (Stemprok and Voldan, 1974; Farges et al., 2006). Greaney et al. (2017) who showed that while Mo can be incorporated in sulphide minerals hosted in subduction-related plutonic rocks (average 2.6 ppm), and could even sometimes be present in undetectable (small) molybdenite, it is more abundant in basaltic to andesitic volcanic glasses (average 5 ppm) and Fe-Ti oxides such as titanite, ilmenite and magnetite (average 6.4 ppm). In fact, Mo does not always exhibit strong chalcophile behaviour, particularly in primary magmatic systems (e.g. Yang et al., 2015. Greaney et al., 2017).

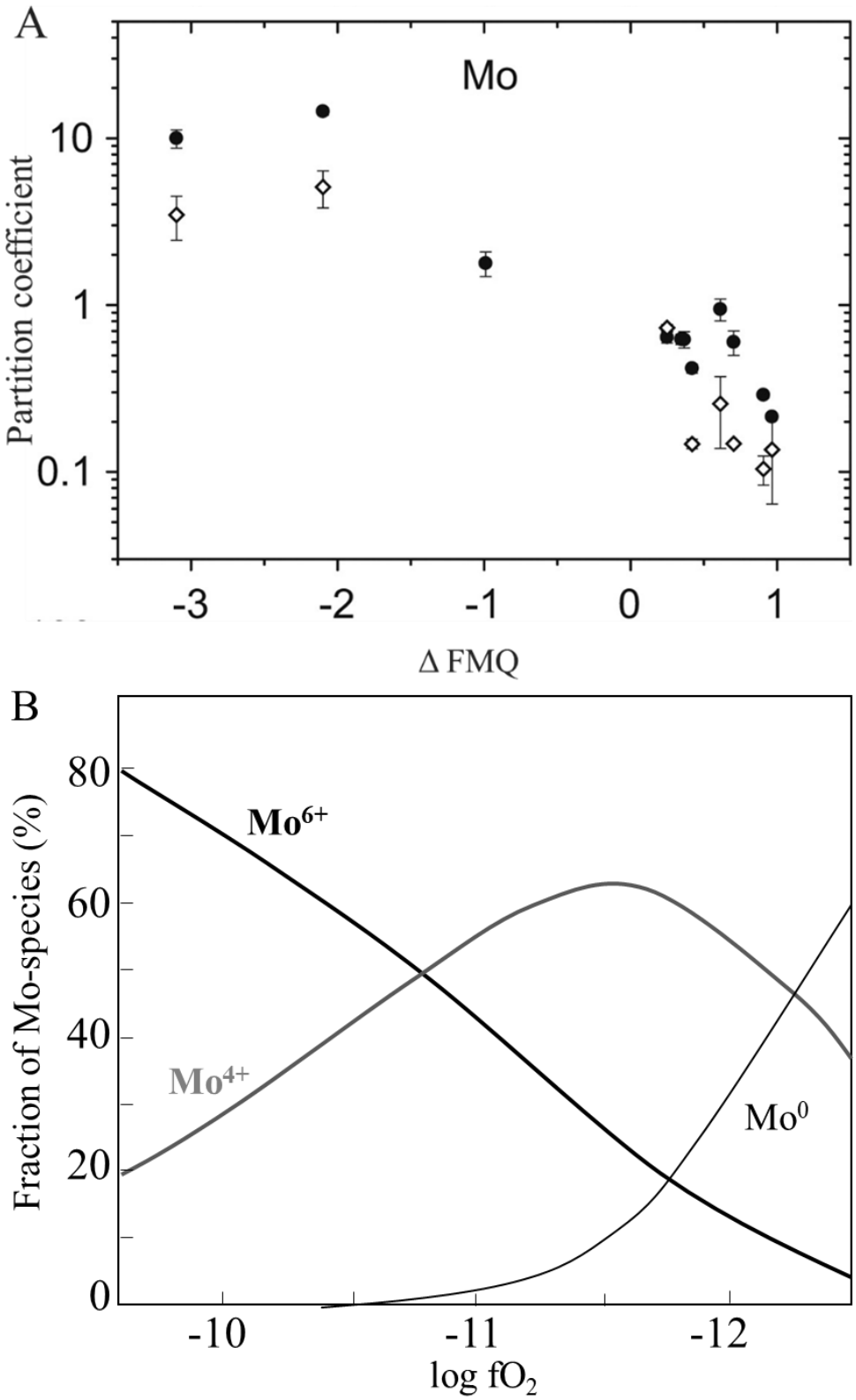

Figure 4.4. A) partition coefficients for Mo between MSS and silicate melt (SM) (black dots) and sulphide liquid and SM (open diamonds) as a function log fO_2 relative to FMQ (from Li and Audétat, 2012) B) Assumed proportions of Mo^{4+}, Mo^{6+} and metallic Mo^0 at 1400°C as a function of oxygen fugacity (log fO_2) (modified from Holzheid et al., 1994)

Relatively low Mo contents have been reported in ultramafic rocks and xenoliths (Liang et al., 2017). However, the mean Mo concentration of 0.19 ppm reported in the ultramafic samples reported by Liang et al. (2017) is higher than would be expected from a typical mantle source, possibly implying that Mo is more abundant in the mantle than commonly thought (e.g. Greber et al., 2015; Wang and Becker, 2018). Alternatively, Liang et al. (2017) proposed that one possible reason for Mo-enrichment of the subcontinental lithosphere source regions of these rocks was the subduction of a fluid-mediated Mo to depth, consistent with previous studies (Siebert et al., 2005, Freymuth et al., 2015, Konig et al., 2016).

4.1.3.3. The chalcophile nature of Mo

In cases where sulphur is readily available, it has been demonstrated that while the siderophile and chalcophile natures of Mo are roughly similar, its lithophile behaviour can be much less (e.g. Kudora and Sandell, 1954; Lodders and Palme, 1991). It has also been suggested that Fe ± Ni ± Cu-sulphide melts could act as repository for Mo in parts of the mantle (e.g. König et al., 2008; Voegelin et al., 2012; Liang et al., 2017). Indeed, at relatively low oxygen fugacities, Mo will readily partition from a silicate phase into a sulphide liquid ($D^{SL/SM}$ = ~5) or MSS ($D^{MSS/SM}$ = ~14.5) (e.g. Fig. 5) (Li and Audétat, 2012). Little is known however, about the Fe-Ni-Cu-S-Mo system at the pressures and temperatures at which diamonds grow (see chapter 3).

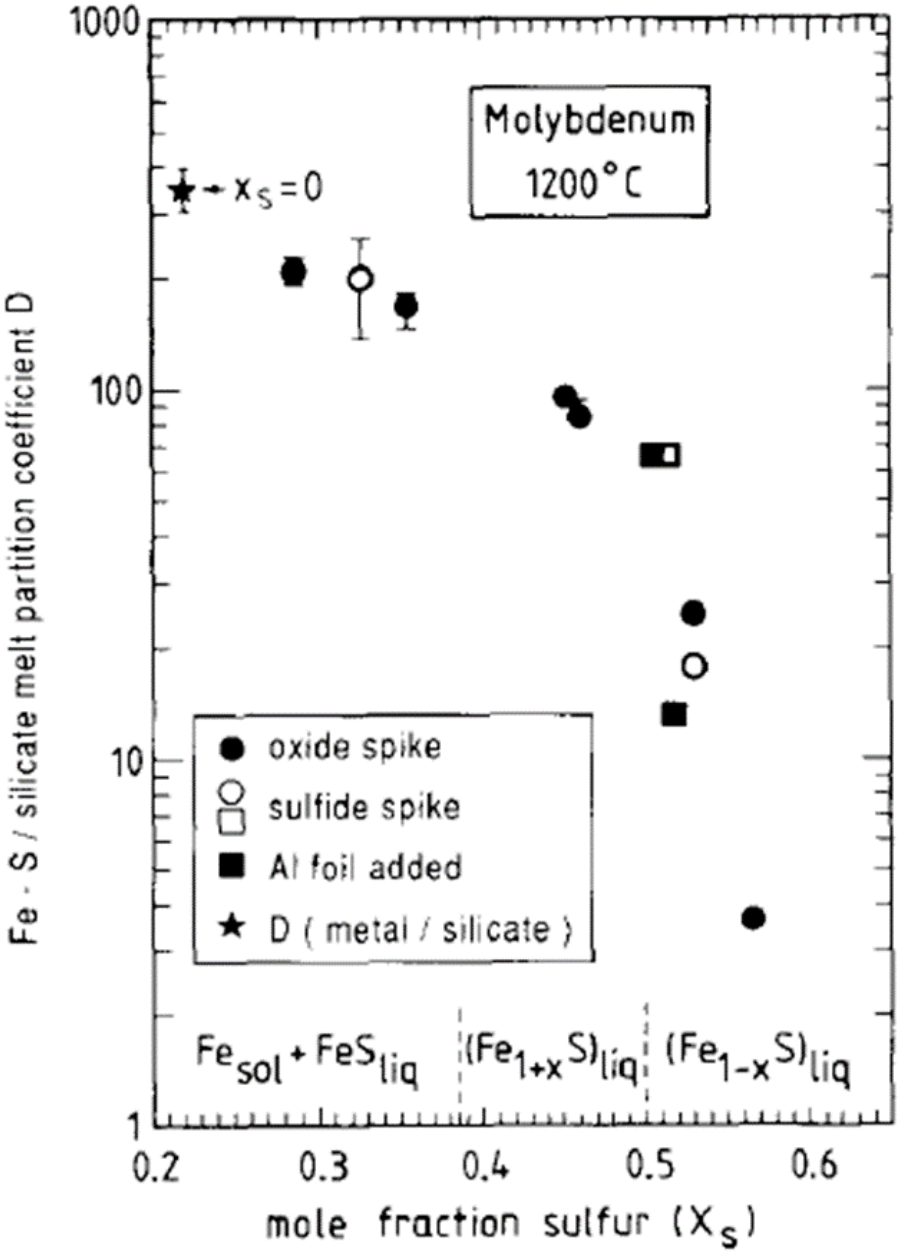

Figure 4.5. Experimental results for Mo partitioning between sulphide and silicate melt at 1200 °C, from Lodders and Palme (1991). The affinity of Mo for an Fe-sulphide phase decreases dramatically when >0.5 mole fraction sulphur is present.

Farges et al. (2006) investigated the structure and stability of different Mo moieties in magmatic systems. Although common magmatic components such as H_2O and halogens were found to have little effect on the behaviour of Mo, it was observed that sulphur occurring as S^{2-} could complex Mo even at moderate oxygen fugacities if sulphur fugacity was sufficiently high to form sulphide groups (S^{2-}), by forming Mo^{6+}=S bonds (Farges et al., 2006). However,

Lodders and Palme (1991) showed that a high (>0.5 mole fraction sulphur) sulphur fugacity (fS_2) decreased the solubility of Mo in a $Fe_{(1-x)}S$ phase. Its Fe content was positively correlated with higher Mo contents (Fig. 4.5) (Lodders and Palme, 1991). It has also been shown that in ore-forming settings, the presence of CO_2 in a Mo-bearing fluid extends the stability field of molybdenite to higher oxygen fugacities (Darling, 1994).

Mengason et al. (2011) observed that during fractional crystallisation within a rhyolitic melt, pyrrhotite, and an immiscible Fe–S–O melt system at ~1042 °C, oxidised felsic melts could lose up to 14% of their initial Mo through its removal within an Fe–S–O melt. No separate molybdenite phase was identified in the experimental run results, and the authors showed that Mo could be hosted in up to 1800 ppm and 5500 ppm concentrations in pyrrhotite and Fe-S-O melt, respectively (Mengason et al., 2011). The depletion of metals such as Mo in arc-magmas, was attributed to its partitioning from a silicate melt into a fractionating sulphide phase, before it could partition into a volatile-rich ore-forming fluid (e.g. Candela and Holland, 1986; Candela and Bouton, 1990, Lynton et al., 1993; Mengason et al., 2011). The main controls on the behaviour of Mo and its incorporation into a sulphide phase are therefore oxygen fugacity, sulphur fugacity and Fe content.

Mo has rarely been reported as a trace element in natural sulphide minerals. Huston et al., (1995) measured 15-95 ppm median concentrations in sphalerite, and several high (540-6740 ppm) concentrations in pyrite grains. Orberger et al. (2003) also analysed high (~ 5000 ppm) concentrations of Mo in sphalerite, while lower values (generally <3.4 ppm) were measured in sphalerite by Cook et al. (2009). In both scenarios, it has been suggested that Mo was likely substituted as Mo^{3+} (originally dissolved in a fluid/melt) into the sphalerite or pyrite lattice (e.g. Evans et al., 1978; Cook and Chryssoulis, 1990; Huston et al., 1995).

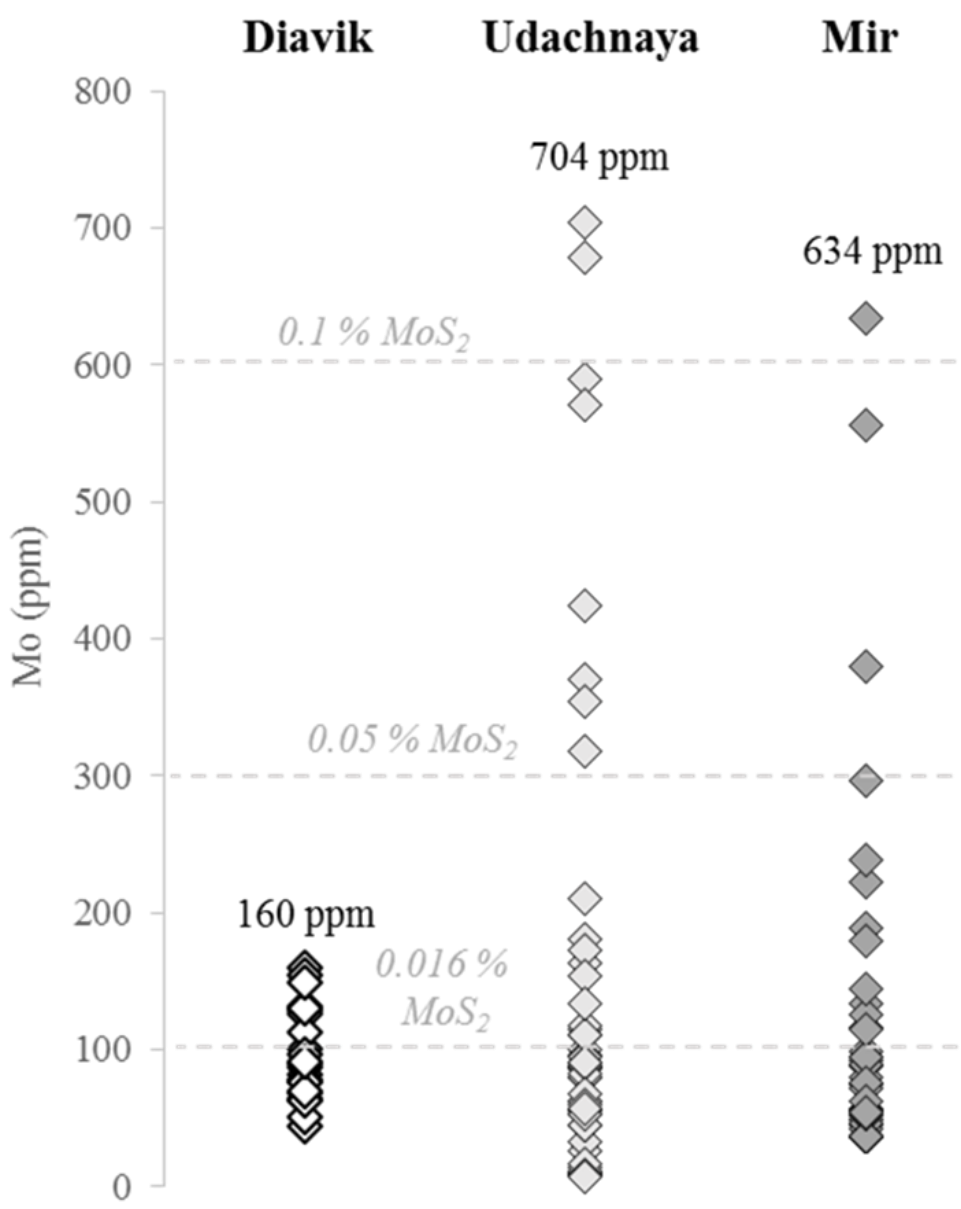

Figure 4.6. Mo concentrations (ppm) measured in diamond-hosted sulphide inclusions from Diavik (Canada), Udachnaya and Mir (Yakutia, Russia) (Aulbach et al., 2009; Bulanova et al., 1996; Wiggers de Vries et al., 2013a). Dashed lines show amounts of molybdenite (MoS_2) that could form at given Mo concentrations.

Despite the common association of chalcopyrite with molybdenite, no literature has been found reporting the Mo content of chalcopyrite, nor the Cu content of molybdenite. Similarly, no Mo concentrations have been analysed in natural mantle-derived pyrrhotite or pentlandite grains. Furthermore, no published work appears to have been published reporting molybdenite as inclusions in primary mantle-derived silicate minerals. However, Davies et al. (2002; 2003)

discovered a bi-mineralic molybdenite-pyrope garnet inclusion hosted in an alluvial diamond from Bingara (New South Wales, Australia). Furthermore, appreciable Mo concentrations have been reported in sulphide inclusions hosted in diamonds from Mir (<634 ppm), Udachnaya (<704 ppm) and Diavik (160 ppm) (Wiggers de Vries et al., 2013a; Bulanova et al., 1996; Aulbach et al., 2012) (Fig. 4.6).

4.1.4. Affinity of Re with molybdenite

Molybdenite has two well-established polytypes, stable 2H (hexagonal) and a less common, metastable 3R (rhombohedral) Mo (e.g. Stein et al., 1998). Though Re contents in 3R polytypes may be higher (Watanabe and Soeda 1981) and a positive correlation between impurities and 3R structure has been noted (Newberry 1979), there is no evidence that molybdenite polytypism affects the Re-Os systematics (Stein et al., 1998; Voudouris et al., 2009; 2013). Molybdenite is the principal host of Re on Earth due to the shared geochemical properties of Mo and Re; both are transition metals of similar atomic size (139 and 137 pm respectively) and can therefore substitute for one another. It has been experimentally determined that molybdenite ca host up to 2.7 wt. % Re substituting for Mo (Drabek et al, 2010). Higher concentrations have nonetheless been reported in natural samples (e.g. 4.2 wt. %; Melfos et al., 2001; 4.7 wt. % Voudouris et al., 2009). However, molybdenite is seldom found to contain more than 0.1 wt. % Re in nature. Upon further saturation in Re, a rare rheniite (ReS_2) phase can form in association with Re-rich molybdenite (e.g. Voudouris, 2009).

Because of the common use of diamond-hosted sulphide inclusions in Re-Os dating of diamond growth events, it is important to understand the source of Mo in Mo-enriched regions of the mantle, the factors controlling the presence of molybdenite, its mode of capture and its effect on the Re budget of a sulphide inclusion in realistic scenarios.

4.2. Samples and methods

4.2.1. Samples

In addition to the 7 Mir diamonds that were studied in Chapter 3, a total of 45 inclusions and one inclusion cloud in 20 sulphide inclusion-bearing diamonds from 6 different localities have been studied. The Mir diamonds are characterised in Chapter 2. Udachnaya diamond plate 3648 has previously been studied in detail (e.g. Bulanova et al., 1996; Pearson et al., 1999).

Seventy-eight whole Argyle diamonds were selected for study at the Rio Tinto (sorting centre in Antwerp), based on the presence within them of inclusions that exhibited dark rosette fractures characteristic of sulphide inclusions. Sixty-eight of those diamonds were subsequently laser-cut into two or three pieces (two off-cuts, or two off-cuts and a plate). Argyle diamond shapes varied between whole, well-defined and clear-brown octa, clear macle shapes and deformed, octahedra. An additional 9 diamonds from a pre-existing collection were also studied. The inclusions studied in these are held in plates or off-cuts of distorted clear octa diamonds, with the exception of one pink diamond. A total of 12 unexposed and 2 exposed inclusions in 10 Argyle diamonds have been studied by Raman.

Fewer samples were studied from other localities. Three Murowa diamond off-cuts from a pre-existing collection were also investigated. The 3 diamonds contain a total of 2 unexposed and 3 partially exposed sulphide inclusions. The 3 exposed sulphide inclusions analysed by Raman in the 3 Murowa samples consist of single inclusions in the centre of clear octahedrally shaped diamonds. Some Dachine diamonds have been studied by Smith et al. (2016). The Dachine diamonds are small (< 1.5 mm) and vary in shape and colour. The 10 studied diamonds contain 13 exposed sulphide inclusions as well as 4 unexposed inclusions. The 8 diamonds from Juina-5, 3 from Collier-4 and 3 from Machado River vary in size and shape. A total of 6 unexposed and 8 exposed inclusions from Juina-5 were studied, alongside 3 inclusions in 3 diamonds from

Collier-4 and from Machado River. The 2 samples from Orapa, 3 from Letlhakane, 2 from Damtshaa and 5 from Jwaneng are not described here. Two whole diamonds from Diavik were also studied by Raman and found to contain at least one sulphide inclusion each.

4.2.2. Methods

All diamonds reported on here were analysed by Raman spectroscopy. The Raman methods employed here and the synchrotron x-ray microtomography (X-CT) technique applied to Mir diamonds 1584, 1591 and 1607 are described in Chapter 3. X-CT data was processed with Image J and/or with the Avizo 8.0 X-CT data visualisation software.

4.3. Results

4.3.1. Raman

4.3.1.1. Yakutian diamonds

Out of all sample suites studied, the Yakutian diamonds from Mir and Udachnaya diamond 3648 contain the most sulphide inclusions (min. 7 inclusions in each). Molybdenite is the most commonly analysed mineral by Raman in this suite, apparently occurring inside all but 4 out of 7 intact sulphide inclusions in diamond 1703. The three inclusions 1703-4, 1703-5 and 1703-6 which contain molybdenite are located within the core/intermediate zone of the diamond (Appendix A). Molybdenite was not identified by Raman in another inclusion in diamond 1700 (inclusion 1700-1; Table A2), but the inclusion had been pre-exposed so the molybdenite may have been polished away.

The Mir diamonds contain few non-sulphide inclusions relative to sulphides. All four silicate inclusions analysed in Mir diamonds 1584i and 1607 occur as bi-mineralic assemblages coexisting with sulphide. Mir diamond 1607 contains three bi-mineralic molybdenite-bearing omphacite-sulphide inclusions in its intermediate growth zone (e.g. Chapter 2, Fig. 2.7.B), and

diamond 1584i hosts an inclusion consisting of coesite and sulphide (chalcopyrite and molybdenite were identified by Raman). Two rutile (TiO_2) inclusions occurring in the core growth zones of diamond 1584 did not contain molybdenite. Molybdenite and anatase (TiO_2) however occur seemingly intergrown together in the centre of Mir diamond 1607 (inclusion 1607-1; Appendix A, fig. A1). The inclusion had been previously exposed by polishing, although no healed fractures had observed between it and the outside of the diamond.

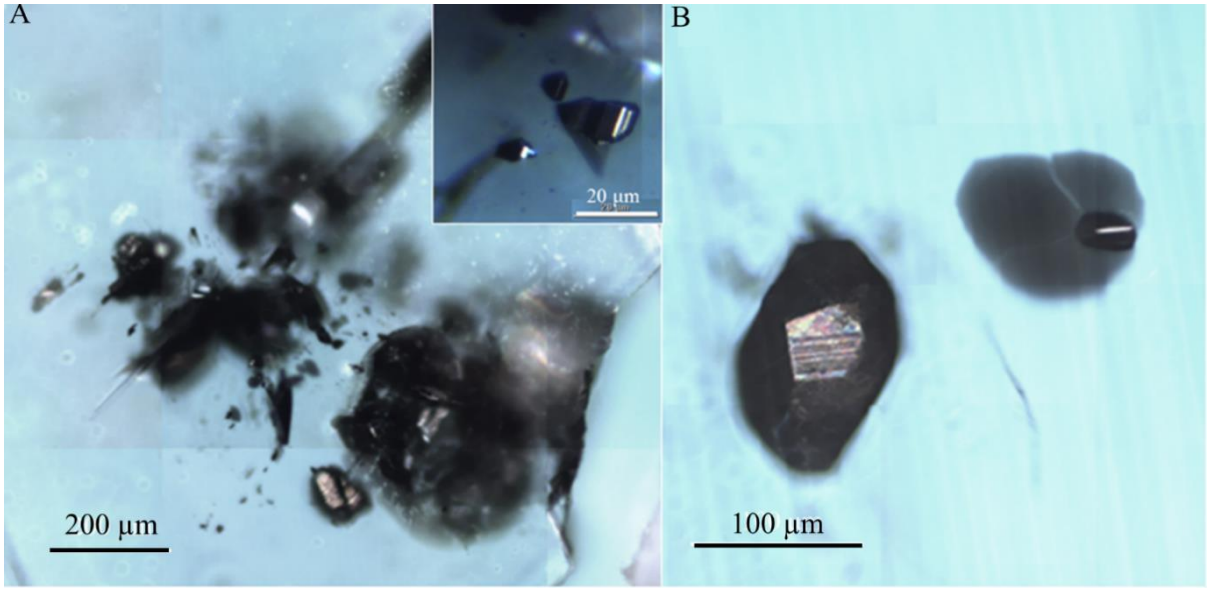

Figure 4.7. A) Raman optical image of the central molybenite-bearing inclusion cluster in Udachnaya diamond 3648 and inset, a close-up of some molybdenite-bearing sulphide inclusions within the cluster. B) Raman optical image of two neighbouring sulphide inclusions occurring in the outer growth zones of diamond 3648 (intermediate part of the central plate). One inclusion (left) has a large rusty-looking euhedral body, and the other inclusion (right) is smaller, more rounded and surrounded by flat rosette fractures.

Diamond 3648 from Udachnaya contains distinctive-looking sulphide inclusions distributed from its core and rim growth zones (e.g. Figs. 4.7.A and 4.7.B). Raman reveals that the core region of the diamond-plate contains an inclusion cluster consisting of olivine and sulphide (molybdenite). Chalcopyrite was not observed by Raman, nor were pyrrhotite or pentlandite. Two unexposed sulphide inclusions occur in the intermediate and two in the rim growth zones of the diamond. Molybdenite was only analysed in two of these, where it forms in single discreet points.

4.3.1.2. Argyle diamonds

21 diamonds from Argyle were found to contain 26 probable sulphide inclusions (only 18 of which yielded a diagnostic Raman signal for chalcopyrite and/or molybdenite). The sulphide inclusions hosted in Argyle diamonds can exhibit different appearances, varying in size (~50 µm - ~120 µm) and shape (e.g. fig. 4.8). Some inclusions display the characteristic rosette-like fracture systems extending from the inclusion body (e.g. Fig. 4.8.A), but in some diamonds, the inclusions lack fractures altogether (e.g. Fig. 4.8.B). Nonetheless, when a Raman signal could not be obtained, sulphide inclusions were identified by the sub-angular shape of the inclusion body and its opacity when viewed in transmitted light.

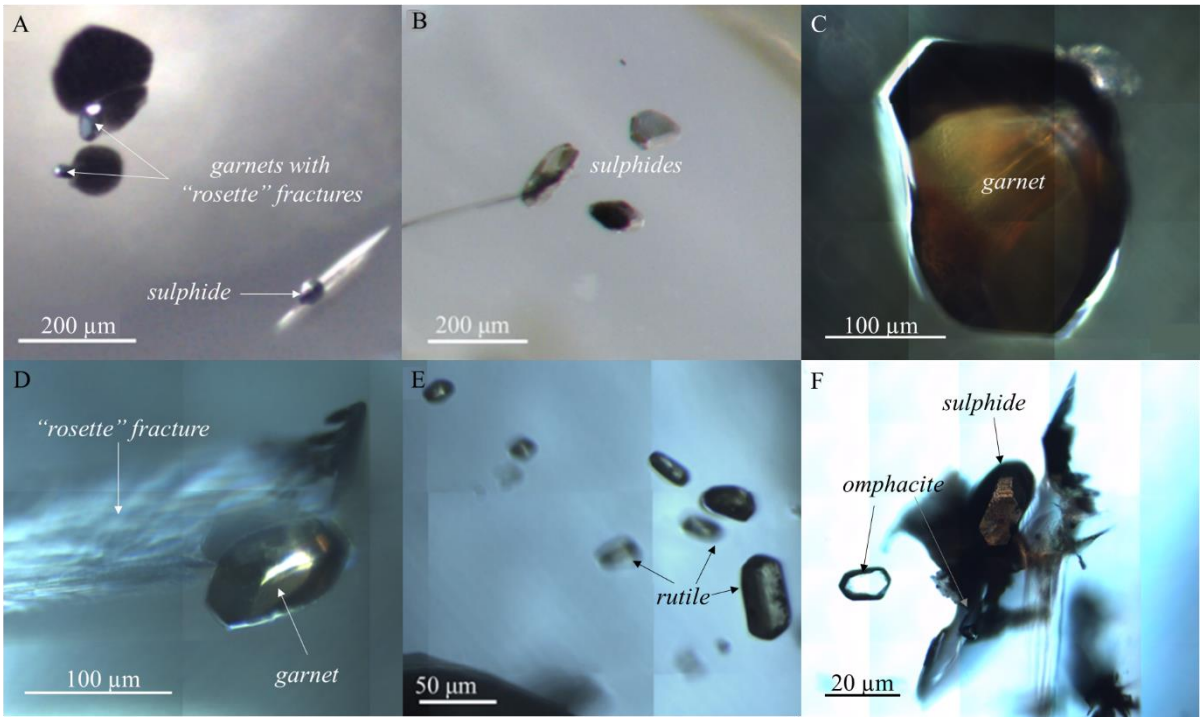

Figure 4.8. Optical Raman images of Argyle diamonds A) L40-1 showing two colourless garnet inclusions surrounded by dark rosette fractures, and one sulphide inclusion with fractures orientated along a different crystallographic plane; B) 104 showing one partly exposed (centre) and two unexposed sulphide inclusions which lack characteristic rosette fractures; C) an orange garnet inclusion in diamond L45-2; D) a garnet inclusion with rosette-like fractures extending from its body in diamond L30-1; E) a cluster of elongated rutile inclusions in diamond L38-C and F) clear omphacite inclusions occur near a euhedral sulphide inclusion in diamond L45-1.

Sulphide inclusions in Argyle diamonds are not always accompanied by silicate minerals in the same diamonds. In all Argyle diamonds studied by Raman, garnet was the most commonly analysed inclusion (>60% of diamonds), and most frequently encountered silicate inclusion in sulphide-bearing diamonds (~20% of diamonds; e.g. 4.8.A, C and D), followed by rutile (e.g. Fig. 4.8.E) and omphacite (Fig. 4.8.F). Several silicate inclusions in diamonds from Argyle contain rosette-like fracture systems (e.g. Fig. 4.8.A and D), but their inclusion body is sub-transparent in transmitted light illumination and often emits a diagnostic Raman signal. Occasionally, oxide minerals such as rutile, which occur as inclusions in >10% of studied diamonds, can appear opaque, but they generally exhibit a more euhedral shape than the sulphide inclusions observed (e.g. Fig. 4.8.C), as well as frequently being Raman active. Molybdenite occurs in at least 15 out of 26 studied sulphide inclusions in 21 Argyle diamonds. It can form as a disseminated phase at the edges of the inclusion body (e.g. Fig. 4.9.A) or as a single, discreet points, confined to one end of the inclusion (e.g. Fig. 4.9.B)

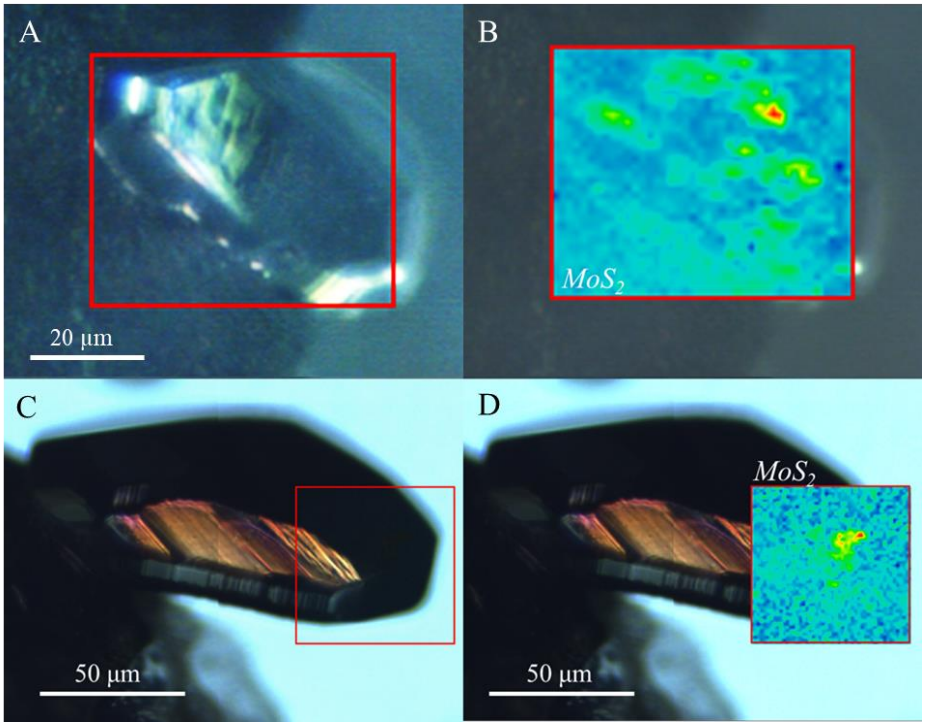

Figure 4.9. Optical Raman images (A, C) and peak height Raman maps (B, D) showing the distribution of molybdenite (MoS_2) in sulphide inclusions from Argyle diamonds L26-1 (A, B) and L17-C (C, D).

4.3.1.3. Diamonds from Dachine and other localities

Inclusions in 10 diamonds from Dachine, 4 from Murowa, 14 from the three sub-lithospheric localities (Juina-5, Collier-4 and Machado River) are described here. The two Diavik diamonds where molybdenite is reported here are whole stones, and no further observations other than the presence of a Raman signal for molybdenite could be made without a polished diamond window.

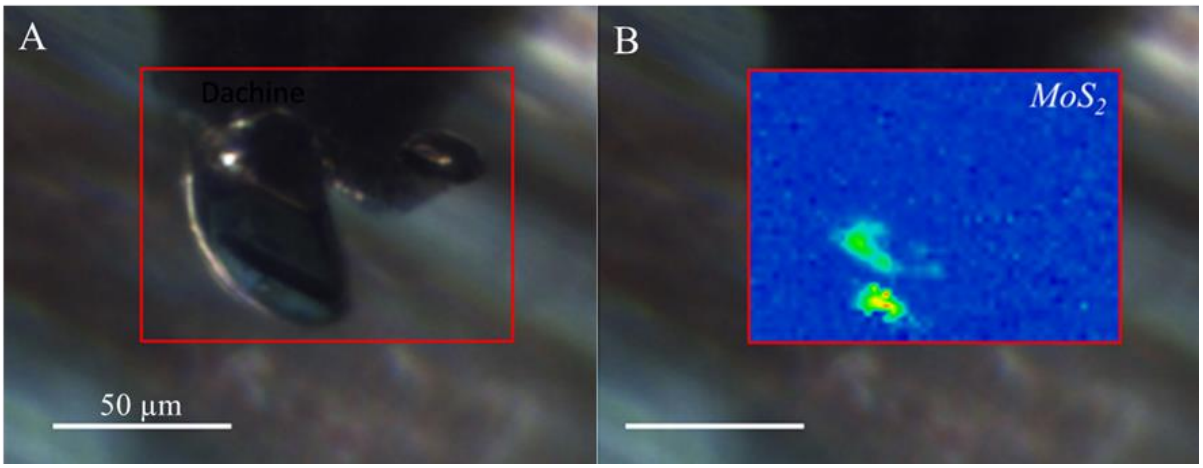

Figure 4.10. Dachine diamond Dac-BS-4A-5 contains a molybdenite-bearing sulphide inclusion located near the "edge" of the diamond (A, B). Optical Raman image (C) and peak height Raman maps (D) show the distribution of molybdenite (MoS_2) within the inclusion

.

Diamonds from Dachine were found to contain molybdenite in 3 out of 4 unexposed sulphide inclusions. After sulphides and graphite, the most commonly found inclusion type was spessartine garnet (hosted in 2 sulphide inclusion-bearing diamonds). In 2 out of 3 diamonds, the molybdenite-bearing inclusions are located near the edge of the diamond (e.g. Fig. 4.10.A). In the inclusions, molybdenite is commonly confined to one end of the inclusion and is not always encountered in sulphide inclusions adjacent to one another (e.g. Figs. 4.10.B and 4.10.C).

4 out of 5 sulphide inclusions in 3 peridotitic diamonds from Murowa were found to contain molybdenite. In each case, the sulphide inclusions are in the centre (presumed core region) of the diamond (Fig. 4.11.A). Molybdenite is seemingly dispersed across the inclusion body and diamond (Fig. 4.11.B and 4.11.C).

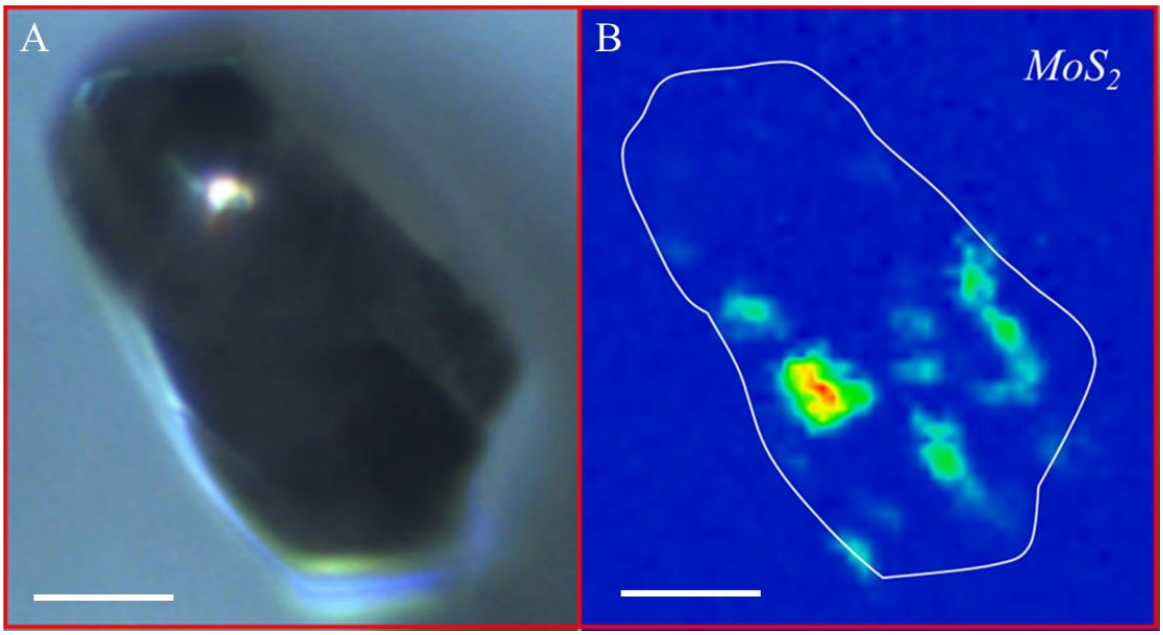

Figure 4.11. Optical Raman images (A) and peak height Raman map (B) showing the distribution of molybdenite (MoS_2) in an unexposed diamond-hosted sulphide inclusion from Murowa (Zimbabwe) (Mur D13). Scales = 10 µm

10+ sulphide inclusions in 8 sub-lithospheric diamonds from Juina-5, 3 in 3 diamonds from Collier-4 and 3 in 3 diamonds from Machado River were analysed by Raman. Molybdenite was only identified as a single small (<10 µm) unexposed inclusion in Juina-5 diamond Ju5-03. The inclusions hosted in this diamond include a former Ca-perovskite and a calcite inclusion (Chapter 2, Figs. 2.12 and 2.13). In the Juina-5 diamonds, sulphide inclusions are typically small (<25 µm) and pyrite and chalcopyrite were the most commonly analysed minerals in these. Molybdenite was not identified by Raman in any inclusions in Collier-4 or Machado River diamonds.

4.3.2. X-CT (x-ray tomography)

Synchrotron x-ray microtomography of inclusion an Mir diamond 1607 shows a brighter phase (Fig. 4.12.A) within the sulphide inclusion. Pyrrhotite has an average density of 4.61 g/cm^3, whilst molybdenite is significantly denser and should therefore appear brighter in the CT image (~5 g/cm^3). The dark rim that is seen in the image is interpreted in chapter 2. Pentlandite has a density of 4.95 g/cm^3, whilst chalcopyrite is likely the less dense phase (4.19 g/cm^3) occurring adjacent to the bright veinlet. Molybdenite is also observed by X-CT in a bimineralic omphacite-sulphide inclusion (1607-5). Figure 4.12.B shows that molybdenite also appears to form at the contact between higher density sulphide and lower density omphacite. Both inclusions shown in figure 4.12 also exhibit a low-density rim at their edges, a feature which is discussed in Chapter 2.

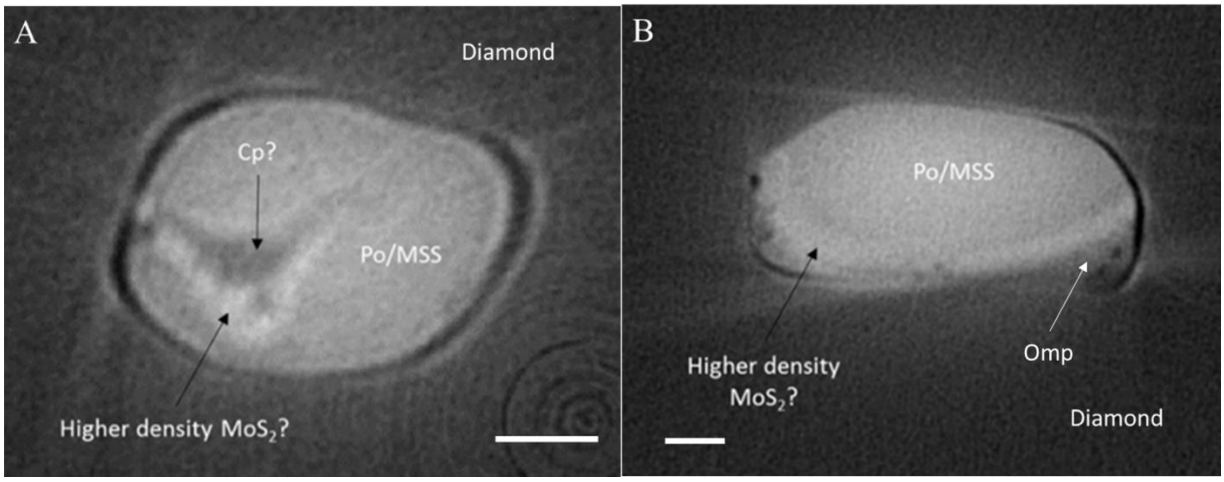

Figure 4.12. Synchrotron x-ray microtomography (X-CT) of sulphide inclusions from Mir diamonds show a higher density (brighter) phase likely corresponding to molybdenite (MoS_2) inside a sulphide inclusion in diamond 1584-i (A) and in diamond-hosted inclusion 1607-5 (B). Inside the inclusion in diamond 1584-i, molybdenite likely coexists with lower density chalcopyrite (Cp) in sulphide (Po/MSS) whilst inclusion 1607-5 is a bimineralic inclusion consisting of omphacite (omp) and sulphide. Scales = 5 µm

4.4. Discussion

4.4.1. Origin of molybdenite in diamond-hosted inclusions

Mo can have siderophile, chalcophile and/or lithophile affinities. The presence of molybdenite in diamond-hosted sulphide inclusions implies that the mantle source region of the diamonds was enriched in Mo, although the reasons for this are unclear. Table 4.1 provides a summary of the parageneses, ages and conditions of growth of diamonds belonging to the same suites as the ones that were studied.

4.4.1.1. Surface-derived origin

Molybdenite is not a common phase in mantle-derived sulphide inclusions and has so far only been identified as a primary sulphide in diamonds and carbonatite magmas (e.g. Davies et al., 2002; Song et al., 2016). Carbonatite magmas are associated with subduction, and it has been shown that a redox reaction between carbonatitic melt and sulphide-bearing eclogite could lead to diamond formation (Jacob et al., 2011). The high concentrations of Mo in the mantle required to form molybdenite may therefore arise through enrichment by a surface-derived fluid or melt component and/or conditions that are specific to the formation of diamond (e.g. Bulanova et al., 1995; 1996; Wiggers de Vries et al., 2013a).

Diamonds from Mir and Udachnaya – in which molybdenite is arguably most common – were formed under changing P-T-fO_2 conditions and were derived from a fluid that was temporally changing in composition (Harte et al., 1999, Hauri et al., 2002, Smart et al., 2011; Wiggers de Vries et al., 2013a; 2013b). Nucleation of Yakutian diamonds was shown to have occurred in the presence of a volatile-rich silicate fluid or melt which was also enriched in HFSEs and accompanied by a carbonatitic component (e.g. Bulanova et al., 1998). It has also been shown that Fe-Ni sulphides melts were an important component of the Yakutian diamond-forming

media, although at Udachnaya, diamond growth primarily from immiscible sulphide melts has been contended (e.g. Anand et al., 2004).

Eclogite xenoliths at Mir and Udachnaya sample ancient subducted oceanic crust (e.g. Anand et al., 2004). High thermal gradients in the Archean are thought to have caused decarbonation or carbonate melting of subducted lithosphere at relatively shallow depths (Dasgupta and Hirschmann, 2010). It has therefore been proposed that organic carbon-rich subducted material entering the diamond stability field was more abundant in the Archean (prior to the first Great Oxidation event, GOE-I). It is however unclear whether significant changes in composition of subducted material and resulting diamond forming reactions occurred after the GOE.

The close association of molybdenite and anatase in the central growth region of Mir diamond 1607 points to a possible link between Mo and a TiO_2 phase hosted in eclogite, which was subsequently metasomatised by sulphide melts. The mineral inclusions observed by Bulanova et al. (1998) in the central growth zones of Yakutian diamonds indicated diamond growth under reducing conditions, with fO_2 being controlled by the iron-wüstite (IW) equilibrium. In fact, Goncharov et al. (2012) also found that all Udachnaya garnet peridotites they studied plotted between the IW and wustite-magnetite (WM) buffers, whilst diamondiferous eclogites from Mir and Udachnaya plotted near the WM buffer equilibrium, supporting Yakutian diamond formation in a reduced environment where Mo occurs as sulphide-favoured Mo^{4+}.

.

Table 2.1. *Summary of characteristics of studied diamonds and their formation media (caption on next page).*

Location	Type	Diamond ages (Ga)	Host	Eruption age (Ma)	Fluids	Oxygen fugacity/log fO_2	Subducted carbon?	Depth (km)	T (°C)
Argyle	E (?)	1.58-1.18	lamproite	1180	Silicic-hydrous	WM - IW	Yes	150-280	1100-1500
Collier-4	SD (?)	~0.1	kimberlite	93	Oxidising C-O-H/mixed	FMQ – FMQ -3	Yes	300-700 (SD)	1,170–1,300
Dachine	E	n/a	komatiite-boninite	1900	Carbon-saturated liquid	low oxygen fugacity	Yes	200-250	800-1000
Damtshaa	E	n/a	kimberlite	93	C-rich (C-O-H, carbonatite)	-	Yes	190	1000-1100
Diavik	P	3.5-3.3, 2.1-1.8	kimberlite	53	carbonatitic-saline	FMQ -3.8 to FMQ +1	Yes	145	1100-1200
Juina-5	SD	~0.1, 0.6	kimberlite	92-95	Oxidising C-O-H/mixed	FMQ – FMQ -3	Yes	>410 (SD)	1411-1534
Jwaneng	E	1.54	kimberlite	240	Carbonatitic-hydrous	WM-IW	Unclear	150-225	<1000-1150
Letlhakane	E	0.25, 1.1, 2.33	kimberlite	93	-	-	Yes	210	n/a
Machado River	SD (?)	n/a	alluvial	n/a	Oxidised CO_2/carbonate	n/a	Yes	>230	1050-1250
Mir group 1	E	2.1	kimberlite	360	Light carbon-rich	FMQ -3 to FMQ -5	Yes	~180	1075-1175
Mir group 2	E	1-0.9	kimberlite	360	Protokimberlitic carbonate–silicate	FMQ -3 to FMQ -5	No	~120	1100-1180
Murowa	P	>3.3	kimberlite	538	LREE, K, P, H_2O and carbonate-rich	-	Likely	~200	1030-1250
Orapa	E	2.1-1, 0.99, 0.14, 1.1, 1.7	kimberlite	93	Carbonatitic-hydrous	-	Yes	~160	-
Udachnaya	P	3.5-3.1 Ga, 2-1.8	kimberlite	367	Carbonatitic - saline	FMQ -0.9 to FMQ-3.4	Yes	150-200	1150-1166

Table 4.1. (Continued from previous page) *Characteristics of the diamonds which have been analysed by Raman so far for the presence of molybdenite, obtained from literature: Argyle – Jaques et al. (1986; 1990), Richardson (1986), Pidgeon et al. (1989), Richardson et al. (1990), Liu et al. (1990), Burgess et al. (1992), Honda et al. (2012); Collier-4 – Bulanova et al. (2008; 2010), Walter et al. (2008; 2011), Kaminsky et al. (2009; 2010), Smith et al. (2010), Araujo et al. (2013), Burnham et al. (2015); Dachine – Capdevila et al. (1999), Cartigny (2010), Smith et al. (2016); Damtshaa – Deines et al. (2009), Ickert et al. (2013), Gress et al. (2017); Diavik – Klein-BenDavid et al. (2004; 2007), Tomlinson et al. (2006), Donnelly et al. (2007), Aulbach et al. (2009), Van Rythoven et al. (2009); Juina-5 – Harte et al. (1999), Kaminsky et al. (2001), Hayman et al. (2005), Brenker et al. (2007), Walter et al. (2011), Bulanova et al. (2010), Araujo et al. (2013), Thomson (2014), Thomson et al. (2014; 2016); Jwaneng – Burgess et al. (1992), Schrauder et al. (1994a; 1996), Gurney et al. (1995), Deines et al. (1997), Cartigny et al. (1998), Richardson et al. (1998; 2004), Shirey et al. (2002), Stachel et al. (2004), Honda et al. (2004; 2011), Thomassot et al. (2009; 2017), Gress et al. (2018), Davies et al. (2018); Letlhakane – Shirey et al. (2002; 2003), Deines and Harris (2004), Deines et al. (2009), Timmerman et al. (2017), Gress et al. (2017) ; Machado River – Bulanova et al. (2008), Schmitz et al. (2012), Burnham et al. (2015; 2016); Mir –Bulanova et al. (1995; 1996; 2014), Garanin et al. (1990), Sobolev et al. (1991; 1998; 2004), Rudnick et al. (1993), Griffin et al. (1993), Taylor et al. (1998), Wiggers de Vries et al. (2013a); Murowa – Klein-BenDavid et al. (2009), Smith et al. (2004 ; 2009), Bulanova et al. (2012), Moss et al. (2013); Orapa – Gurney et al. (1984), Chaussidon et al. (1987), Deines et al. (1991; 1993; 1995; 2004); Burgess et al. (1992; 2004), Cartigny et al. (1999), Farquhar et al. (2002), Shirey et al. (2002; 2008), Phillips et al. (2004; 2008), Stachel et al. (2004), Timmerman et al. (2017; 2018); Udachnaya – Rudnick et al. (1993), Taylor et al. (1995), Bulanova et al. (1995; 1996; 2003), Pearson et al. (1998; 1999), Hauri et al. (1998). The localities where molybdenite has not been observed are shaded. SD = super-deep samples. – indicates that no straight-forward data was found in literature.*

It is conceivable that some Mo was subducted as Mo^{6+} into the diamond-forming regions as MoO_3 incorporated in a TiO_2 phase, which upon interaction with sulphide melts in the upper mantle, partitioned into the sulphide melt/MSS. Alternatively, Mo may also have been subducted into the diamond-forming region as surface-derived sulphides preconcentrated in trace metals. Large variabilities in $\delta^{13}C$ which are commonly observed in eclogitic diamonds can arise from various processes at the surface, which require oxygen. Because of the close association of Mo and oxygen at the surface of the Earth over time, observing strictly recycled $\delta^{13}C$ values for diamonds which host molybdenite-bearing sulphide inclusions could therefore help constrain whether Mo and carbon were derived from the same source.

4.4.1.2. Mantle origin

Knowledge about the Mo budget of the mantle is likely limited by the paucity of pristine samples from the mantle, and the complexity of the factors controlling its behaviour in the mantle. Two distinctive groups of sulphide-bearing diamonds have been characterised in literature. An older generation of Mir diamonds (Group 1) were formed from low $\delta^{13}C$ fluids/melts derived from subducted oceanic crust ~2.1 Ga, while a younger population of diamonds (Group 2) contain mantle-like $\delta^{13}C$ values and their growth was related to later magmatic activity in the local lithosphere ~0.9 Ga (Wiggers de Vries et al., 2013a; Bulanova et al., 2014) (Table 4.2).

The central plate of Mir diamond 1703 was studied by Bulanova et al. (2014) and was shown to have grown in a two-stage model; the core portion of the diamond has depleted $\delta^{13}C$ values (-16.6 ‰) whilst the intermediate and rim zones have more mantle-like $\delta^{13}C$ compositions (-6.8 ‰). The diamond therefore samples the separate growth events which formed the Group 1 and Group 2 diamonds. The absence of molybdenite in inclusions 1703-1, -2, -3 and -7 could be coincidental. Alternatively, it could reflect on a different composition and/or origin of the diamond-forming fluid.

Molybdenite is relatively common in komatiitic diamonds from Dachine, where it occurs in 3 out of 4 unexposed inclusions. The Dachine diamonds were shown to have grown in a metal-enriched environment, as well as exhibiting a clear signature of Early Proterozoic subduction (Smith et al., 2016). In peridotitic diamonds, molybdenite occurs inside at least 4 sulphide inclusions in 3 peridotitic diamonds from Murowa, at least 2 in 2 diamonds from Diavik and is abundant in inclusions in Udachnaya diamond 3648. The lithospheric mantle source region of the Murowa, Diavik and Udachnaya diamonds has been shown to be highly depleted (e.g. Smith et al., 2009; Creighton et al., 2008; Pearson et al., 1999).

Mo, as a typically incompatible element (e.g. Newsom and Palme, 1984; Greaney et al., 2017) is therefore not expected to be enriched in these regions of the mantle. Mo occurring as MoS_2 in diamond-hosted sulphide inclusions could therefore derive from the mantle, only if there is another mechanism other than subduction of oceanic crust (e.g. changing fO_2 and fS_2 conditions), locally concentrating in the diamond-forming region. Alternatively, the P/T path of the sulphide inclusions during their cooling and unmixing could determine whether MoS_2 is crystallised or remains in the bulk of the MSS (Chapter 3 discussion), but to begin to answer these questions, the bulk Mo concentrations of inclusions where MoS_2 is identified by Raman and those where it is absent need to be compared.

4.4.2. Apparent absence of molybdenite

In addition to the four out of seven sulphide inclusions in Mir diamond 1703 where molybdenite was not found, molybdenite was not identified in 7 inclusions in 5 diamonds Jwaneng (Botswana), 3 inclusions in 3 diamonds from Collier-4 or 3 inclusions in 3 diamonds from Machado River (Juina Area, Brazil). Possible reasons for this are considered below.

First, the possibility of a sampling bias is discussed. Then, a scenario is considered where molybdenite is a common occurrence in the sulphide inclusions of many diamonds, and where Mo was a common component of Proterozoic oceanic crust that was subducted into the diamond-forming regions of the Earth's mantle. Geological reasons for the absence of molybdenite in diamonds from Jwaneng and from the Juina area are then proposed.

4.4.2.1. Sampling bias

The apparent absence of molybdenite in diamonds from these localities could be explained by a sampling bias. Compared to the Argyle, Dachine, Siberian and the sublithospheric suite diamonds, not as many sulphide inclusions were studied from the Botswanan diamonds,

including Jwaneng. The sublithospheric diamond-hosted inclusions in turn are generally smaller inclusions (<~25 μm) hosted in smaller diamonds, and additionally 8 of the 14 inclusions studied from Juina-5 had been pre-exposed by polishing. It is therefore possible that molybdenite could be present in sulphide inclusions from Jwaneng and sublithospheric diamonds and has simply not been found. It is also possible that the molybdenite-bearing sulphide inclusions in the studied sample set are anomalous among the global diamond-hosted sulphide inclusion population.

4.4.2.2. Incorporation of Archean sulphides

Thomassot et al. (2009) determined the sulphur isotope compositions of their sulphide inclusions, observing a sulphur mass-independent fractionation (S-MIF) signal which indicated that Archean sulphide material had been captured into the relatively younger Jwaneng diamonds. The S-MIF signature disappears in the rock record after the first Great Oxidation event (GOE-I) ~2.45 Ga (e.g. Farquhar et al., 2000), coinciding with the appearance of Mo in sedimentary material at the surface. If molybdenite has a subducted oceanic crust origin (e.g. hosted in a sulphide phase), we would not expect to see it before the GOE-I – the point before which molybdenite was not being weathered oxidatively and released into the oceans, and ultimately subduction zones.

Molybdenite occurs in the same growth region as two of the inclusions in Udachnaya diamond 3648 which were assigned a mid-Archean Re-Os isochron age (Pearson et al., 1999) and some inclusions in this diamond also contained appreciable Mo concentrations (<~700 ppm; Bulanova et al., 1996). If the diamond growth event of 3648 first began around 3.1-3.5 Ga (Pearson et al., 1999), the molybdenite it hosts is unlikely to have had a sedimentary sulphide origin, and the absence of molybdenite in Jwaneng sulphide inclusions cannot be accounted for by the age of the subducted material or the sulphide. Instead, Thomassot et al. (2009) showed

that Jwaneng diamonds were crystallised from a mantle-derived carbon-bearing fluid. Therefore, the source and nature of the fluid could control its Mo budget.

4.4.2.3. Different diamond-forming reactions

Lodders and Palme (1991) showed that the partition coefficient of Mo between Fe-sulphide and silicate melts around 1200 °C (GPa) increased with increasing Fe content of the system and decreased dramatically with increasing S content (Fig. 4.5). The sublithospheric diamonds were formed by the interaction of oxidised (C-O-H) fluids and, surprisingly, also contain numerous pyrite (FeS_2) inclusions. This implies that one possible reason for the absence of Mo in at least some sub-lithospheric diamonds could be that they were formed under high sulphur fugacity required to form pyrite.

Although the close association of anatase with molybdenite in lithospheric Mir diamond 1607 points to a common origin between the two, many other controls are likely to influence the Mo budget of subducting material. Indeed, one inclusion in a Collier-4 diamond (J15) consists of an intergrowth of chalcopyrite, pyrrhotite and anatase. TiO_2 is a common accessory phase in eclogitic diamonds but is rare in sub-lithospheric diamonds, where it can be present as a garnet exsolution product (e.g. Beyer and Frost, 2017). It is therefore likely that this inclusion has a lithospheric origin, and therefore, reasons for the absence of molybdenite other than S or TiO_2 content should also be considered.

One possible factor that could determine the presence or absence of molybdenite in diamond-hosted sulphide inclusions is the history and composition of the fluid that is forming diamond and the nature of the diamond-forming reaction. Studies of fluid inclusions in fibrous diamonds have indicated that there can be four end-members of diamond-forming fluids: a) hydrous-

silicic melt enriched in H_2O, Si, Al and K; b) a Cl, K and Na-brine; c) C, Mg, Ca, Fe, K and Na-enriched carbonatitic melt; and d) a less common Mg-rich carbonatitic melt.

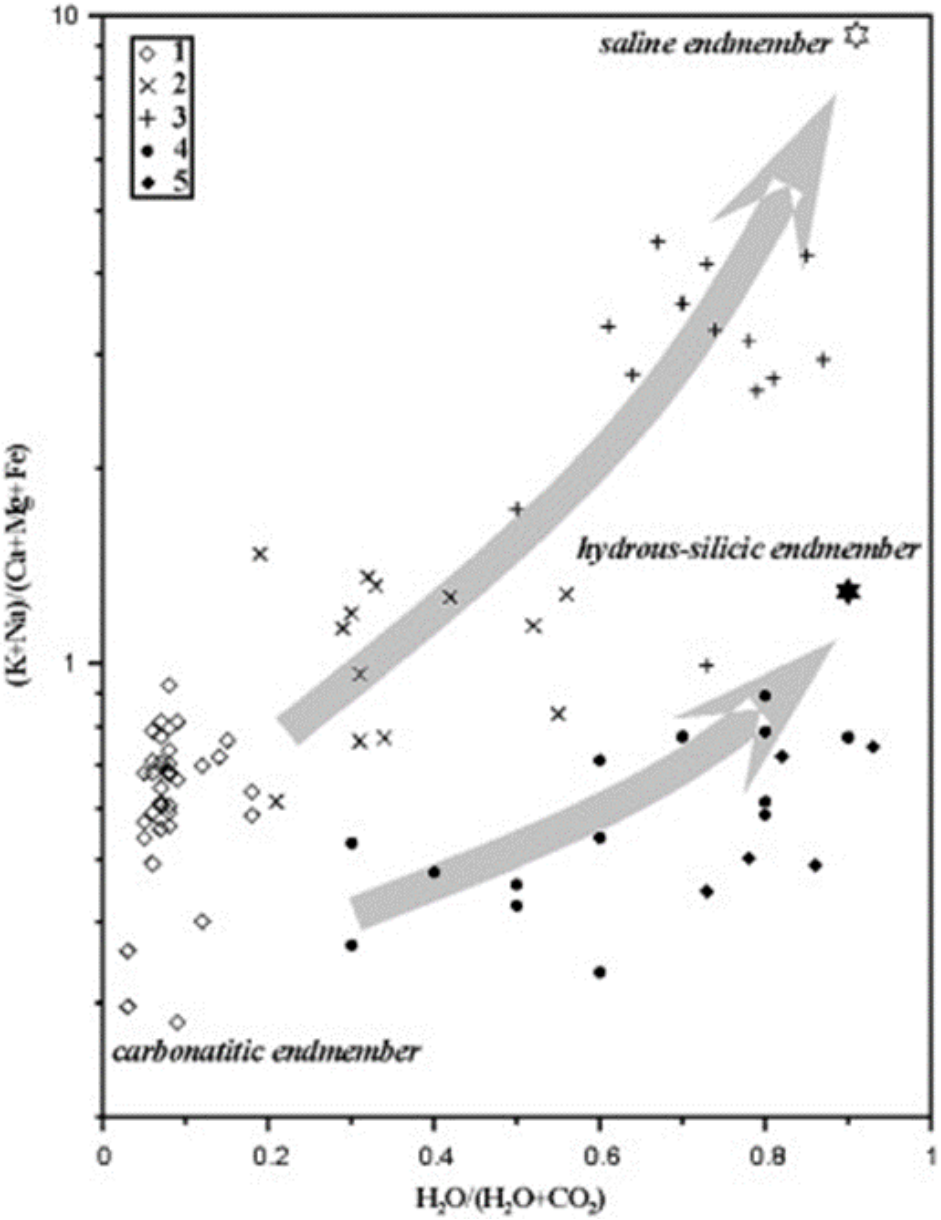

Figure 4.13. Compositions of fluids forming diamonds from 1) Udachnaya, 2) Snap Lake, 3) Diavik, 4) Jwaneng, 5) Brazil (from Zedgenizov et al., 2007).

Figure 4.13 shows the fluid compositions of diamonds from 1) Udachnaya, 2) Snap Lake (Canada), 3) Diavik, 4) Jwaneng and 5) Brazilian diamonds. The compositions of Jwaneng and Brazilian diamond-forming fluids plot along the fluid evolution line toward a hydrous-silicic endmember whilst diamonds from Udachnaya and Diavik were formed in the presence of

carbonatitic and saline end-member fluids, respectively (Zedgenizov et al., 2007). A carbonatitic melt component has also been reported both at Jwaneng and in sub-lithospheric diamonds from the Juina area according to the literature (e.g. Schrauder and Navon, 1994; Bulanova et al., 2010; Thomson et al., 2016). There is no obvious relationship between the composition of the known diamond-forming fluids and the presence or absence of molybdenite in diamonds of a specific suite, although further studies could determine this.

4.4.3. Re partitioning between different sulphides

Although it has been suggested that Re partitions into chalcopyrite over pyrrhotite ± pentlandite during cooling and chemical differentiation of a Fe-Ni-Cu sulphide melt (e.g. Richardson et al., 2002), this is contradictory to the Re and Os values that have been reported in literature. Likely due to the small size of diamond-hosted sulphide inclusions (commonly <150 μm), no in-situ measurements of the relative proportions of Re and Os in the individual phases (chalcopyrite, pentlandite, pyrrhotite) have been found in the literature.

Table 4.2. shows the partition coefficients which were estimated from published relative concentrations of Re and Os in molybdenite, chalcopyrite, pyrrhotite and pentlandite in sulphides originating in different magmatic settings. In 12 out of 14 cases, the data show that Re is enriched (up to ~56 times) in pyrrhotite relative to chalcopyrite. Indeed, experimental data on the partitioning of Re and Os (among other PGEs and HSEs) between MSS and ISS (which later form pyrrhotite ± pentlandite and chalcopyrite, respectively) has also been used to show that Re and Os both partition into MSS over melt/liquid (e.g. Brenan et al., 2002), and is expected to behave this way during sulphide exsolution.

Authors	$D_{Re}^{mo/po}$	$D_{Re}^{mo/cp}$	$D_{Re}^{cp/po}$	$D_{Re}^{po/cp}$	$D_{Re}^{po/pn}$	$D_{Re}^{pn/po}$	$D_{Re}^{pn/cp}$	Geological setting
Ackerman et al., 2013			1.71			2.22	1.29	Peridotites and pyroxenites
Barnes et al., 2006				29.17		1.23	36	Noril'sk PGE-sulphide deposit
Barnes et al., 2008				6.09		1.45	8.81	Various PGE-ore deposits
Barra et al., 2003		190021						Baghdad porphyry Cu-Mo deposit
Chen et al., 2015				25.66	2.14		12	Yaochong granite & Mo deposit
Dare et al., 2010				2.14	1.35		1.58	Sudbury PGE-Ni-Cu deposit
Dare et al., 2011				2.8	1.23		2.28	Sudbury PGE-Ni-Cu deposit
Duran et al., 2016				1.32		9.03	11.97	Lac des Iles Pd deposits (Canada)
Godel & Barnes, 2008				6.76		2.64	17.88	J-M reef (Stillwater Complex)
Liu et al., 2012		240.42						Duobaoshan porphyry Cu-Mo deposit
Mathur et al., 2002		19845						Candelaria Cu-Au deposit
O'Driscoll et al., 2009			3.71					Rum ultramafic-mafic Layered Suite
Piña et al., 2012				4.94	1.45		3.4	Aguablanca Ni-Cu sulphide deposit
Piña et al., 2013				2.44	1.71		1.43	Beni Bousera Cr-Ni mineralisation
Piña et al., 2016				26.31				Great Dyke of Zimbabwe (MSZ)
Wang et al., 2015				1.68		1.07	1.81	Tudun Cu-Ni sulphide deposit
Zu et al., 2015	87089							Hongshan Cu deposit

Table 4.2. *Partition coefficients for Re between molybdenite (mo), chalcopyrite (cp), pyrrhotite (po) and pentlandite (pn) calculated from the average values of Re contents published in the literature. MSZ = Main Sulphide Zone.*

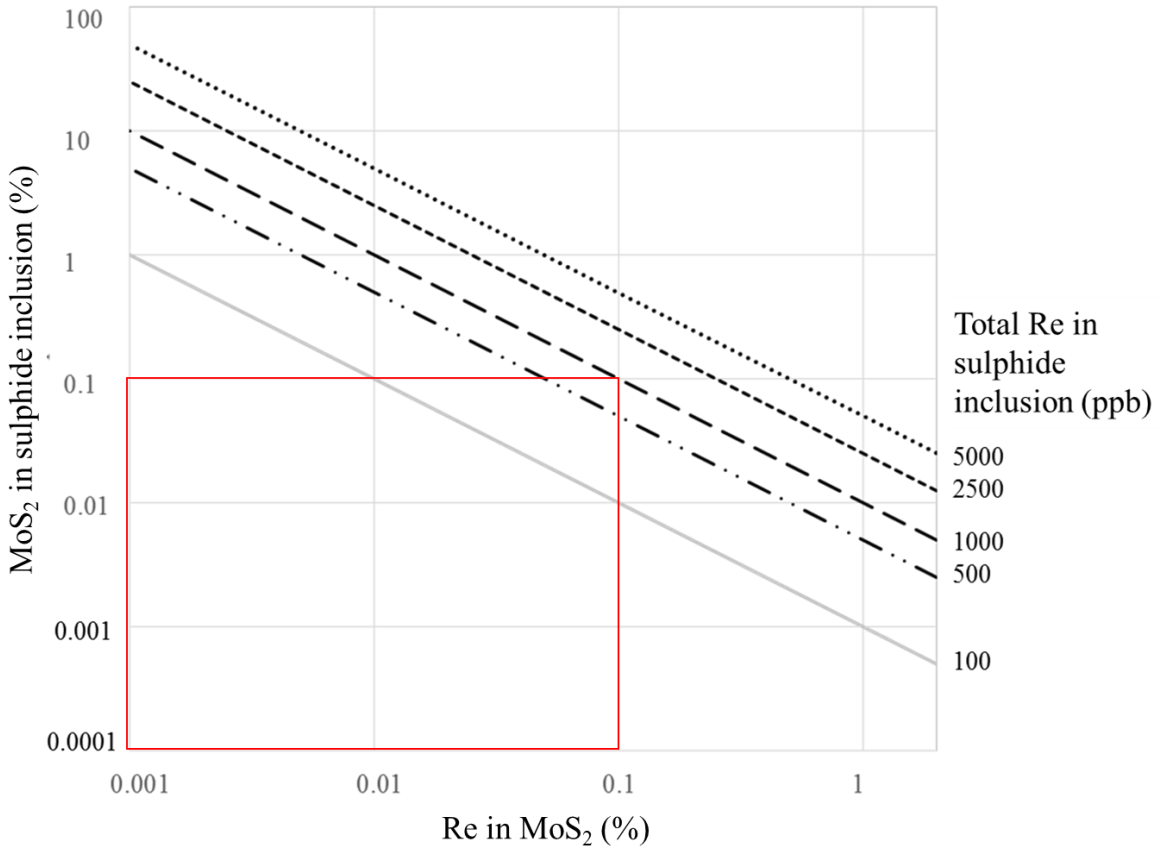

Figure 4.14. shows the amount of molybdenite (MoS_2) that would need to be present in a sulphide inclusion for it to host the total of the available Re (100-5000 ppb), as a function of the amount of Re (wt. %) it can contain. 0.1 wt; % molybdenite in a sulphide inclusion could host up to 1000 ppb Re (realistic amounts are therefore enclosed inside the red rectangle).

In order to determine if a small (<0.1 wt. % MoS_2) amount of molybdenite could host all of the Re available in an inclusion, the amount of molybdenite hosting 0.1 wt. % Re that would need to be present (Fig. 4.14) as well as the concentration of Re in a molybdenite forming <0.1 wt. % of the sulphide inclusions are plotted. Although a reasonable amount of molybdenite (0.1 wt. %) could amply host all of the Re budget of an inclusion which was relatively poor in Re (e.g. <500 ppb), it is not expected to contain more 20 % of an inclusion's total Re, if the inclusion is enriched in Re (e.g. >5000 ppb).

4.4.4. The effect on Re-Os ages of diamonds

4.4.4.1. Re-Os model ages of diamond-hosted sulphide inclusions

The Re-Os compositions of sulphide inclusions in diamonds have been gathered from literature (Pearson et al., 1998a; 1998b; Richardson et al., 2001; Richardson et al., 2004; Westerlund et al., 2004; 2006; Richardson and Shirey, 2008; Aulbach et al., 2009a; 2009b; Laiginhas et al., 2009; Smith et al., 2009; Smit et al., 2010; Wiggers de Vries et al., 2013a; Smit et al., 2016; Aulbach et al., 2018).

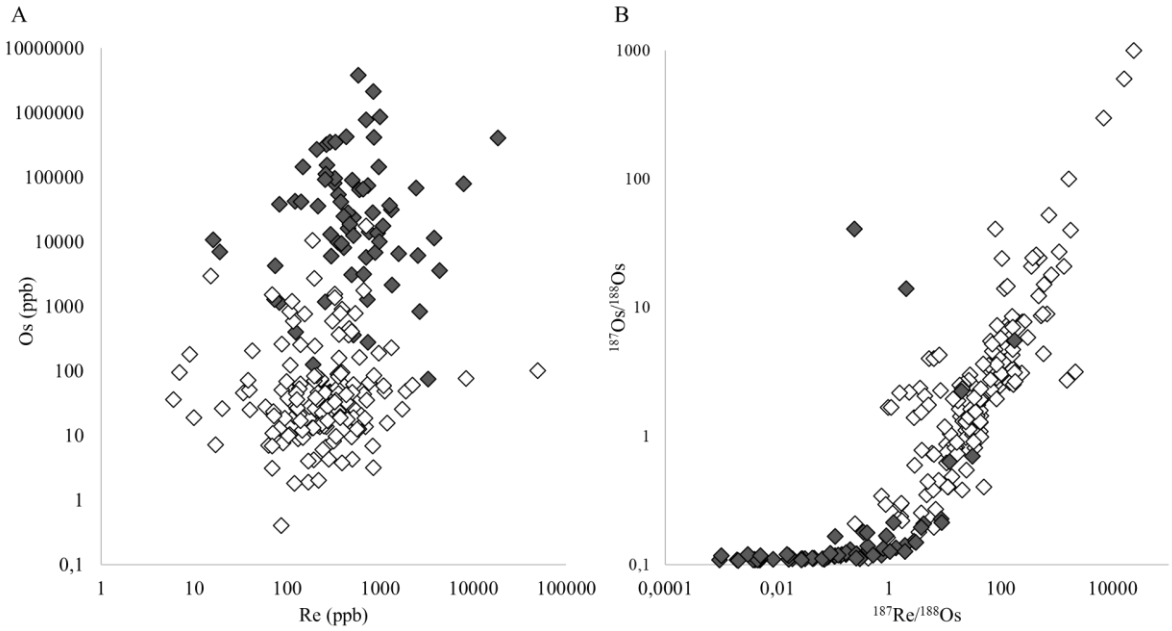

Figure 4.15. A) Re and Os contents (ppb) and B) $^{187}Re/^{188}Os$ and $^{187}Os/^{188}Os$ compositions of natural eclogitic (open symbols) and peridotitic (closed symbols) diamond-hosted sulphide inclusions from literature.

The effect of Re-loss through molybdenite non-recovery is greatest on the age of a sulphide inclusion which evolved with a slightly super-chondritic $^{187}Re/^{188}Os$ composition, and numerous improbable and impossible ages of diamonds have been published in literature. However, the sulphide inclusions in many diamond populations (in particular ones belonging to the eclogitic suite) exhibit $^{187}Re/^{188}Os$ ratio >10 (e.g. Fig. 4.15).

Fig. 4.16. shows that the Re-Os model age (T_{MA}) that have been obtained from literature plotted against the $^{187}Re/^{188}Os$ compositions of sulphide inclusions in diamonds reported in literature for molybdenite-bearing localities of Mir and Diavik diamonds, and for eclogitic Zimmi diamonds (Zimbabwe; Smit et al., 2016). Diamonds from Zimmi were not studied here, but the Re-Os data was used to show a trend (Fig 4.16.C). Indeed, unrealistic model ages ages (T_{MA} >4.5 Ga) were obtained from inclusions with $^{187}Re/^{188}Os$ ratios ≤20. However, eclogitic diamonds exhibit larger variations in their Re/Os contents due to the incompatible nature of Re relative to Os, and typically have higher $^{187}Re/^{188}Os$ ratios than peridotitic diamonds. This implies that Re-loss through non-recovery of a Re-enriched phase is less important for the Re-Os T_{MA} determination of eclogitic diamonds.

Furthermore, model ages are generally accepted to be unreliable because their calculation relies on projecting back to an undisturbed BSE mantle source. Although many of the T_{MA} obtained have been impossible (future ages or ages older than the Earth), reasonable T_{MA} have nonetheless been obtained, which have also been consistent with isochron ages, presently the preferred method of Re-Os age determination (e.g. Shirey et al., 2013; Harvey et al., 2016 and references therein).

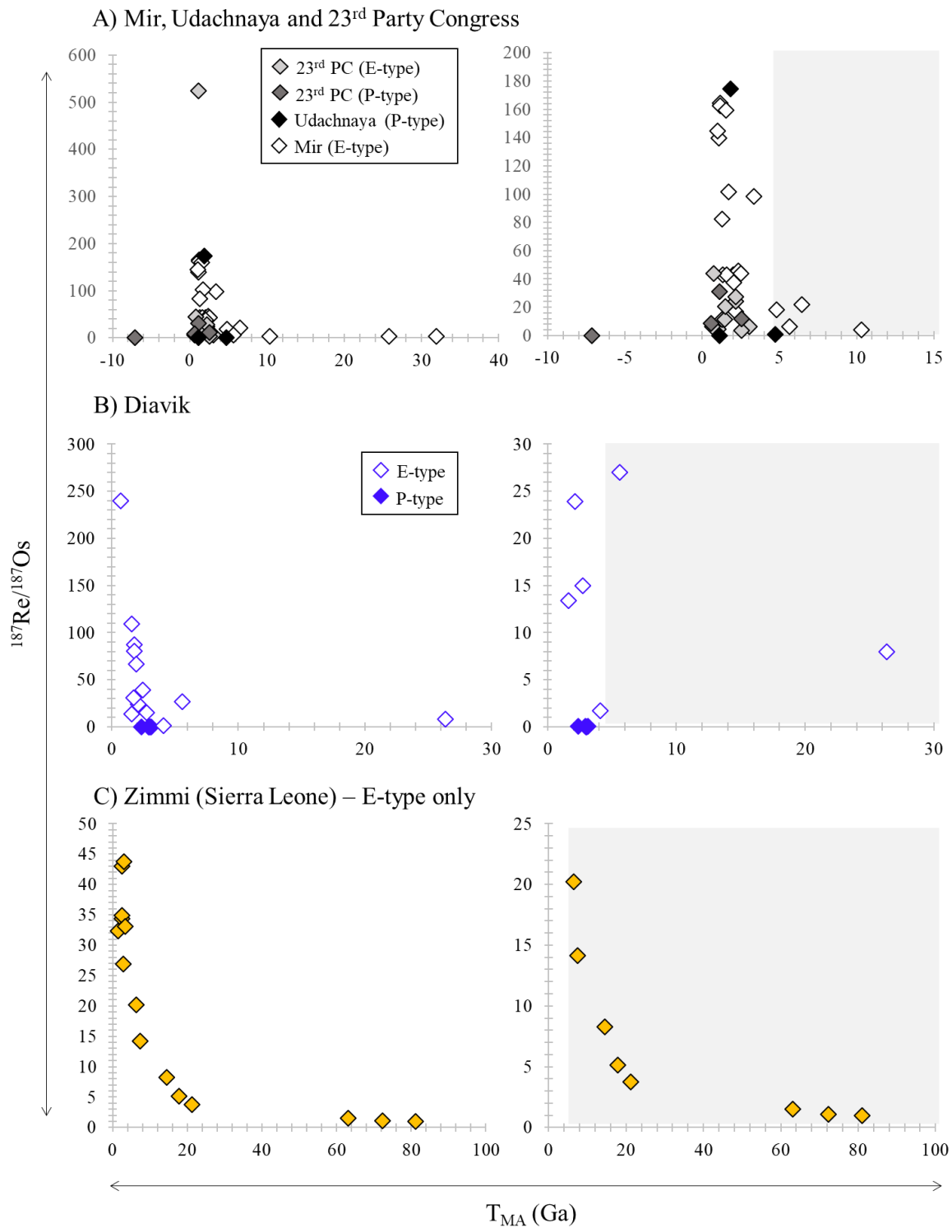

Figure 4.16. $^{187}Re/^{188}Os$ ratios of natural diamond-hosted sulphide inclusions from A) Mir, 23rd Party Congress and Udachnaya (Yakutia) (Wiggers de Vries et al., 2013a), B) Diavik (Canada) (Aulbach et al., 2009) and C) Zimmi (Sierra Leone) (Smit et al., 2016) plotted against calculated model ages (T_{MA}). The shaded boxes cover ages older than the Earth. The red vertical line shown in some of the figures corresponds to the chondritic uniform reservoir (CHUR) value for $^{187}Re/^{188}Os$

4.4.4.2. Recovery of protogenetic Re-bearing molybdenite

It is possible that molybdenite was captured as a single phase of its own and did not undergo re-equilibration with a co-existing sulphide melt (e.g. Fig. 4.17). In such a scenario, recovering molybdenite during sulphide extraction from diamond might lead to an overestimation of the Re and likely the ^{187}Os contents of an inclusion. The recovery for analysis of varying amounts of molybdenite (containing varying amounts of Re) would cause scatter in an isochron, as well as lead to an age under-estimation.

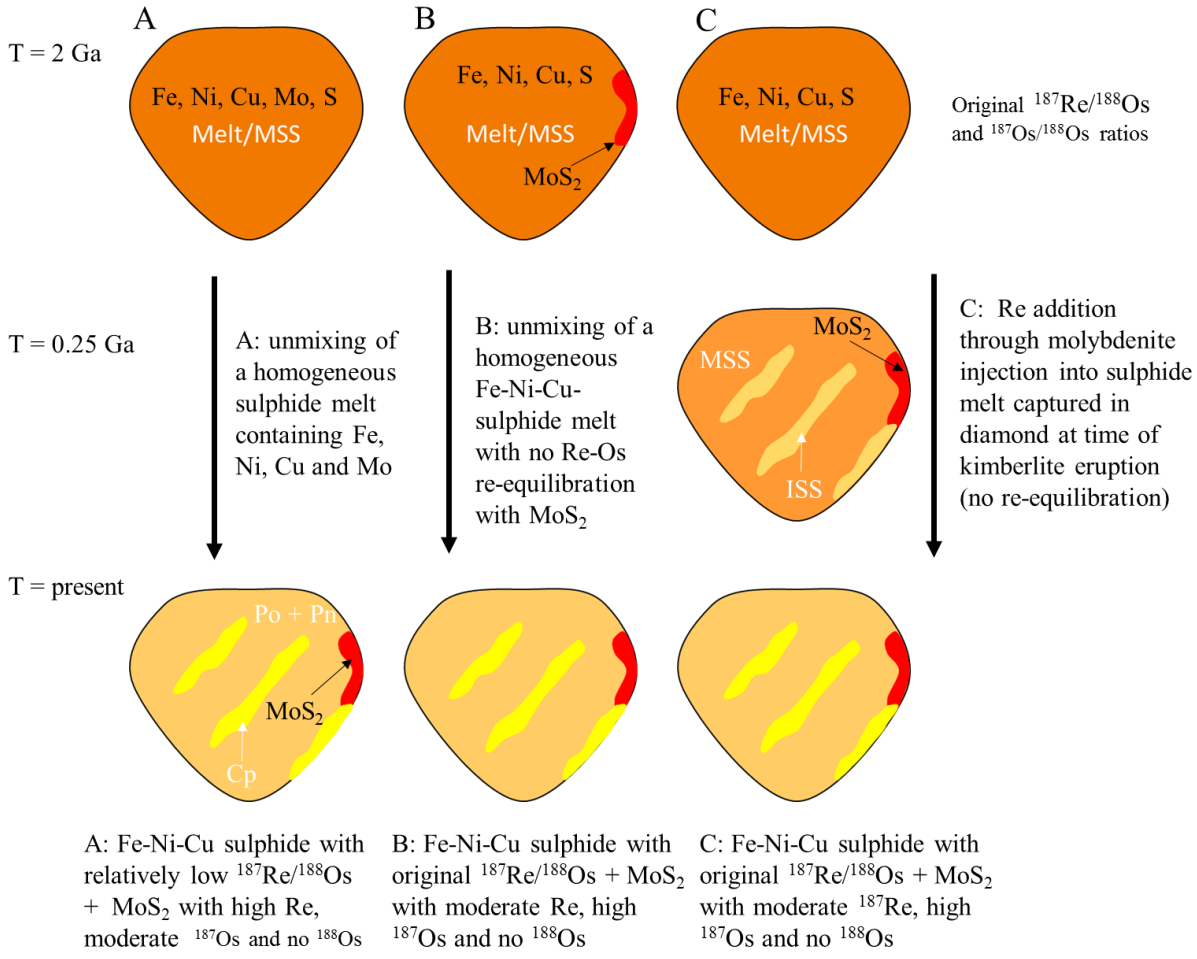

Figure 4.17. Schematic diagrams outlining three different unmixing pathways and modes of initial capture of molybdenite that is considered as having A) unmixed from an originally homogeneous Mo-bearing sulphide melt, B) become enclosed in diamond as a protogenetic Re-bearing mineral, or C) been introduced epigenetically as molybdenite into the sulphide inclusion at a later date (e.g. Through a healed fracture).

With long mantle residence times, the recovery for analysis of molybdenite may cause some scatter in an isochron, but it would not dramatically disturb the age due to the growth of ^{187}Os. If a relatively young and Re-rich molybdenite phase was enclosed in diamond alongside sulphide, sometime close to the time of kimberlite eruption, the Re-Os bulk composition of the inclusion could lead to high $^{187}Re/^{188}Os$ ratios, as well as seemingly young radiometric diamond ages. In the case of Udachnaya diamond 3648, this scenario is more unlikely because if the sulphide inclusion was recovered entirely along with protogenetic Re-bearing molybdenite during sulphide extraction, the diamond growth event should have occurred prior to the assigned 3.5 Ga crystallisation time (in that the 3.5 Ga is actually too young) (Pearson et al., 1999). The most likely scenario nonetheless remains that molybdenite was unmixed from an original Mo-bearing sulphide melt which was captured as a homogeneous phase during diamond growth.

4.4.5. Other reasons for Re-Os age discrepancies

Incomplete recovery of a sulphide inclusion during its extraction for Re-Os dating (e.g. Smit et al., 2010; Wiggers de Vries et al., 2013a) or the presence of healed fractures connecting the inclusion to the surface of the diamond or connecting with other inclusions (whereby re-equilibration of Re and Os isotope compositions could have occurred; e.g. Pearson et al., 1999) have commonly been proposed to account for some incongruous model ages and/or large scatter in isochrons. As mentioned in section 4.3.3., Re concentrations in molybdenite samples rarely exceed 0.1 wt. %, and as such, if an inclusion contained more than 5000 ppb of Re (e.g. Fig. 4.14) molybdenite would not be expected to sequester more than ~ 20 % of that inclusion's Re. Below, other geological explanations for inaccurate radiometric ages being calculated are discussed, if a sulphide inclusion was entirely recovered for analysis (i.e. without any loss of material).

4.4.5.1. Capture of residual sulphides from metasomatised peridotite

Spetsius et al. (2002) analysed the Os isotope compositions of sulphide inclusions in Palaeozoic zircons from the Mir kimberlite by LA-MC-ICPMS. The >2.3 Ga Re-Os T_{RD} and T_{MA} model ages that were obtained were much older than the host zircons (346 to 395 Ma), which were dated by U-Pb (Spetsius et al., 2002). It was suggested that the zircons grew on a metasomatised peridotite substrate and captured within them, ancient residual sulphides which underwent little or no modification isotopic composition (Spetsius et al., 2002). In such a scenario involving diamond growth, the sulphide inclusion would retain a Re/Os composition indicative of an older age than the diamond-forming event, unless the inclusion was fully re-equilibrated.

4.4.5.2. Capture of protogenetic material

Thomassot et al. (2009) analysed the stable C, N and S isotope compositions of diamonds from Jwaneng (Botswana) and their sulphide inclusions. A negative sulphur mass-independent (S-MIF) signal preserved in eclogitic diamond-hosted sulphide inclusions, was attributed to the involvement of ancient (>2.45 Ga) recycled sulphur. It was suggested that diamond crystallisation took place in the presence of a mantle-derived carbon-bearing fluid phase, which led to Re-Os re-equilibration of pre-existing sedimentary sulphide minerals. This has important implications for the interpretation of sulphide inclusion-bearing diamond Re-Os ages because the incorporation of a significant amount of mantle-related sulphur during a diamond growth event into the original sulphide could lead to a re-equilibration of the Re–Os isotope composition in any inclusion, thereby accounting for some scatter on Re-Os isochrons.

4.4.5.3. Presence of unrecovered Platinum Group Minerals (PGM)

Platinum group elements (PGE; Pt, Pd, Rh, Ir and Os) typically behave as strongly chalcophile and siderophile elements, existing entirely in sulphide phases in moderately melt-depleted

mantle peridotites (e.g. Brenan et al. 2016). In highly melt-depleted and/or altered peridotites however, highly siderophile elements (HSE; PGE +) are commonly hosted in platinum-group minerals (PGM) and alloys, formed through reactions involving fluids or melts (e.g., Luguet et al. 2007; Lorand et al. 2013) that have formed from base metal sulphides (BMS) as a consequence of reactions involving melts or fluids (Harvey et al., 2016). Such PGM are important to identify when considering the Os isotope systematics of the mantle.

In cratonic peridotites, sulphides can be relatively enriched in highly siderophile elements (HSE) due to their extensive melting history (e.g. Luguet et al., 2007), or alternatively, different PGM may have existed as alloys in highly refractory mantle residue (e.g. as Pt-rich microphases) and were subsequently re-sulphidised and captured by sulphide during melt extraction (Aulbach et al., 2016 and references therein). Alternatively, PGM may have unmixed from a HSE-rich monosulphide during subsolidus cooling (e.g. Lorand and Luguet, 2016). Such platinum group minerals include laurite RuS_2, Ru-Os Ir sulphides, Re-Os-Ir sulpharsenides, Pt-Ir Os alloys and Pt-Fe alloys (Luguet et al., 2007; Lorand et al., 2013; Lorand and Luguet, 2016). The melting and recycling of the Os-rich compositions of such PGM are thought to generate some of the Os-isotope heterogeneities of the upper mantle. Indeed, the presence and analysis of PGM in diamond-hosted sulphide inclusions could make their radiometric ages appear older than they are.

4.4.5.4. Scatter caused by dating preparation techniques

A further explanation for some of the scatter in isochrons and errors in model ages, could arise from the sulphide digestion and micro-distillation procedures employed in preparation for Re-Os dating of single sulphide inclusions. Bragagni et al. (2018) developed a sulphide reference material for testing sample digestion and chemical separation techniques (following Pearson et al., 1998). These included a pre-digestion step in HBr and/or HCl, and the duration and

temperature of the pre-digestion and micro-distillation steps were also evaluated. Bragagni et al. (2018) observed that depending on the procedure used, the HSE contents of the sulphides varied significantly in reference to the standard that was used. Such variations were deemed to be the results of incomplete digestion of sulphide relative to the Os spike, Os spike-loss during digestion (resulting in an overestimation of the Os content relative to the spike) and/or possibly, the presence of undigested sub-µm-sized PGM.

4.5. Conclusions

The occurrence of molybdenite in diamond-hosted sulphide inclusions is unexpected, and its origin is unclear. It has seldom been reported in diamonds described in literature, likely due to the fact that Raman spectroscopy is not the most obvious tool to use on the study of opaque sulphides. Davies et al. (2002; 2003) reported molybdenite as a bimineralic inclusion with grossular garnet included in a diamond from Bingara (New South Wales). Its occurrence was not interpreted but titanite was also found for the first time in diamonds from the same assemblage (Davies et al., 2002), perhaps providing additional clues to the possibly close association between Mo and Ti. The carbon which formed the Bingara diamonds was also shown to have a deeply subducted crustal source (Davies et al., 2002; 2003).

We have reported on the possible pervasiveness of molybdenite in diamond-hosted sulphide inclusions from Mir, Udachnaya (Yakutia), Dachine (French Guyana), Murowa (Zimbabwe), Orapa, Letlhakane and Damtshaa (Botswana), Diavik and Argyle, and it is therefore evident that molybdenite is a common inclusion phase among these diamond populations. The apparent absence of molybdenite in the majority of the sub-lithospheric diamonds and the studied Jwaneng inclusions potentially reflects on different diamond-forming conditions, availability of Mo and/or a sampling bias.

If the timing of diamond formation is connected to the availability of subducted Mo, the apparent absence of molybdenite in diamond-hosted sulphide inclusions from Jwaneng, could be explained by diamond formation involving mantle-derived carbon and pre-existing Archean sulphides (Thomassot et al., 2007). In fact, the presence of molybdenite in a single inclusion in a sub-lithospheric Juina-5 diamond likely eliminates depth as being a limiting factor for molybdenite, and instead, it could also be related to the fO_2 and fS_2 conditions of diamond formation.

Further work should focus on analysing the carbon isotope compositions of the diamond growth zones hosting molybdenite-bearing sulphide inclusions, to investigate whether the Mo and C may have had a common subducted origin. Mo isotope analyses of the inclusions would be difficult due to the small volume of the molybdenite. Additionally, determining and contrasting the concentrations of Mo and other trace metals (e.g. Se, Cd, Cu… for example by synchrotron-based x-ray fluorescence) in sulphide inclusions hosted in a variety of diamonds, could also help in exploring the source and behaviour of such metals in the diamond-forming regions of the Earth's mantle. Finally, whilst a better understanding of the parameters controlling the presence or absence of molybdenite in diamond-hosted inclusions is important for ensuring accurate Re-Os age determinations are made, it can also help in providing an invaluable insight into the global Mo cycle.

Chapter 5. Preliminary stable sulphur isotope compositions of sulphide inclusions in diamonds

5.1. Introduction

Diamond-hosted sulphide inclusions sample sulphur-bearing material residing at depth in the Earth's mantle, providing an insight into the nature of certain diamond-forming reactions (Chapter 2). To date, studies of the chemical and stable isotope composition of diamond-hosted sulphide inclusions have largely been aimed at lithospheric diamonds, which are more commonly available for study than sub-lithospheric ones. Sulphides included in lithospheric diamonds can provide a valuable insight into the nature of craton-forming events, and the behaviour of sulphur in the subcontinental lithospheric mantle. Sub-lithospheric diamonds on the other hand can sample otherwise inaccessible regions of the Earth's lower mantle and offer a snapshot of the recycling of volatiles to depths exceeding 410 km (e.g. Bulanova et al., 2010; Walter et al., 2011; Thomson et al., 2014; 2016).

The mineralogy and isotopic composition of sulphide minerals included in eclogitic lithospheric diamonds and subduction-related sub-lithospheric diamonds can provide an insight into the behaviour and fate of sulphur-bearing material being recycled into the Earth's interior. Indeed, the isotopic signatures of sulphur can help trace the origin of sulphur in a variety of sulphur-bearing rocks and minerals. Comparing the chemical and sulphur isotope

signatures of the sulphide inclusions hosted in lithospheric and sub-lithospheric diamonds can therefore help place constraints on the recycling of sulphur to depth.

5.1.1. Sulphur isotope geochemistry

Sulphur isotopes provide a powerful spatial and temporal geochemical tracer of sulphur-bearing material and investigating its behaviour whilst undergoing a variety of processes at the surface and within the Earth. Sulphur isotope systematics in geological sciences were first explored with early publications by Thode et al. (1949) and Szabo et al. (1950) and has since become a valuable sub-discipline of both surface and mantle geosciences**.**

Sulphur has 16 protons and 16, 17, 18, 19 or 20 neutrons, and therefore has five naturally occurring isotopes (^{32}S, ^{33}S, ^{34}S, ^{35}S and ^{36}S). All isotopes are stable, except for ^{35}S, which is a cosmic ray spallation product of ^{40}Ar. On Earth, the ^{32}S, ^{33}S, ^{34}S and ^{36}S isotopes have approximate natural abundances of 95.02, 0.72, 4.21 and 0.02 % respectively (MacNamara and Thode, 1950). Since stable isotope geochemistry is chiefly concerned with the changes in the ratios of isotopes between different phases arising from isotope fractionation, rather than their absolute abundances, isotope ratios are normally expressed as the ratio of a minor (less abundant) to the major (most abundant) isotope of the element; the principal ratio of interest for sulphide minerals is $^{34}S/^{32}S$.

Sulphur isotope fractionation processes typically only cause small variations in the sulphur isotope ratios, and therefore, a delta (δ) notation, as parts per thousand variation relative to a reference material is used to express the isotopic composition of a phase. All units are expressed in parts per mille (‰) relative to a meteoritic sulphur isotope reference called Vienna Canyon Diablo Troilite (V-CDT) standard, which is thought to represent the primordial sulphur isotope

composition of the Earth (e.g. Nielsen et al., 1991; Seal et al., 2006). The $^{34}S/^{32}S$ composition of a material is defined as:

$$\delta^{34}S = \left(\frac{\left({}^{34S}/_{32S}\right)sample - \left({}^{34S}/_{32S}\right)reference}{\left({}^{34S}/_{32S}\right)reference}\right)x1000$$

Although the delta notation $\delta^{34}S$ is the most commonly used, multiple sulphur isotopes analyses of the $^{33}S/^{32}S$, $^{36}S/^{32}S$ and $^{34}S/^{32}S$ ratios are useful in providing additional clues for identifying the sources of sulphur and mixing between different reservoirs (discussed in the next section).

5.1.1.1. Sulphur isotope fractionation

Variations in the sulphur isotope compositions of sulphide minerals and associated sulphate minerals or aqueous species are caused by the preferential partitioning (or fractionation) of sulphur isotopes among sulphur-bearing species. The partitioning behaviour of stable sulphur isotopes, also known as isotope fractionation, is controlled by equilibrium and kinetic effects. Isotope fractionation commonly results from mass-dependent variations in the thermodynamic properties of molecules (e.g. Seal et al., 2006), as they react at different rates depending on their masses (e.g. O'Neil 1986). It is generally easier to destabilise bonds involving lighter isotopes (e.g. ^{32}S) while heavier isotopes form stronger bonds.

Isotopic variations among different minerals commonly arise from differences in the temperature of a system and oxidation-reduction processes (e.g. Rees et al., 1978; O'Neil et al., 1986; Seal et al., 2006). Indeed, redox reactions play an important role in driving isotope fractionation, with oxidised material being enriched in $\delta^{34}S$, relative to reduced material that is depleted in $\delta^{34}S$ (^{34}S enrichment follows $SO_4^{2-} > SO_3^{2-} > Sx° > S^{2-}$) (e.g. Sakai, 1968; Bachinski, 1969). Some of the factors affecting sulphur isotope fractionation at a range of temperatures have been summarised by Seal et al. (2006). At low temperatures, isotope

fractionation is kinetically controlled (e.g. through irreversible, physical and/or bacterially mediated processes). For example, sulphate-reducing bacteria preferentially reduce $^{32}SO_4^{2-}$, producing sulphides which are depleted in ^{34}S (e.g. Harrison and Thode, 1958; Kaplan and Rittenberg, 1964). At high temperatures however, reactions typically occur under equilibrium conditions, and fractionation is largely controlled by the chemical composition and the crystal structure of a phase, as well as the pressure and temperature of a system (e.g. O'Neill et al., 1986). This involves chemical exchange between sulphate (SO_4^{2-}) and sulphide (S^{2-}) species, as well as between sulphides with different compositions (Seal et al., 2006 and references therein).

Mass-dependent fractionation

Sulphur isotope mass-dependent fractionation arises from differences in mass of the isotopes. Indeed, the different isotope ratios of interest ($^{33}S/^{32}S$, $^{34}S/^{32}S$ and $^{36}S/^{32}S$) are expected to vary systematically relative to one another depending on their masses; i.e. variations in $^{34}S/^{32}S$ will commonly be twice that of $^{33}S/^{32}S$, and variations in $^{36}S/^{32}S$ will be twice that of $^{34}S/^{32}S$, resulting in linear fractionation trends (e.g. Urey, 1947; Hulston and Thode, 1965; Seal et al., 2006). These linear arrays commonly have slopes of 0.5156 (for $\delta^{33}S$ and $\delta^{34}S$) and 1.91 (for $\delta^{33}S$ and $\delta^{34}S$) (e.g. Hulston and Thode, 1965).

Mass-independent fractionation

Non-linear isotopic fractionation trends can arise from mass-independent fractionation processes. Unexpected variations in the $^{33}S/^{32}S$ and $^{36}S/^{32}S$ ratios of sulphide and sulphate minerals in Precambrian rocks were first reported by Farquhar et al. (2000). The mass-independent sulphur effect was then seen to be dependent on light wavelength by Farquhar et al., (2001) who conducted photolysis experiments on SO_2 at a range of wavelengths. They

showed that UV light with wavelengths shorter than 200 nm was likely to penetrate the Earth's early oxygen-poor atmosphere, causing volcanic SO_2 to break down into elemental sulphur (S^0) and sulphate (SO_4) with clear anomalous (i.e. non-zero) $\Delta^{33}S$ and $\Delta^{36}S$ signatures (e.g. Fig. 5.1).

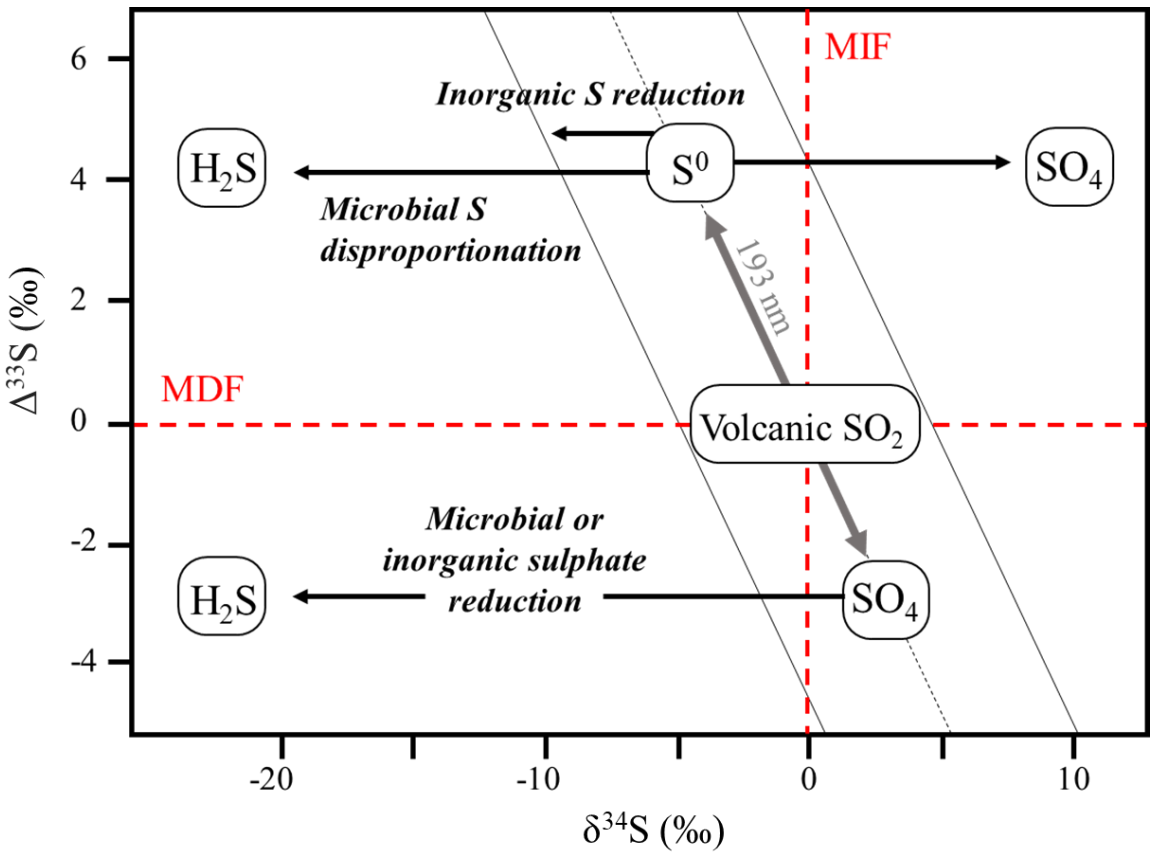

Figure 5.1. Schematic diagram of sulphur isotope systematics ($\delta^{34}S$ vs $\Delta^{3}3S$) in an Archean atmosphere modified from Philippot et al., (2007). The red dotted lines define the ordinarily expected $\delta^{34}S$ and $\Delta^{33}S$ values for natural samples. UV-light induced photolysis of volcanically derived SO_2 and H_2S results in aerosol and gas production, which exhibit both mass-dependent and mass-independent (S-MIF, $\Delta 33S$) isotope and mass-dependent isotope fractionation (MDF-S, $\delta 34S$), the latter arising from UV radiation at ~193 nm.

Anomalous $\Delta^{33}S$ and $\Delta^{36}S$ values have since been recorded in a variety of ancient materials including sedimentary sulphides and sulphates, sulphides in Martian meteorites (e.g. Farquhar et al., 2007), mantle plume-derived sulphides (e.g. Cabral et al., 2013; Delavault et al., 2016), mantle sulphates (Kitayama et al., 2017) as well as sulphide inclusions hosted in lithospheric diamonds (Farquhar et al., 2002; Thomassot et al., 2009; Cartigny et al., 2009; Smit et al.,

2019). Indeed, it is well accepted that on Earth, mass-independent fractionation of sulphur was operating in Hadean and Archean times (prior to the first Great Oxidation Event, GOE-I ~2.45 Ga), in a poorly oxygenated atmosphere (Fig. 5.2) (Farquhar et al., 2000; 2002; 2003).

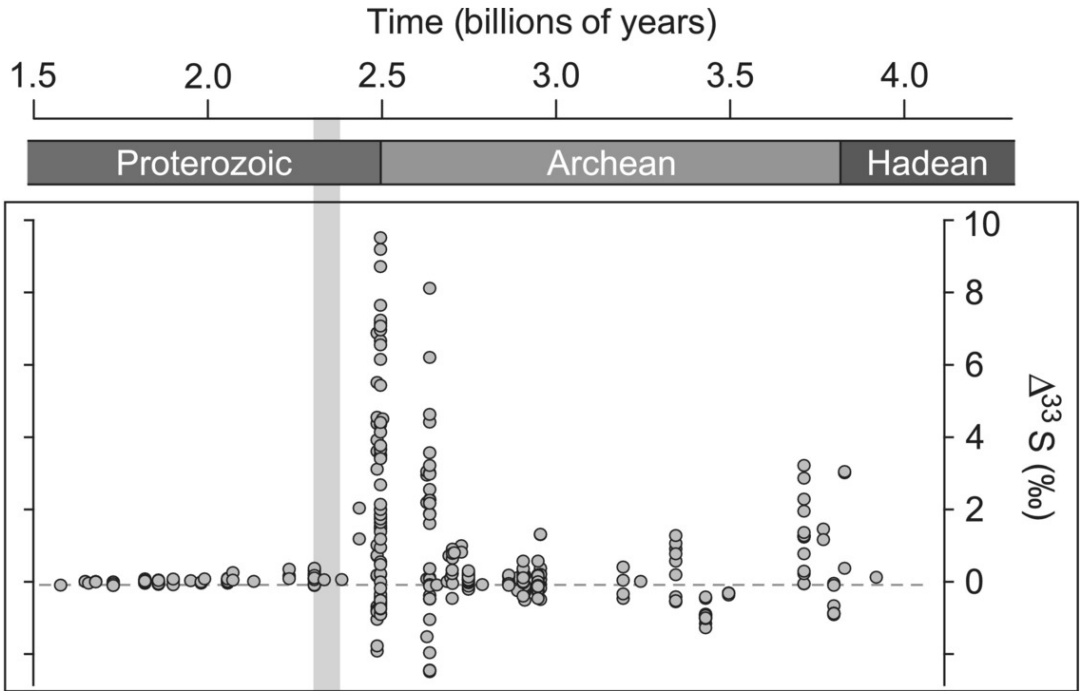

Figure 5.2. Diagram from Catling and Kasting (2017) which shows the overall disappearance of a sulphur mass-independent signature ($\Delta^{33}S \neq 0$) in sedimentary sulphide minerals (grey circles) after the first Great Oxidation Event ca. 2.45 Ga (shown by the grey bar).

The presence of non-zero $\Delta^{33}S$ therefore evidences the incorporation of Archean, mass-independently fractionated sulphur. The deviations from mass-dependent fractionation line are expressed as non-zero $\Delta^{33}S$, which are defined as:

$$\Delta^{33}S = \delta^{33}S - 1000\left(\left(1 - \frac{\delta^{33}S}{1000}\right)0.515 - 1\right)$$

And

$$\Delta^{36}S = \delta^{36}S - 1000\left(\left(1 - \frac{\delta^{36}S}{1000}\right)1.91 - 1\right)$$

The use of capital delta (Δ) notations is necessary for assessing the effects of fractionation of the four isotopes because the abundances of sulphur with masses 33 and 36 are very low (0.75 % and 0.02 % respectively) (e.g. Ono et al., 2006; Farquhar et al., 2007. Barré et al., 2018).

5.1.2. Sulphur isotope geochemistry of natural samples

The $\delta^{34}S$ values of sulphides are commonly used to constrain the sources of sulphur, its redox state in the sulphide mineral and to trace processes of interaction with oxidised or reduced fluids post-sulphide crystallisation (e.g. Crossley et al. 2018). Importantly, and as is mentioned in section 5.1.1.1., oxidation processes produce $\delta^{34}S$-enriched species, whilst reduction reactions typically deplete a starting material in $\delta^{34}S$. Sulphides therefore generally inherit lighter $\delta^{34}S$ compositions than sulphates.

5.1.2.1. The sedimentary sulphur isotope record

Sulphur isotope reservoirs at the Earth's surface are dominated by sulphides and oceanic sulphate (e.g. Canfield et al., 2014). Figure 5.3 shows the $\delta^{34}S$ and $\Delta^{33}S$ compositions of a variety of sulphide and sulphate minerals reported in literature. Large variations in the $\delta^{34}S$ compositions of sulphide minerals (primarily pyrite) hosted in sedimentary rocks (e.g. Fig 5.4) have been closely associated with the sulphur isotope composition of sulphate dissolved in contemporaneous seawater, at least since 2.45 Ga, as the result of the activity of sulphate-reducing bacteria in marine settings (e.g. O'Neil et al., 1986; Seal et al., 2006).

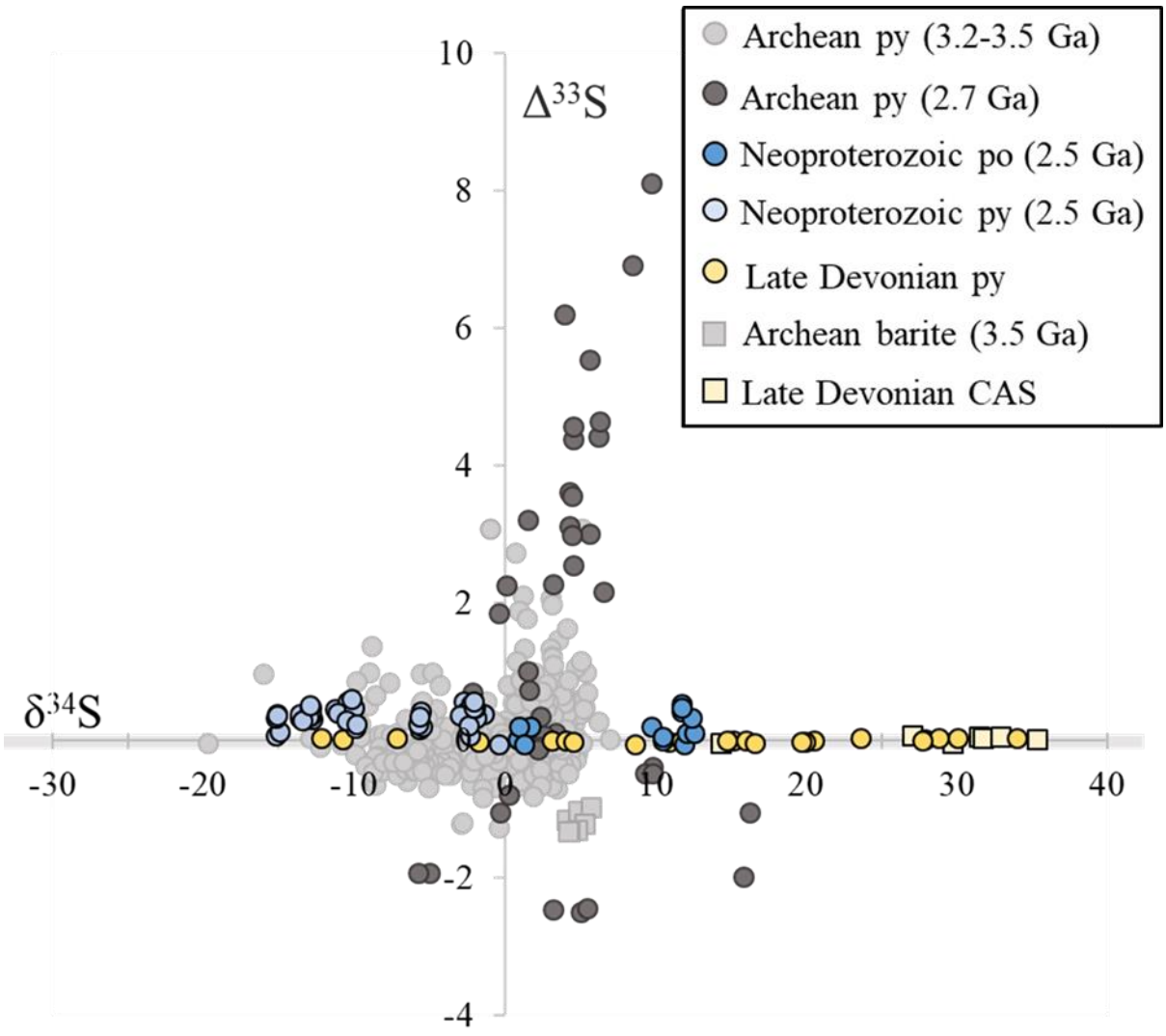

Figure 5.3. $\delta^{34}S$ and $\Delta^{33}S$ compositions of Archean, Neoproterozoic and Late Devonian sedimentary sulphides (pyrite – py, and pyrrhotite – po) and sulphates (barite and carbonate-associated sulphates (CAS) measured by Ono et al. (2003), Shen et al. (2009), Bühn et al. (2012), Roerdink et al. (2013) and Sim et al. (2015).

Figure 5.4. from Canfield and Raiswell (1999) shows that the $\delta^{34}S$ of seawater itself has varied over time; modern seawater has a globally homogeneous value of 21 +-0.2 ‰ (Rees et al., 1978), while modern sedimentary sulphides can exhibit large variations in their isotopic compositions ($\delta^{34}S$ -50 to 20 ‰). The $\delta^{34}S$ isotope composition of marine sulphides has varied significantly since the end of the Archean as a result of the increased activity of atmospheric oxygen. Another marked change in the sulphur isotope composition of sedimentary sulphides

has been observed ca. 0.7 Ga, with negative $\delta^{34}S$ values predominating in pyrite hosted in rocks younger than ~0.66 Ga (e.g. Fig. 5.4).

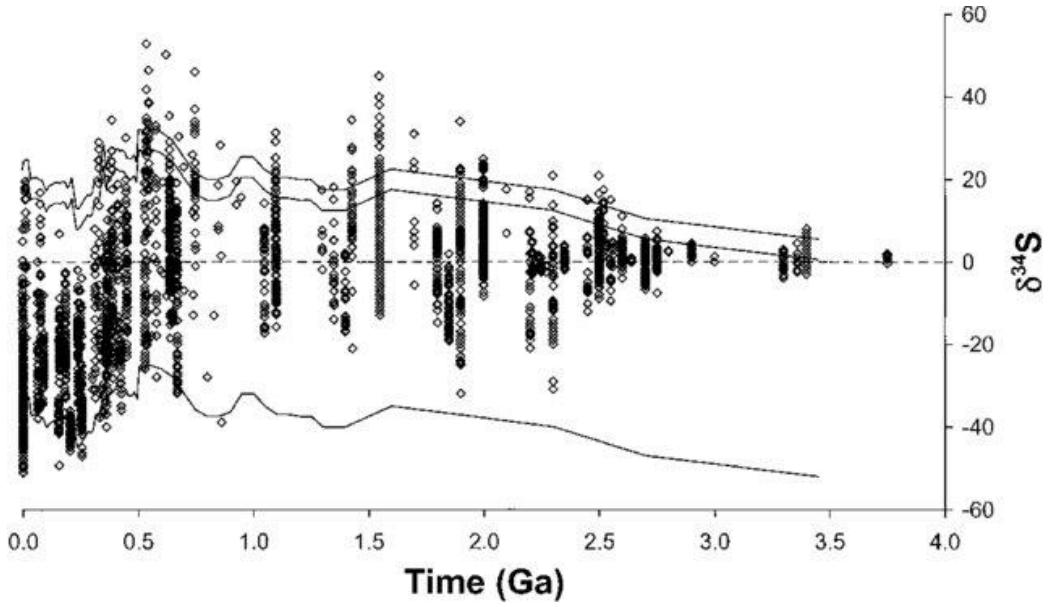

Figure 5.4. Figure from Canfield and Raiswell (1999) showing the variation in the $\delta^{34}S$ of sedimentary sulphides over time (circular symbols). The variation in the $\delta^{34}S$ composition of seawater sulphate is also shown as encompassed between two lines on the positive side of 0 ‰ (with a width of 5 ‰) as well as displaced below (by ‰) for reference

.

5.1.2.2. Sulphur isotopes in subduction zones

The sulphur isotope compositions of sulphur-bearing surface and crustal reservoirs are relatively well characterised, as are the exchange mechanisms involved in isotopic fractionation. In subduction zones however, the input of sulphur into the mantle, and its behaviour during subduction are less well constrained. Positive $\delta^{34}S$ values have consistently been measured in sulphides, sulphates, volcanic glasses and melt inclusions from various volcanic settings (e.g. Alt et al., 1993; 1995; 2012; DeHoog et al., 2001; Crossley et al., 2018). It has been suggested that in arc volcanic settings, these values generally evidence the infiltration of subducted metasomatic (sulphate-bearing) seawater sulphur into the mantle source of the studied materials (e.g. Alt et al., 1993).

Crossley et al. (2018) showed that despite ready devolatilisation of sulphur during subduction, serpentinite-hosted sulphides could retain an isotope composition characteristic of seafloor materials. The samples studied were Jurassic in age (when seawater sulphate $\delta^{34}S$ was ~ 17 ‰), and the sulphides analysed contained high $\delta^{34}S$ values (1.9-15.5 ‰), which were consistent with a hydrothermal origin of seafloor sulphate reduction (Crossley et al., 2018). Alt et al. (2012) had also observed $\delta^{34}S$ enrichment in serpentinised oceanic peridotites having undergone dehydration and desulphurisation (at 700 °C and 16-1.9 GPa) and suggested that the isotopically fractionated dehydration products of serpentinites could be transported deeper into the mantle. However, Alt et al. (1995) had observed that the mean $\delta^{34}S$ composition of altered oceanic crust was only 0.9 ‰, and that subducted basaltic crust was therefore unlikely to be a significant contributor to the high $\delta^{34}S$ values generally observed in arc volcanic rocks.

Sulphides hosted in sedimentary massive sulphide deposits as well as in volcanic settings can typically exhibit large variations in their sulphur isotopes compositions, particularly when the $\delta^{34}S$ values are light (e.g. Eldridge et al., 1993; Velasco et al., 1998). In modern sea-floor hydrothermal vent deposits, negative $\delta^{34}S$ values have also been observed (Peter and Shanks, 1992; Seewald et al., 1994; Herzig et al., 1998; Alfonso et al., 2003). These usually indicate that the sulphur-bearing species inherited its signature from bacterially mediated reduction of seawater sulphate (Zhao et al. (2007).

5.1.2.3. Sulphur isotope geochemistry of the mantle

The abundances of stable sulphur isotopes in the solid Earth vary depending on their mass (c.f. Section 5.1.1.1), during common igneous and metamorphic processes. The resulting sulphur isotope ratios provide a means of investigating the presence of surface-derived materials in the continental lithospheric mantle (e.g. Smit et al., 2019). The $\delta^{34}S$ composition of the mantle was

initially considered to be 0±2 ‰ (Nielsen, 1979). Labidi et al. (2014) more recently determined the canonically referenced $\delta^{34}S$ value to be -1±2 ‰, rather than being centred around 0.

Various processes are known to give rise to sulphur isotopic heterogeneity in the mantle, and it has been shown that incompatible element-enriched components can be recycled into the mantle and resurface in mid-ocean ridge basalts (MORB) and ocean island basalts (OIB) (e.g. Chaussidon et al., 1989; Labidi et al., 2013; 2014; Dixon et al., 2017). The temperature of a subducting slab entering the mantle is a key variable in determining the volatile content of a subducting slab, and the depths to which they can be subducted (section 1.3.3.; Santosh et al., 2010).

Significant studies have also been conducted investigating the stable sulphur isotope compositions of sulphide and sulphate minerals included in mantle xenoliths, plume-derived materials, carbonatites and kimberlitic rocks (e.g. Kanehira et al., 1973; Mitchell and Krouse, 1975; Gerlach and Thomas, 1986; Chaussidon et al., 1989; Ionov et al., 1992; Labidi et al., 2013; 2014; 2015; Cabral et al., 2013; Delavault et al., 2016; Kitayama et al., 2017). Such publications have commonly revealed the presence of recycled signatures, as well as the preservation of relics of ancient subducted sedimentary materials (Cabral et al., 2013; Delavault et al., 2016), shedding light on the complex temporal evolution of the terrestrial sulphur cycle, and highlighting the isotopically heterogeneous nature of the mantle.

Figure 5.5 shows the $\delta^{34}S$ and $\Delta^{33}S$ compositions of plume-derived sulphide minerals as those of diamond-hosted sulphide inclusions which are discussed in the next section.

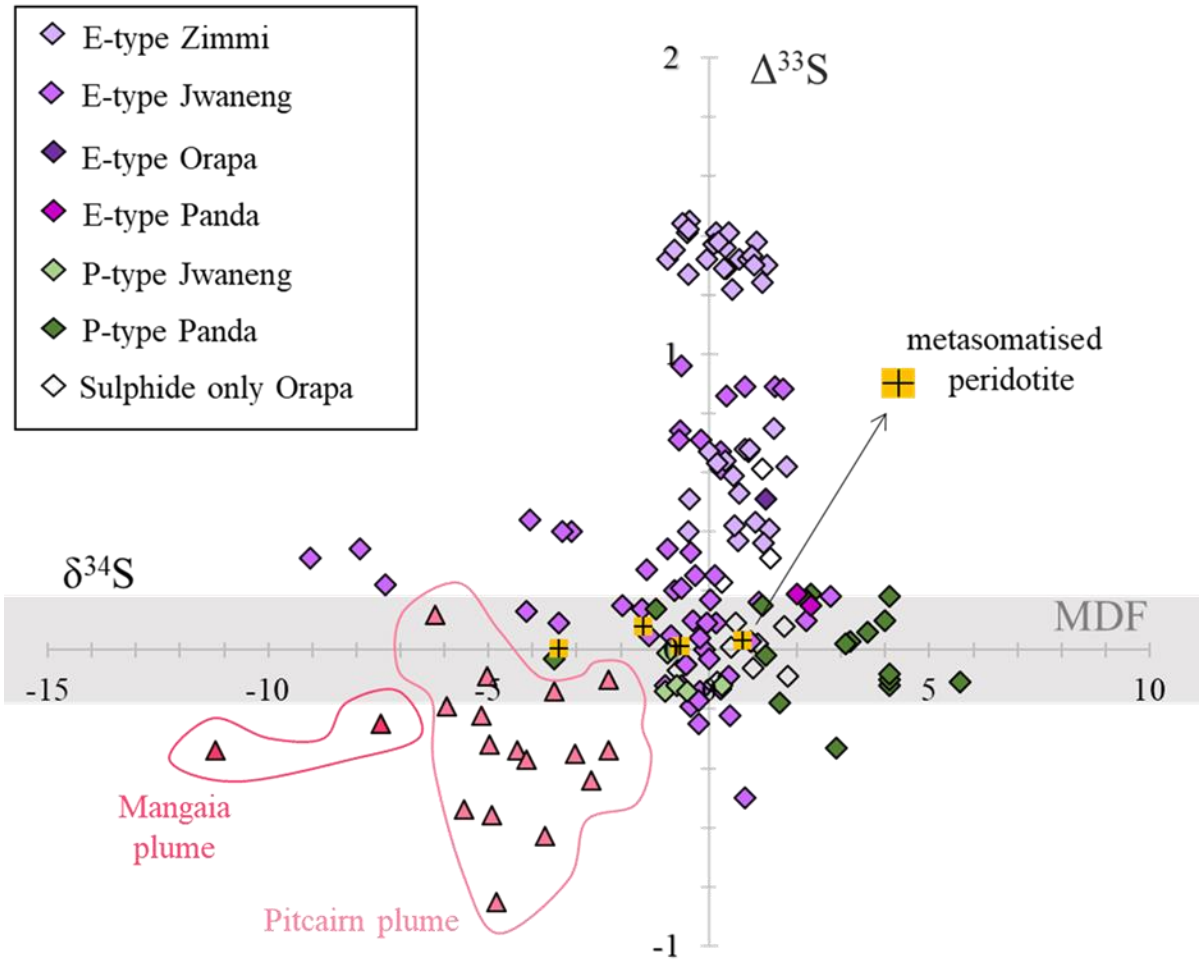

Figure 5.5. $\delta^{34}S$ and $\Delta^{33}S$ compositions of diamond-hosted sulphide inclusions Farquhar et al. 2002; Thomassot et al. 2009; Cartigny et al. 2009; Smit et al., 2019), sulphide inclusions in plume-hosted mantle xenoliths (Cabral et al. 2013; Delavault et al. 2016) and metasomatised peridotite xenoliths (Giuliani et al. 2016)

5.1.2.4. Sulphur isotope compositions of sulphide inclusions in diamonds

The sulphur isotope compositions of diamond-hosted sulphide inclusions were first analysed by ion microprobe by Chaussidon et al. (1987), who observed positive $\delta^{34}S$ values (+2.3± 1.4 ‰ - +8.2± 0.9 ‰) in two inclusions in peridotitic diamonds from Premier (South Africa), and four in eclogitic diamonds from Orapa (Botswana). This deviation from the mantle value was interpreted as evidence for a recycled input into diamond-forming regions of the Earth's mantle. Eldridge et al. (1991) then measured the sulphur isotope compositions of sulphide inclusions in African diamonds, which displayed much greater $\delta^{34}S$ variability across 25‰ (-

11 to 14‰). Whilst the large spread in $\delta^{34}S$ was observed in eclogitic diamonds, signalling the addition of subducted oceanic crust and recycled sediments to their source region, sulphide inclusions with higher Ni contents (hosted in peridotitic diamonds) showed little variation from 0% (Eldridge et al., 1991) (c.f. Figure 5.6)

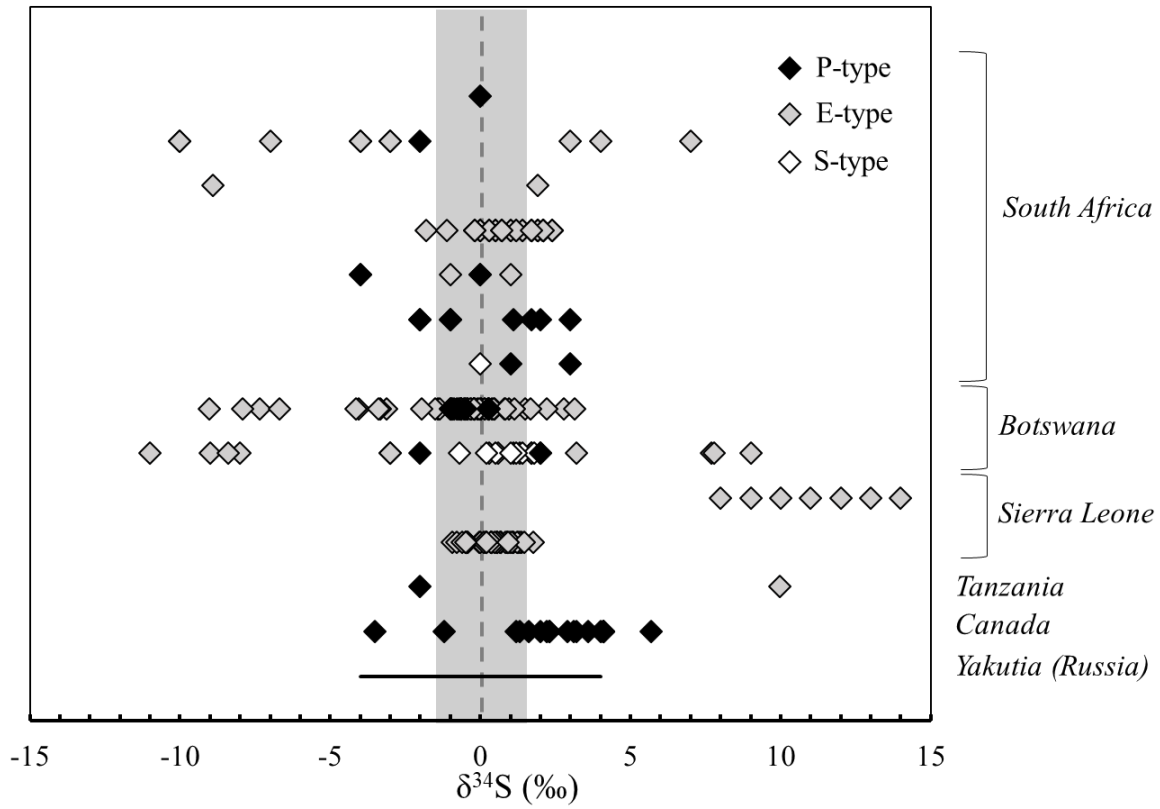

Figure 5.6. $\delta^{34}S$ compositions of eclogitic (E-type), peridotitic (P-type) and "sulphide-only" (S-type) bearing diamond-hosted sulphide inclusions from worldwide localities, reported by Chaussidon et al., (1987), Eldridge et al. (1991), Rudnick et al. (1993), Farquhar et al. (2002), Westerlund et al. (2004), Thomassot et al. (2009; 2017), Cartigny et al., (2009) and Smit et al., (2019).

Rudnick et al. (1993) measured the $^{34}S/^{32}S$ ratios, and Pb/Pb isotope compositions of Yakutian diamonds from the Mir, 23rd Party Congress and Udachnaya kimberlite pipes, observing narrow ranges of $\delta^{34}S$ values for both E- and P-type sulphide inclusions (-4 to +4 ‰), plotting near the mantle $\delta^{34}S$ range (0 ± 3 ‰). However, it was suggested that since subducted oceanic lithosphere can exhibit mantle-like sulphur isotope signatures (e.g. Ohmoto and Rye, 1979;

Sakai et al., 1984) a recycled component could not be "ruled out", and in fact, the high U/Pb compositions measured in the same inclusions perhaps reflected on the involvement of a subducted basaltic component (Zindler and Hart, 1986; Sun and McDonough, 1989; Rudnick et al., 1993).

Later work conducted by Westerlund et al. (2004) on sulphide inclusions in ~2.5 by-old E-type diamonds from Klipspringer also revealed a relatively narrow $\delta^{34}S$ range (-1.8 to +2.4 ‰; average ~1), comparable to values observed in slightly altered MORB or in sub-lithospheric mantle sources. In this case again, a recycled origin of sulphur could not be ruled out because subducted MORB does not excusively exhibit large variations in $\delta^{34}S$, and in fact, diamond growth at Klipspringer was proposed to have a occurred through the local remobilisation of eclogite-derived C-H-N-S fluids, during an early Proterozoic thermal event (Westerlund et al., 2004).

In 2002, Farquhar et al. identified a S-MIF signal in sulphide inclusions in diamonds from Orapa, which implied that Archean sulphur had been transferred into the relatively unmixed diamond-forming region in the mantle. Four sulphur isotope analyses, which are required to calculate $\Delta^{33}S$ were only made possible then, because they require a higher instrumental sensitivity which had not been obtainable before. Since then, various authors have reported a S-MIF signal in lithospheric diamond-hosted sulphide inclusions, demonstrating that Archean sulphur-bearing material can be included in relatively younger diamond populations (e.g. Cartigny et al., 2009, Thomassot et al. 2009, Smit et al. 2019).

Indeed, anomalous S-MIF ($\Delta^{33}S$ and $\Delta^{36}S \neq 0$) signatures are generally robust, and can be preserved despite undergoing metamorphism, subduction processes and arc magmatism (Selvaraja et al., 2017; Muller et al., 2017; Smit et al., 2019). It has also been shown that Archean signatures can be preserved at high temperatures (>1300 °C) in the convecting mantle

source of some ocean island basalts (Cabral et al., 2013; Delavault et al., 2016). Most recently, Smit et al. (2019) measured the sulphur isotope compositions of sulphide inclusions hosted in Neoproterozoic diamonds from West Africa, which clearly confirmed that S-MIF signatures could be preserved despite being introduced into the convecting mantle, and revealed that such anomalous compositions could be preserved for billions of years beneath relatively cool cratons which had avoided the mixing effects of mantle convection.

Stable sulphur isotope analyses provide a means of investigating the source of sulphur in sulphide inclusions in diamonds and help constrain some of the reaction pathways undertaken by sulphur-bearing phases during subduction. In this chapter, the potential origins of sulphur in "komatiitic" diamonds from Dachine (French Guiana), sublithospheric diamonds Juina-5 and Collier-4 (Brazil), and eclogitic lithospheric diamonds from Mir (Yakutia) are explored. The nature and significance of sulphide inclusions in diamonds formed through different reactions at different depths are relatively poorly constrained, as are the behaviour and fate of sulphur-bearing materials being recycled into the mantle. Together with observations of their mineralogy, the sulphur isotope compositions of sulphides included in diamond are therefore used to investigate the origin and nature of the sulphur involved in different diamond-forming reactions.

5.2. Materials and methods

5.2.1. Raman spectroscopy

Raman spectroscopy was used to determine the mineralogy of unexposed diamond-hosted sulphide inclusions and other inclusions when they occur in the same diamonds. The Raman configurations that were used were identical to the ones in outlined in chapters 2-4.

5.2.2. Scanning electron microscopy (SEM) and electron probe analyses (EPMA)

Determining the mineralogy of the analysed matrix of the inclusions is essential for performing sulphur isotope measurement corrections, since sulphur isotopes naturally fractionate differently in varying sulphide minerals. Electron dispersive x-ray spectroscopy (EDS) by scanning electron microscopy (SEM) was used to determine the stoichiometry of 4 exposed Juina-5, 1 Collier-4 and 5 Mir sulphide inclusions. The data was acquired using a ~2-3 µm spot size and 20 KeV accelerating voltage. The chemical composition of the studied Dachine inclusions had previously been determined by Smith et al. (2016). 4 sulphide inclusions in 4 diamonds from Juina-5, 1 from Collier-4 and 5 inclusions in 4 diamonds from Dachine were also mapped by electron microprobe (EPMA) to investigate their major element (Fe, Ni and Cu) distributions at 20 KeV and with a ~2-3 µm beam size. Since the inclusions in the sublithospheric (Juina-5 and Collier-4) and Dachine diamonds are relatively small in size (<25 µm), elemental maps were considered equally useful for estimating the mineralogy of the samples, seeing as the spot size used in secondary ion mass spectrometry (~20 x 20 µm) was usually large enough to encompass the whole of these inclusions (c.f. Appendix B, Figs. B1 and B2).

5.2.3. Secondary ion mass spectrometry (SIMS)

5.2.3.1. Sample preparation

A total of 18 exposed inclusions in 3 diamonds from Mir (Yakutia), 5 from Dachine (French Guiana), and in 4 sublithospheric diamonds from Juina-5 and 1 Collier-4 (Brazil) have been analysed by SIMS. The 13 diamonds that were analysed were mounted into indium which is typically very pure and devoid of any S. A hydraulic press was used to make the polished surfaces of the samples and their inclusions uniformly flat, because reliable SIMS measurements are dependent on the analysed samples having little to no (<3 µm) internal

topography. Subsequently, the samples were coated in gold in order to optimise electrical conductivity across the sample holder.

5.2.3.2. Analytical procedure

Secondary ion mass spectrometry was performed using a Cameca 1280 HR ion microprobe, at the Centre de Recherches Pétrographiques et Géochimiques (CRPG) in Nancy using a primary 1.5 nA Cs+ source. The four stable sulphur isotopes (^{32}S, ^{33}S, ^{34}S and ^{36}S) were measured simultaneously in multicollection mode using three Faraday cups, with a spot size of around 20 µm. Sample chamber pressure was kept below 7.23×10^{-9} Torr during each of the sample measurements and count rates varied between 2.5^7 to 1.17^9 and 7.3^7 to 2.14^9 counts per second (cps) for the measured samples and standards respectively. Analyses of the sulphide inclusions lasted 7 minutes on average; the sample was pre-sputtered for 180 s each time for Faraday cup background measurements, prior to 40 sample measurement cycles, each lasting 6 s. An electron multiplier was used for measuring the least abundant sulphur isotope ^{36}S.

The advantages of using secondary ion mass spectrometry over Laser Ablation Inductively Coupled Plasma Mass Spectrometry (LA-ICPMS) include the higher spatial resolution and sensitivity provided by SIMS, as well as the fact that LA-ICPMS is more destructive to the samples than SIMS; pits produced by SIMS analyses are typically only several micron deep (e.g. Hauri et al., 2016).

5.2.3.3. Instrumental mass fractionation (IMF) corrections

Raw measured isotope ratios are shifted from the absolute ratios due to the large instrumental mass fractionation (IMF) effects (collectively referred to as instrumental bias) that arise from several processes during SIMS analyses; mass fractionation of isotopes occurs during a) the production and acceleration of ions from the analysed sample (known as sputtering), b) the

transmission of the resulting secondary ions through the instrument and c) the detection of the ions (e.g., Hervig et al., 1992; Riciputi et al., 1998; Valley and Kita, 2009; Kozdon et al., 2010). IMF is a complex phenomenon which is influenced by various factors including the mineralogy of the analysed sample, the intensity of the primary ion beam, the pressure within the sample chamber, the X-Y position of the stage and the intensity of the electrostatic deflectors permitting the mass differentiation of the measured isotopes.

In order to obtain confident results, IMF has been corrected for using the measured and known values of a series of standard reference materials:

$$IMF\ (‰)\ = (\frac{measured\ R_{ref}}{true\ R_{ref}})$$

Where R is the measured or true ratio of the isotopes of interest (e.g. $^{34}S/^{32}S$) in the reference (ref) material.

5.2.3.4. Standard reference materials

A group of matrix-matched standards having known sulphur isotope compositions are typically used to correct for instrumental mass fractionation (IMF) effects (see above formula). The standards used consist of the same mineral groups as the analysed sulphide inclusions (pyrite, pyrrhotite, pentlandite and chalcopyrite); average IMF effects of the standards are then resolved in relation to the known (previously determined) composition of the standard.

Six sulphide standards with different compositions (pyrrhotite – $Fe_{(1-X)}S$, pyrite – FeS_2, pentlandite – $FeNi_9S_8$, chalcopyrite – $CuFeS_2$ and galena – PbS) were measured multiple times (n = >6) before the samples were analysed and at regular intervals during the measurement sessions, to calibrate the instrumental mass fractionation (IMF) line of sulphur isotopes during the analyses. During the analytical session, one standard (StdInsideRing) was placed onto the

sample holder alongside the diamonds and ran as unknowns to check instrumental calibration before and several times throughout the sample measurement sessions (the measurement sequence that was followed is described in appendix B; table B3).

Table 5.1. Standard reference materials

Name	Composition	$^{33}S/^{32}S$	$^{34}S/^{32}S$	$\delta^{34}S$ (‰)	$\Delta^{33}S$ (‰)	Source
Galice	Pyrite FeS_2	0.00787220	0.04410620	-1.28	0.02	**A**
Mif-Po	Pyrrhotite $Fe_{1-X}S$	0.00791530	0.04442084	5.83	1.83	**A**

Table 5.1. Sulphur isotope compositions of the standard reference materials used for instrumental mass fractionation (IMF) corrections from A – Delavault et al. (2016);

Here, IMF corrections were made following the procedure described by Delavault et al. (2016) and the results were expressed relative to Canyon Diablo Troilite (CDT) ($^{34}S/^{32}S_{CDT}$ = 0.0441626 and $^{33}S/^{32}S_{CDT}$ = 0.00787729; Ding et al., 2001) Only the sulphur isotope compositions of two of the standards, for pyrite (galice) and the mass-independently fractionated pyrrhotite (Mif-Po), were known (table 5.1); for chalcopyrite and pentlandite the IMF values of the standards (Cp Norilsk and Pn Norilsk) were calculated from the supplementary information available in Delavault et al. (2016). The standard reference materials used in IMF calculations exhibit a large range of $\delta^{34}S$ compositions (-1.51 to 18.28 ‰). The errors on of samples and standards expressed as 2σ, are reported in the tables in appendix B; B1 and B3). Only one standard (Mif-Po) consists of a mass-independently fractionated pyrrhotite grain ($\Delta^{33}S$ = 1.70 to 2.07 ‰), while the rest of the standards have mass-dependently fractionated compositions ($\Delta^{33}S$ = 0 to 0.5 ‰).

In the analytical session, the raw SIMS analyses of standard reference materials performed throughout the sample measurement sessions defined an instrumental fractionation line (IFL)

with a slope (β) of , with a y-intercept (ε) of (β differs slightly from the theoretical value of 0.515 defined according to mass fractionation laws). The reported $\Delta^{33}S$ values essentially correspond to variations perpendicular the slope β of the IFL. The stability of the β value was monitored throughout the analytical sessions with repeat measurements of the different standards (n < 11). Precisions of 0.45 ‰ and 0.27 ‰ or better for repeat measurements of $\delta^{34}S$ and $\delta^{33}S$ respectively were obtained in the pyrite (Galice $\delta^{34}S$ = 0.24 ‰ and $\delta^{33}S$ = 0.14 ‰), chalcopyrite (Cp Norilsk $\delta^{34}S$ = 45 ‰ and $\delta^{33}S$ = 25 ‰) and mass-independently fractionated pyrrhotite (Mif-Po $\delta^{34}S$ = 38 ‰ and $\delta^{33}S$ = 27 ‰) standard grains. The pentlandite standard grain measurements (n = 15) yielded precisions of 0.67 ‰ and 1.22 ‰ for $\delta^{33}S$ and $\delta^{34}S$ respectively.

5.3. Results

The results for the preliminary sulphur isotope results are presented in the following sections. Here, only the $\delta^{34}S$ compositions of the inclusions and whether a clear $\Delta^{33}S$ signature was observed are focused on. The $\Delta^{36}S$ values will not be discussed in this chapter because of the large uncertainties associated with the instrumental mass fractionation (IMF) corrections and known standard compositions. Figure 5.7 plots the published sulphur isotope compositions of diamond-hosted sulphide inclusions, mantle plume xenoliths and metasomatised peridotite xenoliths alongside the compositions of the Mir, Dachine, Juina-5 and Collier-4 diamonds that were analysed in this study.

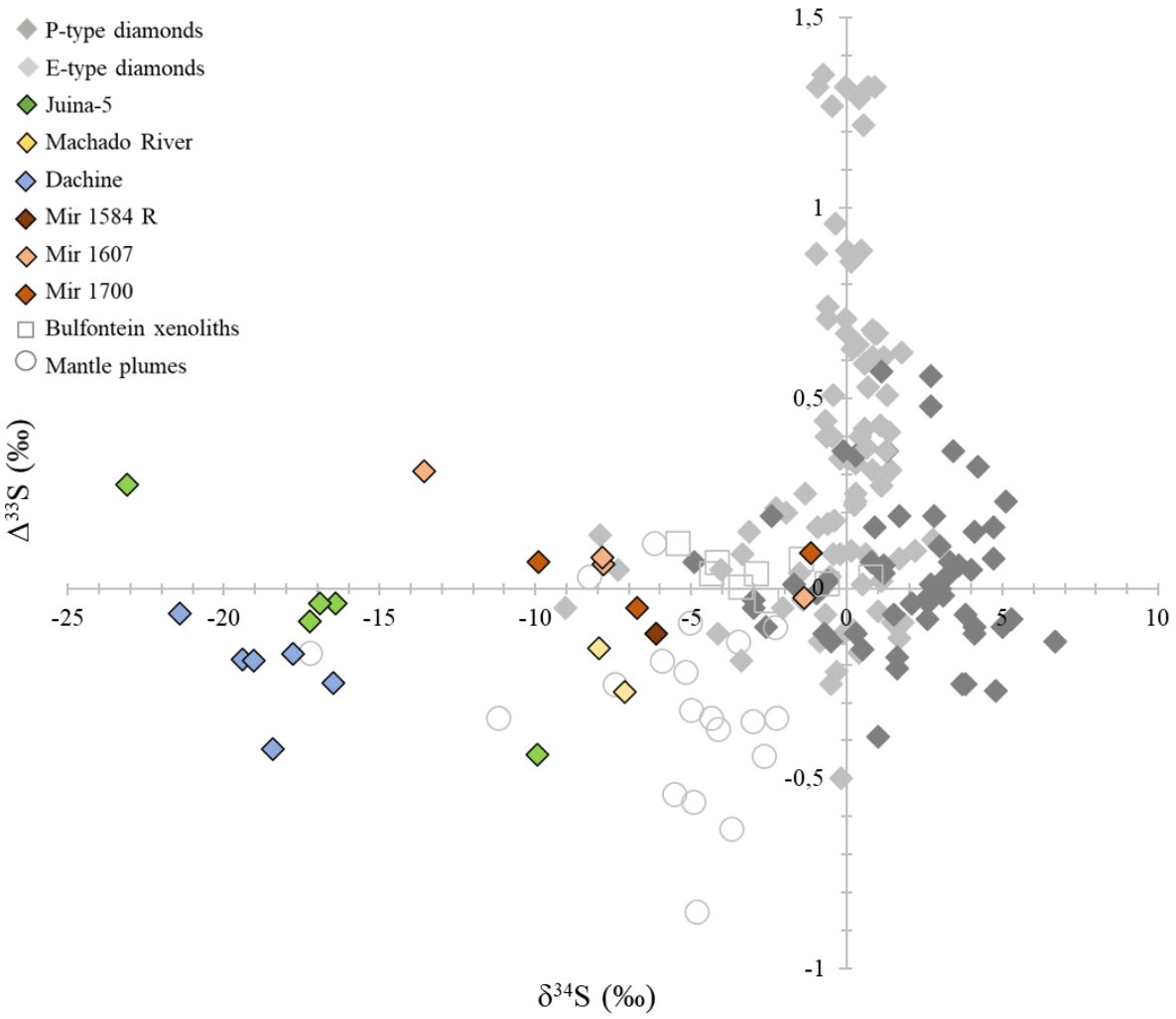

Figure 5.7. Preliminary $\delta^{34}S$ and $\Delta^{33}S$ compositions of sulphide inclusions in diamonds from Dachine (French Guiana), Juina-5 and Collier-4 (Brazil), and Mir (Yakutia) – in colour – compared with the published compositions of eclogitic and peridotitic diamonds from Jwaneng, Orapa, Panda and Zimmi, mantle plume xenoliths and metasomatised peridotite xenoliths (see figure 5.5).

5.3.1. Dachine

Six measurements of six exposed inclusions in five Dachine diamonds reveal light $\delta^{34}S$ compositions (-16.5 to -21.4 ‰) (Appendix B, table B1). Two inclusions in Dachine diamond Dac-BS-4A8 exhibit some variation in their $\delta^{34}S$ compositions (-19.39 ± 0.086 and -17.78 ± 0.058 ‰). Overall, the group of inclusions which were analysed exhibit relatively little scatter in their $\delta^{34}S$, and their measured $\Delta^{33}S$ values do not deviate significantly from 0 with the exception of one inclusion in diamonds Dac-BS-4B10 ($\Delta^{33}S$ = 0.42 ‰). However, the inclusion

in diamond Dac-BS-4B10 is approximately 10 µm wide resulting in significantly lower count rates for ^{32}S (2.5 x 10^7 cps) and has a significantly larger internal error on its $^{33}S/^{32}S$ ratios (7.8 x 10^{-3} ± 1.1 x 10^{-5}) and propagated error on $\delta^{33}S$ (-9.96 ± 1.4 ‰) (Appendix B, table B1), which makes the measured $\Delta^{33}S$ anomaly unreliable.

5.3.2. Juina-5 and Collier-4

Seven sulphur isotope measurements on four inclusions in diamonds from Juina-5 and one inclusion in Collier-4 diamond J6 reveal variably light $\delta^{34}S$ compositions (-7.13 to -23.11 ‰). In the four Juina-5 samples from which data was obtained, $\delta^{34}S$ values range from -9.93 ± 0.042 ‰ in diamond Ju5-53 to -23.11 ± 0.095 ‰ in diamond Ju5-120. With the exception of a pyrite inclusion in diamond Ju5-54, the inclusions consist of predominantly of pyrrhotite with minor proportions of pentlandite (<16 %) and chalcopyrite (<5 %) (c.f. Appendix B, Fig. B1 and B2). The relatively large (~25 x 50 µm) inclusion in the Collier-4 diamond J6 was analysed in two different parts areas within the inclusion (Appendix Fig. B2); the results indicate that its $\delta^{34}S$ composition is light (-7.94 ± 0.029 and -7.13 ± 0.032 ‰), but heavier than that of any of the Juina-5 inclusions.

The $\Delta^{33}S$ values of the samples from Juina-5 and Collier-4 show little or no deviation from zero (-0.46 to 0.33 ‰). Of the five measurements on the four Juina-5 inclusions, the inclusion in diamond Ju5-120 exhibits a slightly positive $\Delta^{33}S$ value (0.27 ‰), and one measurement of the inclusion in Collier-4 diamond J6 reveals slightly negative one (-0.27 ‰; Appendix B, table B1). However, the errors on these are likely to be so great that a geologically significant reason for these results will not be determined.

5.3.3. Mir

Eight sulphur isotope measurements were performed on six exposed inclusions in lithospheric diamonds from Mir (1584-rim, 1607 and 1700). The $\delta^{34}S$ compositions of the inclusions are highly variable, ranging from -1.14 to -13.56 ‰. Four out of six of the inclusions in the three analysed diamonds exhibit relatively light $\delta^{34}S$ signatures (-6.13 ± 0.081 to -13.56 ± 0.084 ‰), while two inclusions in diamonds 1607 and 1700 reveal heavier $\delta^{34}S$ compositions (-1.37 and -1.14 ‰ respectively). Only one inclusion in diamond 1607 (1607-a, which consists of pyrrhotite) exhibits a slightly positive Δ33S value (0.307 ‰), with the Δ33S compositions of the remaining inclusions ranging between -0.117 and 0.094 ‰.

In diamond 1607, two of the three exposed inclusions (1607-a and 1607-b) exhibit light $\delta^{34}S$ values and the third (1607-c), which is situated in an outer zone in the diamond (c.f. Appendix A, Figs. A1 and A2) has a more positive $\delta^{34}S$ composition (-1.37 ± 0.056 ‰). Inclusion 1607-b, which was analysed twice exhibiting only slight intragrain variability (-7.8 and -7.85 ± 0.022 ‰). In diamond 1700, repeat measurements of inclusion 1700-1 which is located in the core of the diamond (Appendix A, Figs. A1 and A2) reveal a larger variation in $\delta^{34}S$ within the inclusion but greater error on each analysis (-6.73 and -9.91 ± 0.12 ‰) (Appendix B, table B1). An inclusion (1700-2) located at the boundary between the intermediate and growth zones of diamond 1700 (Appendix, Fig. A1 and A2) has a heavier $\delta^{34}S$ composition (-1.14 ± 0.115 ‰).

5.4. Discussion

Diamonds from Dachine (French Guiana), the Juina area (Brazil) and Mir (Yakutia) have been used in this study because of the different ages, depths and mechanisms of formation that have been assigned to each of the diamond populations (e.g. Smith et al., 2016; Bulanova et al., 2010; Wiggers de Vries, 2013). In the following sections, the preliminary stable sulphur isotope

results acquired in this study are interpreted considering the formation conditions and ages of the diamond populations to which the samples belong. An attempt is also made at comparing these with results with the average carbon isotope compositions of the diamonds from each locality.

5.4.1. Sulphur isotope compositions

5.4.1.1. Dachine

Diamonds from Dachine (French Guiana), are unique among worldwide diamond populations, being generally termed as komatiitic diamonds since they have been shown to be derived from a komatiite-boninite host which was emplaced ca. 2.2 Ga during an arc-forming Paleoproterozoic subduction zone setting (e.g. Smith et al., 2016). The diamonds are therefore relatively old, although no radiometric dates of the inclusions have been published in literature so far. A relatively deep origin has also been speculated for diamonds from Dachine; Smith et al. (2016) reported on a majoritic garnet inclusion in a Dachine diamond, implying that at least some of the diamonds were formed at depths of ~250 km.

The sulphur isotope compositions of the 6 analysed sulphide inclusions in Dachine diamonds unanimously display extremely light $\delta^{34}S$ compositions which range between - 16.73 and - 21.57 ‰, indicative of a recycled origin. The compositions generally plot within a relatively well constrained range of values (e.g. Fig. 5.7). This could imply that the sulphur in the Dachine sulphide inclusions have a common source of subducted sulphur, or that the processes transforming the sulphur-bearing materials involved in Dachine diamond formation occurred under similar conditions. It has been suggested that the Dachine diamonds formed shortly before their eruption ca. 2.2 Ga (Capdevila et al., 1999; Cartigny et al., 2010; Smith et al., 2016) and therefore, the absence of a clear anomalous $\Delta^{33}S$ signature (indicative of Archean sedimentary material deposited prior to 2.45 Ga) can be expected.

5.4.1.2. Sublithospheric diamonds

Diamonds from the Juina area in Brazil (Juina-5 and Collier-4) have been found hosted in Mesozoic (<250 My old) kimberlites (Heaman et al., 1998; Kaminsky et al., 2010), which were likely erupted into a Proterozoic (1.55-1.8 Gy old) basement (Tassinari et al., 2000). Diamonds from the Juina area have been the subject of extensive studies, particularly for their non-sulphide inclusions and general diamond characteristics (Harte et al., 1999; Kaminsky et al., 2001; Hutchison et al., 2001; Hayman et al., 2005; Brenker et al., 2007; Walter et al., 2008; Kaminsky et al., 2009; Bulanova et al., 2010; Walter et al., 2011; Araujo et al., 2013; Zedgenizov et al., 2014; Thomson, 2014; Thomson et al., 2014; 2016; Burnham et al., 2015; 2016). Only two radiometric ages have been assigned to the inclusions in sub-lithospheric diamonds, including a single 602 my old age obtained through Re-Os dating by Shirey et al. (2015) and a Cretaceous (~101 my) U-Pb age of a Ca–Si–Ti inclusion has also been published (Bulanova et al., 2010). Nitrogen aggregation studies, however, cannot be used to ascertain mantle residence times as the Juina area diamonds contain low nitrogen contents (<20 ppm).

Previous workers have indicated that diamonds from the Juina area were likely formed as a result of the interaction between oxidised surface-derived C-O-H-bearing fluids/melts deriving from a relatively young (~90-190 My old) subducting slab with an otherwise reduced deeper mantle, at depths ranging between ~300 and 800 km (e.g. Walter et al., 2011; Thomson et al., 2014; 2016; Burnham et al., 2015; 2016). However, the processes modifying sulphur-bearing material being subducted into diamond-forming regions remain unclear due to uncertainties about their host lithology, the pressure and temperature conditions they underwent during their transport into the mantle and the redox pathways they are subjected to. The four Juina-5 samples that were analysed exhibit variably light $\delta^{34}S$ compositions (-9.93 to -23.11 ‰), which are characteristic of recycled sulphur and consistent with a possible common source for sulphur

and the oxidised C-O-H fluids that formed the diamonds (c.f. Chapter 2). A clearly anomalous $\Delta^{33}S$ signature was not recorded in the studied inclusions and is not expected if the diamonds are young (~101 My, Bulanova et al., 2010) and capturing contemporaneously formed inclusion material (e.g. Pyrite, Chapter 2). It is also possible that the analysed sulphide inclusions belong to distinctive diamond populations sampled by the Juina-5 kimberlite.

Despite the insufficient amount of sulphur isotope data presented here, an intriguing observation however is the difference between the sulphur isotope compositions of the sulphide inclusions hosted in Juina-5 diamonds and the one which was analysed in Collier-4 diamond J6. The Juina-5 samples exhibit lighter $\delta^{34}S$ signatures than the inclusion in the Collier-4 diamond (which was analysed twice), which has a relatively heavier $\delta^{34}S$ composition (average = -7.53 ‰).

5.4.1.3. Mir

The studied diamonds from Mir contain sulphide inclusions distributed across different growth zones of the diamonds (Appendix Fig A1, A2; B3). Sulphide inclusion-bearing diamonds from Mir have been sub-categorised by Wiggers de Vries et al. (2013; Bulanova et al., 2014) as belonging to Groups 1 and 2 (see Chapter 4). The Group 1 Mir diamonds are characterised by relatively low Cu (<1.28 wt. %) and Ni (<2.87 wt. %) pyrrhotites and were shown to have formed first ~2.1 Ga at ~180 km depths from carbon that was originally surface-derived. The younger Group 2 population grew later and at shallower depths from mantle-like carbon and contain more chalcopyrite (Cu 1.04-4.18 wt. %) and pentlandite (Ni 5.8-7.75 wt. %) (Wiggers de Vries et al., 2013; Bulanova et al., 2014).

The studied Mir diamonds exhibit significantly different $\delta^{34}S$ compositions between inclusions and across their growth zones (Mir 1607 and 1700) (Fig. B3). The variability in $\delta^{34}S$ between

mantle-like (e.g. -1.37 ‰ in 1607-c and -1.14 ‰ in 1700-2) and recycled (e.g. -6.13 to -13.56 ‰ in inclusions 1584R-a, 1607-a, 1607-b and 1700-1) signatures is not unexpected, seeing as it is still undetermined which sulphide inclusion-bearing group the diamonds belong to (c.f. Wiggers de Vries et al., 2013). However, of the inclusions studied here, the samples exhibiting heavier $\delta^{34}S$ compositions are relatively richer in Cu and Ni on average (Appendix B, table B2) while the inclusions characterised by light $\delta^{34}S$ values consist predominantly of pyrrhotite with the exceptions of inclusions 1584R-a and 1607-b. Indeed, in diamond 1700, the central inclusion analysed (points Mir 1700-1-1 and 1700-1-2) consists of relatively low Ni and Cu pyrrhotite (Appendix B, table B2) exhibiting light $\delta^{34}S$ compositions (-6.73 and -9.91 ‰). The inclusion in an outer growth zone of diamond 1700 (Mir 1700-2) has appreciable Cu and Ni contents and exhibits a heavier mantle-like $\delta^{34}S$ signature (-1.14 ‰). In diamond 1607, no clear correlation is observed between the bulk Ni and Cu contents and the $\delta^{34}S$ values; of the three inclusions analysed, two inclusions (Mir 1607-a and 1607-b) exhibit relatively light $\delta^{34}S$ compositions, and one inclusion (Mir 1607-c) in an outer growth zone of the diamond (Appendix A, B) reveals a heavier $\delta^{34}S$ value (Fig. 5.7; B3).

Overall, the differences in major element compositions of the inclusions distributed across growth zones in diamonds 1700 and 1607 are not enough to imply that they belong to Group 1 and 2 Mir diamonds respectively. However, the positioning of the inclusions in the diamonds shows that the inclusions with heavier $\delta^{34}S$ compositions (1607-b and 1700-2) were encapsulated in diamond at a later stage than the inclusions with lighter $\delta^{34}S$ signatures (1607-a, b and 1700-1) (Fig. B3) Therefore, the variable sulphur isotope results could be consistent with different sources of sulphur being involved in the formation of different growth zones of single diamond crystals (e.g. Mir diamond 1704; c.f. Chapter 4; Bulanova et al., 2014).

At Mir, the formation of the sulphide inclusion-bearing diamonds is thought to have occurred around 0.9-1.1 and 2.1 Ga (Wiggers de Vries et al., 2013a) and there has not been any evidence published suggested that the sulphur present in them pre-dates the first Great Oxidation Event (~2.45 Ga) after which the S-MIF signal waned, and then disappeared from the rock record (Fig. 5.2 and 5.3). The $\delta^{34}S$ compositions of the sulphide inclusions measured by Rudnick et al (1993) for Siberian diamonds from Mir, 23rd Party Congress and Udachnaya (Yakutia, Russia) were reported to range near mantle values (-4 to +4 ‰) (Fig. 5.6), and therefore differ to at least 4 out of 6 inclusions in the studied Mir diamonds.

5.4.2. Carbon isotope compositions

Figure 5.8. shows the relationship between the average C isotope compositions ($\delta^{13}C$) of the studied diamond populations available in the literature and the S ($\delta^{34}S$) isotope signatures measured in their sulphide inclusions. Plotted are also the C and S isotope compositions measured in diamonds from Panda (Canada) and Jwaneng (Botswana) (Cartigny et al., 2009; Thomassot et al., 2009).

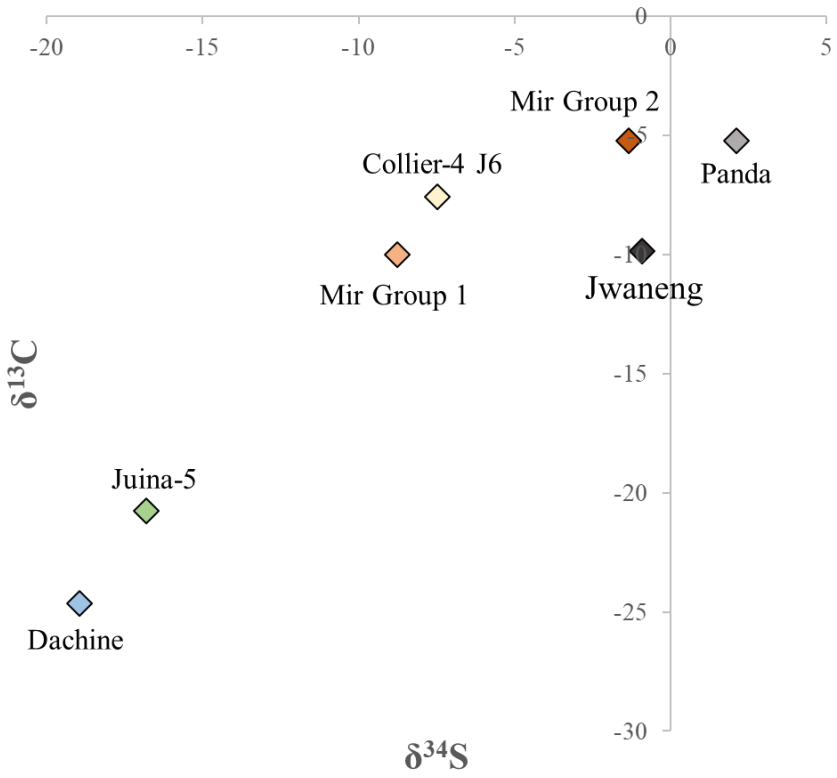

Figure 5.8. Published average carbon isotope compositions ($\delta^{13}C$) for diamonds from Panda (Cartigny et al., 2009), Jwaneng (Thomassot et al., 2009), Mir (Wiggers de Vries et al., 2013; see text in section 5.4.3. for explanation of determining group 1 and group 2 Mir inclusions), Collier-4 diamond J6, Juina-5 and Dachine, plotted against their average $\delta^{34}S$ compositions. Sulphur isotope compositions for diamonds from the Panda and Jwaneng kimberlite were measured by Cartigny et al. (2009) and Thomassot et al. (2009).

5.4.2.1. Dachine

Dachine diamonds record a sedimentary carbon source as suggested by their extremely light C isotope compositions ($\delta^{13}C$ = -36.07 to -18.78 ‰). It was suggested that the carbon forming the Dachine diamonds was initially deposited in a marine setting in early Proterozoic times, and that the processes of diamond crystallisation and exhumation from their growth regions are likely to have occurred rapidly over a relatively short timescale, as indicated by the N defects in the diamonds and their morphology (Smith et al., 2016). It has also been proposed that diamonds at Dachine formed through direct crystallisation of volatiles associated with the formation of their host komatiite melt (Capdevila et al., 1999; Cartigny, 2010).

Too few samples were analysed in this study to determine a general trend between the sulphur and carbon isotope compositions that is representative of the whole Dachine diamond population. Furthermore, the samples studied here were not analysed for their carbon isotope compositions and these may differ from those of the diamonds studied by Smith et al., 2016). However, the extremely light $\delta^{34}S$ values correlate well with the light, recycled $\delta^{13}C$ compositions which characterise the Dachine diamond population (Fig. 5.8). Carbon isotope measurements and potential Re-Os dating of similar unexposed inclusions would help constrain the origin and nature of the sulphides enclosed in the Dachine diamonds.

5.4.2.2. Sublithospheric diamonds

The sulphide inclusions in sublithospheric diamonds from Juina-5 and Collier-4 exhibit $\delta^{34}S$ signatures which correlate well with their light carbon isotope compositions (Fig. 5.7 and 5.8). The majority of sublithospheric diamonds at Juina-5 are composed of isotopically light carbon (average -20.76 ‰) which reflect the light sulphur isotope compositions recorded in the studied diamonds (Fig. 5.8.A; Thomson et al., 2014). Of the four analysed Juina-5 samples, three have previously been studied for their carbon isotope compositions by Thomson et al. (2014); the mean $\delta^{13}C$ values of diamonds Ju5-03 (-14.5 ‰), Ju5-53 (-24.7 ‰) and Ju5-54 (-21.6 ‰) do not individually correlate with their sulphur isotopes compositions ($\delta^{34}S$ = -16.42, -9.93 and -16.93 ‰ respectively. However, a range of $\delta^{13}C$ values have been recorded in different growth zones of the diamonds (4.7 ‰ in Ju5-03, 1.8 ‰ in Ju5-53 and 13.5 ‰ in Ju5-54) (Thomson et al., 2014), and therefore, carbon isotope measurements should be performed of the zones in which the studied sulphide inclusions are hosted

Collier-4 sublithospheric diamonds have been subcategorised into three groups (Bulanova et al., 2010); diamond J6 belongs to the Group 1 of Collier-4 diamonds which exhibit heavier mantle-like carbon isotope compositions (-5 to -10‰) although still retaining a recycled carbon

signature (Fig. 5..8.A; Bulanova et al., 2010). Despite the absence of sublithospheric-type (i.e. polyphase) silicate inclusions in Collier-4 diamond J6, the sample has previously been studied for its nitrogen contents and nitrogen aggregation values, and the group of diamonds it belongs to was shown to have formed at asthenospheric to transition depths with an input derived from a mafic to ultramafic portion of subducted oceanic lithosphere (Bulanova et al., 2010). The sulphur isotope data that was acquired in Collier-4 diamond J6 is somewhat reconcilable with its average carbon isotope composition ($\delta^{13}C$ -7.56 ‰) which is heavier than that of the Juina-5 diamonds (Bulanova et al., 2010), perhaps indicating higher degrees of mixing with mantle sulphur.

5.4.2.3. Mir

In Wiggers de Vries (2013), Group 1 pyrrhotite-bearing diamonds record a recycled carbon isotope signature (-12.08 to -31.36 ‰), while group 2 sulphide inclusions are hosted in diamonds which grew from a carbon source with more mantle-like $\delta^{13}C$ compositions (-3.4 to -7.6 ‰). In figure 5.8, the sulphide inclusions in Mir diamonds that reveal light sulphur isotope compositions have been classed as belonging to Group 1 and the ones with heavy signatures to Group 2, on the basis of their $\delta^{34}S$ compositions and their position in diamond (Fig. B3). This would imply that the sulphur and carbon involved in the formation of inclusions 1584R-a, 1607-a, 1607-b and 1700-1 and their host diamond have a recycled, subduction-related origin, whilst a mantle source for both carbon and sulphur is possibly involved in the formation of inclusions 1607-c and 1700-2. Determining the carbon isotope compositions of the diamond growth zones in which the studied inclusions occur would help determine if they belong to Group 1 or Group 2 Mir diamond inclusions and investigate whether the sulphur and diamond-forming carbon have a common origin. However, the interpretation of the measured sulphur

isotope compositions requires most future attention, seeing as only 6 inclusions in 3 diamonds were studied.

5.5. Conclusions

Sulphide inclusions in diamonds from Dachine (French Guiana), Juina-5 and Collier-4 (Brazil) and Mir (Yakutia, Russia) exhibit significantly different sulphur isotope compositions among and within their populations (Fig. 5.7). Previous workers have shown that significant variations in the sulphur isotope compositions ($\delta^{34}S$ and $\Delta^{33}S$) of diamond-hosted sulphide inclusions occur among worldwide populations (Fig. 5.6 and 5.7) (Chaussidon et al., 1987; Eldridge et al., 1991; Rudnick et al., 1993; Farquhar et al., 2002; Westerlund et al., 2004; Thomassot et al., 2009; 2017; Cartigny et al., 2009; Smit et al., 2019). Light $\delta^{34}S$ values have previously been recorded in some lithospheric diamonds indicating a surface-derived origin for the sulphides they host ($\delta^{34}S$ = <-11 ‰ in eclogitic diamonds, e.g. Eldridge et al., 1991). Archean S-MIF ($\Delta^{33}S \neq 0 \pm 0.2$) anomalies have also been "recorded" in diamonds, demonstrating that at least some of the sulphide inclusions materials were deposited prior to the first Great Oxidation event (ca. 2.45 Ga) and recycled into the Earth's mantle where they remained relatively undisturbed for billions of years (e.g. Thomassot et al., 2009; Cartigny et al., 2009, Smit et al., 2019).

No distinctive $\Delta^{33}S$ anomaly was observed in the diamonds from Dachine, Juina area or Mir, possibly due to the relatively young formation ages of the diamonds and their inclusion incorporation mechanisms (<2.45 Ga; Smith et al., 2016; Bulanova et al., 2010; Wiggers de Vries et al., 2013). Here however, the studied inclusions from Dachine and Juina-5 exhibit extremely light $\delta^{34}S$ compositions (<-21.57 and <-23.21 ‰ respectively), providing evidence for involvement of a recycled sulphur-bearing component related to the formation of the komatiitic Dachine diamonds and sublithospheric diamonds from the Juina area. Two of the

three studied Mir diamonds exhibit relative differences in their $\delta^{34}S$ values, across different growth zones. The distinctive mineralogies of the inclusions may also help group the inclusions as belonging to Group 1 or Group 2 Mir diamonds, which formed at different times and from distinctive carbon sources (recycled vs. mantle carbon respectively) (e.g. Wiggers de Vries et al., 2013)

Overall, the sulphur and carbon isotopes signatures of sulphide inclusion-hosting diamond populations appear to be well correlated (Fig. 5.8); indeed, light average $\delta_{34}S$ signatures have been measured in sulphide inclusions hosted by diamonds generally characterised by light, carbon isotope compositions with a recycled origin. This indicates that the sulphur and carbon involved in the formation of sulphide inclusion-bearing diamonds may potentially derive from a common source. However, further sulphur isotope analyses in conjunction with carbon isotope measurements are needed in order to investigate this and deliberate on the role of sulphur, as well as its nature during diamond-forming events. In fact, different sulphur-bearing materials could be expected to be involved differently with the formation of their diamond hosts, and therefore the nature of the sulphur in diamond-hosted sulphide inclusions should be investigated to better understand its involvement in diamond-forming reactions.

6. Concluding remarks

The study of mineral inclusions in natural diamonds offers a promising insight into the nature of the diamond-forming regions of the mantle and the volatile budget of the Earth's interior. Sulphide inclusions are common features in diamonds worldwide and their abundance in diamonds relative to normal mantle contents suggests that sulphur-bearing material may play an important role in the formation of certain diamonds. Sulphur is among the five most abundant elements on Earth, where it imposes strong controls on both surface and mantle processes. Sulphur is highly sensitive to redox and compositional variations in rocks and fluids where it typically occurs as sulphide or sulphate; its presence and speciation in subduction zones and in mantle environments depends mainly on the sulphur and oxygen fugacity of a system, and its volatile content, and to a lesser extent, pressure and temperature. Sulphur predominates as Fe-Ni-Cu sulphide melts in the diamond-forming regions of the Earth's mantle, where they act as the principal hosts of chalcophile (sulphur-loving) and siderophile (iron-loving) elements. The unique chemistry of diamond-hosted sulphide inclusions also allows for their use in Re-Os radiometric dating of diamond-forming events, understanding the mantle processes associated with the construction of continents over time, as well as providing clues to the nature of the involvement of sulphur-bearing materials in diamond-forming reactions (e.g. Shirey and Walker, 1998; Pearson et al., 1998; Harvey et al., 2016).

Diamonds are inherently associated with fluids in the mantle, and the second chapter provides an overview of the compositions of diamond-forming fluids, as well as exploring the compatibility of sulphur and other volatiles species associated with diamond growth. Diamond-forming reactions involving sulphides that have been reported in literature are summarised; it has been shown experimentally that sulphide melts could participate in the formation of

diamond by acting as reducing agents on oxidised subducting slabs (Pal'yanov et al. 2007), providing direct growth media for diamonds (Zhimulev et al., 2016), acting as recipients of carbon in the lower upper mantle (Zhang et al., 2015; 2018) or by promoting diamond stability in certain otherwise reduced regions of the Earth's mantle (Tsuno and Dasgupta, 2015). Petrological observations of volatile phases that are associated with sulphide inclusions in diamonds are relatively scarce, however. In the second chapter, computed x-ray microtomography, Raman spectroscopy and Fourier-Transform infrared spectroscopy data provide evidence of a low-density phase occurring as a film around sulphide inclusions and as micro inclusions associated with sulphides in diamonds from Mir and Udachnaya (Yakutia, Russia). In the studied Udachnaya diamond, the low-density phases consist of carbonate and a hydrous silicic phase, whilst at Mir, the composition of the low-density rim is unknown. Nonetheless, it appears that the study of sulphide inclusions in diamonds from both localities can provide clues about the nature of the fluids forming sulphide inclusion-bearing diamonds and the conditions that prevailed in their source regions.

In the third chapter, we report the discovery of molybdenite (MoS_2) as a primary exsolved sulphide in intact diamond-hosted sulphide inclusions from Mir, Udachnaya (Yakutia), Argyle (Australia), Dachine (French Guiana), Orapa, Letlhakane, Damtshaa (Botswana), Murowa (Zimbabwe), Diavik (Canada) and Juina-5 (Brazil). Sulphide inclusions typically unmix into an assemblage of Fe, Ni and Cu sulphides upon cooling, and the presence of molybdenite is likely to impose strong controls on the distribution of Re and Os within the inclusions. Indeed, molybdenite is the principal host of Re on Earth, and its apparent tendency to migrate toward the edges of inclusions and in some cases into the surrounding thermal decompression fractures, would make it harder to recover during the extraction of the sulphide from diamond for dating. Indeed, we show that Re-loss through the potential non-recovery of molybdenite

from diamond-hosted sulphide inclusions being extracted for Re-Os radiometric dating could provide one explanation for some of the unusual Re-Os ages obtained in the literature.

The previously unrecognised occurrence of molybdenite in diamond-hosted sulphide inclusions poses interesting questions about the processes controlling Mo enrichment in the mantle source regions of diamonds, which are discussed in Chapter 4. Depending on the prevailing redox conditions and sulphur availability of a system, Mo can exhibit siderophile (Fe-loving), chalcophile (S-loving) or lithophile (silicate-loving) affinities. The presence of Mo in diamond-forming mantle domains in sufficiently high concentrations to form molybdenite may require its transfer from a predominantly young (<2.45 Ga), oxidised subducting slab where Mo is for example hosted in rutile – its primary non-sulphide mineral host – into a relatively reduced, sulphide-bearing mantle. However, further work is needed to constrain the origin of Mo in diamond-hosted sulphide inclusions, for example involving carbon isotopes of the diamonds, compositional studies of associated fluids, or even Mo isotopes of the sulphide inclusions.

The fifth chapter presents the preliminary results of stable sulphur isotope analyses of sulphide inclusions in diamonds from Dachine (French Guiana), Juina-5 and Collier-4 (Brazil) and Mir (Yakutia), which offer information regarding the source and nature of the sulphur in them. The results reveal extremely light $\delta^{34}S$ compositions for inclusions in five diamonds from Dachine and five from the Brazilian localities, clearly reflecting the presence of surface-derived, subducted sulphur-bearing materials. For Mir diamonds, both light (i.e. recycled) and heavier mantle-like $\delta^{34}S$ compositions are observed in inclusions occurring in different growth zones of two of the three studied diamonds. Interestingly, an apparent relationship is observed between the sulphur isotopes of sulphide inclusions and carbon isotope compositions of their

host diamonds (reported in the literature), potentially reconciling the preliminary sulphur isotope results with the known formation mechanisms of the diamonds.

Sulphide inclusions in diamonds represent unique samples of diamond-forming regions of the Earth's mantle. The unique chemistry of sulphides allows for their use in gaining a better understanding of the processes leading to diamond formation, as well as the timing of their onset. The mineralogy, chemical and isotopic composition of exposed and unexposed sulphide inclusions in natural diamonds originating from worldwide sources have been reported here. Owing to some of the unexpected features associated with sulphide inclusions and the complexity of their study however, further work is required to investigate the potential involvement of sulphides in diamond-forming reactions and related mantle processes nature, as well as the timing and nature of these events.

References

Ackerman, L., Pitcher, L., Strnad, L., Puchtel, I.S., Jelínek, E., Walker, R.J. and Rohovec, J., 2013. Highly siderophile element geochemistry of peridotites and pyroxenites from Horní Bory, Bohemian Massif: Implications for HSE behaviour in subduction-related upper mantle. *Geochimica et Cosmochimica Acta*, 100, pp.158-175.

Adam, J. and Green, T., 2006. Trace element partitioning between mica-and amphibole-bearing garnet lherzolite and hydrous basanitic melt: 1. Experimental results and the investigation of controls on partitioning behaviour. *Contributions to Mineralogy and Petrology*, 152(1), pp.1-17.

Alard, O., Griffin, W.L., Lorand, J.P., Jackson, S.E. and O'Reilly, S.Y., 2000. Non-chondritic distribution of the highly siderophile elements in mantle sulphides. *Nature*, 407(6806), pp.891.

Alard, O., Lorand, J.P., Reisberg, L., Bodinier, J.L., Dautria, J.M. and O'reilly, S.Y., 2011. Volatile-rich metasomatism in Montferrier xenoliths (Southern France): Implications for the abundances of chalcophile and highly siderophile elements in the subcontinental mantle. *Journal of Petrology*, 52(10), pp.2009-2045.

Alfonso, P., Prol-Ledesma, R.M., Canet, C., Melgarejo, J.C. and Fallick, A.E., 2003. Sulfur isotope geochemistry of the submarine hydrothermalcoastal vents of Punta Mita, Mexico. *Journal of Geochemical Exploration*, *78*, pp.301-304.

Alt, J.C., Shanks III, W.C. and Jackson, M.C., 1993. Cycling of sulfur in subduction zones: The geochemistry of sulfur in the Mariana Island Arc and back-arc trough. *Earth and Planetary Science Letters*, *119*(4), pp.477-494.

Alt, J.C., Zuleger, E. and Erzinger, J., 1995. Mineralogy and stable isotopic compositions of the hydrothermally altered lower sheeted dike complex, Hole 504B, Leg 140. In Proceedings of the Ocean Drilling Program, Scientific Results (Vol. 137, No. 140, pp. 155-166). Ocean Drilling Program.

Alt, J.C., Laverne, C., Coggon, R.M., Teagle, D.A., Banerjee, N.R., Morgan, S., Smith-Duque, C.E., Harris, M. and Galli, L., 2010. Subsurface structure of a submarine hydrothermal system in ocean crust formed at the East Pacific Rise, ODP/IODP Site 1256. Geochemistry, Geophysics, Geosystems, 11(10).

Alt, J.C., Shanks III, W.C., Crispini, L., Gaggero, L., Schwarzenbach, E.M., Früh-Green, G.L. and Bernasconi, S.M., 2012. Uptake of carbon and sulfur during seafloor serpentinization and the effects of subduction metamorphism in Ligurian peridotites. *Chemical Geology*, *322*, pp.268-277.

Anand, M., Taylor, L.A., Misra, K.C., Carlson, W.D. and Sobolev, N.V., 2004. Nature of diamonds in Yakutian eclogites: views from eclogite tomography and mineral inclusions in diamonds. *Lithos*, 77(1-4), pp.333-348.

Anbar, A.D., Duan, Y., Lyons, T.W., Arnold, G.L., Kendall, B., Creaser, R.A., Kaufman, A.J., Gordon, G.W., Scott, C., Garvin, J. and Buick, R., 2007. A whiff of oxygen before the great oxidation event? *Science*, 317(5846), pp.1903-1906.

Anbar, A.D., 2008. Elements and evolution. *Science*, 322(5907), pp.1481-1483.

Andersen, T., Griffin, W.L. and O'Reilly, S.Y., 1987. Primary sulphide melt inclusions in mantle-derived megacrysts and pyroxenites. *Lithos*, 20(4), pp.279-294.

Anderson, D.L., Sammis, C. and Jordan, T., 1971. Composition and evolution of the mantle and core. *Science*, 171(3976), pp.1103-1112.

Anthony, J.W., Bideaux, R.A., Bladh, K.W. and Nichols, M.C., (eds.) 2003. *Molybdenite—Handbook of Mineralogy*. Mineralogical Society of America, Chantilly, VA.

Anzolini, C., Nestola, F., Mazzucchelli, M.L., Alvaro, M., Nimis, P., Gianese, A., Morganti, S., Marone, F., Campione, M., Hutchison, M.T. and Harris, J.W., 2019. Depth of diamond formation obtained from single periclase inclusions. *Geology*, 47(3), pp.219-222.

Araújo, D.P., Griffin, W.L., O'Reilly, S.Y., Grant, K.J., Ireland, T., Holden, P. and van Achterbergh, E., 2009. Microinclusions in monocrystalline octahedral diamonds and coated diamonds from Diavik, Slave Craton: Clues to diamond genesis. *Lithos*, 112, pp.724-735.

Araujo, D.P., Gaspar, J.C., Bulanova, G.P., Smith, C.B., Kohn, S.C., Walter, M.J. and Hauri, E.H., 2013. Juina diamonds from kimberlites and alluvials: a comparison of morphology, spectral characteristics and carbon isotope composition. In *Proceedings of 10th International Kimberlite Conference* (pp. 255-269). Springer, New Delhi.

De Paula, J., 2010. *Atkins' Physical Chemistry*. Oxford University Press.

Aulbach, S., Griffin, W.L., Pearson, N.J., O'Reilly, S.Y., Kivi, K. and Doyle, B.J., 2004. Mantle formation and evolution, Slave Craton: constraints from HSE abundances and Re–Os isotope systematics of sulfide inclusions in mantle xenocrysts. *Chemical Geology*, 208(1-4), pp.61-88.

Aulbach, S., Stachel, T., Creaser, R.A., Heaman, L.M., Shirey, S.B., Muehlenbachs, K., Eichenberg, D. and Harris, J.W., 2009. Sulphide survival and diamond genesis during formation and evolution of Archaean subcontinental lithosphere: A comparison between the Slave and Kaapvaal cratons. *Lithos*, 112, pp.747-757.a

Aulbach, S., Shirey, S.B., Stachel, T., Creighton, S., Muehlenbachs, K. and Harris, J.W., 2009. Diamond formation episodes at the southern margin of the Kaapvaal Craton: Re–Os systematics of sulfide inclusions from the Jagersfontein Mine. *Contributions to Mineralogy and Petrology*, 157(4), pp.525-540.b

Aulbach, S., Stachel, T., Seitz, H.M. and Brey, G.P., 2012. Chalcophile and siderophile elements in sulphide inclusions in eclogitic diamonds and metal cycling in a Paleoproterozoic subduction zone. *Geochimica et Cosmochimica Acta*, 93, pp.278-299.

Aulbach, S., Mungall, J.E. and Pearson, D.G., 2016. Distribution and processing of highly siderophile elements in cratonic mantle lithosphere. *Reviews in Mineralogy and Geochemistry*, *81*(1), pp.239-304.

Aulbach, S., Creaser, R.A., Stachel, T., Heaman, L.M., Chinn, I.L. and Kong, J., 2018. Diamond ages from Victor (Superior Craton): Intra-mantle cycling of volatiles (C, N, S) during supercontinent reorganisation. *Earth and Planetary Science Letters*, 490, pp.77-87.

Bachinski, D.J., 1969. Bond strength and sulfur isotopic fractionation in coexisting sulfides. *Economic Geology*, *64*(1), pp.56-65.

Bali, E., Keppler, H. and Audetat, A., 2012. The mobility of W and Mo in subduction zone fluids and the Mo–W–Th–U systematics of island arc magmas. *Earth and Planetary Science Letters*, 351, pp.195-207.

Ballhaus, C., Tredoux, M. and Späth, A., 2001. Phase relations in the Fe–Ni–Cu–PGE–S system at magmatic temperature and application to massive sulphide ores of the Sudbury igneous complex. *Journal of Petrology*, 42(10), pp.1911-1926.

Ballhaus, C. and Ulmer, P., 1995. Platinum-group elements in the Merensky Reef: II. Experimental solubilities of platinum and palladium in Fe1− xS from 950 to 450° C under controlled *f*S2 and *f*H2. *Geochimica et Cosmochimica Acta*, 59(23), pp.4881-4888.

Barling, J., Arnold, G.L. and Anbar, A.D., 2001. Natural mass-dependent variations in the isotopic composition of molybdenum. Earth and Planetary Science Letters, 193(3-4), pp.447-457.

Barnes, S.J., Cox, R.A. and Zientek, M.L., 2006. Platinum-group element, gold, silver and base metal distribution in compositionally zoned sulfide droplets from the Medvezky Creek Mine, Noril'sk, Russia. *Contributions to Mineralogy and Petrology*, 152(2), pp.187-200.

Barnes, S. J., Prichard, H. M., Cox, R. A., Fisher, P. C., & Godel, B. (2008). The location of the chalcophile and siderophile elements in platinum-group element ore deposits (a textural, microbeam and whole rock geochemical study): Implications for the formation of the deposits. *Chemical Geology*, 248(3-4), 295-317.

Barra, F., Ruiz, J., Mathur, R. and Titley, S., 2003. A Re–Os study of sulfide minerals from the Bagdad porphyry Cu–Mo deposit, northern Arizona, USA. *Mineralium Deposita*, 38(5), pp.585-596.

Barré, G., Thomassot, E., Cartigny, P., Michels, R., Truche, L., Strzerzynski, P., Guillot, S., Lorgeoux, C. and Assayag, N., 2018, September. How Multiple Sulfur Isotopes (δ33S, δ34S, δ36S) Help Unravel the Context of Thermochemical Sulfate Reaction during Metamorphic Events: Application to Subducted Evaporites from the French Alps. In *First EAGE/IFPEN Conference on Sulfur Risk Management in Exploration and Production*.

Barron, L.M., Mernagh, T.P. and Barron, B.J., 2008. Using strain birefringence in diamond to estimate the remnant pressure on an inclusion. *Australian Journal of Earth Sciences*, 55(2), pp.159-165.

Barton, P.B., 1973. Solid solutions in the system Cu-Fe-S, Part I; the Cu-S and CuFe-S joins. *Economic Geology*, 68(4), pp.455-465.

Bataleva, Y., Palyanov, Y. and Borzdov, Y., 2018. Sulfide formation as a result of sulfate subduction into silicate mantle (Experimental modeling under high p, t-parameters). *Minerals*, 8(9), p.373.

Bénard, A., Klimm, K., Woodland, A.B., Arculus, R.J., Wilke, M., Botcharnikov, R.E., Shimizu, N., Nebel, O., Rivard, C. and Ionov, D.A., 2018. Oxidising agents in sub-arc mantle melts link slab devolatilisation and arc magmas. *Nature communications*, 9(1), p.3500.

Berner, R.A., 1984. Sedimentary pyrite formation: an update. *Geochimica et cosmochimica Acta*, 48(4), pp.605-615.

Berner, R.A., 1999. Atmospheric oxygen over Phanerozoic time. *Proceedings of the National Academy of Sciences*, 96(20), pp.10955-10957.

Berrang, P.G. and Grill, E.V., 1974. The effect of manganese oxide scavenging on molybdenum in Saanich Inlet, British Columbia. *Marine Chemistry*, 2(2), pp.125-148.

Bertine, K.K., 1972. The deposition of molybdenum in anoxic waters. *Marine Chemistry*, 1(1), pp.43-53.

Bertine, K.K. and Turekian, K.K., 1973. Molybdenum in marine deposits. *Geochimica et Cosmochimica Acta*, 37(6), pp.1415-1434.

Beyer, C. and Frost, D.J., 2017. The depth of sub-lithospheric diamond formation and the redistribution of carbon in the deep mantle. *Earth and Planetary Science Letters*, *461*, pp.30-39.

Bockrath, C., Ballhaus, C. and Holzheid, A., 2004. Fractionation of the platinum-group elements during mantle melting. *Science*, 305(5692), pp.1951-1953.

Borges, M.P.A.C., Moura, M.A., Lenharo, S.L.R., Smith, C.B. and Araujo, D.P., 2016. Mineralogical characterization of diamonds from Roosevelt Indigenous Reserve, Brazil, using non-destructive methods. *Lithos*, 265, pp.182-198.

Botcharnikov, R.E., Behrens, H., Holtz, F., Koepke, J. and Sato, H., 2004. Sulfur and chlorine solubility in Mt. Unzen rhyodacitic melt at 850 C and 200 MPa. *Chemical Geology*, 213(1-3), pp.207-225.

Boyd, S.R., Mattey, D.P., Pillinger, C.T., Milledge, H.J., Mendelssohn, M. and Seal, M., 1987. Multiple growth events during diamond genesis: an integrated study of carbon and nitrogen isotopes and nitrogen aggregation state in coated stones. *Earth and Planetary Science Letters*, 86(2-4), pp.341-353.

Bragagni, A., Van Acken, D., Fonseca, R.O., Speelmanns, I.M., Wainwright, A.N., Heuser, A., Nowell, G.M. and Luguet, A., 2018. Re-Os and HSE in individual base metal sulfide grains: Evaluating micro-analytical procedures using a sulfide reference material. *Chemical geology*, 493, pp.426-440.

Brenan, J.M., 2002. Re–Os fractionation in magmatic sulfide melt by monosulfide solid solution. *Earth and Planetary Science Letters*, 199(3-4), pp.257-268.

Brenan, J.M., Bennett, N.R. and Zajacz, Z., 2016. Experimental results on fractionation of the highly siderophile elements (HSE) at variable pressures and temperatures during planetary and magmatic differentiation. *Reviews in Mineralogy and Geochemistry*, *81*(1), pp.1-87.

Brenker, F.E., Vollmer, C., Vincze, L., Vekemans, B., Szymanski, A., Janssens, K., Szaloki, I., Nasdala, L., Joswig, W. and Kaminsky, F., 2007. Carbonates from the lower part of transition zone or even the lower mantle. *Earth and Planetary Science Letters*, *260*(1-2), pp.1-9.

Bühn, B., Santos, R.V., Dardenne, M.A. and de Oliveira, C.G., 2012. Mass-dependent and mass-independent sulfur isotope fractionation (δ34S and δ33S) from Brazilian Archean and Proterozoic sulfide deposits by laser ablation multi-collector ICP-MS. *Chemical Geology*, *312*, pp.163-176.

Bulanova, G.P. and Pavlova, L.P., 1987. The magnesite peridotite association in diamond from the'Mir'pipe. In *Akademiia Nauk SSSR Doklady*, 295, pp. 1452-1456.

Bulanova, G.P., Novgorodov, P.G. and Pavlova, L.A., 1988. The first find of a melt inclusion in diamond from the Mir pipe. *Geokhimiia*, pp.756-765.

Bulanova, G.P., 1995. The formation of diamond. *Journal of Geochemical Exploratio*n, 53(1-3), pp.1-23.

Bulanova, G.P., Griffin, W.L., Ryan, C.G., Shestakova, O.Y. and Barnes, S.J., 1996. Trace elements in sulfide inclusions from Yakutian diamonds. *Contributions to Mineralogy and Petrology*, 124(2), pp.111-125.

Bulanova, G.P., Griffin, W.L. and Ryan, C.G., 1998. Nucleation environment of diamonds from Yakutian kimberlites. *Mineralogical Magazine*, 62(3), pp.409-419.

Bulanova, G.P., Shelkov, D., Milledge, H.J., Hauri, E.H., Smith, C.B. and Chris, B., 1999. Nature of eclogitic diamonds from Yakutian kimberlites: evidence from isotopic composition and chemistry of inclusions. In *Proceedings of the 7th International Kimberlite Conference*, 57, p. 65.

Bulanova, G.P., Pearson, D.G., Hauri, E.H. and Griffin, B.J., 2002. Carbon and nitrogen isotope systematics within a sector-growth diamond from the Mir kimberlite, Yakutia. *Chemical Geology*, 188(1-2), pp.105-123.

Bulanova, G.P., Pearson, D.G., Hauri, E.H., Milledge, H.J. and Barashkov, Y.P., 2003, June. Dynamics of diamond growth: evidence from isotope and FTIR trends. In *International Kimberlite Conference: Extended Abstracts*, 8.

Bulanova, G.P., Muchemwa, E., Pearson, D.G., Griffin, B.J., Kelley, S.P., Klemme, S. and Smith, C.B., 2004. Syngenetic inclusions of yimengite in diamond from Sese kimberlite (Zimbabwe)—evidence for metasomatic conditions of growth. *Lithos*, 77(1-4), pp.181-192.

Bulanova, G.P., Varshavsky, A.V. and Kotegov, V.A., 2005. A venture into the interior of natural diamond: genetic information and implications for the gem industry: part I: the main types of internal growth structures. *Journal of Gemmology*, 29(7/8), p.377.

Bulanova, G.P., Smith, C.B., Walter, M.J., Blundy, J., Gobbo, L. and Kohn, S.C., 2008, October. Proto-kimberlitic ultra-deep diamonds from Collier 4 kimberlite pipe, Juina, Brazil. In *International Kimberlite Conference: Extended Abstracts*, 9.

Bulanova, G.P., Walter, M.J., Smith, C.B., Kohn, S.C., Armstrong, L.S., Blundy, J. and Gobbo, L., 2010. Mineral inclusions in sublithospheric diamonds from Collier 4 kimberlite pipe, Juina, Brazil: subducted protoliths, carbonated melts and primary kimberlite magmatism. *Contributions to Mineralogy and Petrology*, 160(4), pp.489-510.

Bulanova, G.P., Marks, A., Smith, C.B., Kohn, S.C., Walter, M.J., Gaillou, E., Shirey, S.B., Trautman, R. and Griffin, B.J., 2012, February. Diamonds from Sese and Murowa kimberlites (Zimbabwe)–evidence of extreme peridotitic lithosphere depletion and Ti-REE metasomatism. In *International Kimberlite Conference: Extended Abstracts*, 10.

Bulanova, G.P., de Vries, D.W., Pearson, D.G., Beard, A., Mikhail, S., Smelov, A.P. and Davies, G.R., 2014. An eclogitic diamond from Mir pipe (Yakutia), recording two growth events from different isotopic sources. *Chemical Geology*, 381, pp.40-54.

Bureau, H., Langenhorst, F., Auzende, A.L., Frost, D.J., Estève, I. and Siebert, J., 2012. The growth of fibrous, cloudy and polycrystalline diamonds. *Geochimica et Cosmochimica Acta*, 77, pp.202-214.

Burgess, R., Turner, G. and Harris, J.W., 1992. 40Ar-39Ar laser probe studies of clinopyroxene inclusions in eclogitic diamonds. *Geochimica et Cosmochimica Acta*, 56(1), pp.389-402.

Burgess, R., Kiviets, G.B. and Harris, J.W., 1994. Ar–Ar age determinations of eclogitic clinopyroxene and garnet inclusions in diamonds from the Venetia and Orapa kimberlites. *Lithos*, 77(1-4), pp.113-124.

Burgess, R., Layzelle, E., Turner, G. and Harris, J.W., 2002. Constraints on the age and halogen composition of mantle fluids in Siberian coated diamonds. *Earth and Planetary Science Letters*, 197(3-4), pp.193-203.

Burgess, R., Kiviets, G.B. and Harris, J.W., 2004. Ar–Ar age determinations of eclogitic clinopyroxene and garnet inclusions in diamonds from the Venetia and Orapa kimberlites. *Lithos*, 77(1-4), pp.113-124.

Burgess, R., Cartigny, P., Harrison, D., Hobson, E. and Harris, J., 2009. Volatile composition of microinclusions in diamonds from the Panda kimberlite, Canada: Implications for chemical and isotopic heterogeneity in the mantle. *Geochimica et Cosmochimica Acta*, 73(6), pp.1779-1794.

Burkemper, L.K. and Agee, C.B., 2010, March. The effect of pressure and temperature on molybdenum solubility in silicate melts. In *Lunar and Planetary Science Conference* (Vol. 41, p. 1376).

Burnham, A.D., Thomson, A.R., Bulanova, G.P., Kohn, S.C., Smith, C.B. and Walter, M.J., 2015. Stable isotope evidence for crustal recycling as recorded by superdeep diamonds. *Earth and Planetary Science Letters*, 432, pp.374-380.

Burnham, A.D., Bulanova, G.P., Smith, C.B., Whitehead, S.C., Kohn, S.C., Gobbo, L. and Walter, M.J., 2016. Diamonds from the Machado River alluvial deposit, Rondônia, Brazil, derived from both lithospheric and sublithospheric mantle. *Lithos*, 265, pp.199-213.

Burton, K.W., Schiano, P., Birck, J.L., Allegre, C.J., Rehkämper, M., Halliday, A.N. and Dawson, J.B., 2000. The distribution and behaviour of rhenium and osmium amongst mantle minerals and the age of the lithospheric mantle beneath Tanzania. *Earth and Planetary Science Letters*, 183(1-2), pp.93-106.

Cabral, R.A., Jackson, M.G., Rose-Koga, E.F., Koga, K.T., Whitehouse, M.J., Antonelli, M.A., Farquhar, J., Day, J.M. and Hauri, E.H., 2013. Anomalous sulphur isotopes in plume lavas reveal deep mantle storage of Archaean crust. *Nature*, 496(7446), p.490.

Calvert, S.E. and Pedersen, T.F., 1993. Geochemistry of recent oxic and anoxic marine sediments: implications for the geological record. *Marine Geology*, 113(1-2), pp.67-88.

Campbell, I.H. and Squire, R.J., 2010. The mountains that triggered the Late Neoproterozoic increase in oxygen: the Second Great Oxidation Event. *Geochimica et Cosmochimica Acta*, 74(15), pp.4187-4206.

Candela, P.A. and Holland, H.D., 1984. The partitioning of copper and molybdenum between silicate melts and aqueous fluids. *Geochimica et Cosmochimica Acta*, 48(2), pp.373-380.

Candela, P.A. and Holland, H.D., 1986. A mass transfer model for copper and molybdenum in magmatic hydrothermal systems; the origin of porphyry-type ore deposits. *Economic Geology*, *81*(1), pp.1-19.

Candela, P.A. and Bouton, S.L., 1990. The influence of oxygen fugacity on tungsten and molybdenum partitioning between silicate melts and ilmenite. *Economic Geology*, 85(3), pp.633-640.

Canfield D.E., 1993. Organic Matter Oxidation in Marine Sediments. In: Wollast R., Mackenzie F.T., Chou L. (eds.) Interactions of C, N, P and S Biogeochemical Cycles and Global Change. NATO ASI Series (Series I: Global Environmental Change), vol 4. Springer, Berlin, Heidelberg

Canfield, D.E. and Raiswell, R., 1999. The evolution of the sulfur cycle. *American Journal of Science*, 299(7-9), pp.697-723.

Canfield, D.E., 2004. The evolution of the Earth surface sulfur reservoir. *American Journal of Science*, 304(10), pp.839-861.

Canfield, D.E., Ngombi-Pemba, L., Hammarlund, E.U., Bengtson, S., Chaussidon, M., Gauthier-Lafaye, F., Meunier, A., Riboulleau, A., Rollion-Bard, C., Rouxel, O. and Asael, D., 2013. Oxygen dynamics in the aftermath of the Great Oxidation of Earth's atmosphere. *Proceedings of the National Academy of Sciences*, 110(42), pp.16736-16741.

Canil, D. and Fellows, S.A., 2017. Sulphide–sulphate stability and melting in subducted sediment and its role in arc mantle redox and chalcophile cycling in space and time. *Earth and Planetary Science Letters*, 470, pp.73-86.

Capdevila, R., Arndt, N., Letendre, J. and Sauvage, J.F., 1999. Diamonds in volcaniclastic komatiite from French Guiana. *Nature*, *399*(6735), p.456.

Carlson, J.A., Kirkley, M.B., Thomas, E.M. and Hillier, W.D., 1999a. Recent Canadian kimberlite discoveries. In *The JB Dawson Volume, Proceedings of the VIIth International Kimberlite Conference, Cape Town* (pp. 81-89).

Carlson, S.M., Hillier, W.D., Hood, C.T., Pryde, R.P. and Skelton, D.N., 1999b. The Buffalo Hills kimberlites: a newly-discovered diamondiferous kimberlite province in north-central Alberta, Canada. In *Proceedings of the 7th International Kimberlite Conference, Cape Town, South Africa*. Edited by JJ Gurney, JL Gurney, MD Pascoev and SH Richardson. Red Roof Design, Cape Town, South Africa (pp. 109-116).

Carlson, R.W., 2005. Application of the Pt–Re–Os isotopic systems to mantle geochemistry and geochronology. *Lithos*, 82(3-4), pp.249-272.

Carroll, M.R. and Rutherford, M.J., 1985. Sulfide and sulfate saturation in hydrous silicate melts. J*ournal of Geophysical Research: Solid Earth*, 90(S02), pp.C601-C612.

Cartigny, P., Harris, J.W. and Javoy, M., 1998. Eclogitic diamond formation at Jwaneng: no room for a recycled component. *Science*, 280(5368), pp.1421-1424.

Cartigny, P., Harris, J.W. and Javoy, M., 1999. Eclogitic, peridotitic and metamorphic diamonds and the problems of carbon recycling—the case of Orapa (Botswana). In *The JB Dawson Volume—Proceedings of the Seventh International Kimberlite Conference, Cape Town. Red Roof Design, Cape Town* (pp. 117-124).

Cartigny, P., 2005. Stable isotopes and the origin of diamond. *Elements*, 1(2), pp.79-84.

Cartigny, P., Farquhar, J., Thomassot, E., Harris, J.W., Wing, B., Masterson, A., McKeegan, K. and Stachel, T., 2009. A mantle origin for Paleoarchean peridotitic diamonds from the Panda kimberlite, Slave Craton: evidence from ^{13}C-, ^{15}N-and ^{33}, ^{34}S-stable isotope systematics. *Lithos*, *112*, pp.852-864.

Cartigny, P., 2010. Mantle-related carbonados? Geochemical insights from diamonds from the Dachine komatiite (French Guiana). *Earth and Planetary Science Letters*, 296(3-4), pp.329-339.

Casalini, M., Avanzinelli, R., Tommasini, S., Elliott, T. and Conticelli, S., 2019. Ce/Mo and Molybdenum Isotope Systematics in Subduction-related Orogenic Potassic Magmas of Central-Southern Italy. *Geochemistry, Geophysics, Geosystems*, 20(6), pp.2753-2768.

Chaussidon, M., Albarede, F. and Sheppard, S.M.F., 1987. Sulphur isotope heterogeneity in the mantle from ion microprobe measurements of sulphide inclusions in diamonds. *Nature*, 330(6145), p.242.

Chaussidon, M., Albarède, F. and Sheppard, S.M., 1989. Sulphur isotope variations in the mantle from ion microprobe analyses of micro-sulphide inclusions. *Earth and Planetary Science Letters*, *92*(2), pp.144-156.

Chen, J.M. and Wang, C.S., 1974. Second order Raman spectrum of MoS_2. *Solid State Communications*, 14(9), pp.857-860.

Chen, M., Mao, J., Li, C., Zhang, Z. and Dang, Y., 2015. Re–Os isochron ages for arsenopyrite from Carlin-like gold deposits in the Yunnan–Guizhou–Guangxi "golden triangle", southwestern China. *Ore Geology Reviews*, *64*, pp.316-327.

Chepurov, A.I., 1988. Role of sulfide melt in natural diamond formation. *Geology and Geophysics*, 29(8), pp.119-124.

Chowdhury, P. and Dasgupta, R., 2019. Effect of sulfate on the basaltic liquidus and Sulfur Concentration at Anhydrite Saturation (SCAS) of hydrous basalts–Implications for sulfur cycle in subduction zones. *Chemical Geology*, 522, pp.162-174.

Chrenko, R.M., McDonald, R.S. and Darrow, K.A., 1967. Infra-red spectra of diamond coat. *Nature*, 213(5075), p.474.

Cook, N.J. and Chryssoulis, S.L., 1990. Concentrations of invisible gold in the common sulfides. *The Canadian Mineralogist*, *28*(1), pp.1-16.

Creighton, S., Stachel, T., McLean, H., Muehlenbachs, K., Simonetti, A., Eichenberg, D. and Luth, R., 2008. Diamondiferous peridotitic microxenoliths from the Diavik Diamond Mine, NT. *Contributions to Mineralogy and Petrology*, *155*(5), pp.541-554.

Crook, A.R., 1904. Molybdenite at Crown Point, Washington. *Bulletin of the Geological Society of America*, 15(1), pp.283-288.

Crossley, R.J., Evans, K.A., Jeon, H. and Kilburn, M.R., 2018. Insights into sulfur cycling at subduction zones from in-situ isotopic analysis of sulfides in high-pressure serpentinites and 'hybrid'samples from Alpine Corsica. *Chemical Geology*, *493*, pp.359-378.

Croswell, K., 1995. The alchemy of the heavens: searching for meaning in the Milky Way. Anchor Books.

Crusius, J., Calvert, S., Pedersen, T. and Sage, D., 1996. Rhenium and molybdenum enrichments in sediments as indicators of oxic, suboxic and sulfidic conditions of deposition. *Earth and Planetary Science Letters*, 145(1-4), pp.65-78.

Dare, S.A., Barnes, S.J. and Prichard, H.M., 2010. The distribution of platinum group elements (PGE) and other chalcophile elements among sulfides from the Creighton Ni–Cu–PGE sulfide deposit, Sudbury, Canada, and the origin of palladium in pentlandite. *Mineralium Deposita*, *45*(8), pp.765-793.

Dare, S.A., Barnes, S.J., Prichard, H.M. and Fisher, P.C., 2011. Chalcophile and platinum-group element (PGE) concentrations in the sulfide minerals from the McCreedy East deposit, Sudbury, Canada, and the origin of PGE in pyrite. *Mineralium Deposita*, 46(4), pp.381-407.

Darling, R.S., 1994. Fluid inclusion and phase equilibrium studies at the Cannivan Gulch molybdenum deposit, Montana, USA: Effect of CO2 on molybdenite-powellite stability. *Geochimica et cosmochimica acta*, *58*(2), pp.749-760.

Dasgupta, R., Buono, A., Whelan, G. and Walker, D., 2009. High-pressure melting relations in Fe–C–S systems: Implications for formation, evolution, and structure of metallic cores in planetary bodies. *Geochimica et Cosmochimica Acta*, 73(21), pp.6678-6691.

Dasgupta, R. and Hirschmann, M.M., 2010. The deep carbon cycle and melting in Earth's interior. *Earth and Planetary Science Letters*, *298*(1-2), pp.1-13.

Davies, R.M., O'Reilly, S.Y. and Griffin, W.L., 1998a. Characteristics of alluvial diamonds from Bingara and Wellington, eastern Australia. In *International Kimberlite Conference: Extended Abstracts* (Vol. 7, pp. 173-175).

Davies, R.M., O'Reilly, S.Y. and Griffin, W.L., 1998b. Dynamic growth structures in diamonds from Bingara, NSW, Australia. In *International Kimberlite Conference: Extended Abstracts* (Vol. 7, pp. 176-178).

Davies, R.M., O'reilly, S.Y. and Griffin, W.L., 1999. Diamonds from Wellington, NSW: insights into the origin of eastern Australian diamonds. *Mineralogical Magazine*, 63(4), pp.447-471.

Davies, R.M., O'Reilly, S.Y. and Griffin, W.L., 2002. Multiple origins of alluvial diamonds from New South Wales, Australia. *Economic Geology*, 97(1), pp.109-123.

Davies, R.M., Griffin, W.L., O'Reilly, S.Y. and Andrew, A.S., 2003. Unusual mineral inclusions and carbon isotopes of alluvial diamonds from Bingara, eastern Australia. *Lithos*, 69(1-2), pp.51-66.

Davies, G.R., van den Heuvel, Q., Matveev, S., Drury, M.R., Chinn, I.L. and Gress, M.U., 2018. A combined cathodoluminescence and electron backscatter diffraction examination of the growth relationships between Jwaneng diamonds and their eclogitic inclusions. *Mineralogy and Petrology*, 112(1), pp.231-242.

Davis, G.L., Sobolev, N.V. and Khar'kiv, A.D., 1980. New data on the age of Yakutian kimberlites obtained by uranium-lead study of zircons. *Doklady Akademii Nauk SSSR*, 254(1), pp.175-179.

Debret, B., Millet, M.A., Pons, M.L., Bouilhol, P., Inglis, E. and Williams, H., 2016. Isotopic evidence for iron mobility during subduction. *Geology*, 44(3), pp.215-218.

Debret, B. and Sverjensky, D.A., 2017. Highly oxidising fluids generated during serpentinite breakdown in subduction zones. *Scientific reports*, 7(1), pp.1-6.

De Hoog, J.C.M., Taylor, B.E. and Van Bergen, M.J., 2001. Sulfur isotope systematics of basaltic lavas from Indonesia: implications for the sulfur cycle in subduction zones. *Earth and Planetary Science Letters*, *189*(3-4), pp.237-252.

Deines, P., Harris, J.W., Robinson, D.N., Gurney, J.J. and Shee, S.R., 1991. Carbon and oxygen isotope variations in diamond and graphite eclogites from Orapa, Botswana, and the nitrogen content of their diamonds. *Geochimica et Cosmochimica Acta*, 55(2), pp.515-524.

Deines, P., Harris, J.W. and Gurney, J.J., 1993. Depth-related carbon isotope and nitrogen concentration variability in the mantle below the Orapa kimberlite, Botswana, Africa. *Geochimica et Cosmochimica Acta*, 57(12), pp.2781-2796.

Deines, P. and Harris, J.W., 1995. Sulfide inclusion chemistry and carbon isotopes of African diamonds. *Geochimica et Cosmochimica Acta*, 59(15), pp.3173-3188.

Deines, P., Harris, J.W. and Gurney, J.J., 1997. Carbon isotope ratios, nitrogen content and aggregation state, and inclusion chemistry of diamonds from Jwaneng, Botswana. *Geochimica et Cosmochimica Acta*, 61(18), pp.3993-4005.

Deines, P. and Harris, J.W., 2004. New insights into the occurrence of 13C-depleted carbon in the mantle from two closely associated kimberlites: Letlhakane and Orapa, Botswana. *Lithos*, 77(1-4), pp.125-142.

Deines, P., Stachel, T. and Harris, J.W., 2009. Systematic regional variations in diamond carbon isotopic composition and inclusion chemistry beneath the Orapa kimberlite cluster, in Botswana. *Lithos*, 112, pp.776-784.

Delavault, H., Chauvel, C., Thomassot, E., Devey, C.W. and Dazas, B., 2016. Sulfur and lead isotopic evidence of relic Archean sediments in the Pitcairn mantle plume. *Proceedings of the National Academy of Sciences*, *113*(46), pp.12952-12956.

Delpech, G., Lorand, J.P., Grégoire, M., Cottin, J.Y. and O'Reilly, S.Y., 2012. In-situ geochemistry of sulfides in highly metasomatized mantle xenoliths from Kerguelen, southern Indian Ocean. *Lithos*, 154, pp.296-314.

Dickinson, R.G. and Pauling, L., 1923. The crystal structure of molybdenite. *Journal of the American Chemical Society*, 45(6), pp.1466-1471.

Ding T, et al. (2001) Calibrated sulfur isotope abundance ratios of three IAEA sulfur isotope reference materials and V-CDT with a reassessment of the atomic weight of sulfur. *Geochimica et Cosmochimica Acta,* 65(15), pp. 2433-2437.

Dixon, J.E., Bindeman, I.N., Kingsley, R.H., Simons, K.K., Le Roux, P.J., Hajewski, T.R., Swart, P., Langmuir, C.H., Ryan, J.G., Walowski, K.J. and Wada, I., 2017. Light stable isotopic compositions of enriched mantle sources: Resolving the dehydration paradox. *Geochemistry, Geophysics, Geosystems*, *18*(11), pp.3801-3839.

Dobson, D.P., Crichton, W.A., VoCadlo, L., Jones, A.P., Wang, Y., Uchida, T., Rivers, M., Sutton, S. and Brodholt, J.P., 2000. In situ measurement of viscosity of liquids in the Fe-FeS system at high pressures and temperatures. *American Mineralogist*, 85(11-12), pp.1838-1842.

Donnelly, C.L., Stachel, T., Creighton, S., Muehlenbachs, K. and Whiteford, S., 2007. Diamonds and their mineral inclusions from the A154 South pipe, Diavik Diamond Mine, Northwest territories, Canada. *Lithos*, 98(1-4), pp.160-176.

Drábek, M., Rieder, M. and Böhmová, V., 2010. The Re–Mo–S system: new data on phase relations between 400 and 1200 C. *European Journal of Mineralogy*, *22*(4), pp.479-484.

Du, Y., Qin, X., Barnes, C.G., Cao, Y., Dong, Q. and Du, Y., 2014. Sulphide melt evolution in upper mantle to upper crust magmas, Tongling, China. *Geoscience Frontiers*, 5(2), pp.237-248.

Duran, C.J., Barnes, S.J. and Corkery, J.T., 2016. Trace element distribution in primary sulfides and Fe–Ti oxides from the sulfide-rich pods of the Lac des Iles Pd deposits, Western Ontario, Canada: constraints on processes controlling the composition of the ore and the use of pentlandite compositions in exploration. *Journal of Geochemical Exploration*, *166*, pp.45-63.

Ebel, D.S. and Naldrett, A.J., 1996. Fractional crystallization of sulfide ore liquids at high temperature. *Economic Geology*, 91(3), pp.607-621.

Ebel, D.S. and Naldrett, A.J., 1997. Crystallization of sulfide liquids and the interpretation of ore composition. *Canadian Journal of Earth Sciences*, 34(4), pp.352-365.

Egami, F., 1974. Inorganic types of fermentation and anaerobic respirations in the evolution of energy-yielding metabolism. In *Cosmochemical evolution and the origins of life* (pp. 405-413). Springer, Dordrecht.

Eldridge, C.S., Compston, W., Williams, I.S., Harris, J.W. and Bristow, J.W., 1991. Isotope evidence for the involvement of recycled sediments in diamond formation. *Nature*, 353(6345), p.649.

Eldridge, C.S., Williams, N. and Walshe, J.L., 1993. Sulfur isotope variability in sediment-hosted massive sulfide deposits as determined using the ion microprobe SHRIMP; II, A study of the HYC Deposit at McArthur River, Northern Territory, Australia. *Economic Geology*, *88*(1), pp.1-26.

Emerson, S.R. and Huested, S.S., 1991. Ocean anoxia and the concentrations of molybdenum and vanadium in seawater. *Marine Chemistry*, 34(3-4), pp.177-196.

Erickson, B.E. and Helz, G.R., 2000. Molybdenum (VI) speciation in sulfidic waters:: stability and lability of thiomolybdates. *Geochimica et Cosmochimica Acta*, 64(7), pp.1149-1158.

Evans, G., Morgan, P., Evans, W.E., Evans, T.R. and Woodside, J.M., 1978. Faulting and halokinetics in the northeastern Mediterranean between Cyprus and Turkey. *Geology*, *6*(7), pp.392-396.

Evans, K.A., 2012. The redox budget of subduction zones. *Earth Science Reviews*, 113(1-2), pp.11-32.

Evans, K.A. and Powell, R., 2015. The effect of subduction on the sulphur, carbon and redox budget of lithospheric mantle. *Journal of Metamorphic Geology*, 33(6), pp.649-670.

Farges, F., Siewert, R., Brown Jr, G.E., Guesdon, A. and Morin, G., 2006. Structural environments around molybdenum in silicate glasses and melts. I. Influence of composition and oxygen fugacity on the local structure of molybdenum. *The Canadian Mineralogist*, 44(3), pp.731-753.

Farquhar, J., Bao, H. and Thiemens, M., 2000. Atmospheric influence of Earth's earliest sulfur cycle. *Science*, 289(5480), pp.756-758.

Farquhar, J., Savarino, J., Airieau, S. and Thiemens, M.H., 2001. Observation of wavelength-sensitive mass-independent sulfur isotope effects during SO2 photolysis: Implications for the early atmosphere. *Journal of Geophysical Research: Planets*, 106(E12), pp.32829-32839.

Farquhar, J., Wing, B.A., McKeegan, K.D., Harris, J.W., Cartigny, P. and Thiemens, M.H., 2002. Mass-independent sulfur of inclusions in diamond and sulfur recycling on early Earth. *Science*, 298(5602), pp.2369-2372.

Farquhar, J. and Wing, B.A., 2003. Multiple sulfur isotopes and the evolution of the atmosphere. *Earth and Planetary Science Letters*, 213(1-2), pp.1-13.

Farquhar, J., Kim, S.T. and Masterson, A., 2007. Implications from sulfur isotopes of the Nakhla meteorite for the origin of sulfate on Mars. *Earth and Planetary Science Letters*, *264*(1-2), pp.1-8.

Fedortchouk, Y., Matveev, S. and Carlson, J.A., 2010. H2O and CO2 in kimberlitic fluid as recorded by diamonds and olivines in several Ekati Diamond Mine kimberlites, Northwest Territories, Canada. *Earth and Planetary Science Letters*, 289(3-4), pp.549-559.

Fesq, H.W., Bibby, D.M., Erasmus, C.S., Kable, E.J.D. and Sellschop, J.P.F., 1975. A comparative trace element study of diamonds from Premier, Finsch and Jagersfontein mines, South Africa. In *Physics and Chemistry of the Earth* (pp. 817-836). Pergamon.

Fincham, C.J.B. and Richardson, F.D., 1954. The behaviour of sulphur in silicate and aluminate melts. *Proceedings of the Royal Society of London. Series A. Mathematical and Physical Sciences*, 223(1152), pp.40-62.

Fitton, J.G., 1995. Coupled molybdenum and niobium depletion in continental basalts. *Earth and Planetary Science Letters*, *136*(3-4), pp.715-721.

Fleet, M.E., MacRae, N.D. and Herzberg, C.T., 1977. Partition of nickel between olivine and sulfide: A test for immiscible sulfide liquids. *Contributions to Mineralogy and Petrology*, 65(2), pp.191-197.

Fleet, M.E., 2006. Phase equilibria at high temperatures. *Reviews in Mineralogy and Geochemistry*, 61(1), pp.365-419.

Fonseca, R.O., Campbell, I.H., O'Neill, H.S.C. and Fitzgerald, J.D., 2008. Oxygen solubility and speciation in sulphide-rich mattes. *Geochimica et Cosmochimica Acta*, 72(11), pp.2619-2635.

Fortin, M.A., Riddle, J., Desjardins-Langlais, Y. and Baker, D.R., 2015. The effect of water on the sulfur concentration at sulfide saturation (SCSS) in natural melts. *Geochimica et Cosmochimica Acta*, 160, pp.100-116.

François, R., 1988. A study on the regulation of the concentrations of some trace metals (Rb, Sr, Zn, Pb, Cu, V, Cr, Ni, Mn and Mo) in Saanich Inlet sediments, British Columbia, Canada. *Marine Geology*, 83(1-4), pp.285-308.

Freymuth, H., Vils, F., Willbold, M., Taylor, R.N. and Elliott, T., 2015. Molybdenum mobility and isotopic fractionation during subduction at the Mariana arc. *Earth and Planetary Science Letters*, 432, pp.176-186.

Frondel, J.W. and Wickman, F.E., 1970. Molybdenite polytypes in theory and occurrence. II. Some naturally-occurring polytypes of molybdenite. *American Mineralogist: Journal of Earth and Planetary Materials*, 55(11-12), pp.1857-1875.

Frost, D.J. and McCammon, C.A., 2008. The redox state of Earth's mantle. *Annual Reviews of Earth and Planetary Science*, 36, pp.389-420.

Gaetani, G.A. and Grove, T.L., 1999. Wetting of mantle olivine by sulfide melt: implications for Re/Os ratios in mantle peridotite and late-stage core formation. *Earth and Planetary Science Letters*, *169*(1-2), pp.147-163.

Gaillu, E., Shrey, S.B., Bulanova, G.P., Marks, B., Smith, C.B., Wang, J., Kohn, S.C. and Walter, M.J., 2012, February. Sulfide inclusion Re-Os ages and carbon, nitrogen of diamonds from the Murowa kimberlites: implications for Zimbabwe craton evolution. In *International Kimberlite Conference: Extended Abstracts* (Vol. 10).

Galer, S.J.G. and O'nions, R.K., 1986. Magmagenesis and the mapping of chemical and isotopic variations in the mantle. *Chemical Geology*, 56(1-2), pp.45-61.

Garanin, V.K. and Kudryavtseva, G.P., 1990. Morphology, physical properties and paragenesis of inclusion-bearing diamonds from Yakutian kimberlites. *Lithos*, 25(1-3), pp.211-217.

Gerlach, T.M. and Thomas, D.M., 1986. Carbon and sulphur isotopic composition of Kilauea parental magma. *Nature*, *319*(6053), p.480.

Giardini, A.A. and Melton, C.E., 1975. The nature of cloud-like inclusions in two Arkansas diamonds. *American Mineralogist: Journal of Earth and Planetary Materials*, 60(9-10), pp.931-933.

Giuliani, A., Fiorentini, M.L., Martin, L.A.J., Farquhar, J., Phillips, D., Griffin, W.L. and LaFlamme, C., 2016. Sulfur isotope composition of metasomatised mantle xenoliths from the Bultfontein kimberlite (Kimberley, South Africa): Contribution from subducted sediments and the effect of sulfide alteration on S isotope systematics. *Earth and Planetary Science Letters* 445, pp.114-124.

Godel, B. and Barnes, S.J., 2008. Platinum-group elements in sulfide minerals and the whole rocks of the JM Reef (Stillwater Complex): Implication for the formation of the reef. *Chemical Geology*, 248(3-4), pp.272-294.

Goncharov, A.G., Ionov, D.A., Doucet, L.S. and Pokhilenko, L.N., 2012. Thermal state, oxygen fugacity and C□ O□ H fluid speciation in cratonic lithospheric mantle: New data on peridotite xenoliths from the Udachnaya kimberlite, Siberia. *Earth and Planetary Science Letters*, 357, pp.99-110.

Greaney, A.T., Rudnick, R.L., Gaschnig, R.M., Whalen, J.B., Luais, B. and Clemens, J.D., 2018. Geochemistry of molybdenum in the continental crust. *Geochimica et Cosmochimica Acta*, 238, pp.36-54.

Gréau, Y., Alard, O., Griffin, W.L., Huang, J.X. and O'Reilly, S.Y., 2013. Sulfides and chalcophile elements in Roberts Victor eclogites: unravelling a sulfide-rich metasomatic event. *Chemical Geology*, 354, pp.73-92.

Greaney, A.T., Rudnick, R.L., Romaniello, S.J., Johnson, A., Gaschnig, R.M. and Anbar, A.D., 2017, December. Molybdenum isotopes reveal oxidation of Earth's continental crust during the 2.4 Ga Great Oxidation Event. In *AGU Fall Meeting Abstracts*, pp. V24C-02.

Greber, N.D., Puchtel, I.S., Nägler, T.F. and Mezger, K., 2015. Komatiites constrain molybdenum isotope composition of the Earth's mantle. *Earth and Planetary Science Letters*, 421, pp.129-138.

Gregory, D.D., Large, R.R., Halpin, J.A., Steadman, J.A., Hickman, A.H., Ireland, T.R. and Holden, P., 2015. The chemical conditions of the late Archean Hamersley basin inferred from whole rock and pyrite geochemistry with $\Delta^{33}S$ and $\delta^{34}S$ isotope analyses. *Geochimica et Cosmochimica Acta*, 149, pp.223-250.a

Gregory, D.D., Large, R.R., Halpin, J.A., Baturina, E.L., Lyons, T.W., Wu, S., Danyushevsky, L., Sack, P.J., Chappaz, A., Maslennikov, V.V. and Bull, S.W., 2015. Trace element content of sedimentary pyrite in black shales. *Economic Geology*, 110(6), pp.1389-1410.b

Gress, M.U., Timmerman, S., van den Heuvel, Q., Schulten, E., Chinn, I.L., Koornneef, J.M. and Davies, G.R., 2017a, September. Variation in diamond growth events recorded in Botswanan diamonds. In *International Kimberlite Conference: Extended Abstracts* (Vol. 11).

Gress, M.U., Pearson, D.G., Timmerman, S., Chinn, I.L., Koornneef, J.M. and Davies, G.R., 2017b, September. Three phases of diamond growth spanning> 2.0 Ga beneath Letlhakane established by Re-Os and Sm-Nd systematics of individual eclogitic sulphide, garnet and clinopyroxene inclusions. In *International Kimberlite Conference: Extended Abstracts* (Vol. 11).

Gress, M.U., Howell, D., Chinn, I.L., Speich, L., Kohn, S.C., van den Heuvel, Q., Schulten, E., Pals, A.S. and Davies, G.R., 2018. Episodic diamond growth beneath the Kaapvaal Craton at Jwaneng Mine, Botswana. *Mineralogy and Petrology*, 112(1), pp.219-229.

Griffin, W.L., Sobolev, N.V., Ryan, C.G., Pokhilenko, N.P., Win, T.T. and Yefimova, E.S., 1993. Trace elements in garnets and chromites: diamond formation in the Siberian lithosphere. *Lithos*, 29(3-4), pp.235-256.

Gudmundsson, G. and Wood, B.J., 1995. Experimental tests of garnet peridotite oxygen barometry. *Contributions to Mineralogy and Petrology*, 119(1), pp.56-67.

Guntoro, P.I., Jokilaakso, A., Hellstén, N. and Taskinen, P., 2018. Copper matte-slag reaction sequences and separation processes in matte smelting. *Journal of Mining and Metallurgy, Section B: Metallurgy*, 54(3), pp.301-311.

Gurney, J.J., Harris, J.W. and Rickard, R.S., 1982. Silicate and oxide inclusions in diamonds from the Finsch kimberlite pipe. *Kimberlites, Diatremes, and Diamonds: Their geology, petrology, and geochemistry*, 15, pp.1-15.

Gurney, J.J., Harris, J.W. and Rickard, R.S., 1984. Silicate and Oxide Inclusions in Diamonds from the Orapa Mine, Botswana. In *Developments in Petrology* (Vol. 11, No. 2, pp. 3-9). Elsevier.

Gurney, J.J., Harris, J.W., Otter, M.L. and Rickard, R.S., 1995, September. Jwaneng diamond inclusions. In *International Kimberlite Conference: Extended Abstracts* (Vol. 6, pp. 208-210).

Gurney, J.J., Hildebrand, P.R., Carlson, J.A., Fedortchouk, Y. and Dyck, D.R., 2004. The morphological characteristics of diamonds from the Ekati property, Northwest Territories, Canada. *Lithos*, 77(1-4), pp.21-38.

Gurney, J.J., Helmstaedt, H.H., Richardson, S.H. and Shirey, S.B., 2010. Diamonds through time. *Economic Geology*, 105(3), pp.689-712.

Gutscher, M.A., Maury, R., Eissen, J.P. and Bourdon, E., 2000. Can slab melting be caused by flat subduction?. *Geology*, 28(6), pp.535-538.

Haggerty, S.E., 1986. Diamond genesis in a multiply-constrained model. *Nature*, 320(6057), p.34.

Hannington, M.D., de Ronde, C.D. and Petersen, S., 2005. Sea-floor tectonics and submarine hydrothermal systems. *Economic Geology* 100th Anniversary Volume. Society of Economic Geologists, Littelton, Colorado, USA, pp. 111-141.

Harris, J.W., 1968. Recognition of diamond inclusions. 1. Syngenetic mineral inclusions. *Industrial Diamond Review*, 28(334), p.402.

Harris, J.W., 1972. Black material on mineral inclusions and in internal fracture planes in diamond. *Contributions to mineralogy and petrology*, 35(1), pp.22-33.

Harrison, A.G. and Thode, H.G., 1958. Mechanism of the bacterial reduction of sulphate from isotope fractionation studies. *Transactions of the Faraday Society*, *54*, pp.84-92.

Hart, S.R. and Gaetani, G.A., 2006. Mantle Pb paradoxes: the sulfide solution. *Contributions to Mineralogy and Petrology*, 152(3), pp.295-308.

Hart, S.R. and Zindler, A., 1986. In search of a bulk-Earth composition. *Chemical Geology*, *57*(3-4), pp.247-267.

Harte, B. and Richardson, S., 2012. Mineral inclusions in diamonds track the evolution of a Mesozoic subducted slab beneath West Gondwanaland. *Gondwana Research*, 21(1), pp.236-245.

Harte, B., Fitzsimons, I.C.W., Harris, J.W. and Otter, M.L., 1999. Carbon isotope ratios and nitrogen abundances in relation to cathodoluminescence characteristics for some diamonds from the Kaapvaal Province, S. Africa. *Mineralogical Magazine*, *63*(6), pp.829-856.

Harvey, J., Gannoun, A., Burton, K.W., Rogers, N.W., Alard, O. and Parkinson, I.J., 2006. Ancient melt extraction from the oceanic upper mantle revealed by Re–Os isotopes in abyssal peridotites from the Mid-Atlantic ridge. *Earth and Planetary Science Letters*, 244(3-4), pp.606-621.

Harvey, J., Dale, C.W., Gannoun, A. and Burton, K.W., 2011. Osmium mass balance in peridotite and the effects of mantle-derived sulphides on basalt petrogenesis. *Geochimica et Cosmochimica Acta*, 75(19), pp.5574-5596.

Harvey, J., Warren, J.M. and Shirey, S.B., 2016. Mantle sulfides and their role in Re–Os and Pb isotope geochronology. *Reviews in Mineralogy and Geochemistry*, 81(1), pp.579-649.

Hattori, K. and Hart, S.R., 1991. Osmium-isotope ratios of platinum-group minerals associated with ultramafic intrusions: Os-isotopic evolution of the oceanic mantle. *Earth and Planetary Science Letters*, *107*(3-4), pp.499-514.

Haughton, D.R., Roeder, P.L. and Skinner, B.J., 1974. Solubility of sulfur in mafic magmas. *Economic Geology*, 69(4), pp.451-467.

Hauri, E.H., Pearson, D.G., Bulanova, G.P. and Milledge, H.J., 1998, April. Microscale variations in C and N isotopes within mantle diamonds revealed by SIMS. In *International Kimberlite Conference: Extended Abstracts* (Vol. 7, No. 1, pp. 317-319).

Hauri, E.H., Papineau, D., Wang, J. and Hillion, F., 2016. High-precision analysis of multiple sulfur isotopes using NanoSIMS. *Chemical Geology*, 420, pp.148-161.

Hauri, E.H., Wang, J., Pearson, D.G. and Bulanova, G.P., 2002. Microanalysis of δ13C, δ15N, and N abundances in diamonds by secondary ion mass spectrometry. *Chemical Geology*, *185*(1-2), pp.149-163.

Hayman, P.C., Kopylova, M.G. and Kaminsky, F.V., 2005. Lower mantle diamonds from Rio Soriso (Juina area, Mato Grosso, Brazil). *Contributions to Mineralogy and Petrology*, 149(4), pp.430-445.

Heaman, L., Teixeira, N.A., Gobbo, L. and Gaspar, J.C., 1998, April. U-Pb mantle zircon ages for kimberlites from the Juina Paranatinga Provinces, Brazil. In *International Kimberlite Conference: Extended Abstracts* (Vol. 7, No. 1, pp. 322-324).

Helffrich, G., Kendall, J.M., Hammond, J.O. and Carroll, M.R., 2011. Sulfide melts and long-term low seismic wavespeeds in lithospheric and asthenospheric mantle. *Geophysical Research Letters*, 38(11), L11301

Helmstaedt, H. and Schulze, D.J., 1989. Southern African kimberlites and their mantle sample: implications for Archean tectonics and lithosphere evolution. *Kimberlites and related rocks*, 1, pp.358-368.

Helz, G.R., Miller, C.V., Charnock, J.M., Mosselmans, J.F.W., Pattrick, R.A.D., Garner, C.D. and Vaughan, D.J., 1996. Mechanism of molybdenum removal from the sea and its

concentration in black shales: EXAFS evidence. *Geochimica et Cosmochimica Acta*, 60(19), pp.3631-3642.

Helz, G.R. and Vorlicek, T.P., 2019. Precipitation of molybdenum from euxinic waters and the role of organic matter. *Chemical Geology*, 509, pp.178-193.

Hervig, R.L., Williams, P., Thomas, R.M., Schauer, S.N. and Steele, I.M., 1992. Microanalysis of oxygen isotopes in insulators by secondary ion mass spectrometry. *International Journal of Mass Spectrometry and Ion Processes*, 120(1-2), pp.45-63.

Herzig, P.M., Hannington, M.D. and Arribas Jr, A., 1998. Sulfur isotopic composition of hydrothermal precipitates from the Lau back-arc: implications for magmatic contributions to seafloor hydrothermal systems. *Mineralium Deposita*, *33*(3), pp.226-237.

Hillgren, V.J., 1993. Partitioning behavior of moderately siderophile elements in Ni-rich systems: Implications for the earth and moon (Doctoral Dissertation, University of Arizona, USA)

Hintenberger, H., Herr, W. and Voshage, H., 1954. Radiogenic osmium fromrhenium-containing molybdenite. *Physical Review*, 95(6), p.1690.

Hiskey, C.F. and Meloche, V.W., 1940. Determination of Rhenium in molybdenite minerals. *Industrial & Engineering Chemistry, Analytical Edition*, 12(9), pp.503-506.

Hofmann, A.W. and White, W.M., 1982. Mantle plumes from ancient oceanic crust. *Earth and Planetary Science Letters*, 57(2), pp.421-436.

Holland, H.D., 2006. The oxygenation of the atmosphere and oceans. *Philosophical Transactions of the Royal Society B: Biological Science*s, 361(1470), pp.903-915.

Holzheid, A., Borisov, A. and Palme, H., 1994. The effect of oxygen fugacity and temperature on solubilities of nickel, cobalt, and molybdenum in silicate melts. *Geochimica et Cosmochimica Acta*, 58(8), pp.1975-1981.

Honda, M., Phillips, D., Harris, J.W. and Yatsevich, I., 2004. Unusual noble gas compositions in polycrystalline diamonds: preliminary results from the Jwaneng kimberlite, Botswana. *Chemical Geology*, 203(3-4), pp.347-358.

Honda, M., Phillips, D., Harris, J.W. and Matsumoto, T., 2011. He, Ne and Ar in peridotitic and eclogitic paragenesis diamonds from the Jwaneng kimberlite, Botswana—Implications for mantle evolution and diamond formation ages. *Earth and Planetary Science Letters*, 301(1-2), pp.43-51.

Honda, M., Phillips, D., Kendrick, M.A., Gagan, M.K. and Taylor, W.R., 2012. Noble gas and carbon isotope ratios in Argyle diamonds, Western Australia: Evidence for a deeply subducted volatile component. *Australian Journal of Earth Sciences*, 59(8), pp.1135-1142.

Howell, D., Wood, I.G., Dobson, D.P., Jones, A.P., Nasdala, L. and Harris, J.W., 2010. Quantifying strain birefringence halos around inclusions in diamond. *Contributions to Mineralogy and Petrology*, 160(5), pp.705-717.

Howell, D., 2012. Strain-induced birefringence in natural diamond: a review. *European Journal of Mineralogy*, 24(4), pp.575-585.

Hulston, J.R. and Thode, H.G., 1965. Variations in the S33, S34, and S36 contents of meteorites and their relation to chemical and nuclear effects. *Journal of Geophysical Research*, *70*(14), pp.3475-3484.

Huston, D.L., Power, M., Gemmell, J.B., Large, R.R., Lang, B., Vulkan, U. and Stein, G., 1995. Current Literature Survey of Geochemistry. *Australian Journal of Earth Sciences*, *42*(6), pp.549-555.

Hutchison, M.T., Hursthouse, M.B. and Light, M.E., 2001. Mineral inclusions in diamonds: associations and chemical distinctions around the 670-km discontinuity. *Contributions to Mineralogy and Petrology*, *142*(1), pp.119-126.

Ickert, R.B., Stachel, T., Stern, R.A. and Harris, J.W., 2013. Diamond from recycled crustal carbon documented by coupled δ18O–δ13C measurements of diamonds and their inclusions. *Earth and Planetary Science Letters*, 364, pp.85-97.

Ionov, D.A., Hoefs, J., Wedepohl, K.H. and Wiechert, U., 1992. Content and isotopic composition of sulphur in ultramafic xenoliths from central Asia. *Earth and Planetary Science Letters*, *111*(2-4), pp.269-286.

Izraeli, E.S., Harris, J.W. and Navon, O., 2001. Brine inclusions in diamonds: a new upper mantle fluid. *Earth and Planetary Science Letters*, 187(3-4), pp.323-332.

Izraeli, E.S., Harris, J.W. and Navon, O., 2004. Fluid and mineral inclusions in cloudy diamonds from Koffiefontein, South Africa. *Geochimica et Cosmochimica Acta*, 68(11), pp.2561-2575.

Jablon, B.M. and Navon, O., 2016. Most diamonds were created equal. *Earth and Planetary Science Letters*, 443, pp.41-47.

Jacob, D.E., Wirth, R., Enzmann, F., Kronz, A. and Schreiber, A., 2011. Nano-inclusion suite and high resolution micro-computed-tomography of polycrystalline diamond (framesite) from Orapa, Botswana. *Earth and Planetary Science Letters*, *308*(3-4), pp.307-316.

Jaques, A.L., Sheraton, J.W., Hall, A.E., Smith, C.B., Sun, S.S., Drew, R. and Foudoulis, C., 1986, September. Composition of crystalline inclusions and C-isotopic composition of Argyle and Ellendale diamonds. In *International Kimberlite Conference: Extended Abstracts* (Vol. 4, pp. 426-428).

Jaques, A.L., O'Neill, H.S.C., Smith, C.B., Moon, J. and Chappell, B.W., 1990. Diamondiferous peridotite xenoliths from the Argyle (AK1) lamproite pipe, Western Australia. *Contributions to Mineralogy and Petrology*, 104(3), pp.255-276.

Jago, B.C., Morrison, G.G. and Little, T.L., 1994. Metal zonation patterns and microtextural and micromineralogical evidence for alkali-and halogen-rich fluids in the genesis of the Victor Deep and McCreedy East footwall copper orebodies, Sudbury Igneous Complex. In: Lightfoot, P.C. and Naldrett, A.J. (eds.) *Proceedings of the Sudbury-Noril'sk Symposium*, pp. 65-76. Ontario Geological Survey Special Publication, 5.

Jenner, F.E., O'Neill, H.S.C., Arculus, R.J. and Mavrogenes, J.A., 2010. The magnetite crisis in the evolution of arc-related magmas and the initial concentration of Au, Ag and Cu. *Journal of Petrology*, 51(12), pp.2445-2464.

Jégo, S. and Dasgupta, R., 2014. The fate of sulfur during fluid-present melting of subducting basaltic crust at variable oxygen fugacity. *Journal of Petrology*, 55(6), pp.1019-1050.

John, D.A. and Taylor, R.D., 2016. By-products of porphyry copper and molybdenum deposits. *Reviews in Economic Geology*, 18, p. 137–164.

Johnson, A.C., Romaniello, S.J., Reinhard, C.T., Gregory, D.D., Garcia-Robledo, E., Revsbech, N.P., Canfield, D.E., Lyons, T.W. and Anbar, A.D., 2019. Experimental determination of pyrite and molybdenite oxidation kinetics at nanomolar oxygen concentrations. *Geochimica et Cosmochimica Acta*, 249, pp.160-172.

Jorgenson, C., 2017. Sulphur solubility of carbonatites as a mass transfer agent in the mantle. Masters Thesis (Dalhousie University, Halifax, Nova Scotia)

Jugo, P.J., Luth, R.W. and Richards, J.P., 2005. Experimental data on the speciation of sulfur as a function of oxygen fugacity in basaltic melts. *Geochimica et Cosmochimica Acta*, 69(2), pp.497-503.

Jugo, P.J., 2009. Sulfur content at sulfide saturation in oxidized magmas. *Geology*, 37(5), pp.415-418.

Jugo, P.J., Wilke, M. and Botcharnikov, R.E., 2010. Sulfur K-edge XANES analysis of natural and synthetic basaltic glasses: Implications for S speciation and S content as function of oxygen fugacity. *Geochimica et Cosmochimica Acta*, 74(20), pp.5926-5938.

Jørgensen, B.B., 1982. Mineralization of organic matter in the sea bed—the role of sulphate reduction. *Nature*, 296(5858), p.643.

Kalinowski, A., 2002. An experimental investigation into the causes and effects of sulfide partial melting at Broken Hill, NSW, Australia (Doctoral dissertation, Honours Thesis, The Australian National University, Canberra, Australia).

Kaminsky, F., Zakharchenko, O., Davies, R., Griffin, W., Khachatryan-Blinova, G. and Shiryaev, A., 2001. Superdeep diamonds from the Juina area, Mato Grosso State, Brazil. *Contributions to Mineralogy and Petrology*, *140*(6), pp.734-753.

Kaminsky, F.V., Khachatryan, G.K., Andreazza, P., Araujo, D. and Griffin, W.L., 2009. Super-deep diamonds from kimberlites in the Juina area, Mato Grosso State, Brazil. *Lithos*, 112, pp.833-842.

Kaminsky, F., Wirth, R., Matsyuk, S., Schreiber, A. and Thomas, R., 2009. Nyerereite and nahcolite inclusions in diamond: evidence for lower-mantle carbonatitic magmas. *Mineralogical Magazine*, *73*(5), pp.797-816.

Kaminsky, F.V., Sablukov, S.M., Belousova, E.A., Andreazza, P., Tremblay, M. and Griffin, W.L., 2010. Kimberlitic sources of super-deep diamonds in the Juina area, Mato Grosso State, Brazil. *Lithos*, *114*(1-2), pp.16-29.

Kaminsky, F.V. and Wirth, R., 2011. Iron carbide inclusions in lower-mantle diamond from Juina, Brazil. *The Canadian Mineralogist*, *49*(2), pp.555-572.

Kaminsky, F., 2012. Mineralogy of the lower mantle: A review of 'super-deep'mineral inclusions in diamond. *Earth-Science Reviews*, *110*(1-4), pp.127-147.

Kaminsky, F.V., Wirth, R. and Schreiber, A., 2013. Carbonatitic inclusions in deep mantle diamond from Juina, Brazil: new minerals in the carbonate-halide association. *The Canadian Mineralogist*, *51*(5), pp.669-688.

Kaminsky, F.V., Ryabchikov, I.D., McCammon, C.A., Longo, M., Abakumov, A.M., Turner, S. and Heidari, H., 2015. Oxidation potential in the Earth's lower mantle as recorded by ferropericlase inclusions in diamond. *Earth and Planetary Science Letters*, *417*, pp.49-56.

Kaminsky, F. and Wirth, R., 2017. Nitride, carbonitride and nitrocarbide inclusions in lower-mantle diamonds: A key to the balance of nitrogen in the Earth. *European Geosciences Union General Assembly Abstract No. EGU2017-1751, Vienna, Austria*.

Kanehira, K., Yui, S., Sakai, H. and Sasaki, A., 1973. Sulphide globules and sulphur isotope ratios in the abyssal tholeiite from the Mid-Atlantic Ridge near 30 N latitude. *Geochemical Journal*, *7*(2), pp.89-96.

Kaplan, I.R. and Rittenberg, S.C., 1964. Microbiological fractionation of sulphur isotopes. *Microbiology*, *34*(2), pp.195-212.

Keays, R.R., 1987. Principles of mobilization (dissolution) of metals in mafic and ultramafic rocks—the role of immiscible magmatic sulphides in the generation of hydrothermal gold and volcanogenic massive sulphide deposits. *Ore Geology Reviews*, 2(1-3), pp.47-63.

Kendrick, M.A., Jackson, M.G., Kent, A.J., Hauri, E.H., Wallace, P.J. and Woodhead, J., 2014. Contrasting behaviours of CO2, S, H2O and halogens (F, Cl, Br, and I) in enriched-mantle melts from Pitcairn and Society seamounts. *Chemical Geology*, 370, pp.69-81.

Keppler, H. and Wyllie, P.J., 1991. Partitioning of copper, tin, molybdenum, tungsten, uranium and thorium between melt and aqueous fluid in the systems haplogranite–water–hydrogen chloride and haplogranite–water–hydrogen fluoride. *Contributions to Mineralogy and Petrology*, 109, pp.139-150.

Kesson, S.E. and Ringwood, A.E., 1989. Slab-mantle interactions: 2. The formation of diamonds. *Chemical Geology*, 78(2), pp.97-118.

Kidane, A., Koch-Müller, M., Morales, L., Wiedenbeck, M. and De Wit, M., 2015, April. Carbon isotope ratios and impurities in diamonds from Southern Africa. In *EGU General Assembly Conference Abstracts* (Vol. 17).

Kidane, A.T., Koch-Müller, M., Wiedenbeck, M. and de Wit, M.J., 2017. Tracking sources of selected diamonds from Southern Africa based on carbon isotopic and chemical impurities. *South African Journal of Geology*, 120(3), pp.371-384.

Kinny, P.D., Compston, W., Bristow, J.W. and Williams, I.S., 1989. Archaean mantle xenocrysts in a Permian kimberlite: two generations of kimberlitic zircon in Jwaneng DK2, southern Botswana. *Kimberlites and related rocks*, 2, pp.833-842.

Kinny, P.D., Griffin, B., Heaman, L.M., Brakhfogel, F.F. and Spetsius, Z.V., 1997. SHRIMP U-Pb ages of perovskite from Yakutian kimberlites. *Geologiya i geofizika*, 38, pp.91-99.

Kiseeva, E.S., Fonseca, R.O. and Smythe, D.J., 2017. Chalcophile elements and sulfides in the upper mantle. *Elements*, 13(2), pp.111-116.

Kita, N.T., Ushikubo, T., Fu, B. and Valley, J.W., 2009. High precision SIMS oxygen isotope analysis and the effect of sample topography. *Chemical Geology*, 264(1-4), pp.43-57.

Kitayama, Y., Thomassot, E., Galy, A., Golovin, A., Korsakov, A., d'Eyrames, E., Assayag, N., Bouden, N. and Ionov, D., 2017. Co-magmatic sulfides and sulfates in the Udachnaya-East pipe (Siberia): A record of the redox state and isotopic composition of sulfur in kimberlites and their mantle sources. *Chemical Geology*, 455, pp.315-330.

Klein-BenDavid, O., Izraeli, E.S., Hauri, E. and Navon, O., 2004. Mantle fluid evolution—a tale of one diamond. *Lithos*, 77(1-4), pp.243-253.

Klein-BenDavid, O., Izraeli, E.S., Hauri, E. and Navon, O., 2007. Fluid inclusions in diamonds from the Diavik mine, Canada and the evolution of diamond-forming fluids. *Geochimica et Cosmochimica Acta*, 71(3), pp.723-744.

Klein-BenDavid, O. and Pearson, D.G., 2009. Origins of subcalcic garnets and their relation to diamond forming fluids—case studies from Ekati (NWT-Canada) and Murowa (Zimbabwe). *Geochimica et Cosmochimica Acta*, 73(3), pp.837-855.

Klein-BenDavid, O., Logvinova, A.M., Schrauder, M., Spetius, Z.V., Weiss, Y., Hauri, E.H., Kaminsky, F.V., Sobolev, N.V. and Navon, O., 2009. High-Mg carbonatitic microinclusions in some Yakutian diamonds—a new type of diamond-forming fluid. *Lithos*, 112, pp.648-659.

Klein-BenDavid, O., Pearson, D.G., Nowell, G.M., Ottley, C., McNeill, J.C., Logvinova, A. and Sobolev, N.V., 2014. The sources and time-integrated evolution of diamond-forming fluids–Trace elements and isotopic evidence. *Geochimica et Cosmochimica Acta*, 125, pp.146-169.

Klimm, K. and Botcharnikov, R.E., 2010. The determination of sulfate and sulfide species in hydrous silicate glasses using Raman spectroscopy. *American Mineralogist*, 95(10), pp.1574-1579.

Klimm, K., Kohn, S.C., O'Dell, L.A., Botcharnikov, R.E. and Smith, M.E., 2012. The dissolution mechanism of sulphur in hydrous silicate melts. I: Assessment of analytical techniques in determining the sulphur speciation in iron-free to iron-poor glasses. *Chemical Geology*, 322, pp.237-249. a

Klimm, K., Kohn, S.C. and Botcharnikov, R.E., 2012. The dissolution mechanism of sulphur in hydrous silicate melts. II: Solubility and speciation of sulphur in hydrous silicate melts as a function of fO_2. *Chemical Geology*, 322, pp.250-267.

Kohn, S.C., Speich, L., Smith, C.B. and Bulanova, G.P., 2016. FTIR thermochronometry of natural diamonds: a closer look. *Lithos*, 265, pp.148-158.

Kong, J.M., Boucher, D.R. and Scott-Smith, B.H., 1998. Exploration and geology of the Attawapiskat kimberlites, James Bay lowland, northern Ontario, Canada. In *International Kimberlite Conference: Extended Abstracts* (Vol. 7, pp. 446-448).

Kozdon, R., Kita, N.T., Huberty, J.M., Fournelle, J.H., Johnson, C.A. and Valley, J.W., 2010. In situ sulfur isotope analysis of sulfide minerals by SIMS: Precision and accuracy, with application to thermometry of~ 3.5 Ga Pilbara cherts. *Chemical Geology*, 275(3-4), pp.243-253.

König, S., Münker, C., Schuth, S. and Garbe-Schönberg, D., 2008. Mobility of tungsten in subduction zones. *Earth and Planetary Science Letters*, 274(1-2), pp.82-92.

König, S., Wille, M., Voegelin, A. and Schoenberg, R., 2016. Molybdenum isotope systematics in subduction zones. *Earth and Planetary Science Letters*, 447, pp.95-102.

Koornneef, J.M., Gress, M.U., Chinn, I.L., Jelsma, H.A., Harris, J.W. and Davies, G.R., 2017. Archaean and Proterozoic diamond growth from contrasting styles of large-scale magmatism. *Nature communications*, 8(1), p.648.

Kopylova, M., Navon, O., Dubrovinsky, L. and Khachatryan, G., 2010. Carbonatitic mineralogy of natural diamond-forming fluids. *Earth and Planetary Science Letters*, 291(1-4), pp.126-137.

Kress, V., 2007. Thermochemistry of sulfide liquids III: Ni-bearing liquids at 1 bar. *Contributions to Mineralogy and Petrology*, 154(2), pp.191-204.

Kuroda, P.K. and Sandell, E.B., 1954. Geochemistry of molybdenum. *Geochimica et Cosmochimica Acta*, *6*(1), pp.35-63.

Labidi, J., Cartigny, P. and Moreira, M., 2013. Non-chondritic sulphur isotope composition of the terrestrial mantle. *Nature*, 501(7466), p.208.

Labidi, J., Cartigny, P., Hamelin, C., Moreira, M. and Dosso, L., 2014. Sulfur isotope budget (32S, 33S, 34S and 36S) in Pacific–Antarctic ridge basalts: A record of mantle source heterogeneity and hydrothermal sulfide assimilation. *Geochimica et Cosmochimica Acta*, *133*, pp.47-67.

Lafuente, B., Downs, R.T., Yang, H. and Stone, N., 2015. The power of databases: the RRUFF project. In *Highlights in mineralogical crystallography*, Armbruster, T. & Danisi, RM, (eds.) W. De Gruyter, Berlin, Germany, 1, p.30.

Langford, R.E., Melton, C.E. and Giardini, A.A., 1974. Diamond growth by sulphide reduction of CO_2. *Nature*, 249(5458), p.647.

Large, R.R., Halpin, J.A., Danyushevsky, L.V., Maslennikov, V.V., Bull, S.W., Long, J.A., Gregory, D.D., Lounejeva, E., Lyons, T.W., Sack, P.J. and McGoldrick, P.J., 2014. Trace element content of sedimentary pyrite as a new proxy for deep-time ocean–atmosphere evolution. *Earth and Planetary Science Letters*, 389, pp.209-220.

Laurenz, V., Rubie, D.C., Frost, D.J. and Vogel, A.K., 2016. The importance of sulfur for the behavior of highly-siderophile elements during Earth's differentiation. *Geochimica et Cosmochimica Acta*, 194, pp.123-138.

Lewis, I.R. and Edwards, H., 2001. Handbook of Raman spectroscopy: from the research laboratory to the process line. CRC Press.

Li, C., Naldrett, A.J., Coats, C.J.A. and Johannessen, P., 1992. Platinum, palladium, gold, copper-rich stringers at the Strathcona Mine, Sudbury; their enrichment by fractionation of a sulfide liquid. *Economic Geology*, 87(6), pp.1584-1598.

Li, C. and Ripley, E.M., 2006. Formation of Pt–Fe alloy by desulfurization of Pt–Pd sulfide in the J–M reef of the Stillwater complex, Montana. *The Canadian Mineralogist*, 44(4), pp.895-903.

Li, C. and Ripley, E.M., 2009. Sulfur contents at sulfide-liquid or anhydrite saturation in silicate melts: empirical equations and example applications. *Economic Geology*, 104(3), pp.405-412.

Li, S., Junkin, W.D., Gaschnig, R.M., Ash, R.D., Piccoli, P.M., Candela, P.A. and Rudnick, R.L., 2019. Molybdenum contents of sulfides in ancient glacial diamictites: implications for molybdenum delivery to the oceans prior to the Great Oxidation Event. *Geochimica et Cosmochimica Acta*.

Li, Y. and Audétat, A., 2012. Partitioning of V, Mn, Co, Ni, Cu, Zn, As, Mo, Ag, Sn, Sb, W, Au, Pb, and Bi between sulfide phases and hydrous basanite melt at upper mantle conditions. *Earth and Planetary Science Letters*, 355, pp.327-340.

Liang, Y.H., Halliday, A.N., Siebert, C., Fitton, J.G., Burton, K.W., Wang, K.L. and Harvey, J., 2017. Molybdenum isotope fractionation in the mantle. *Geochimica et Cosmochimica Acta*, 199, pp.91-111.

Litvin, Y.A., Butvina, V.G., Bobrov, A.V. and Zharikov, V.A., 2002. The first synthesis of diamond in sulfide-carbon systems: The role of sulfides in diamond genesis. *Doklady Earth Sciences*, 382, pp. 40-43

Litvin, Y.A. and Butvina, V.G., 2004. Diamond-forming media in the system eclogite-carbonatite-sulfide-carbon: Experiments at 6.0-8.5 GPa. *Petrology*, 12(4), pp.377-387.

Litvin, Y.A., Shushkanova, A.V. and Zharikov, V.A., 2005, June. Immiscibility of sulfide-silicate melts in the mantle: Role in the syngenesis of diamond and inclusions (based on experiments at 7.0 GPa). *Doklady Earth Sciences*, 403(5), pp. 719

Liu, L.G., Mernagh, T.P. and Jaques, A.L., 1990. A mineralogical Raman spectroscopy study on eclogitic garnet inclusions in diamonds from Argyle. *Contributions to Mineralogy and Petrology*, 105(2), pp.156-161.

Liu, Y., Samaha, N. and Baker, D.R., 2006, May. Sulfur Concentration at Sulfide Saturation in Anhydrous Silicate Melts at Crustal Conditions. In *AGU Spring Meeting Abstracts*.

Liu, Y., Samaha, N.T. and Baker, D.R., 2007. Sulfur concentration at sulfide saturation (SCSS) in magmatic silicate melts. *Geochimica et Cosmochimica Acta*, 71(7), pp.1783-1799.

Liu, J., Wu, G., Li, Y., Zhu, M. and Zhong, W., 2012. Re–Os sulfide (chalcopyrite, pyrite and molybdenite) systematics and fluid inclusion study of the Duobaoshan porphyry Cu (Mo) deposit, Heilongjiang Province, China. *Journal of Asian Earth Sciences*, *49*, pp.300-312.

Lodders, K. and Palme, H., 1991. On the chalcophile character of molybdenum: determination of sulfide/silicate partition coefficients of Mo and W. *Earth and Planetary Science Letters*, *103*(1-4), pp.311-324.

Logvinova, A.M., Wirth, R., Tomilenko, A.A., Afanas'ev, V.P. and Sobolev, N.V., 2011. The phase composition of crystal-fluid nanoinclusions in alluvial diamonds in the northeastern Siberian Platform. *Russian Geology and Geophysics*, 52(11), pp.1286-1297.

Logvinova, A.M., Taylor, L.A., Fedorova, E.N., Yelisseyev, A.P., Wirth, R., Howarth, G., Reutsky, V.N. and Sobolev, N.V., 2015. A unique diamondiferous peridotite xenolith from the

Udachnaya kimberlite pipe, Yakutia: role of subduction in diamond formation. *Russian Geology and Geophysics*, 56(1-2), pp.306-320.

Longo, M., McCammon, C., Bulanova, G., Kaminsky, F.V. and Tappert, R., 2009, December. Oxygen fugacity determined from iron oxidation state in natural (Mg, Fe) O ferropericlase: new insights for lower mantle diamond formation. In *AGU Fall Meeting Abstracts*.

Longo, M., McCammon, C., Bulanova, G., Kaminsky, F. and Tappert, R., 2010, May. Oxygen fugacities determined from iron oxidation state in natural (Mg, Fe) O ferropericlase: new insights into lower mantle diamond formation. In *EGU General Assembly Conference Abstracts* (Vol. 12, p. 13549).

Lorand, J.P., Luguet, A. and Alard, O., 2013. Platinum-group element systematics and petrogenetic processing of the continental upper mantle: A review. *Lithos*, *164*, pp.2-21.

Lorand, J.P. and Luguet, A., 2016. Chalcophile and siderophile elements in mantle rocks: Trace elements controlled by trace minerals. *Reviews in Mineralogy and Geochemistry*, *81*(1), pp.441-488.

Luck, J.M. and Allègre, C.J., 1982. The study of molybdenites through the187Re-187Os chronometer. *Earth and Planetary Science Letters*, 61(2), pp.291-296.

Luguet, A., Shirey, S.B., Lorand, J.P., Horan, M.F. and Carlson, R.W., 2007. Residual platinum-group minerals from highly depleted harzburgites of the Lherz massif (France) and their role in HSE fractionation of the mantle. *Geochimica et Cosmochimica Acta*, *71*(12), pp.3082-3097.

Luth, R.W. and Stachel, T., 2014. The buffering capacity of lithospheric mantle: implications for diamond formation. *Contributions to Mineralogy and Petrology*, 168(5), p.1083.

Lynton, S.J., Candela, P.A. and Piccoli, P.M., 1993. An experimental study of the partitioning of copper between pyrrhotite and a high silica rhyolitic melt. *Economic Geology*, *88*(4), pp.901-915.

Lyons, T.W., Reinhard, C.T. and Planavsky, N.J., 2014. The rise of oxygen in Earth's early ocean and atmosphere. *Nature*, 506(7488), p.307.

MacLean, W.H. and Shimazaki, H., 1976. The partition of Co, Ni, Cu, and Zn between sulfide and silicate liquids. *Economic Geology*, 71(6), pp.1049-1057.

MacNamara, J. and Thode, H.G., 1950. Comparison of the isotopic constitution of terrestrial and meteoritic sulfur. *Physical Review*, *78*(3), p.307.

Maier, W.D. and Barnes, S.J., 1996. Unusually high concentrations of magnetite at Caraiba and other Cu-sulfide deposits in the Curaca Valley, Bahia, Brazil. *Canadian Mineralogist*, 34(4), pp.717-731.

Manheim, F.T. and Landergren, S., 1974. Molybdenum. in: K.H. Wedepohl (Ed.), *Handbook of Geochemistry*, Springer, Berlin, pp. 42-B-1–42-O-2

Markey, R., Stein, H.J., Hannah, J.L., Zimmerman, A., Selby, D. and Creaser, R.A., 2007. Standardizing Re–Os geochronology: a new molybdenite reference material (Henderson, USA) and the stoichiometry of Os salts. *Chemical Geology*, 244(1-2), pp.74-87.

Martin, C.E., 1991. Osmium isotopic characteristics of mantle-derived rocks. *Geochimica et Cosmochimica Acta*, 55(5), pp.1421-1434.

Marx, P.C., 1972. Pyrrhotine and the origin of terrestrial diamonds. *Mineralogical Magazine*, 38(297), pp.636-638.

Masotta, M. and Keppler, H., 2015. Anhydrite solubility in differentiated arc magmas. *Geochimica et Cosmochimica Acta*, 158, pp.79-102.

Mathur, R., Marschik, R., Ruiz, J., Munizaga, F., Leveille, R.A. and Martin, W., 2002. Age of mineralization of the Candelaria Fe oxide Cu-Au deposit and the origin of the Chilean iron belt, based on Re-Os isotopes. *Economic Geology*, 97(1), pp.59-71.

Mavrogenes, J.A. and O'Neill, H.S.C., 1999. The relative effects of pressure, temperature and oxygen fugacity on the solubility of sulfide in mafic magmas. *Geochimica et Cosmochimica Acta*, 63(7-8), pp.1173-1180.

McCammon, C.A., Stachel, T. and Harris, J.W., 2004. Iron oxidation state in lower mantle mineral assemblages: II. Inclusions in diamonds from Kankan, Guinea. *Earth and Planetary Science Letters*, 222(2), pp.423-434.

McCarthy, T.S. and Allan, J.G., 2007. A possible new alluvial diamond field related to the Klipspringer kimberlite swarm, South Africa. *South African Journal of Geology*, 110(4), pp.503-510.

McCormick, K.A., Lesher, C.M., McDonald, A.M., Fedorowich, J.S. and James, R.S., 2002. Chlorine and alkali geochemical halos in the footwall breccia and sublayer norite at the margin of the Strathcona embayment, Sudbury structure, Ontario. *Economic Geology*, 97(7), pp.1509-1519.

McDonald, I., Hughes, H.S., Butler, I.B., Harris, J.W. and Muir, D., 2017. Homogenisation of sulphide inclusions within diamonds: A new approach to diamond inclusion geochemistry. *Geochimica et Cosmochimica Acta*, 216, pp.335-357.

McDonough, W.F. and Sun, S.S., 1995. The composition of the Earth. *Chemical Geology*, *120*(3-4), pp.223-253.

McManus, J., Berelson, W.M., Severmann, S., Poulson, R.L., Hammond, D.E., Klinkhammer, G.P. and Holm, C., 2006. Molybdenum and uranium geochemistry in continental margin sediments: paleoproxy potential. *Geochimica et Cosmochimica Acta*, 70(18), pp.4643-4662.

Melfos, V., Vavelidis, M., Christofides, G. and Seidel, E., 2002. Origin and evolution of the Tertiary Maronia porphyry copper-molybdenum deposit, Thrace, Greece. *Mineralium Deposita*, *37*(6-7), pp.648-668.

Melton, G.L., Stachel, T., Stern, R.A., Carlson, J. and Harris, J.W., 2013. Infrared spectral and carbon isotopic characteristics of micro-and macro-diamonds from the Panda kimberlite (Central Slave Craton, Canada). *Lithos*, 177, pp.110-119.

Mengason, M.J., Candela, P.A. and Piccoli, P.M., 2011. Molybdenum, tungsten and manganese partitioning in the system pyrrhotite–Fe–S–O melt–rhyolite melt: impact of sulfide segregation on arc magma evolution. *Geochimica et Cosmochimica Acta*, 75(22), pp.7018-7030.

Mernagh, T.P. and Trudu, A.G., 1993. A laser Raman microprobe study of some geologically important sulphide minerals. *Chemical Geology*, 103(1-4), pp.113-127.

Métrich, N. and Mandeville, C.W., 2010. Sulfur in magmas. *Elements*, 6(2), pp.81-86.

Meyer, H.O.A, 1987. Inclusions in diamond. In Nixon, P.H., (ed.), *Mantle xenoliths*: Chichester, England, John Wiley and Sons, p. 501-522

Meyer, H.O.A., Milledge, H.J. and Sutherland, F.L., 1995, September. Unusual diamonds and unique inclusions from New South Wales, Australia. In *International Kimberlite Conference: Extended Abstracts* (Vol. 6, pp. 379-381).

Milani, S., Nestola, F., Angel, R.J., Nimis, P. and Harris, J.W., 2016. Crystallographic orientations of olivine inclusions in diamonds. *Lithos*, 265, pp.312-316.

Miller, C.E., Kopylova, M. and Smith, E., 2014. Mineral inclusions in fibrous diamonds: constraints on cratonic mantle refertilization and diamond formation. *Mineralogy and Petrology*, 108(3), pp.317-331.

Mingxiang, M., 2016. Great Oxidation Event in history of the Earth: An important clue for the further understanding of evolution of palaeogeographical background. *Journal of Palaeogeography* (Chinese Edition), (3), p.3.

Mitchell, R.H. and Krouse, H.R., 1975. Sulphur isotope geochemistry of carbonatites. *Geochimica et Cosmochimica Acta*, *39*(11), pp.1505-1513.

Moh, G.H., 1978. High-temperature metal sulfide chemistry. In *Topics in current chemistry* (pp. 107-151). Springer, Berlin, Heidelberg.

Moretti, R. and Ottonello, G., 2005. Solubility and speciation of sulfur in silicate melts: The Conjugated Toop-Samis-Flood-Grjotheim (CTSFG) model. *Geochimica et Cosmochimica Acta*, 69(4), pp.801-823.

Morford, J.L. and Emerson, S., 1999. The geochemistry of redox sensitive trace metals in sediments. *Geochimica et Cosmochimica Acta*, 63(11-12), pp.1735-1750.

Morgan, J.W. and Anders, E., 1980. Chemical composition of earth, Venus, and Mercury. *Proceedings of the National Academy of Sciences*, 77(12), pp.6973-6977.

Morris, A.W., 1975, January. Dissolved molybdenum and vanadium in the northeast Atlantic Ocean. In *Deep Sea Research and Oceanographic Abstracts* (Vol. 22, No. 1, pp. 49-54). Elsevier.

Moss, S., Webb, K., Hetman, C. and Manyumbu, A., 2013. Geology of the K1 and K2 kimberlite pipes at Murowa, Zimbabwe. In *Proceedings of 10th International Kimberlite Conference* (pp. 35-50). Springer, New Delhi.

Muller, É., Philippot, P., Rollion-Bard, C., Cartigny, P., Assayag, N., Marin-Carbonne, J., Mohan, M.R. and Sarma, D.S., 2017. Primary sulfur isotope signatures preserved in high-grade Archean barite deposits of the Sargur Group, Dharwar Craton, India. *Precambrian Research*, *295*, pp.38-47.

Mungall, J.E. and Brenan, J.M., 2003. Experimental evidence for the chalcophile behavior of the halogens. *The Canadian Mineralogist*, 41(1), pp.207-220.

Mungall, J.E. and Su, S., 2005. Interfacial tension between magmatic sulfide and silicate liquids: Constraints on kinetics of sulfide liquation and sulfide migration through silicate rocks. *Earth and Planetary Science Letters*, 234(1-2), pp.135-149.

Mungall, J.E., 2007. Crystallization of magmatic sulfides: An empirical model and application to Sudbury ores. *Geochimica et Cosmochimica Acta*, 71(11), pp.2809-2819.

Naldrett, A.J., 1969. A portion of the system Fe–S–O between 900 and 1080 C and its application to sulfide ore magmas. *Journal of Petrology*, 10(2), pp.171-201.

Naldrett, A.J., 2004. Magmatic sulfide deposits: Geology, geochemistry and exploration, Berlin/Heidelberg/New York

Nash, W.M., Smythe, D.J. and Wood, B.J., 2019. Compositional and temperature effects on sulfur speciation and solubility in silicate melts. *Earth and Planetary Science Letters*, 507, pp.187-198.

Navon, O., Hutcheon, I.D., Rossman, G.R. and Wasserburg, G.J., 1988. Mantle-derived fluids in diamond micro-inclusions. *Nature*, 335(6193), p.784.

Navon, O., 1991. High internal pressures in diamond fluid inclusions determined by infrared absorption. *Nature*, 353(6346), p.746.

Navon, O., 1998, April. Diamond formation in the Earth's mantle. In *International Kimberlite Conference: Extended Abstracts* (Vol. 7, No. 1, pp. 618-621).

Navon, O., 1999. Formation of diamonds in the Earth's mantle. In *Proceedings of the 7th International Kimberlite Conference* (pp. 584-604). Red Roof Designs Cape Town.

Navon, O., Izraeli, E.S. and Klein-BenDavid, O., 2003, June. Fluid inclusions in diamonds-the carbonatitic connection. In *International Kimberlite Conference: Extended Abstracts* (Vol. 8).

Nestola, F., Nimis, P., Angel, R.J., Milani, S., Bruno, M., Prencipe, M. and Harris, J.W., 2014. Olivine with diamond-imposed morphology included in diamonds. Syngenesis or protogenesis?. *International Geology Review*, 56(13), pp.1658-1667.

Nestola, F., Jung, H. and Taylor, L.A., 2017. Mineral inclusions in diamonds may be synchronous but not syngenetic. *Nature communications*, 8, p.14168.

Newberry, R.J., 1979. Polytypism in molybdenite (II): Relationships between polytypism, ore deposition/alteration stages and rhenium contents. *American Mineralogist*, *64*, pp.768-775.

Newsom, H.E. and Palme, H., 1984. The depletion of siderophile elements in the Earth's mantle: new evidence from molybdenum and tungsten. *Earth and Planetary Science Letters*, 69(2), pp.354-364.

Nielsen, H., 1979. Sulfur isotopes. In *Lectures in isotope geology* (pp. 283-312). Springer, Berlin, Heidelberg.

Nielsen, H., Pilot, J., Grinenko, L.N., Grinenko, V.A., Lein, A.Y., Smith, J.W. and Pankina, R.G., 1991. Lithospheric sources of sulphur. In: Krouse, H.R., Grinenko, V.A. (eds.), *Stable Isotopes, Natural and Anthropogenic Sulfur in the Environment*. Scope 43, 65–132

Nimis, P., Alvaro, M., Nestola, F., Angel, R.J., Marquardt, K., Rustioni, G., Harris, J.W. and Marone, F., 2016. First evidence of hydrous silicic fluid films around solid inclusions in gem-quality diamonds. *Lithos*, 260, pp.384-389.

Nimis, P., Angel, R.J., Alvaro, M., Nestola, F., Harris, J.W., Casati, N. and Marone, F., 2019. Crystallographic orientations of magnesiochromite inclusions in diamonds: what do they tell us?. *Contributions to Mineralogy and Petrology*, 174(4), p.29.

Nisbet, E.G., Cheadle, M.J., Arndt, N.T. and Bickle, M.J., 1993. Constraining the potential temperature of the Archaean mantle: a review of the evidence from komatiites. *Lithos*, 30(3-4), pp.291-307.

Noll Jr, P.D., Newsom, H.E., Leeman, W.P. and Ryan, J.G., 1996. The role of hydrothermal fluids in the production of subduction zone magmas: evidence from siderophile and chalcophile trace elements and boron. *Geochimica et Cosmochimica Acta*, 60(4), pp.587-611.

O'Driscoll, B., Day, J.M., Daly, J.S., Walker, R.J. and McDonough, W.F., 2009. Rhenium–osmium isotopes and platinum-group elements in the Rum Layered Suite, Scotland: Implications for Cr-spinel seam formation and the composition of the Iceland mantle anomaly. *Earth and Planetary Science Letters*, 286(1-2), pp.41-51.

O'Neil, J.R., 1986. Theoretical and experimental aspects of isotopic fractionation. *Reviews in Mineralogy*, *16*, pp.1-40.

O'Neill, H.S.C. and Eggins, S.M., 2002. The effect of melt composition on trace element partitioning: an experimental investigation of the activity coefficients of FeO, NiO, CoO, MoO2 and MoO3 in silicate melts. *Chemical Geology*, *186*(1-2), pp.151-181.

O'Neill, H.S.C. and Mavrogenes, J.A., 2002. The sulfide capacity and the sulfur content at sulfide saturation of silicate melts at 1400 C and 1 bar. *Journal of Petrology*, 43(6), pp.1049-1087.

Ohmoto, H. and Rye, R.O., 1979. Isotopes of sulfur and carbon. In Barnes, H.L. (ed.), *Geochemistry of Hydrothermal Ore Deposits*. John Wiley and Sons, p. 509-567

Ohmoto, H., Watanabe, Y., Ikemi, H., Poulson, S.R. and Taylor, B.E., 2006. Sulphur isotope evidence for an oxic Archaean atmosphere. *Nature*, *442*(7105), p.908.

Ono, S., Eigenbrode, J.L., Pavlov, A.A., Kharecha, P., Rumble III, D., Kasting, J.F. and Freeman, K.H., 2003. New insights into Archean sulfur cycle from mass-independent sulfur isotope records from the Hamersley Basin, Australia. *Earth and Planetary Science Letters*, *213*(1-2), pp.15-30.

Ono, S., Wing, B., Johnston, D., Farquhar, J. and Rumble, D., 2006. Mass-dependent fractionation of quadruple stable sulfur isotope system as a new tracer of sulfur biogeochemical cycles. *Geochimica et Cosmochimica Acta*, *70*(9), pp.2238-2252.

Orberger, B., Pasava, J., Gallien, J.P., Daudin, L. and Trocellier, P., 2003. Se, As, Mo, Ag, Cd, In, Sb, Pt, Au, Tl, Re traces in biogenic and abiogenic sulfides from Black Shales (Selwyn Basin, Yukon territories, Canada): a nuclear microprobe study. *Nuclear Instruments and Methods in Physics Research Section B: Beam Interactions with Materials and Atoms*, 210, pp. 441-448.

Padilla, R., Ruiz, M.C. and Sohn, H.Y., 1997. Reduction of molybdenite with carbon in the presence of lime. *Metallurgical and Materials Transactions B*, 28(2), pp.265-274.

Palme, H. and O'Neill, H.S.C., 2003. Cosmochemical estimates of mantle composition. *Treatise on geochemistry*, 2, p.568.

Palot, M., Pearson, D.G., Stern, R., Stachel, T. and Harris, J.W., 2012, February. Multiple growth events, processes and fluid sources involved in the growth of diamonds from Finsch mine, RSA: a micro-analytical study. In *International Kimberlite Conference: Extended Abstracts* (Vol. 10).

Palot, M., Pearson, D.G., Stachel, T., Harris, J.W., Bulanova, G.P. and Chinn, I., 2013. Multiple growth episodes or prolonged formation of diamonds? Inferences from infrared absorption data. In *Proceedings of 10th International Kimberlite Conference* (pp. 281-296). Springer, New Delhi.

Palot, M., Pearson, D.G., Stern, R.A., Stachel, T. and Harris, J.W., 2014. Isotopic constraints on the nature and circulation of deep mantle C–H–O–N fluids: Carbon and nitrogen systematics within ultra-deep diamonds from Kankan (Guinea). *Geochimica et Cosmochimica Acta*, 139, pp.26-46.

Palyanov, Y.N., Borzdov, Y.M., Khokhryakov, A.F., Kupriyanov, I.N. and Sobolev, N.V., 2006. Sulfide melts–graphite interaction at HPHT conditions: Implications for diamond genesis. *Earth and Planetary Science Letters*, 250(1-2), pp.269-280.

Palyanov, Y.N., Borzdov, Y.M., Bataleva, Y.V., Sokol, A.G., Palyanova, G.A. and Kupriyanov, I.N., 2007. Reducing role of sulfides and diamond formation in the Earth's mantle. *Earth and Planetary Science Letters*, 260(1-2), pp.242-256.

Pantaleo, N.S., Newton, M.G., Gogineni, S.V., Melton, C.E. and Giardini, A.A., 1979. Mineral inclusions in four Arkansas diamonds; their nature and significance. *American Mineralogist*, 64(9-10), pp.1059-1062.

Peach, C.L., Mathez, E.A. and Keays, R.R., 1990. Sulfide melt-silicate melt distribution coefficients for noble metals and other chalcophile elements as deduced from MORB: Implications for partial melting. *Geochimica et Cosmochimica Acta*, *54*(12), pp.3379-3389.

Peach, C.L. and Mathez, E.A., 1993. Sulfide melt-silicate melt distribution coefficients for nickel and iron and implications for the distribution of other chalcophile elements. *Geochimica et Cosmochimica Acta*, *57*(13), pp.3013-3021.

Pearson, D.G., Shirey, S.B., Carlson, R.W., Boyd, F.R., Pokhilenko, N.P. and Shimizu, N., 1995. Re-Os, Sm-Nd, and Rb-Sr isotope evidence for thick Archaean lithospheric mantle beneath the Siberian craton modified by multistage metasomatism. *Geochimica et Cosmochimica Acta*, 59(5), pp.959-977.

Pearson, D.G., Shirey, S.B., Bulanova, G.P., Carlson, R.W. and Milledge, H.J., 1998a. Dating diamonds using the Re-Os isotope technique: a study of sulfide inclusions in Siberian diamonds. In *International Kimberlite Conference: Extended Abstracts* (Vol. 7, pp. 661-663).

Pearson, D.G., Shirey, S.B., Harris, J.W. and Carlson, R.W., 1998b. Sulphide inclusions in diamonds from the Koffiefontein kimberlite, S Africa: constraints on diamond ages and mantle Re–Os systematics. *Earth and Planetary Science Letters*, 160(3-4), pp.311-326.

Pearson, D.G., Shirey, S.B., Bulanova, G.P., Carlson, R.W. and Milledge, H.J., 1999. Re-Os isotope measurements of single sulfide inclusions in a Siberian diamond and its nitrogen aggregation systematics. *Geochimica et Cosmochimica Acta*, 63(5), pp.703-711.

Pearson, D.G., Bulanova, G.P., Shirey, S.B., Carlson, R.W., Milledge, H.J. and Barashkov, Y.P., 2000. Re-Os isotope constraints on the ages of Siberian diamonds. In *Journal of conference abstracts* (Vol. 5, p. 776).

Pearson, D.G. and Harris, J.W., 2004. Age constraints for diamonds from Koffiefontein mine, S. Africa, a Re-Os isotope and N-aggregation study. *Geochimica et Cosmochimica Acta*, 68(11), pp. A714

Pearson, D.G. and Wittig, N., 2008. Formation of Archaean continental lithosphere and its diamonds: the root of the problem. *Journal of the Geological Society*, 165(5), pp.895-914.

Peate, D.W., Pearce, J.A., Hawkesworth, C.J., Colley, H., Edwards, C.M. and Hirose, K., 1997. Geochemical variations in Vanuatu arc lavas: the role of subducted material and a variable mantle wedge composition. *Journal of Petrology*, 38(10), pp.1331-1358.

Pedersen, A.K., 1979. Basaltic glass with high-temperature equilibrated immiscible sulphide bodies with native iron from Disko, central West Greenland. *Contributions to Mineralogy and Petrology*, 69(4), pp.397-407.

Peter, J.M. and Shanks III, W.C., 1992. Sulfur, carbon, and oxygen isotope variations in submarine hydrothermal deposits of Guaymas Basin, Gulf of California, USA. *Geochimica et Cosmochimica Acta*, *56*(5), pp.2025-2040.

Philippot, P., Van Zuilen, M., Lepot, K., Thomazo, C., Farquhar, J. and Van Kranendonk, M.J., 2007. Early Archaean microorganisms preferred elemental sulfur, not sulfate. *Science*, 317(5844), pp.1534-1537.

Phillips, D., Onstott, T.C. and Harris, J.W., 1989. 40Ar/39Ar laser-probe dating of diamond inclusions from the Premier kimberlite. *Nature*, 340(6233), p.460.

Phillips, D., Kiviets, G.B., Barton, E.S., Smith, C.B., Viljoen, K.S. and Fourie, L.F., 1998, April. 40Ar/39Ar dating of kimberlites and related rocks: problems and solutions. In International Kimberlite Conference: Extended Abstracts (Vol. 7, pp. 690-692).

Phillips, D., Harris, J.W. and Kiviets, G.B., 2004. 40Ar/39Ar analyses of clinopyroxene inclusions in African diamonds: implications for source ages of detrital diamonds. *Geochimica et Cosmochimica Acta*, 68(1), pp.151-165.

Phillips, D. and Harris, J.W., 2008. Provenance studies from 40Ar/39Ar dating of mineral inclusions in diamonds: Methodological tests on the Orapa kimberlite, Botswana. *Earth and Planetary Science Letters*, 274(1-2), pp.169-178.

Piccoli, P., Candela, P. and Rivers, M., 2000. Interpreting magmatic processes from accessory phases: titanite—a small-scale recorder of large-scale processes. *Earth and Environmental Science Transactions of The Royal Society of Edinburgh*, 91(1-2), pp.257-267.

Pidgeon, R.T., Smith, C.B. and Fanning, C.M., 1989. Kimberlite and lamproite emplacement ages in Western Australia. *Kimberlites and related rocks*, 1, pp.382-391.

Pilipchuk, M.F. and Volkov, I.I., 1974. Behavior of molybdenum in processes of sediment formation and diagenesis in Black Sea. In E.T Degens, D.A Ross (eds.), *The Black Sea—Geology, Chemistry and Biology*, AAPG Mem, pp. 542-553

Piña, R., Gervilla, F., Barnes, S.J., Ortega, L. and Lunar, R., 2012. Distribution of platinum-group and chalcophile elements in the Aguablanca Ni–Cu sulfide deposit (SW Spain): evidence from a LA-ICP-MS study. *Chemical Geology*, 302, pp.61-75.

Piña, R., Gervilla, F., Barnes, S.J., Ortega, L. and Lunar, R., 2013. Partition coefficients of platinum group and chalcophile elements between arsenide and sulfide phases as determined in the Beni Bousera Cr-Ni mineralization (North Morocco). *Economic Geology*, *108*(5), pp.935-951.

Piña, R., Gervilla, F., Barnes, S.J., Oberthür, T. and Lunar, R., 2016. Platinum-group element concentrations in pyrite from the Main Sulfide Zone of the Great Dyke of Zimbabwe. *Mineralium Deposita*, 51(7), pp.853-872.

Plimer, I.R., 1985. Broken Hill Pb-Zn-Ag deposit—a product of mantle metasomatism. *Mineralium Deposita*, 20(3), pp.147-153.

Pons, M.L., Debret, B., Bouilhol, P., Delacour, A. and Williams, H., 2016. Zinc isotope evidence for sulfate-rich fluid transfer across subduction zones. *Nature communications*, 7, p.13794.

Poulson, S.R. and Ohmoto, H., 1990. An evaluation of the solubility of sulfide sulfur in silicate melts from experimental data and natural samples. *Chemical Geology*, 85(1-2), pp.57-75.

Poulson, R.L., Siebert, C., McManus, J. and Berelson, W.M., 2006. Authigenic molybdenum isotope signatures in marine sediments. *Geology*, 34(8), pp.617-620.

Rabbia, O.M., Hernández, L.B., French, D.H., King, R.W. and Ayers, J.C., 2009. The El Teniente porphyry Cu–Mo deposit from a hydrothermal rutile perspective. *Mineralium Deposita*, 44(8), p.849.

Raiswell, R. and Berner, R.A., 1986. Pyrite and organic matter in Phanerozoic normal marine shales. *Geochimica et Cosmochimica Acta*, 50(9), pp.1967-1976.

Ravizza, G., Turekian, K.K. and Hay, B.J., 1991. The geochemistry of rhenium and osmium in recent sediments from the Black Sea. *Geochimica et Cosmochimica Acta*, 55(12), pp.3741-3752.

Rees, C.E., Jenkins, W.J. and Monster, J., 1978. The sulphur isotopic composition of ocean water sulphate. *Geochimica et Cosmochimica Acta*, *42*(4), pp.377-381.

Rege, S., Griffin, W.L., Pearson, N.J., Araújo, D., Zedgenizov, D. and O'Reilly, S.Y., 2010. Trace-element patterns of fibrous and monocrystalline diamonds: Insights into mantle fluids. *Lithos*, 118(3-4), pp.313-337.

Reutskii, V.N., Logvinova, A.M. and Sobolev, N.V., 1999. Carbon isotopic composition of polycrystalline diamond aggregates with chromite inclusions from the Mir kimberlite pipe, Yakutia. *Geochemistry international*, 37(11), pp.1073-1078.

Richardson, S.H., Gurney, J.J., Erlank, A.J. and Harris, J., 1984. Origin of diamonds in old enriched mantle. *Nature*, 310(5974), pp.198-202.

Richardson, S.H., 1986. Latter-day origin of diamonds of eclogitic paragenesis. *Nature*, 322(6080), pp.623-626.

Richardson, S.H., Erlank, A.J., Harris, J.W. and Hart, S.R., 1990. Eclogitic diamonds of Proterozoic age from Cretaceous kimberlites. *Nature*, 346(6279), p.54.

Richardson, S.H., Harris, J.W. and Gurney, J.J., 1993. Three generations of diamonds from old continental mantle. *Nature*, 366(6452), p.256.

Richardson, S.H. and Harris, J.W., 1997. Antiquity of peridotitic diamonds from the Siberian craton. *Earth and Planetary Science Letters*, 151(3-4), pp.271-277.

Richardson, S.H., Chinn, I.L. and Harris, J.W., 1998, April. Age and origin of eclogitic diamonds from the Jwaneng kimberlite, Botswana. In *International Kimberlite Conference: Extended Abstracts* (Vol. 7, pp. 734-736).

Richardson, S.H., Shirey, S.B., Harris, J.W. and Carlson, R.W., 2001. Archean subduction recorded by Re–Os isotopes in eclogitic sulfide inclusions in Kimberley diamonds. *Earth and Planetary Science Letters*, 191(3-4), pp.257-266.

Richardson, S.H., Shirey, S.B. and Harris, J.W., 2003, June. Episodic diamond genesis and Kaapvaal craton evolution. In *International Kimberlite Conference: Extended Abstracts* (Vol. 8).

Richardson, S.H., Shirey, S.B. and Harris, J.W., 2004. Episodic diamond genesis at Jwaneng, Botswana, and implications for Kaapvaal craton evolution. *Lithos*, 77(1-4), pp.143-154.

Richardson, S.H. and Shirey, S.B., 2008. Continental mantle signature of Bushveld magmas and coeval diamonds. *Nature*, *453*(7197), p.910.

Richardson, S.H., Pöml, P.F., Shirey, S.B. and Harris, J.W., 2009. Age and origin of peridotitic diamonds from Venetia, Limpopo Belt, Kaapvaal–Zimbabwe craton. *Lithos*, 112, pp.785-792.

Riciputi, L.R., Paterson, B.A. and Ripperdan, R.L., 1998. Measurement of light stable isotope ratios by SIMS:: Matrix effects for oxygen, carbon, and sulfur isotopes in minerals. *International Journal of Mass Spectrometry*, 178(1-2), pp.81-112.

Rickard, R.S., Harris, J.W., Gurney, J.J. and Cardoso, P., 1989. Mineral inclusions in diamonds from Koffiefontein Mine. *Kimberlites and related rocks*, 2, pp.1054-1062.

Roerdink, D.L., Mason, P.R., Whitehouse, M.J. and Reimer, T., 2013. High-resolution quadruple sulfur isotope analyses of 3.2 Ga pyrite from the Barberton Greenstone Belt in South Africa reveal distinct environmental controls on sulfide isotopic arrays. *Geochimica et Cosmochimica Acta*, *117*, pp.203-215.

Rohrbach, A., Ballhaus, C., Ulmer, P., Golla-Schindler, U. and Schönbohm, D., 2011. Experimental evidence for a reduced metal-saturated upper mantle. *Journal of Petrology*, 52(4), pp.717-731.

Rohrbach, A., Ghosh, S., Schmidt, M.W., Wijbrans, C.H. and Klemme, S., 2014. The stability of Fe–Ni carbides in the Earth's mantle: Evidence for a low Fe–Ni–C melt fraction in the deep mantle. *Earth and Planetary Science Letters*, 388, pp.211-221.

Rubie, D.C., Laurenz, V., Jacobson, S.A., Morbidelli, A., Palme, H., Vogel, A.K. and Frost, D.J., 2016. Highly siderophile elements were stripped from Earth's mantle by iron sulfide segregation. *Science*, 353(6304), pp.1141-1144.

Rudnick, R.L., Eldridge, C.S. and Bulanova, G.P., 1993. Diamond growth history from in situ measurement of Pb and S isotopic compositions of sulfide inclusions. *Geology*, 21(1), pp.13-16.

Rudnick, R.L. and Walker, R.J., 2009. Interpreting ages from Re–Os isotopes in peridotites. *Lithos*, 112, pp.1083-1095.

Rusk, B.G., Reed, M.H., Dilles, J.H., Klemm, L.M. and Heinrich, C.A., 2004. Compositions of magmatic hydrothermal fluids determined by LA-ICP-MS of fluid inclusions from the porphyry copper–molybdenum deposit at Butte, MT. *Chemical Geology*, 210(1-4), pp.173-199.

Rusk, B.G., Reed, M.H. and Dilles, J.H., 2008. Fluid inclusion evidence for magmatic-hydrothermal fluid evolution in the porphyry copper-molybdenum deposit at Butte, Montana. *Economic Geology*, 103(2), pp.307-334.

Ryabchikov, I.D. and Kaminsky, F.V., 2013. Oxygen potential of diamond formation in the lower mantle. *Geology of Ore Deposits*, 55(1), pp.1-12.

Sakai, H., 1968. Isotopic properties of sulfur compounds in hydrothermal processes. *Geochemical Journal*, *2*(1), pp.29-49.

Sakai, H., Des Marais, D.J., Ueda, A. and Moore, J.G., 1984. Concentrations and isotope ratios of carbon, nitrogen and sulfur in ocean-floor basalts. *Geochimica et Cosmochimica Acta*, *48*(12), pp.2433-2441.

Salters, V.J. and Stracke, A., 2004. Composition of the depleted mantle. *Geochemistry, Geophysics, Geosystems*, 5(5), pp. 27.

Santosh, M., Tsunogae, T., Shimizu, H. and Dubessy, J., 2010. Fluid characteristics of retrogressed eclogites and mafic granulites from the Cambrian Gondwana suture zone in southern India. *Contributions to Mineralogy and Petrology*, *159*(3), pp.349-369.

Schmitt, A.K., Zack, T., Kooijman, E., Logvinova, A.M. and Sobolev, N.V., 2019. U–Pb ages of rare rutile inclusions in diamond indicate entrapment synchronous with kimberlite formation. *Lithos*, 350, p.105251.

Schmitz, S., Brenker, F.E., Garrevoet, J., Vekemans, B., Krebs, M., Rudloff, J., Falkenberg, G., Frühling, U., Wellenreuther, G., De Samber, B. and Vincze, L., 2012. Sub-micron and full-field XRF analyses of mantle fluids and melts trapped in cloudy diamonds of ultra-deep sources. *DESY Annual Report*. Photon Science.

Schrauder, M. and Navon, O., 1994. Hydrous and carbonatitic mantle fluids in fibrous diamonds from Jwaneng, Botswana. *Geochimica et Cosmochimica Acta*, 58(2), pp.761-771.a

Schrauder, M., Navon, O., Szafranek, D., Kaminsky, F.V. and Galimov, E.M., 1994. Fluids in Yakutian and Indian diamonds. *Mineralogical Magazine A*, 58, pp.813-814.b

Schrauder, M., Koeberl, C. and Navon, O., 1996. Trace element analyses of fluid-bearing diamonds from Jwaneng, Botswana. *Geochimica et Cosmochimica Acta*, 60(23), pp.4711-4724.

Schulze, D.J., Wiese, D. and Steude, J., 1996. Abundance and distribution of diamonds in eclogite revealed by volume visualization of CT X-ray scans. *The Journal of Geology*, 104(1), pp.109-114.

Schulze, D.J., Harte, B., Edinburgh Ion Microprobe Facility staff, Page, F.Z., Valley, J.W., Channer, D.M.D. and Jaques, A.L., 2013. Anticorrelation between low δ13C of eclogitic diamonds and high δ18O of their coesite and garnet inclusions requires a subduction origin. *Geology*, 41(4), pp.455-458.

Seal, R.R., 2006. Sulfur isotope geochemistry of sulfide minerals. *Reviews in Mineralogy and Geochemistry*, 61(1), pp.633-677.

Seewald, Jeffrey S., William E. Seyfried Jr, and Wayne C. Shanks III. "Variations in the chemical and stable isotope composition of carbon and sulfur species during organic-rich sediment alteration: an experimental and theoretical study of hydrothermal activity at Guaymas Basin, Gulf of California." *Geochimica et Cosmochimica Acta* 58, no. 22 (1994): 5065-5082.

Selvaraja, V., Fiorentini, M.L., LaFlamme, C.K., Wing, B.A. and Bui, T.H., 2017. Anomalous sulfur isotopes trace volatile pathways in magmatic arcs. *Geology*, *45*(5), pp.419-422.

Sharp, W.E., 1966. Pyrrhotite: a common inclusion in South African diamonds. *Nature*, 211(5047), p.402.

Shatsky, V., Ragozin, A., Zedgenizov, D. and Mityukhin, S., 2008. Evidence for multistage evolution in a xenolith of diamond-bearing eclogite from the Udachnaya kimberlite pipe. *Lithos*, 105(3-4), pp.289-300.

Shen, Y., Farquhar, J., Masterson, A., Kaufman, A.J. and Buick, R., 2009. Evaluating the role of microbial sulfate reduction in the early Archean using quadruple isotope systematics. *Earth and Planetary Science Letters*, *279*(3-4), pp.383-391.

Shima, H. and Naldrett, A.J., 1975. Solubility of sulfur in an ultramafic melt and the relevance of the system Fe-SO. *Economic Geology*, 70(5), pp.960-967.

Shimazaki, H. and MacLean, W.H., 1976. An experimental study on the partition of zinc and lead between the silicate and sulfide liquids. *Mineralium Deposita*, 11(2), pp.125-132.

Shimizu, N., Boyd, F.R., Sobolev, N.V. and Pokhilenko, N.P., 1994. Chemical zoning of garnets in peridotites and diamonds. *Mineralogical Magazine A*, 58, p.831.

Shimizu, N. and Sobolev, N.V., 1995. Young peridotitic diamonds from the Mir kimberlite pipe. *Nature*, 375(6530), p.394.

Shimmield, G.B. and Price, N.B., 1986. The behaviour of molybdenum and manganese during early sediment diagenesis—offshore Baja California, Mexico. *Marine Chemistry*, 19(3), pp.261-280.

Shirey, S.B., Harris, J.W., Richardson, S.H., Fouch, M.J., James, D.E., Cartigny, P., Deines, P. and Viljoen, F., 2002. Diamond genesis, seismic structure, and evolution of the Kaapvaal-Zimbabwe craton. *Science*, 297(5587), pp.1683-1686.

Shirey, S.B., Harris, J.W., Richardson, S.H., Fouch, M., James, D.E., Cartigny, P., Deines, P. and Viljoen, F., 2003. Regional patterns in the paragenesis and age of inclusions in diamond, diamond composition, and the lithospheric seismic structure of Southern Africa. *Lithos*, 71(2-4), pp.243-258.

Shirey, S.B., Richardson, S.H. and Harris, J.W., 2004. Integrated models of diamond formation and craton evolution. *Lithos*, 77(1-4), pp.923-944.

Shirey, S.B., Richardson, S.H. and Harris, J.W., 2008, October. Mesoarchean to Mesoproterozoic Re-Os ages for sulfide inclusions in Orapa diamonds and implications for Kaapvaal-Zimbabwe craton development. In *International Kimberlite Conference: Extended Abstracts* (Vol. 9).

Shirey, S.B. and Richardson, S.H., 2011. Start of the Wilson cycle at 3 Ga shown by diamonds from subcontinental mantle. *Science*, 333(6041), pp.434-436.

Shirey, S.B., Cartigny, P., Frost, D.J., Keshav, S., Nestola, F., Nimis, P., Pearson, D.G., Sobolev, N.V. and Walter, M.J., 2013. Diamonds and the geology of mantle carbon. *Reviews in Mineralogy and Geochemistry*, 75(1), pp.355-421.

Shushkanova, A.V. and Litvin, Y.A., 2008. Diamond nucleation and growth in sulfide-carbon melts: an experimental study at 6.0–7.1 GPa. *European Journal of Mineralogy*, 20(3), pp.349-355.a

Shushkanova, A.V. and Litvin, Y.A., 2008. Experimental evidence for liquid immiscibility in the model system CaCO3–pyrope–pyrrhotite at 7.0 GPa: the role of carbonatite and sulfide melts in diamond genesis. *The Canadian Mineralogist*, 46(4), pp.991-1005.b

Siebert, C., Kramers, J.D., Meisel, T., Morel, P. and Nägler, T.F., 2005. PGE, Re-Os, and Mo isotope systematics in Archean and early Proterozoic sedimentary systems as proxies for redox conditions of the early Earth. *Geochimica et Cosmochimica Acta*, *69*(7), pp.1787-1801.

Siebert, C., McManus, J., Bice, A., Poulson, R. and Berelson, W.M., 2006. Molybdenum isotope signatures in continental margin marine sediments. *Earth and Planetary Science Letters*, 241(3-4), pp.723-733.

Sim, M.S., Ono, S. and Hurtgen, M.T., 2015. Sulfur isotope evidence for low and fluctuating sulfate levels in the Late Devonian ocean and the potential link with the mass extinction event. *Earth and Planetary Science Letters*, *419*, pp.52-62.

Simakov, S.K. and Ivanov, M.V., 1997. Specific Features of the Fluid Regime of Eclogite-Type Diamond Formation in Subduction-related Processes within the Upper Mantle. *Earth Science*, 5, pp. 702-704.

Sims, K.W.W., Newsom, H.E. and Gladney, E.S., 1990. Chemical fractionation during formation of the Earth's core and continental crust: clues from As, Sb, W, and Mo. In Newsom, H.E. and Jones, J.H. (eds.) *Origin of Earth*, pp. 291–317, Oxford University Press, New York.

Sims, K.W. and DePaolo, D.J., 1997. Inferences about mantle magma sources from incompatible element concentration ratios in oceanic basalts. *Geochimica et Cosmochimica Acta*, *61*(4), pp.765-784.

Skinner, E.M.W., Bristow, J.W., Smith, C.B., Scott, S. and Dawson, J.B., 1985. Proterozoic kimberlites and lamproites and a preliminary age for the Argyle lamproite pipe, Western Australia. *Transactions of the Geological Society of South Africa*, 88(2), pp.335-340.

Smart, K.A., Chacko, T., Stachel, T., Muehlenbachs, K., Stern, R.A. and Heaman, L.M., 2011. Diamond growth from oxidized carbon sources beneath the Northern Slave Craton, Canada: a δ13C–N study of eclogite-hosted diamonds from the Jericho kimberlite. *Geochimica et Cosmochimica Acta*, *75*(20), pp.6027-6047.

Smit, K.V., Shirey, S.B., Richardson, S.H., le Roex, A.P. and Gurney, J.J., 2010. Re–Os isotopic composition of peridotitic sulphide inclusions in diamonds from Ellendale, Australia: Age constraints on Kimberley cratonic lithosphere. *Geochimica et Cosmochimica Acta*, 74(11), pp.3292-3306.

Smit, K.V., Shirey, S.B. and Wang, W., 2016. Type Ib diamond formation and preservation in the West African lithospheric mantle: Re–Os age constraints from sulphide inclusions in Zimmi diamonds. *Precambrian Research*, 286, pp.152-166.

Smit, K.V., Shirey, S.B., Hauri, E.H., Wang, J., Stachel, T. and Stern, R.A., 2017, September. Neoproterozoic Zimmi diamond formation through infiltration of recycled methane into sulphide-bearing Archaean eclogite. In *International Kimberlite Conference: Extended Abstracts* (Vol. 11).

Smit, K.V., D'Haenens-Johansson, U.F., Howell, D., Loudin, L.C. and Wang, W., 2018. Deformation-related spectroscopic features in natural Type Ib-IaA diamonds from Zimmi (West African craton). *Mineralogy and Petrology*, 112(1), pp.243-257.

Smit, K.V., Shirey, S.B., Hauri, E.H. and Stern, R.A., 2019. Sulfur isotopes in diamonds reveal differences in continent construction. *Science*, 364(6438), pp.383-385.

Smit, K.V. and Shirey, S.B., 2019. How Old Are Diamonds? Are They Forever? *Gems & Gemmology*, 55(1), pp.102-109.

Smith, C.B., 1983. Pb, Sr and Nd isotopic evidence for sources of southern African Cretaceous kimberlites. *Nature*, 304(5921), pp.51-54.

Smith, C.B., Allsop, H.L., Kramers, J.D., Hutchinson, G. and Roddick, J.C., 1985. Emplacement ages of Jurassic-Cretaceous South African kimberlites by the Rb-Sr method on phlogopite and whole-rock samples. *Transactions of the Geological Society of South Africa*, 88(2), pp.249-266.

Smith, C.B., Sims, K., Chimuka, L., Duffin, A., Beard, A.D. and Townend, R., 2004. Kimberlite metasomatism at Murowa and Sese pipes, Zimbabwe. *Lithos*, 76(1-4), pp.219-232.

Smith, C.B., Pearson, D.G., Bulanova, G.P., Beard, A.D., Carlson, R.W., Wittig, N., Sims, K., Chimuka, L. and Muchemwa, E., 2009a. Extremely depleted lithospheric mantle and diamonds beneath the southern Zimbabwe Craton. *Lithos*, 112, pp.1120-1132.

Smith, C.B., Bulanova, G.P., Kohn, S.C., Milledge, H.J., Hall, A.E., Griffin, B.J. and Pearson, D.G., 2009b. Nature and genesis of Kalimantan diamonds. *Lithos*, 112, pp.822-832.

Smith, C.B., Walter, M.J., Bulanova, G.P., Mikhail, S., Burnham, A.D., Gobbo, L. and Kohn, S.C., 2016. Diamonds from Dachine, French Guiana: a unique record of Early Proterozoic subduction. *Lithos, 265,* pp.82-95.

Smith, E.M., Kopylova, M.G., Nowell, G.M., Pearson, D.G. and Ryder, J., 2012. Archean mantle fluids preserved in fibrous diamonds from Wawa, Superior craton. *Geology*, 40(12), pp.1071-1074.

Smith, E.M. and Kopylova, M.G., 2014. Implications of metallic iron for diamonds and nitrogen in the sublithospheric mantle. *Canadian Journal of Earth Sciences*, 51(5), pp.510-516.

Smith, E.M., Kopylova, M.G., Frezzotti, M.L. and Afanasiev, V.P., 2015. Fluid inclusions in Ebelyakh diamonds: Evidence of CO2 liberation in eclogite and the effect of H2O on diamond habit. *Lithos,* 216, pp.106-117.

Smithies, R.H., Champion, D.C. and Cassidy, K.F., 2003. Formation of Earth's early Archaean continental crust. *Precambrian Research*, 127(1-3), pp.89-101.

Smythe, D.J., Wood, B.J. and Kiseeva, E.S., 2017. The S content of silicate melts at sulfide saturation: new experiments and a model incorporating the effects of sulfide composition. *American Mineralogist,* 102(4), pp.795-803.

Sobolev, N.V. and Brown, D.A., 1977. Deep-seated inclusions in kimberlites and the problem of the composition of the upper mantle. *(Translated from the Russian edition, 1974) American Geophysical Union*, Washington, pp. 279.

Sobolev, N.V., Zuev, V.M., Bezborodov, S.M., Ponomarenko, A.I., Spetsius, Z.V., Kuligin, S., Yefimova, E.S., Afanasiev, V.P., Koptil, V.I. and Botkunov, A.I., 1991. Eclogite Paregenesis of Diamonds from Udachnaya and Mir Pipes, Yakutia. In *International Kimberlite Conference: Extended Abstracts* (Vol. 5, pp. 391-391).

Sobolev, N.V., Snyder, G.A., Taylor, L.A., Keller, R.A., Yefimova, E.S., Sobolev, V.N. and Shimizu, N., 1998. Extreme chemical diversity in the mantle during eclogitic diamond formation: evidence from 35 garnet and 5 pyroxene inclusions in a single diamond. *International Geology Review,* 40(7), pp.567-578.

Sobolev, N.V., Logvinova, A.M., Zedgenizov, D.A., Seryotkin, Y.V., Yefimova, E.S., Floss, C. and Taylor, L.A., 2004. Mineral inclusions in microdiamonds and macrodiamonds from kimberlites of Yakutia: a comparative study. *Lithos*, 77(1-4), pp.225-242.

Sobolev, N.V., Shatsky, V.S., Zedgenizov, D.A., Ragozin, A.L. and Reutsky, V.N., 2016. Polycrystalline diamond aggregates from the Mir kimberlite pipe, Yakutia: Evidence for mantle metasomatism. *Lithos*, 265, pp.257-266.

Song, W., Xu, C., Veksler, I.V. and Kynicky, J., 2016. Experimental study of REE, Ba, Sr, Mo and W partitioning between carbonatitic melt and aqueous fluid with implications for rare metal mineralization. *Contributions to Mineralogy and Petrology*, 171(1), p.1.

Spivak, A.V., Litvin, Y.A., Shushkanova, A.V., Litvin, V.Y. and Shiryaev, A.A., 2008. Diamond formation in carbonate-silicate-sulfide-carbon melts: Raman-and IR-microspectroscopy. *European Journal of Mineralogy*, 20(3), pp.341-347.

Spry, P.G. and Wonder, J.D., 1989. Manganese-rich garnet rocks associated with the Broken Hill lead-zinc-silver deposit, New South Wales, Australia. *The Canadian Mineralogist*, 27(2), pp.275-292.

Stachel, T., Brey, G.P. and Harris, J.W., 2000. Kankan diamonds (Guinea) I: from the lithosphere down to the transition zone. *Contributions to Mineralogy and Petrology*, 140(1), pp.1-15.a

Stachel, T., Harris, J.W., Brey, G.P. and Joswig, W., 2000. Kankan diamonds (Guinea) II: lower mantle inclusion parageneses. *Contributions to Mineralogy and Petrology*, 140(1), pp.16-27.b

Stachel, T., Harris, J., Aulbach, S. and Deines, P., 2002. Kankan diamonds (Guinea) III: δ 13 C and nitrogen characteristics of deep diamonds. *Contributions to Mineralogy and Petrology*, 142(4), pp.465-475.

Stachel, T., Harris, J.W., Tappert, R. and Brey, G.P., 2003. Peridotitic diamonds from the Slave and the Kaapvaal cratons—similarities and differences based on a preliminary data set. *Lithos*, 71(2-4), pp.489-503.

Stachel, T., Viljoen, K.S., McDade, P. and Harris, J.W., 2004. Diamondiferous lithospheric roots along the western margin of the Kalahari Craton—the peridotitic inclusion suite in diamonds from Orapa and Jwaneng. *Contributions to Mineralogy and Petrology*, 147(1), pp.32-47.

Stachel, T., Brey, G.P. and Harris, J.W., 2005. Inclusions in sublithospheric diamonds: glimpses of deep Earth. *Elements*, 1(2), pp.73-78.

Stachel, T. and Harris, J.W., 2008. The origin of cratonic diamonds—constraints from mineral inclusions. Ore Geology Reviews, 34(1-2), pp.5-32.

Stachel, T. and Harris, J.W., 2009. Formation of diamond in the Earth's mantle. *Journal of Physics: Condensed Matter*, 21(36), p.364206.

Stachel, T. and Luth, R.W., 2015. Diamond formation—Where, when and how?. *Lithos*, 220, pp.200-220.

Stagno, V., Ojwang, D.O., McCammon, C.A. and Frost, D.J., 2013. The oxidation state of the mantle and the extraction of carbon from Earth's interior. *Nature*, *493*(7430), p.84.

Stein, H.J., Markey, R.J., Morgan, J.W., Du, A. and Sun, Y., 1997. Highly precise and accurate Re-Os ages for molybdenite from the East Qinling molybdenum belt, Shaanxi Province, China. *Economic Geology*, 92(7-8), pp.827-835.

Stein, H.J., Sundblad, K., Markey, R.J., Morgan, J.W. and Motuza, G., 1998. Re-Os ages for Archean molybdenite and pyrite, Kuittila-Kivisuo, Finland and Proterozoic molybdenite, Kabeliai, Lithuania: Testing the chronometer in a metamorphic and metasomatic setting. *Mineralium Deposita*, *33*(4), pp.329-345.

Stein, H.J., Markey, R.J., Morgan, J.W., Hannah, J.L. and Scherstén, A., 2001. The remarkable Re–Os chronometer in molybdenite: how and why it works. *Terra Nova*, 13(6), pp.479-486.

Stein, H., Scherstén, A., Hannah, J. and Markey, R., 2003. Subgrain-scale decoupling of Re and 187Os and assessment of laser ablation ICP-MS spot dating in molybdenite. *Geochimica et Cosmochimica Acta*, 67(19), pp.3673-3686.

Stemprok, M. and Voldan, J., 1974. Homogeneous Silicate-Glasses in Systems Na2O-SiO2-WO3 and Na2O-SiO2-MoO3. *Silikaty*, *18*(1), pp.19-30.

Stiefenhofer, J., Viljoen, K.S. and Marsh, J.S., 1997. Petrology and geochemistry of peridotite xenoliths from the Letlhakane kimberlites, Botswana. *Contributions to Mineralogy and Petrology*, 127(1-2), pp.147-158.

Suer, T.A., Siebert, J., Remusat, L., Menguy, N. and Fiquet, G., 2017. A sulfur-poor terrestrial core inferred from metal–silicate partitioning experiments. *Earth and Planetary Science Letters*, 469, pp.84-97.

Sugaki, A. and Kitakaze, A., 1998. High form of pentlandite and its thermal stability. *American Mineralogist*, 83(1-2), pp.133-140.

Sunagawa, I., 1981. Characteristics of crystal growth in nature as seen from the morphology of mineral crystals. *Bulletin de minéralogie*, 104, pp.81-87.

Sunagawa, I., 1984. Morphology of natural and synthetic diamond crystals. In I. Sunagawa (ed.), *Materials Science of the Earth's Interior*, Terra Science Publishing Company, Tokyo, pp. 303–330.

Suzuki, K. and Masuda, A., 1990. The way to overcome the difficulty in Re-Os dating of molybdenite. *Proceedings of the Japan Academy, Series B*, 66(9), pp.173-176.

Sverjensky, D.A. and Huang, F., 2015. Diamond formation due to a pH drop during fluid–rock interactions. *Nature communications*, 6, p.8702.

Szabo, A., Tudge, A., Macnamara, J. and Thode, H.G., 1950. The distribution of S34 in nature and the sulfur cycle. *Science*, 111(2887), pp.464-465.

Tappert, R., Stachel, T., Harris, J.W., Muehlenbachs, K., Ludwig, T. and Brey, G.P., 2005. Subducting oceanic crust: The source of deep diamonds. *Geology*, 33(7), pp.565-568.

Tassinari, C. C. G., J. S. Bettencourt., M. C. Geraldes, M. J. B. Macambira, and J. M. Lafon, 2000., The Amazonian craton. In Cordani, U., Milani, E., Thomaz, F.A. and Campos, D. (eds.), *Tectonic evolution of South America,* pp. 41–96, Geological Society.

Taylor, L.A., Milledge, H.J., Bulanova, G.P., Snyder, G.A. and Keller, R.A., 1998. Metasomatic eclogitic diamond growth: evidence from multiple diamond inclusions. *International Geology Review*, 40(8), pp.663-676.

Taylor, L.A., Keller, R.A., Snyder, G.A., Wang, W., Carlson, W.D., Hauri, E.H., Mccandless, T., Kim, K.R., Sobolev, N.V. and Bezborodov, S.M., 2000. Diamonds and their mineral inclusions, and what they tell us: A detailed "pull-apart" of a diamondiferous eclogite. *International Geology Review*, 42(11), pp.959-983.

Taylor, L.A., Anand, M., Promprated, P., Floss, C. and Sobolev, N.V., 2003. The significance of mineral inclusions in large diamonds from Yakutia, Russia. *American Mineralogist*, 88(5-6), pp.912-920.

Taylor, L.A. and Anand, M., 2004. Diamonds: time capsules from the Siberian Mantle. *Geochemistry*, 64(1), pp.1-74.

Taylor, L.A. and Liu, Y., 2009. Sulfide inclusions in diamonds: not monosulfide solid solution. *Russian Geology and Geophysics*, 50(12), pp.1201-1211.

Taylor, W.R., Jaques, A.L. and Ridd, M., 1990. Nitrogen-defect aggregation characteristics of some Australasian diamonds; time-temperature constraints on the source regions of pipe and alluvial diamonds. *American Mineralogist*, 75(11-12), pp.1290-1310.

Taylor W.R., Bulanova, G.P. and Milledge H.J., 1995. Quantitative nitrogen aggregation study of some Yakutian diamonds: constraints on the growth, thermal and deformation history of peridotitic and eclogitic diamonds. *Extended abstract 6th international kimberlite conference, Novosibirsk*, pp.608–610

Tenailleau, C., Etschmann, B., Wang, H., Pring, A., Grguric, B.A. and Studer, A., 2005. Thermal expansion of troilite and pyrrhotite determined by in situ cooling (873 to 373 K) neutron powder diffraction measurements. *Mineralogical Magazine*, 69(2), pp.205-216.

Thode, H.G., Macnamara, J. and Collins, C.B., 1949. Natural variations in the isotopic content of sulphur and their significance. *Canadian Journal of Research*, *27*(4), pp.361-373.

Thomassot, E., Cartigny, P., Harris, J.W., Lorand, J.P., Rollion-Bard, C. and Chaussidon, M., 2009. Metasomatic diamond growth: A multi-isotope study (13C, 15N, 33S, 34S) of sulphide inclusions and their host diamonds from Jwaneng (Botswana). *Earth and Planetary Science Letters*, 282(1-4), pp.79-90.

Thomassot, E., Farquhar, J., Bouden, N., Harris, J.W., McKeegan, K., Cliff, J., Wing, B. and Piccoli, P., 2017. The Archean sedimentary sulfur recycling under the Kaapvaal craton revisited from 4S-isotopic compositions in sulfide inclusions in diamonds from Kimberley Pool (South Africa) Jwaneng and Orapa (Botswana). In *International Kimberlite Conference: Extended Abstracts* (Vol. 11).

Thompson, T.G., Johnston, W.R. and Wirth, H.E., 1931. The sulfate-chlorinity ratio in ocean waters. *ICES Journal of Marine Science*, 6(2), pp.246-251.

Thomson, A.R. 2014. The Earth's deep carbon cycle: superdeep diamonds and the fate of recycled carbon (Doctoral dissertation, University of Bristol, UK)

Thomson, A.R., Kohn, S.C., Bulanova, G.P., Smith, C.B., Araujo, D. and Walter, M.J., 2014. Origin of sub-lithospheric diamonds from the Juina-5 kimberlite (Brazil): constraints from carbon isotopes and inclusion compositions. *Contributions to Mineralogy and Petrology*, 168(6), p.1081.

Thomson, A.R., Kohn, S.C., Bulanova, G.P., Smith, C.B., Araujo, D. and Walter, M.J., 2016. Trace element composition of silicate inclusions in sub-lithospheric diamonds from the Juina-5 kimberlite: Evidence for diamond growth from slab melts. *Lithos*, 265, pp.108-124.

Timmerman, S., Koornneef, J.M., Chinn, I.L. and Davies, G.R., 2017. Dated eclogitic diamond growth zones reveal variable recycling of crustal carbon through time. *Earth and Planetary Science Letters*, 463, pp.178-188.

Timmerman, S., Jaques, A.L., Weiss, Y. and Harris, J.W., 2018a. N-δ^{13}C-inclusion profiles of cloudy diamonds from Koffiefontein: Evidence for formation by continuous Rayleigh fractionation and multiple fluids. *Chemical Geology*, 483, pp.31-46.

Timmerman, S., Chinn, I.L., Fisher, D. and Davies, G.R., 2018b. Formation of unusual yellow Orapa diamonds. *Mineralogy and Petrology*, 112(1), pp.209-218.

Titkov, S.V., Bershov, L.V., Scandale, E., Saparin, G.V., Chukichev, M.V. and Speranskiy, A.V., 1998. Nickel structural impurities in natural diamonds. In *International Kimberlite Conference: Extended Abstracts* (Vol. 7, No. 1, pp. 911-913).

Tomkins, A.G. and Evans, K.A., 2015. Separate zones of sulfate and sulfide release from subducted mafic oceanic crust. *Earth and Planetary Science Letters*, 428, pp.73-83.

Tomlinson, E.L., Jones, A.P. and Harris, J.W., 2006. Co-existing fluid and silicate inclusions in mantle diamond. *Earth and Planetary Science Letters*, 250(3-4), pp.581-595.

Tomlinson, E.L. and Müller, W., 2009. A snapshot of mantle metasomatism: trace element analysis of coexisting fluid (LA-ICP-MS) and silicate (SIMS) inclusions in fibrous diamonds. *Earth and Planetary Science Letters*, 279(3-4), pp.362-372.

Tossell, J.A., 2005. Calculating the partitioning of the isotopes of Mo between oxidic and sulfidic species in aqueous solution. *Geochimica et Cosmochimica Acta*, 69(12), pp.2981-2993.

Trefry, J.H., Butterfield, D.B., Metz, S., Massoth, G.J., Trocine, R.P. and Feely, R.A., 1994. Trace metals in hydrothermal solutions from Cleft segment on the southern Juan de Fuca Ridge. *Journal of Geophysical Research: Solid Earth*, 99(B3), pp.4925-4935.

Tribovillard, N., Riboulleau, A., Lyons, T. and Baudin, F., 2004. Enhanced trapping of molybdenum by sulfurized marine organic matter of marine origin in Mesozoic limestones and shales. *Chemical Geology*, 213(4), pp.385-401.

Tsujimura, T. and Kitakaze, A., 2005. Experimental study of sulfur solubility in silicate melts coexisting with graphite as a function of silicate melt composition. *Resource Geology*, 55(1), pp.55-60.

Tsuno, K. and Dasgupta, R., 2015. Fe–Ni–Cu–C–S phase relations at high pressures and temperatures–The role of sulfur in carbon storage and diamond stability at mid-to deep-upper mantle. *Earth and Planetary Science Letters*, 412, pp.132-142.

Ulrich, T. and Mavrogenes, J., 2008. An experimental study of the solubility of molybdenum in H2O and KCl–H2O solutions from 500 C to 800 C, and 150 to 300 MPa. *Geochimica et Cosmochimica Acta*, 72(9), pp.2316-2330.

Urey, H.C., 1947. The thermodynamic properties of isotopic substances. *Journal of the Chemical Society (Resumed)*, pp.562-581.

Van Rythoven, A.D. and Schulze, D.J., 2009. In-situ analysis of diamonds and their inclusions from the Diavik Mine, Northwest Territories, Canada: Mapping diamond growth. *Lithos*, 112, pp.870-879.

Vaughan, D.J., 2006. Sulfide mineralogy and geochemistry: introduction and overview. *Reviews in Mineralogy and Geochemistry*, 61(1), pp.1-5.

Velasco, F., Sánchez-España, J., Boyce, A.J., Fallick, A.E., Sáez, R. and Almodóvar, G.R., 1998. A new sulphur isotopic study of some Iberian Pyrite Belt deposits: evidence of a textural control on sulphur isotope composition. *Mineralium Deposita*, *34*(1), pp.4-18.

Voegelin, A.R., Nägler, T.F., Pettke, T., Neubert, N., Steinmann, M., Pourret, O. and Villa, I.M., 2012. The impact of igneous bedrock weathering on the Mo isotopic composition of stream waters: Natural samples and laboratory experiments. *Geochimica et cosmochimica acta*, *86*, pp.150-165.

Vorlicek, T.P., Kahn, M.D., Kasuya, Y. and ZHENG, G.R., 2004. Capture of molybdenum in pyrite-forming sediments: role of ligand-induced reduction by polysulfides. *Geochimica et Cosmochimica Acta*, 68(3), pp.547-556.

Voudouris, P.C., Melfos, V., Spry, P.G., Bindi, L., Kartal, T., Arikas, K., Moritz, R. and Ortelli, M., 2009. Rhenium-rich molybdenite and rheniite in the Pagoni Rachi Mo–Cu–Te–Ag–Au prospect, northern Greece: implications for the Re geochemistry of porphyry-style Cu–Mo and Mo mineralization. *The Canadian Mineralogist*, *47*(5), pp.1013-1036.

Voudouris, P., Melfos, V., Spry, P.G., Bindi, L., Moritz, R., Ortelli, M. and Kartal, T., 2013. Extremely Re-rich molybdenite from porphyry Cu-Mo-Au prospects in northeastern Greece: Mode of occurrence, causes of enrichment, and implications for gold exploration. *Minerals*, *3*(2), pp.165-191.

Walter, M.J. and Thibault, Y., 1995. Partitioning of tungsten and molybdenum between metallic liquid and silicate melt. *Science*, *270*(5239), pp.1186-1189.

Walter, M.J., Bulanova, G.P., Armstrong, L.S., Keshav, S., Blundy, J.D., Gudfinnsson, G., Lord, O.T., Lennie, A.R., Clark, S.M., Smith, C.B. and Gobbo, L., 2008. Primary carbonatite melt from deeply subducted oceanic crust. *Nature*, 454(7204), p.622.

Walter, M.J., Kohn, S.C., Araujo, D., Bulanova, G.P., Smith, C.B., Gaillou, E., Wang, J., Steele, A. and Shirey, S.B., 2011. Deep mantle cycling of oceanic crust: evidence from diamonds and their mineral inclusions. *Science*, 334(6052), pp.54-57.

Wang, D., 2012. Redox chemistry of molybdenum in natural waters and its involvement in biological evolution. *Frontiers in microbiology*, 3, p.427.

Wang, M., Guo, X., Michalak, P.P., Xia, Q., Xiao, F., Wang, W. and Liu, K., 2015. Origin of the Tudun Cu–Ni sulfide deposit in the Eastern Tianshan, NW China: constraints on the geochemistry of platinum group elements. *Ore Geology Reviews*, 64, pp.445-454.

Wang, Y.H., Zhang, F.F., Liu, J.J., Xue, C.J., Li, B.C. and Xian, X.C., 2018. Ore genesis and hydrothermal evolution of the donggebi porphyry Mo deposit, Xinjiang, Northwest China: evidence from isotopes (C, H, O, S, Pb), fluid inclusions, and molybdenite Re-Os dating. *Economic Geology*, 113(2), pp.463-488.

Wang, Z. and Becker, H., 2018. Molybdenum partitioning behavior and content in the depleted mantle: Insights from Balmuccia and Baldissero mantle tectonites (Ivrea Zone, Italian Alps). *Chemical Geology*, 499, pp.138-150.

Watanabe, M. and Soeda, A., 1981. Distribution of polytype contents of molybdenites from Japan and possible controlling factor in polytypism. *Neues Jahrbuch für Mineralogie. Abhandlungen*, 141(3), pp.258-279.

Wedepohl, K.H., 1995. The composition of the continental crust. *Geochimica et cosmochimica Acta*, 59(7), pp.1217-1232.

Weiss, Y., Kessel, R., Griffin, W.L., Kiflawi, I., Klein-BenDavid, O., Bell, D.R., Harris, J.W. and Navon, O., 2009. A new model for the evolution of diamond-forming fluids: Evidence from microinclusion-bearing diamonds from Kankan, Guinea. *Lithos*, 112, pp.660-674.

Weiss, Y., Kiflawi, I., Davies, N. and Navon, O., 2014. High-density fluids and the growth of monocrystalline diamonds. *Geochimica et Cosmochimica Acta*, 141, pp.145-159.

Westerlund, K., 2000. A geochemical study of diamonds, diamond inclusion minerals and other mantle minerals from the Klipspringer kimberlites, South Africa (Doctoral dissertation, University of Cape Town).

Westerlund, K.J., Gurney, J.J., Carlson, R.W., Shirey, S.B., Hauri, E.H. and Richardson, S.H., 2004. A metasomatic origin for late Archean eclogitic diamonds: Implications from internal morphology of diamonds and Re-Os and S isotope characteristics of their sulfide inclusions from the late Jurassic Klipspringer kimberlites. *South African Journal of Geology*, 107(1-2), pp.119-130.

Westerlund, K.J., Shirey, S.B., Richardson, S.H., Carlson, R.W., Gurney, J.J. and Harris, J.W., 2006. A subduction wedge origin for Paleoarchean peridotitic diamonds and harzburgites from the Panda kimberlite, Slave craton: evidence from Re–Os isotope systematics. *Contributions to Mineralogy and Petrology*, 152(3), p.275.

Wiggers De Vries, D., Pearson, D.G., Bulanova, G.P., Smelov, A.P., Pavlushin, A.D. and Davies, G.R., 2013a. Re–Os dating of sulphide inclusions zonally distributed in single Yakutian diamonds: Evidence for multiple episodes of Proterozoic formation and protracted timescales of diamond growth. *Geochimica et Cosmochimica Acta*, 120, pp.363-394.

Wiggers de Vries, D., Bulanova, G.P., De Corte, K., Pearson, D.G., Craven, J.A. and Davies, G.R., 2013b. Micron-scale coupled carbon isotope and nitrogen abundance variations in diamonds: Evidence for episodic diamond formation beneath the Siberian Craton. *Geochimica et Cosmochimica Acta*, 100, pp.176-199.

Wilding, M.C., Harte, B. and Harris, J.W., 1991, February. Inclusion chemistry, carbon isotopes and nitrogen distribution in Bultfontein diamonds. In *International Kimberlite Conference: Extended Abstracts* (Vol. 5, pp. 459-459).

Wilding, M.C., Harte, B., Fallick, A.E. and Harris, J.W., 1994. Inclusion chemistry, carbon isotopes and nitrogen distribution in diamonds from the Bultfontein Mine, South Africa. In Meyer, H.O.A. and Leonardos, O.H. (eds.), *Diamonds: Characterization, Genesis and Exploration. Proceedings of the Fifth International Kimberlite Conference, Araxa, Brasil*. Companhia de Pesquisa de Recursos Minerais — CPRM, Rio de Janeiro, pp. 116-126

Willbold, M. and Elliott, T., 2017. Molybdenum isotope variations in magmatic rocks. *Chemical Geology*, 449, pp.253-268.

Wilkinson, J.J., 2013. Triggers for the formation of porphyry ore deposits in magmatic arcs. *Nature Geoscience*, 6(11), p.917.

Williamson, M.A. and Rimstidt, J.D., 1994. The kinetics and electrochemical rate-determining step of aqueous pyrite oxidation. *Geochimica et Cosmochimica Acta*, 58(24), pp.5443-5454.

Woodland, A.B., Girnis, A.V., Bulatov, V.K., Brey, G.P. and Höfer, H.E., 2019. Experimental study of sulfur solubility in silicate–carbonate melts at 5–10.5 GPa. *Chemical Geology*, 505, pp.12-22.

Wykes, J.L. and Mavrogenes, J.A., 2005. Hydrous sulfide melting: experimental evidence for the solubility of H2O in sulfide melts. *Economic Geology*, 100(1), pp.157-164.

Wykes, J.L., O'Neill, H.S.C. and Mavrogenes, J.A., 2015. The effect of FeO on the sulfur content at sulfide saturation (SCSS) and the selenium content at selenide saturation of silicate melts. *Journal of Petrology*, 56(7), pp.1407-1424.

Xu, C., Kynicky, J., Chakhmouradian, A.R., Qi, L. and Song, W., 2010. A unique Mo deposit associated with carbonatites in the Qinling orogenic belt, central China. *Lithos*, 118(1-2), pp.50-60.

Yang, J., Siebert, C., Barling, J., Savage, P., Liang, Y.H. and Halliday, A.N., 2015. Absence of molybdenum isotope fractionation during magmatic differentiation at Hekla volcano, Iceland. *Geochimica et Cosmochimica Acta*, *162*, pp.126-136.

Yoshiki-Gravelsins, K.S. and Toguri, J.M., 1993. Oxygen and sulfur solubilities in Ni-Fe-SO melts. *Metallurgical Transactions B*, 24(5), pp.847-856.

Yuryeva, O.P., Rakhmanova, M.I. and Zedgenizov, D.A., 2017. Nature of type IaB diamonds from the Mir kimberlite pipe (Yakutia): evidence from spectroscopic observation. *Physics and Chemistry of Minerals*, 44(9), pp.655-667.

Zack, T., Kronz, A., Foley, S.F. and Rivers, T., 2002. Trace element abundances in rutiles from eclogites and associated garnet mica schists. *Chemical Geology*, 184(1-2), pp.97-122.

Zajacz, Z., 2015. The effect of melt composition on the partitioning of oxidized sulfur between silicate melts and magmatic volatiles. *Geochimica et Cosmochimica Acta*, 158, pp.223-244.

Zedgenizov, D.A., Shiryaev, A.A., Shatsky, V.S. and Kagi, H., 2006. Water-related IR characteristics in natural fibrous diamonds. *Mineralogical Magazine*, 70(2), pp.219-229.

Zedgenizov, D.A., Rege, S., Griffin, W.L., Kagi, H. and Shatsky, V.S., 2007. Composition of trapped fluids in cuboid fibrous diamonds from the Udachnaya kimberlite: LAM-ICPMS analysis. *Chemical Geology*, 240(1-2), pp.151-162.

Zedgenizov, D.A., Ragozin, A.L., Shatsky, V.S., Araujo, D., Griffin, W.L. and Kagi, H., 2009. Mg and Fe-rich carbonate–silicate high-density fluids in cuboid diamonds from the Internationalnaya kimberlite pipe (Yakutia). *Lithos*, 112, pp.638-647.

Zedgenizov, D.A., Kagi, H., Shatsky, V.S. and Ragozin, A.L., 2014. Local variations of carbon isotope composition in diamonds from São-Luis (Brazil): evidence for heterogenous carbon reservoir in sublithospheric mantle. *Chemical Geology*, *363*, pp.114-124.

Zhang, Z., Lentsch, N. and Hirschmann, M.M., 2015. Carbon-saturated monosulfide melting in the shallow mantle: solubility and effect on solidus. *Contributions to Mineralogy and Petrology*, 170(5-6), p.47.

Zhang, Z. and Hirschmann, M.M., 2016. Experimental constraints on mantle sulfide melting up to 8 GPa. *American Mineralogist*, 101(1), pp.181-192.

Zhang, Z., Hastings, P., Von der Handt, A. and Hirschmann, M.M., 2018. Experimental determination of carbon solubility in Fe-Ni-S melts. *Geochimica et Cosmochimica Acta*, 225, pp.66-79.

Zhao, K.D., Jiang, S.Y., Ni, P., Ling, H.F. and Jiang, Y.H., 2007. Sulfur, lead and helium isotopic compositions of sulfide minerals from the Dachang Sn-polymetallic ore district in South China: implication for ore genesis. *Mineralogy and Petrology*, *89*(3-4), pp.251-273.

Zheng, Y., Anderson, R.F., Van Geen, A. and Kuwabara, J., 2000. Authigenic molybdenum formation in marine sediments: a link to pore water sulfide in the Santa Barbara Basin. *Geochimica et Cosmochimica Acta*, 64(24), pp.4165-4178.

Zhimulev, E.I., Chepurov, A.I., Sinyakova, E.F., Sonin, V.M., Chepurov, A.A. and Pokhilenko, N.P., 2012. Diamond crystallization in the Fe-Co-SC and Fe-Ni-SC systems and the role of sulfide-metal melts in the genesis of diamond. *Geochemistry International*, 50(3), pp.205-216.

Zhimulev, E.I., Sonin, V.M., Mironov, A.M. and Chepurov, A.I., 2016. Effect of sulfur concentration on diamond crystallization in the Fe–C–S system at 5.3–5.5 GPa and 1300–1370° C. *Geochemistry International*, 54(5), pp.415-422.

Zu, B., Xue, C., Zhao, Y., Qu, W., Li, C., Symons, D.T. and Du, A., 2015. Late Cretaceous metallogeny in the Zhongdian area: Constraints from Re–Os dating of molybdenite and pyrrhotite from the Hongshan Cu deposit, Yunnan, China. *Ore Geology Reviews*, 64, pp.1-12.

Appendix A

Figure A1. Optical images of the 7 diamonds from Mir, cut and polished on the dodecahedral plane, containing molybdenite-bearing sulphide inclusions.

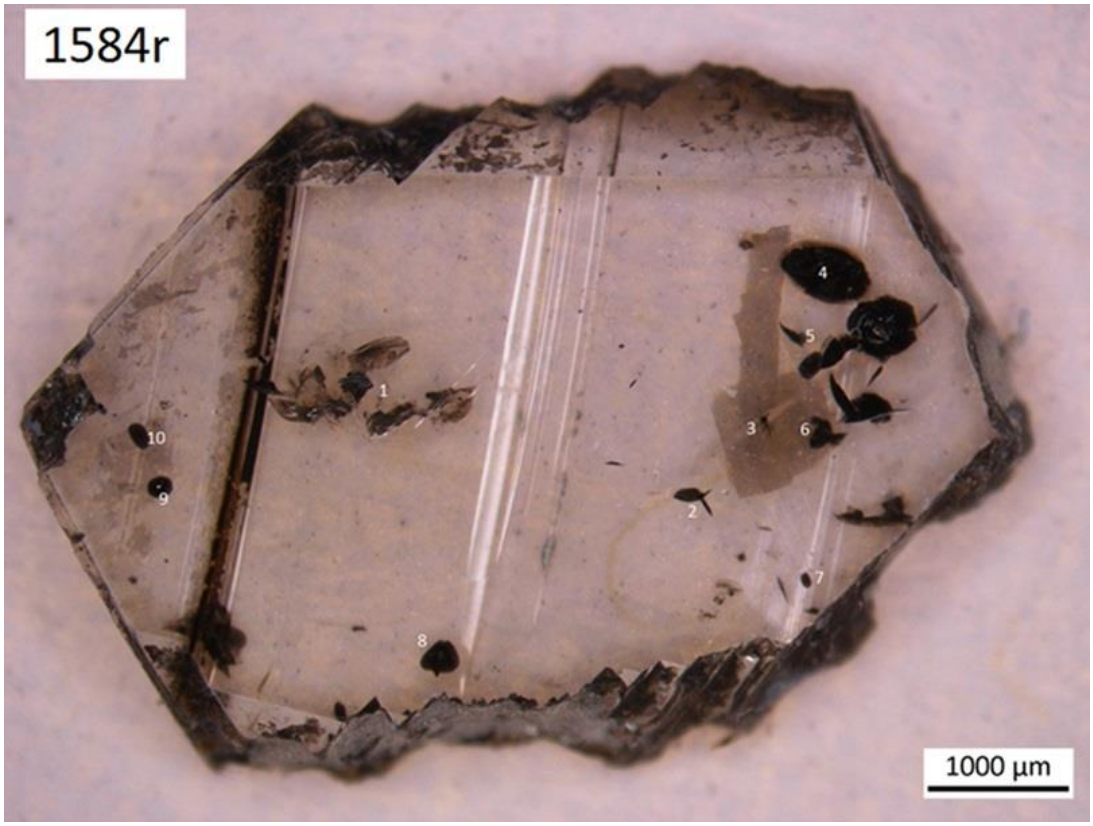


1591
1000 µm
7
8
5
3
2
1
9
6
4

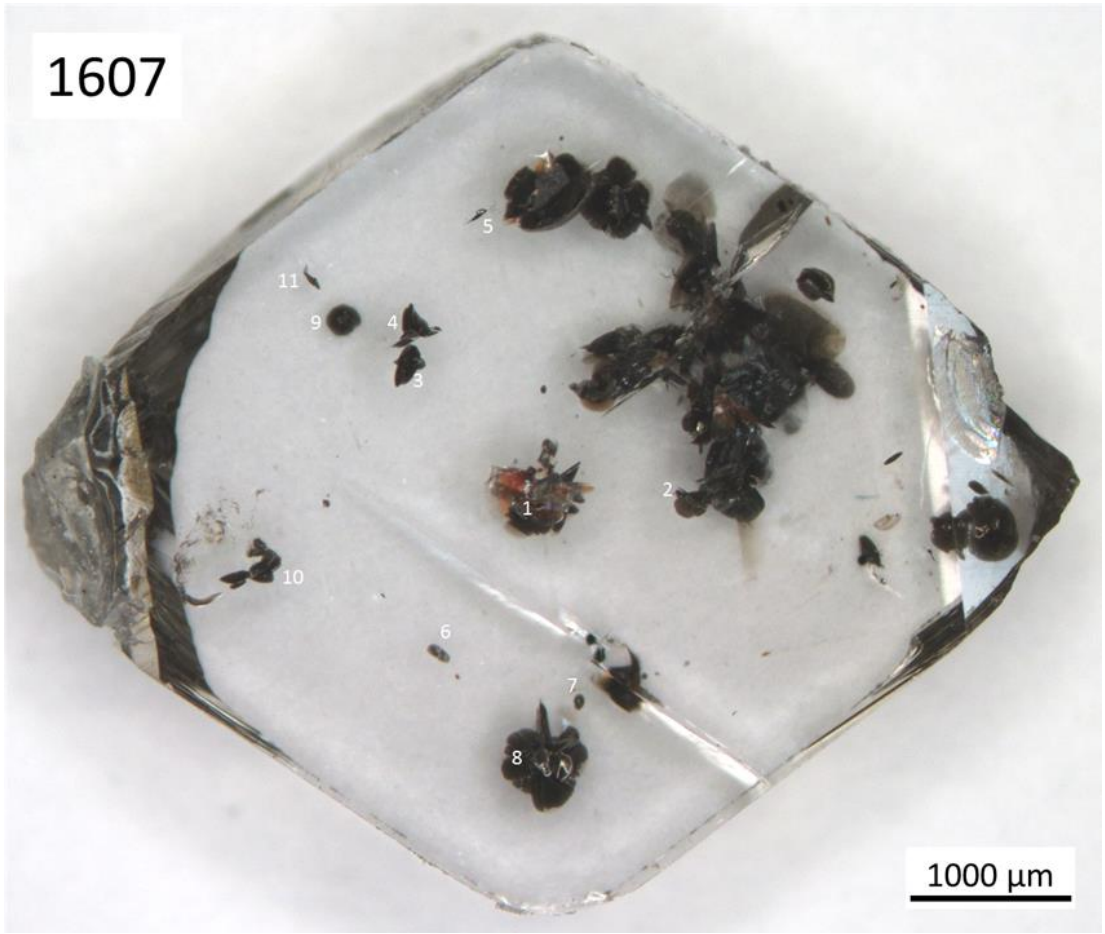
1607
5
11
9
4
3
1
2
10
6
7
8
1000 µm

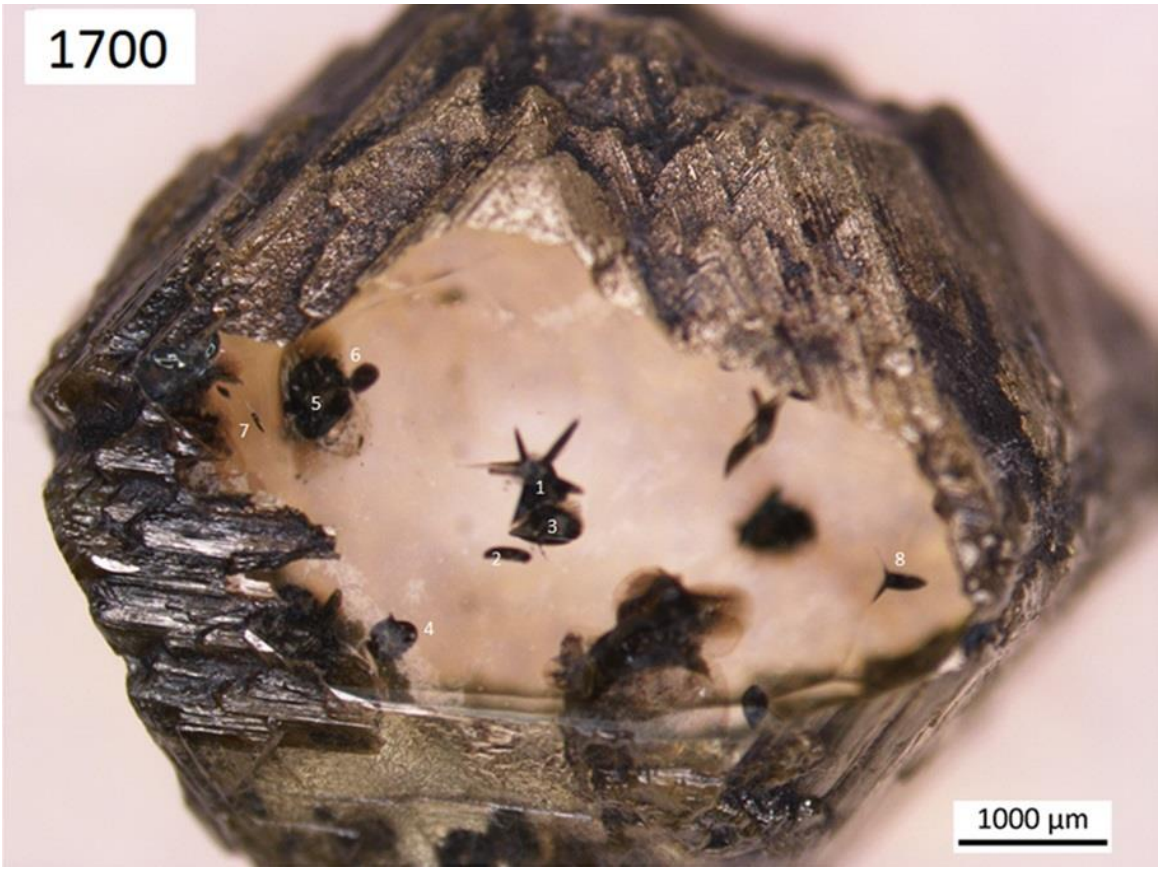
1700
6
5
7
1
3
2
8
4
1000 µm


1702
8
9
6
7
5
15
4
1
3
2
10
14
11
13
12
1000 µm


1703
1
2
3
4
5
6
7
1000 µm


1704
1
2
3
4
5
6
7
8
1000 µm

Table A1. Characteristics of the studied Mir diamond samples.

Note: Sf – sulphide, incl. - inclusions; Omp - omphacite; Cs - coesite; Gt – garnet, Ru – rutile, Mgt - magnetite; Octa - octahedron. Interm. – Intermediate. Res-regr. Zone – zone of resorption and regression. Data from Wiggers de Vries et al. 2013a, and Bulanova et al. (1996, 1999, 2014). Isotope data in additional information from Bulanova et al., 1999. Inclusions positions refer to core or rim zone of diamond.

Diamond # and state (plate or off-cut)	Shape	Presence of molybdenite in sulphide incl.	Associated sulphide phases	Incl. Locations in diamond growth zones	Silicate or oxide incl. also present	Additional information
1584 Interm. plate	Octa	16	Po? ccp	Core, interm. & rim	Omp, Cs	
1584 Rim plate	Octa	10	Po? ccp	Interm. or rim	Ru	
1591 plate	Distorted octa	10	Po? ccp	Core, interm. & rim		$\delta^{13}C$ = -16 ‰, $\delta^{34}S$ = +3 ‰ $\delta^{15}N$= -1.5%,
1607 plate	Distorted (broken) octa	12	Po? ccp	Core, int. & rim	Omp, Anatase	$\delta^{34}S$ = + 4 ‰? $\delta^{34}S$ = +3 ‰?
1700 thick plate	Octa	6	Po? ccp	Interm. Or rim		$\delta^{34}S$ = + 0.9 to -1.3 ‰
1702 off-cut	Octa	15	Po? ccp	Core, interm. & rim		$\delta^{34}S$ = -2.7 to + 0.6 ‰
1703 off-cut	Distorted octa	3	Po	Core/interm. Res-regr. zone	Omp	Core $\delta^{13}C$= -16‰; Res-regr. $\delta^{13}C$ = -7 ‰
1704 off-cut	Distorted octa	5	Po? ccp	Core, int.	Omp	

Table A2. Mir eclogitic diamond sulphide inclusions and whether or not molybdenite was identified by Raman.

Note: The inclusions (e.g. 1584-i-1, 1584-2) are referred to by number (e.g. 1584-I-#), and their location in diamond is shown in Fig. S1. ccp - chalcopyrite, cs – coesite, omp - omphacite clinopyroxene, po - pyrrhotite. -- indicates that molybdenite was not identified by Raman. Coexisting phases left blank occur when no other Raman signal was obtained.

Inclusion	1584-i-1	1584-i-2	1584-i-3	1584-i-4	1584-i-5	1584-i-6	1584-i-7	1584-i-8	1584-i-9	1584-i-10	1584-i-11	1584-i-12	1584-i-13	1584-i-14
Position	core?	int	int	int-rim	Rim	int	int	int-rim	int	int	int	int	int-rim	int-rim
Mo	--	yes	yes	yes	Yes	yes	yes	Yes	yes	yes	yes	yes	yes	yes
Coexisting phases		ccp, cs		ccp	ccp	ccp	ccp	ccp	ccp	ccp	ccp	ccp	ccp	ccp

1584-i-15	1584-i-16	1584-r-1	1584-r-2	1584-r-3	1584-r-4	1584-r-5	1584-r-6	1584-r-7	1584-r-8	1584-r-9	1584-r-10	1591-1	1591-2
int-rim	rim	core	Int	int	rim	Rim	rim	rim	rim	rim	rim	core	core
yes	yes	--	Yes	yes	yes	Yes	yes	yes	yes	yes	yes	yes	yes
ccp	ccp	rutile	ccp	ccp	ccp	ccp	ccp	ccp	ccp	ccp	ccp	ccp	ccp

1591-3	1591-4	1591-5	1591-6	1591-7	1591-8	1591-9	1607-1	1607-2	1607-3	1607-4	1607-5	1607-6	1607-7
core	core	int	int	int	int	Rim	core	int	int?	int	int	int	int
Yes	yes	Yes	yes	yes	Yes	yes	yes	yes	yes	yes	yes	yes	yes
ccp	ccp	ccp	ccp	ccp	ccp		anatase		ccp	ccp	ccp, omp	ccp, omp	ccp, omp

1607-8	1607-9	1607-10	1607-11	1607-12	1700-1	1700-2	1700-3	1700-4	1700-5	1700-6	1702-1	1702-2	1702-3
Int	int	int-rim	Rim	rim	core	int	int	rim	rim	rim	core	core	core
Yes	yes	yes	Yes	yes	--	yes	yes	yes	yes	yes	yes	yes	yes
ccp	ccp	ccp	ccp	ccp	po, ccp						ccp, po	po	ccp, po

1702-4	1702-5	1702-6	1702-7	1702-8	1702-9	1702-10	1702-11	1702-12	1702-13	1702-14	1702-15	1703-1	1703-2
core	core	core-int	core-int	int	int	int-rim	rim	rim	int-rim	rim	rim	int	int
yes	yes	yes	yes	yes	yes	yes	yes	yes	yes	yes	yes	--	--
ccp, po	ccp, po	ccp	ccp	ccp	ccp	ccp	ccp	ccp	ccp	ccp	ccp	po, cpx	ccp

1703-3	1703-4	1703-5	1703-6	1703-7	1704-1	1704-2	1704-3	1704-4	1704-5
Int	int-rim	int	int	int	core/int	core/int	core/int	int	int
--	yes	yes	yes	--	yes	yes	yes	yes	yes
	ccp	ccp	ccp	ccp			ccp	ccp	ccp

Figure A2. Cathodoluminescence images showing the growth regions of 5 of the studied Mir diamonds (from Wiggers de Vries et al. 2013a and Bulanova et al. 1996)

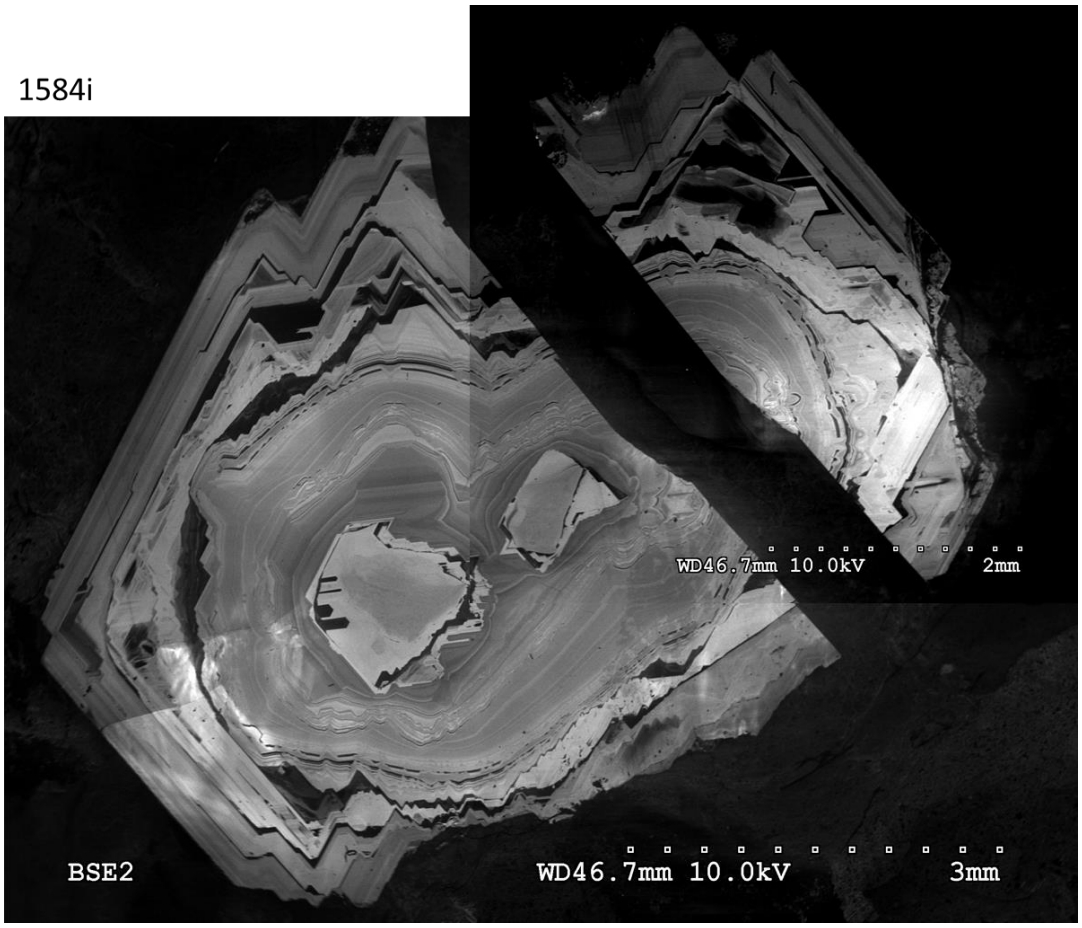

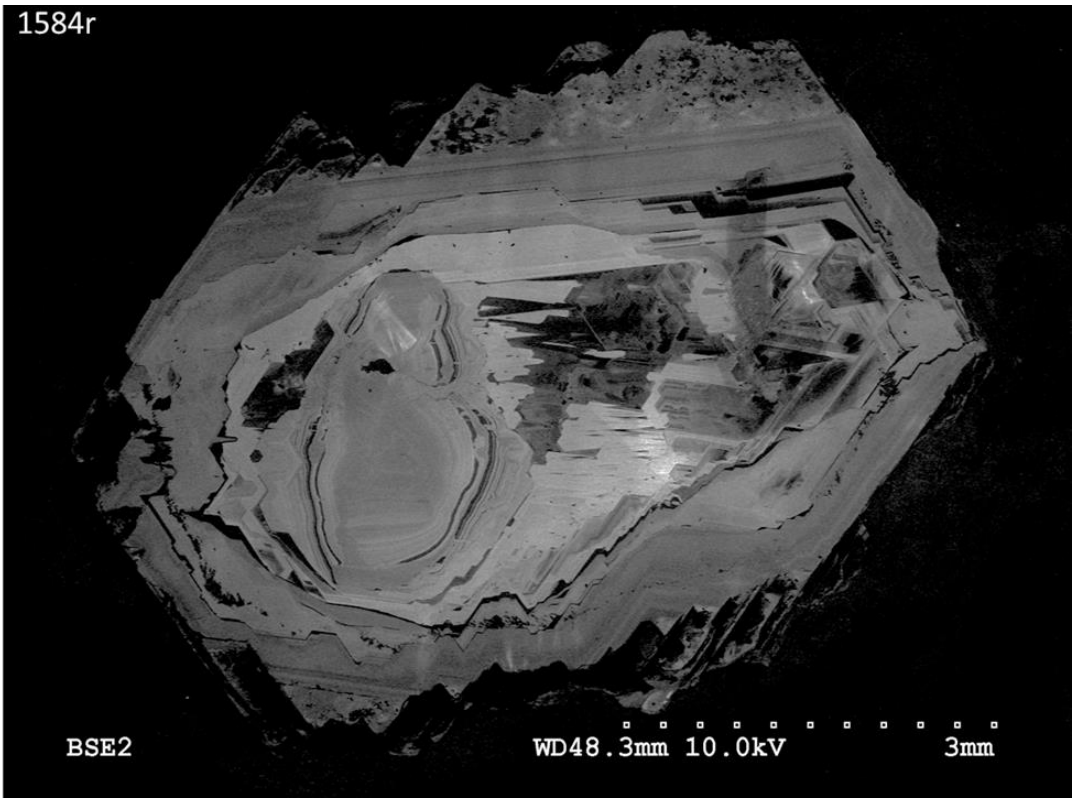

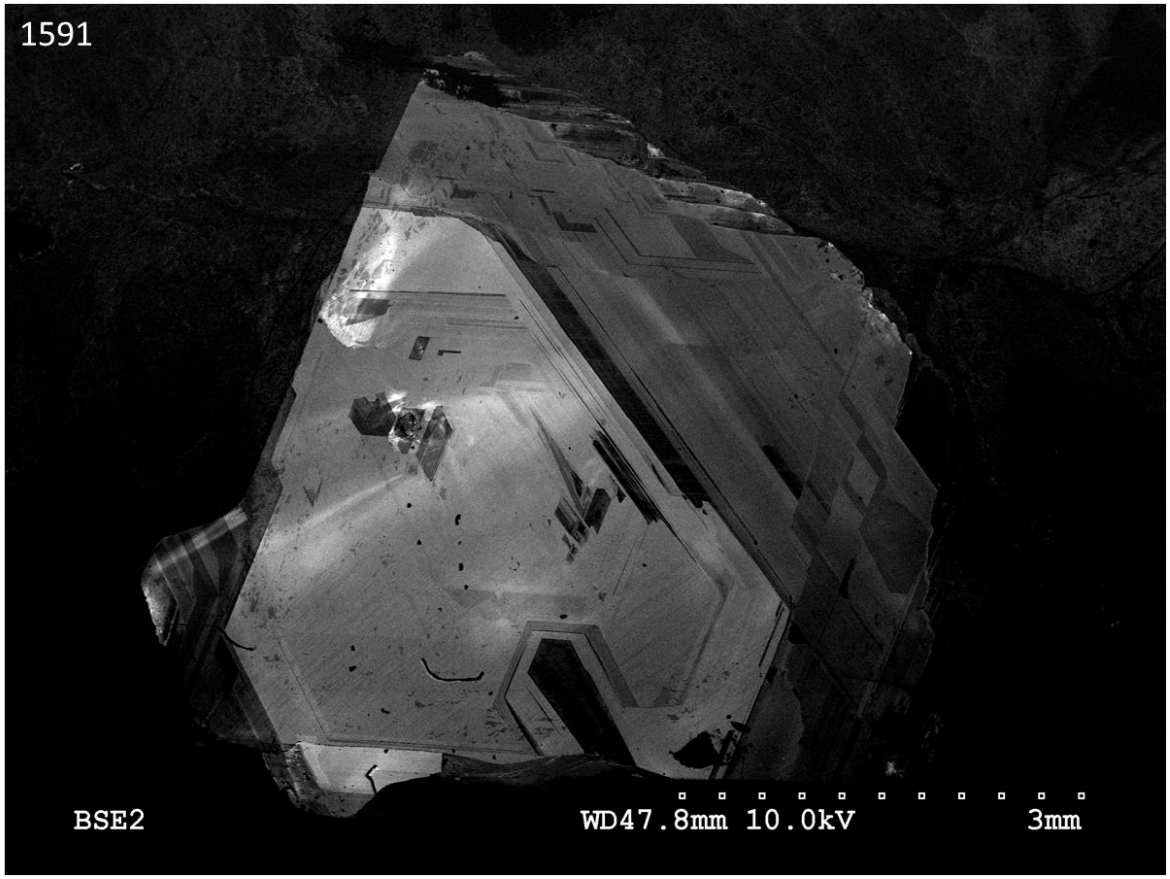
1591
BSE2
WD47.8mm 10.0kV
3mm

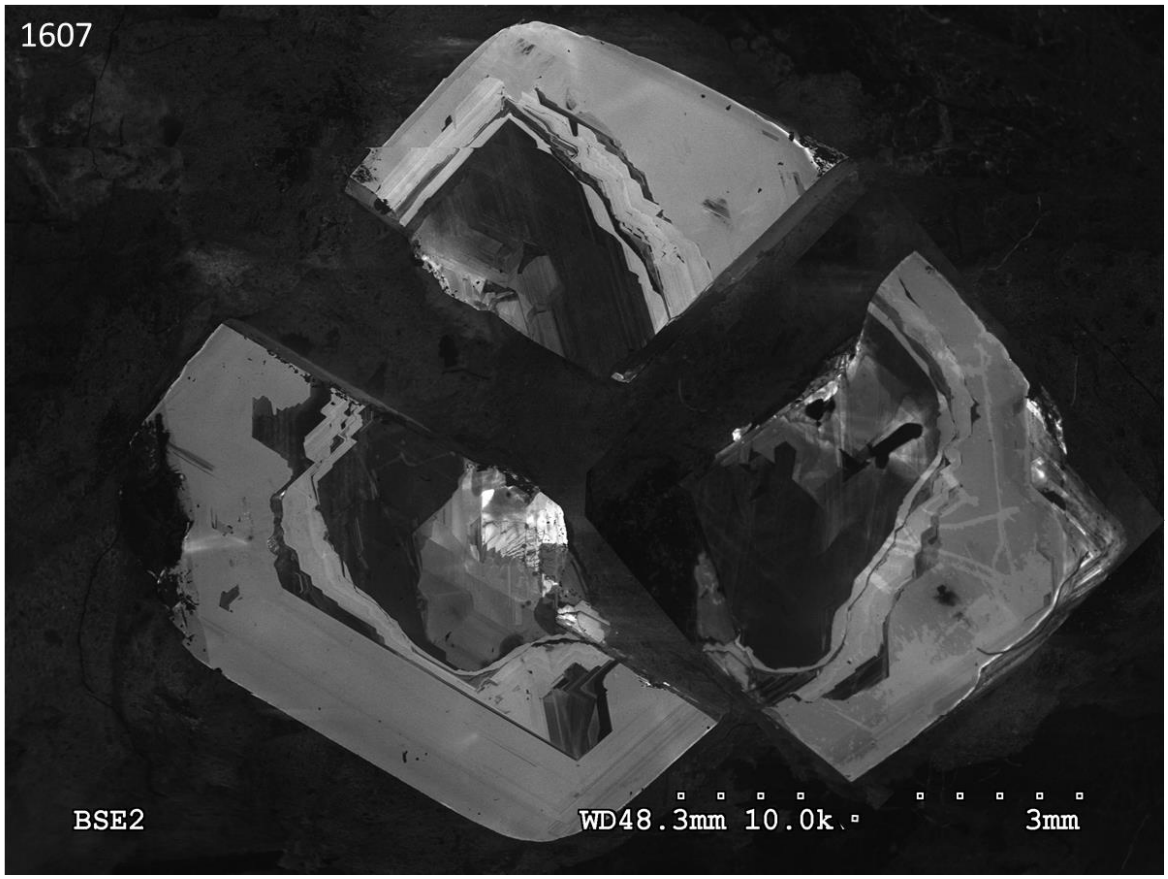
1607
BSE2
WD48.3mm 10.0k
3mm

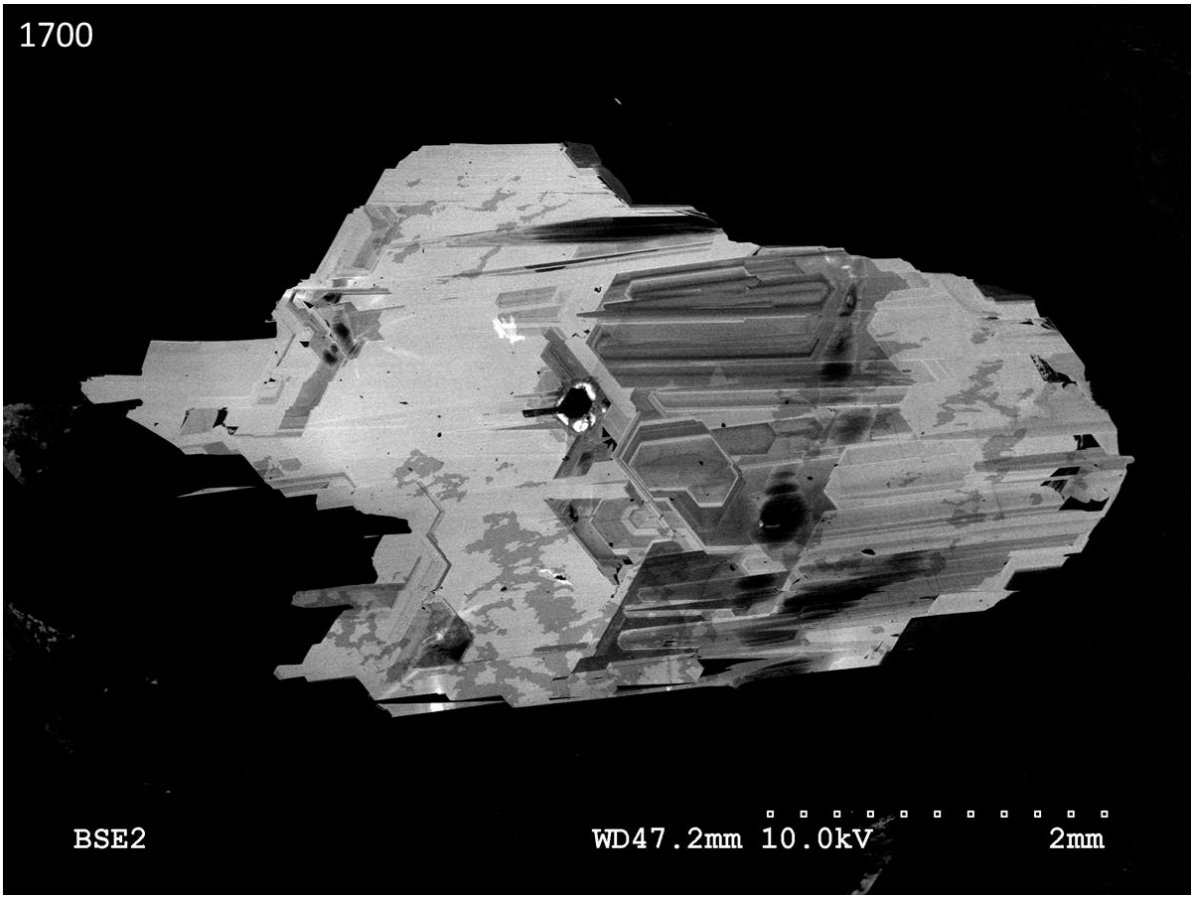
1700
BSE2
WD47.2mm 10.0kV
2mm

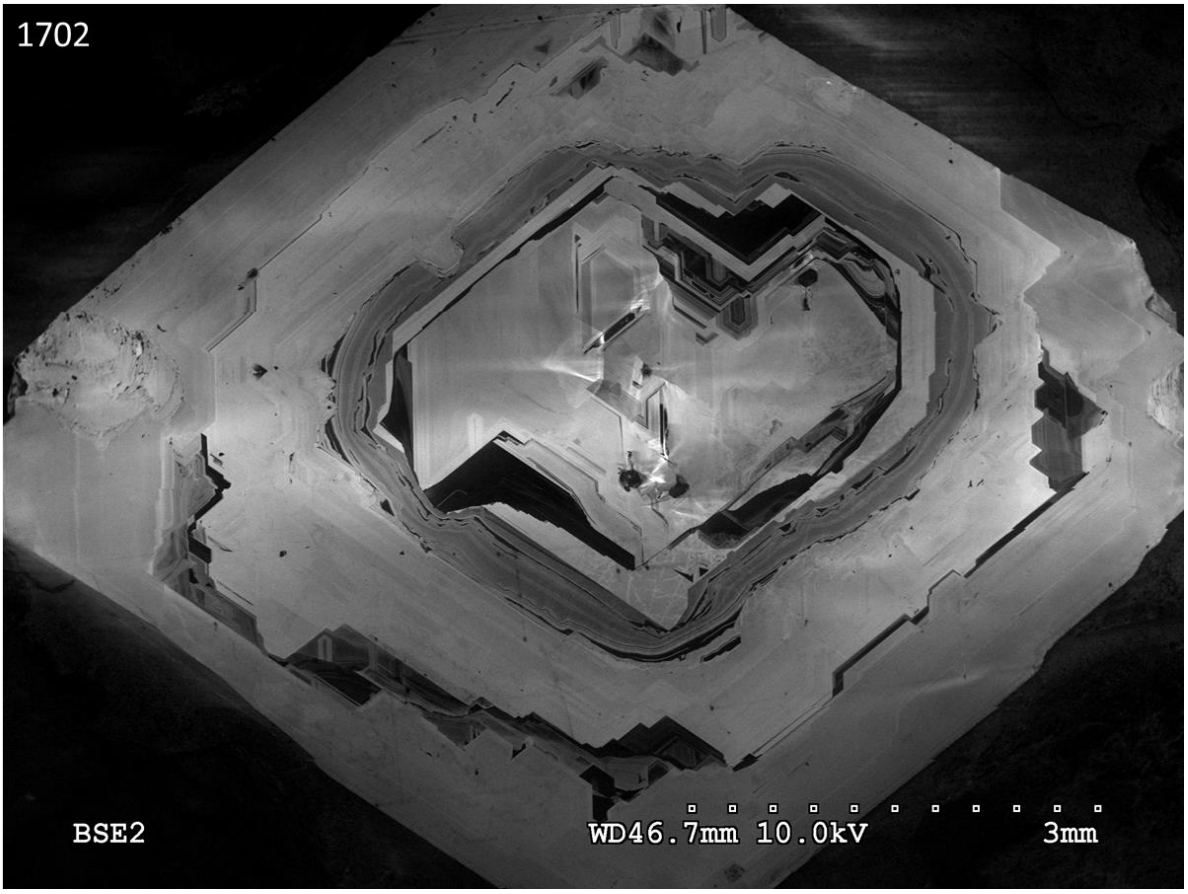
1702
BSE2
WD46.7mm 10.0kV
3mm

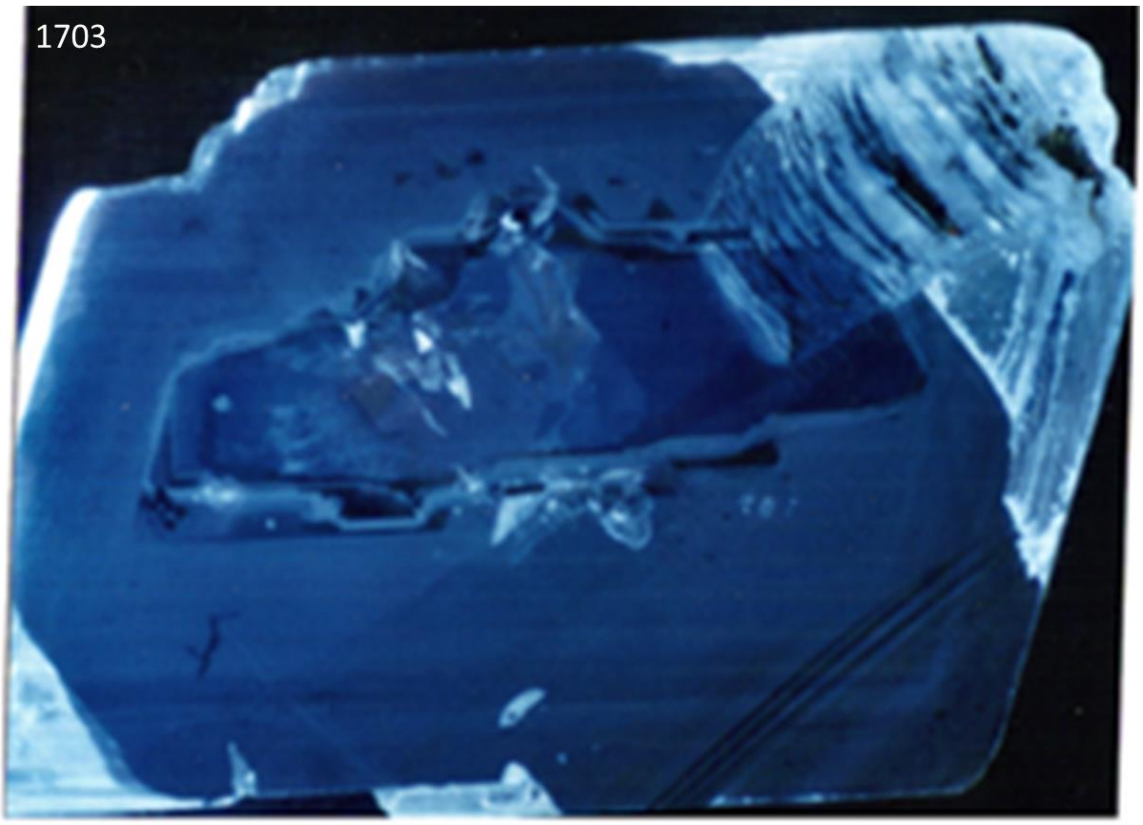

N.B. The diamond sample 1703 was not scanned by SEM-CL here; the above CL map was previously acquired of the diamond by Galina Bulanova

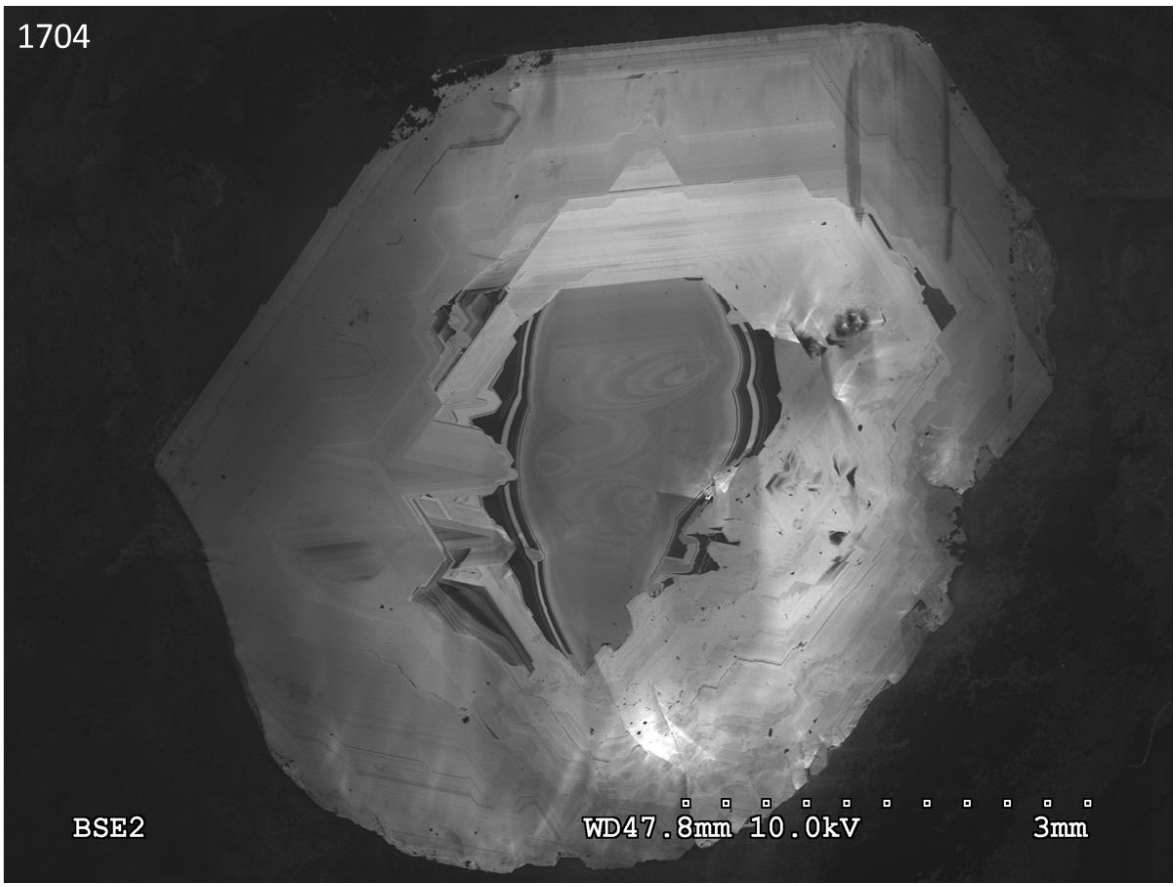

Figure A3. Raman spectrum for pyrrhotite (340, 370 cm^{-1}) and an unidentified sulphide (sharp peak at 286 cm^{-1}) in Mir diamond 1702 acquired with the blue (455 nm) laser.

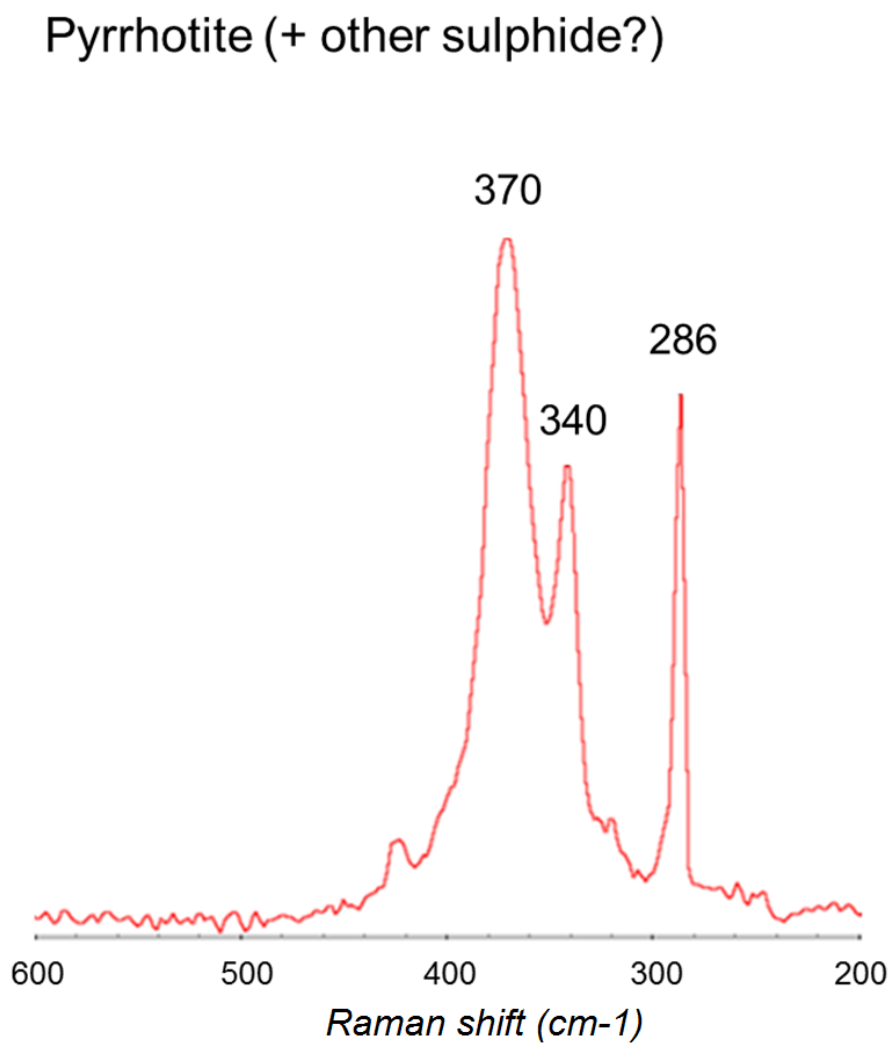

Appendix B

Table B1. Sulphur isotope data

Sample	Mineralogy (proportions)				Instrumental mass fractionation (IMF)		^{32}S cps average intensity (cps)	Raw data (± counting statistic error)						Corrected results (‰ vs. CDT)				
	Cp	Pn	Po	Py	α_{inst} ^{33}S/^{32}S	α_{inst} ^{34}S/^{32}S		^{33}S/^{32}S	Int error (1σ)	^{34}S/^{32}S	Int error (1σ)	true ^{33}/^{32}S	true ^{34}S/^{32}S	**δ^{33}S**	**Error (2σ)**	**δ^{33}S**	**Error (2σ)**	**Δ^{33}S**
4A1@1	0,006	0,008	0,986	0	0,999911	0,998352	1,01E+09	0,007789	3,79E-07	4,31E-02	9,01E-07	0,007789	0,043217	**-11,1505**	0,048631	**-21,4111**	0,020885	**-0,06588**
4A8@1	0,035	0,005	0,96	0	0,999924	0,998399	7,78E+08	0,007803	5,21E-07	4,33E-02	2,51E-06	0,007803	0,043377	**-9,37269**	0,066799	**-17,7857**	0,05788	**-0,17322**
4A8@2	0,03	0,005	0,965	0	0,999923	0,998391	3,93E+08	0,007796	7,99E-07	4,32E-02	3,75E-06	0,007797	0,043306	**-10,2247**	0,102546	**-19,3968**	0,086789	**-0,18786**
4B6@1	0,1	0,14	0,76	0	0,999796	0,998316	6,12E+08	0,007797	5,49E-07	4,32E-02	3,15E-06	0,007798	0,043322	**-10,0414**	0,070431	**-19,0419**	0,072903	**-0,18906**
4B9@1	0,01	0,001	0,989	0	0,99992	0,998367	5,83E+08	0,007807	5,69E-07	4,34E-02	3,13E-06	0,007808	0,043434	**-8,78007**	0,072835	**-16,5**	0,072088	**-0,24829**
4B10@1	0,02	0,005	0,975	0	0,999919	0,998377	25010146	0,007798	1,10E-05	4,33E-02	1,78E-05	0,007799	0,043349	**-9,95747**	1,410617	**-18,434**	0,410761	**-0,42112**
Ju5-03@1	0,04	0,12	0,84	0	0,999798	0,998254	8,67E+08	0,007808	3,06E-07	4,34E-02	1,25E-06	0,00781	0,043437	**-8,53**	0,039148	**-16,4213**	0,028755	**-0,03906**
Ju5-03-rep	0,04	0,12	0,84	0	0,999798	0,998254	3,2E+08	0,007805	9,33E-07	0,043326	1,60E-06	0,007806	0,043401	**-9,00019**	0,119576	**-17,235**	0,037001	**-0,08675**
Ju5-53-1	0,035	0,07	0,895	0	0,999852	0,998313	3,65E+08	0,007832	5,98E-07	0,04365	1,85E-06	0,007833	0,043724	**-5,56466**	0,076315	**-9,93195**	0,04237	**-0,43732**
Ju5-54@1	0,005	0	0	0,995	1,001497	1,001782	6,75E+08	0,00782	5,08E-07	0,043492	3,06E-06	0,007808	0,043415	**-8,79596**	0,065022	**-16,9343**	0,070364	**-0,03867**
Ju5-120@1	0,05	0,16	0,79	0	0,999757	0,998216	1,06E+08	0,007783	2,23E-06	0,043065	4,09E-06	0,007785	0,043142	**-11,6988**	0,286327	**-23,1139**	0,094952	**0,272287**
J6-@1	0,045	0,005	0,95	0	0,999928	0,998414	1,17E+09	0,007843	2,93E-07	4,37E-02	1,29E-06	0,007844	0,043812	**-4,25358**	0,037406	**-7,93937**	0,029573	**-0,1569**
J6-@2	0,045	0,005	0,95	0	0,999928	0,998414	1,06E+09	0,007846	2,74E-07	4,38E-02	1,43E-06	0,007846	0,043848	**-3,95117**	0,034909	**-7,13152**	0,032622	**-0,27206**
1584R-a	0,085	0,4	0,515	0	0,999501	0,99795	6,4E+08	0,007847	6,03E-07	4,38E-02	3,58E-06	0,007851	0,043892	**-3,28061**	0,076843	**-6,13258**	0,081699	**-0,11762**
1607-a	0	0	1	0	0,999918	0,998354	3,52E+08	0,007824	6,55E-07	4,35E-02	3,65E-06	0,007824	0,043564	**-6,70112**	0,08377	**-13,5645**	0,083923	**0,307733**
Mir1607-b	0,1	0,15	0,75	0	0,999785	0,998303	1,01E+09	0,007844	3,29E-07	4,37E-02	9,77E-07	0,007846	0,043818	**-3,96483**	0,041961	**-7,80696**	0,02233	**0,063399**
Mir1607-b-rep	0,1	0,15	0,75	0	0,999785	0,998303	1,01E+09	0,007844	3,66E-07	4,37E-02	9,65E-07	0,007846	0,043816	**-3,97397**	0,046653	**-7,85731**	0,022059	**0,080288**
Mir1607-c	0,13	0,13	0,74	0	0,999817	0,998374	1,08E+09	0,00787	3,51E-07	4,40E-02	2,46E-06	0,007871	0,044102	**-0,73127**	0,04465	**-1,37402**	0,055952	**-0,02341**
Mir1700-1	0,085	0,025	0,89	0	0,999919	0,998446	1,1E+09	0,007849	6,11E-07	4,38E-02	5,36E-06	0,007849	0,043865	**-3,52374**	0,077866	**-6,73316**	0,12242	**-0,05048**
Mir1700-2	0,12	0,2	0,68	0	0,999736	0,998266	1,14E+09	0,007871	4,86E-07	4,40E-02	5,09E-06	0,007873	0,044112	**-0,49573**	0,061789	**-1,14533**	0,115697	**0,094283**
Mir1700-1-rep	0,085	0,025	0,89	0	0,999919	0,998446	1,16E+09	0,007837	5,50E-07	4,37E-02	5,41E-06	0,007837	0,043725	**-5,04648**	0,070244	**-9,91183**	0,123826	**0,07044**

Raw and IMF-corrected (vs. Canyon Diablo Troilite – CDT) sulphur isotope results; Cp = chalcopyrite, Pn = pentlandite, Po = pyrrhotite and Py = pyrrhotite)

Table B2. Chemical composition of exposed sulphide inclusions in studied diamonds acquired by SEM-EDS at 10 nA and 20 KeV

		Major element composition (wt. %)									
Locality	**Sample**	**Fe**	**Ni**	**Cu**	**S**	**Cr**	**Co**	**Zn**	**Mn**	**O**	**Sum**
	4A1	57.8	0.31	0.19	39.1	0.01	-	0.01	-	-	97.42
Dachine	4A8-1	58.9	0.14	1.11	37.9	-	-	-	-	-	98.05
(DAC-BS)*	4A8-2	59	0.17	0.99	37.09	-	-	-	-	-	97.25
	4B6	50.88	5.77	3.39	36.3	-	-	-	-	-	96.34
	4B9	57.8	0.04	0.38	37.4	-	-	-	-	-	95.62
	4B10	59.5	0.2	0.66	37.2	-	-	-	-	-	97.56
	03	57.55	5.05	1.23	32.18	-	-	-	-	-	96.01
Juina-5 (Ju5)	53	64.32	2.84	1.017	27.76	0.47	0.29	-	-	-	96.69
	54	54.1	-	0.162	40.94	-	-	-	-	-	95.20
	120	36.67	20.25	6.214	34.92	0.43	0.23	0.09	-	-	98.05
Collier-4	J6	56.02	0.126	1.49	35.99	0.003	-	-	0.034	-	93.66
	1607-a	49.88	7.848	3.838	38.39	-	-	-	-	-	99.95
	1607-b	41.58	7.31	5.544	30.14	-	-	-	-	13.4	97.97
Mir	1607-c	54.18	-	-	37.76	-	-	-	-	-	91.94
	1584R-a	34.14	19.31	2.68	28.68	-	-	-	-	13.42	84.81
	1700-1	58.61	0.993	2.814	37.33	-	-	-	-	-	99.75
	1700-2	48.90	8.465	4.13	38.5	-	-	-	-	-	99.99

Before sample measurement sessions

Date	Analysis Name	Average ^{32}S intensity (cps)	$^{33}S/^{32}S$	Int. error (1σ)	$^{34}S/^{32}S$	Int. error (1σ)	$\delta^{33}S$	Error (2σ)	$\delta^{34}S$	Error (2σ)	$\Delta^{33}S$
05/12/2017	GaleneEtienne@1	2,14E+09	7,74E-03	3,36E-07	4,26E-02	3,24E-06					
05/12/2017	GaleneEtienne@2	2,09E+09	7,74E-03	3,36E-07	4,26E-02	2,40E-06					
05/12/2017	GaleneEtienne@3	2,07E+09	7,74E-03	2,25E-07	4,26E-02	2,31E-06					
05/12/2017	GaleneEtienne@4	2,10E+09	7,74E-03	2,99E-07	4,26E-02	2,90E-06					
05/12/2017	PyriteEmerald@1	1,83E+09	8,05E-03	2,43E-07	4,61E-02	1,56E-06	21,03	0,03	41,34	0,03	-0,05
05/12/2017	PyriteEmerald@2	1,83E+09	8,06E-03	2,40E-07	4,61E-02	1,68E-06	21,06	0,03	41,28	0,04	0,01
05/12/2017	PyriteEmerald@3	1,83E+09	8,05E-03	2,29E-07	4,61E-02	1,63E-06	20,93	0,03	41,19	0,04	-0,07
05/12/2017	PyriteEmerald@4	1,83E+09	8,05E-03	2,14E-07	4,61E-02	1,61E-06	21,02	0,03	41,26	0,03	-0,02
05/12/2017	CpNorilsk@1	1,82E+09	7,93E-03	5,05E-07	4,47E-02	4,88E-06	7,05	0,06	13,27	0,11	0,24
05/12/2017	CpNorilsk@2	1,80E+09	7,93E-03	4,92E-07	4,47E-02	4,97E-06	7,08	0,06	13,28	0,11	0,26
05/12/2017	CpNorilsk@3	1,85E+09	7,93E-03	7,91E-07	4,47E-02	7,78E-06	6,32	0,10	11,76	0,17	0,28
05/12/2017	CpNorilsk@4	1,82E+09	7,94E-03	4,76E-07	4,47E-02	5,03E-06	7,10	0,06	13,32	0,11	0,26
05/12/2017	PnNorilsk@1	7,32E+07	7,93E-03	2,81E-06	4,47E-02	4,79E-06	7,69	0,35	14,79	0,11	0,11
05/12/2017	PnNorilsk@2	9,96E+07	7,94E-03	2,12E-06	4,48E-02	4,18E-06	9,38	0,27	18,28	0,09	0,01
05/12/2017	PnNorilsk@3	1,86E+09	7,93E-03	5,65E-07	4,47E-02	6,33E-06	7,65	0,07	14,24	0,14	0,34
05/12/2017	PnNorilsk@4	1,82E+09	7,93E-03	7,58E-07	4,46E-02	7,94E-06	7,35	0,10	13,77	0,18	0,28
05/12/2017	Galice@1	1,82E+09	7,88E-03	2,51E-07	4,42E-02	1,79E-06	-0,70	0,03	-1,47	0,04	0,06
05/12/2017	Galice@2	1,71E+09	7,88E-03	2,37E-07	4,42E-02	1,81E-06	-0,76	0,03	-1,45	0,04	-0,01
05/12/2017	Galice@3	1,75E+09	7,89E-03	2,37E-07	4,42E-02	1,55E-06	-0,49	0,03	-1,10	0,04	0,08
05/12/2017	Galice@4	1,73E+09	7,88E-03	2,30E-07	4,42E-02	1,85E-06	-0,75	0,03	-1,51	0,04	0,02
05/12/2017	Mif-Po@1	1,40E+09	7,91E-03	3,96E-07	4,43E-02	3,87E-06	4,30	0,05	5,00	0,09	1,73
05/12/2017	Mif-Po@2	1,39E+09	7,91E-03	3,62E-07	4,43E-02	3,84E-06	4,33	0,05	5,05	0,09	1,73
05/12/2017	Mif-Po@3	1,39E+09	7,91E-03	4,58E-07	4,43E-02	3,70E-06	4,31	0,06	5,08	0,08	1,70
05/12/2017	Mif-Po@4	1,39E+09	7,91E-03	3,99E-07	4,43E-02	3,91E-06	4,34	0,05	5,07	0,09	1,74
06/12/2017	CpNorilsk@5	1,63E+09	7,94E-03	4,47E-07	4,48E-02	4,67E-06	7,23	0,06	13,68	0,10	0,21
06/12/2017	CpNorilsk@6	1,59E+09	7,93E-03	6,73E-07	4,47E-02	6,73E-06	6,99	0,08	13,14	0,15	0,25
06/12/2017	CpNorilsk@7	1,62E+09	7,94E-03	4,59E-07	4,48E-02	4,12E-06	7,29	0,06	13,78	0,09	0,22
06/12/2017	PnNorilsk@5	9,58E+08	7,91E-03	1,00E-06	4,45E-02	9,70E-06	5,97	0,13	11,33	0,22	0,15
06/12/2017	PnNorilsk@6	9,22E+08	7,92E-03	8,85E-07	4,46E-02	8,88E-06	6,30	0,11	12,08	0,20	0,09
06/12/2017	PnNorilsk@7	9,24E+08	7,92E-03	8,60E-07	4,46E-02	8,85E-06	6,41	0,11	12,01	0,20	0,24
06/12/2017	PnNorilsk@8	2,18E+08	7,92E-03	1,32E-06	4,45E-02	2,52E-06	6,42	0,17	11,54	0,06	0,50
06/12/2017	Mif-Po@5	1,22E+09	7,91E-03	3,82E-07	4,43E-02	3,00E-06	4,68	0,05	5,66	0,07	1,76
06/12/2017	Mif-Po@6	1,22E+09	7,91E-03	4,02E-07	4,43E-02	3,16E-06	4,58	0,05	5,58	0,07	1,71
06/12/2017	Galice@5	1,58E+09	7,88E-03	2,58E-07	4,42E-02	1,33E-06	-0,53	0,03	-0,96	0,03	-0,03
06/12/2017	Galice@6	1,58E+09	7,88E-03	3,00E-07	4,42E-02	1,65E-06	-0,58	0,04	-1,17	0,04	0,02

Table B3. Raw and IMF-corrected stable sulphur isotope data of standard reference materials (continued on next page)

During sample measurement sessions

Date	Analysis Name	Average ^{32}S intensity (cps)	$^{33}S/^{32}S$	Int. error (1σ)	$^{34}S/^{32}S$	Int. error (1σ)	$\delta^{33}S$	Error (2σ)	$\delta^{34}S$	Error (2σ)	$\Delta^{33}S$
06/12/2017	StdInsideRing1@1	1,14E+09	7,88E-03	3,04E-07	4,42E-02	9,97E-07					
Sample (Ju5-120-1)											
06/12/2017	StdInsideRing1@3	1,09E+09	7,88E-03	3,04E-07	4,42E-02	1,17E-06					
2 samples (Ju5-53 and Ju5-03-1)											
06/12/2017	StdInsideRing1@4	1,08E+09	7,88E-03	3,59E-07	4,42E-02	1,19E-06					
06/12/2017	StdInsideRing1@5	1,08E+09	7,88E-03	2,60E-07	4,42E-02	1,09E-06					
06/12/2017	StdInsideRing1@6	1,08E+09	7,88E-03	3,21E-07	4,42E-02	1,11E-06					
06/12/2017	StdInsideRing1@7	1,08E+09	7,88E-03	3,06E-07	4,42E-02	1,23E-06					
07/12/2017	GaleneEtienne@5	1,21E+09	7,74E-03	3,65E-07	4,26E-02	1,87E-06					
07/12/2017	GaleneEtienne@6	1,25E+09	7,74E-03	2,75E-07	4,26E-02	1,34E-06					
07/12/2017	GaleneEtienne@7	1,23E+09	7,74E-03	3,30E-07	4,26E-02	1,44E-06					
07/12/2017	PyriteEmerald@5	1,22E+09	8,06E-03	2,63E-07	4,61E-02	1,02E-06					
07/12/2017	PyriteEmerald@6	1,22E+09	8,06E-03	3,31E-07	4,61E-02	9,85E-07					
07/12/2017	PyriteEmerald@7	1,22E+09	8,06E-03	2,50E-07	4,61E-02	9,20E-07					
07/12/2017	CpNorilsk@8	1,20E+09	7,94E-03	3,93E-07	4,48E-02	3,64E-06	7,58	0,05	14,23	0,08	0,28
07/12/2017	CpNorilsk@9	1,18E+09	7,94E-03	4,19E-07	4,48E-02	3,37E-06	7,65	0,05	14,46	0,08	0,23
07/12/2017	PnNorilsk@9	6,73E+08	7,92E-03	6,93E-07	4,46E-02	7,50E-06	6,84	0,09	12,88	0,17	0,23
07/12/2017	PnNorilsk@10	6,69E+08	7,92E-03	7,64E-07	4,46E-02	7,64E-06	6,91	0,10	12,86	0,17	0,31
07/12/2017	Mif-Po@7	9,25E+08	7,91E-03	3,75E-07	4,43E-02	2,43E-06	4,79	0,05	5,81	0,05	1,80
07/12/2017	Mif-Po@8	9,16E+08	7,91E-03	4,35E-07	4,44E-02	2,24E-06	4,80	0,05	5,99	0,05	1,72
07/12/2017	Galice@7	1,19E+09	7,89E-03	2,51E-07	4,42E-02	1,04E-06	-0,44	0,03	-0,82	0,02	-0,01
07/12/2017	Galice@8	1,16E+09	7,89E-03	2,43E-07	4,42E-02	9,82E-07	-0,47	0,03	-0,92	0,02	0,01
07/12/2017	StdInsideRing1@9	1,02E+09	7,88E-03	3,68E-07	4,42E-02	7,93E-07					
2 samples (Ju5-54 and DacBS-4B10)											
07/12/2017	StdInsideRing1@10	8,90E+08	7,88E-03	3,81E-07	4,42E-02	7,27E-07					
07/12/2017	StdInsideRing1@11	1,02E+09	7,88E-03	2,68E-07	4,42E-02	8,31E-07					
2 samples (DacBS-4A1 and Ju5-03-rep)											
07/12/2017	StdInsideRing1@12	1,01E+09	7,88E-03	3,03E-07	4,42E-02	8,81E-07					
07/12/2017	StdInsideRing1@13	9,84E+08	7,88E-03	3,40E-07	4,42E-02	9,14E-07					
07/12/2017	StdInsideRing2@14	6,56E+08	7,93E-03	9,80E-07	4,47E-02	8,86E-06					
07/12/2017	StdInsideRing2@15	5,92E+08	7,94E-03	1,10E-06	4,48E-02	1,10E-05					
Sample measurement (DacBS-4B6)											
07/12/2017	StdInsideRing1@16	5,89E+08	7,94E-03	1,25E-06	4,48E-02	1,33E-05					
07/12/2017	StdInsideRing1@17	5,90E+08	7,94E-03	1,31E-06	4,48E-02	1,37E-05					
08/12/2017	GaleneEtienne@8	1,41E+09	7,74E-03	2,78E-07	4,26E-02	1,17E-06					
08/12/2017	GaleneEtienne@9	1,44E+09	7,74E-03	3,04E-07	4,26E-02	1,78E-06					
08/12/2017	PyriteEmerald@8	1,37E+09	8,06E-03	2,22E-07	4,61E-02	8,87E-07					

08/12/2017	PyriteEmerald@9	1,37E+09	8,06E-03	2,96E-07	4,61E-02	8,73E-07					
08/12/2017	CpNorilsk@10	1,35E+09	7,94E-03	3,96E-07	4,48E-02	3,35E-06	7,71	0,05	14,50	0,07	0,27
08/12/2017	PnNorilsk@11	7,59E+08	7,92E-03	8,15E-07	4,46E-02	7,82E-06	6,86	0,10	12,94	0,18	0,22
08/12/2017	Mif-Po@9	1,03E+09	7,91E-03	3,27E-07	4,44E-02	2,33E-06	4,87	0,04	6,08	0,05	1,75
08/12/2017	Galice@9	1,40E+09	7,89E-03	2,58E-07	4,42E-02	9,04E-07	-0,18	0,03	-0,66	0,02	0,16
08/12/2017	StdInsideRing1@18	1,39E+09	7,89E-03	2,34E-07	4,42E-02	1,27E-06					
08/12/2017	StdInsideRing1@19	1,40E+09	7,89E-03	1,77E-07	4,42E-02	9,21E-07					
2 sample measurements (DacBS-4A8-1 and 4A8-2)											
08/12/2017	StdInsideRing1@20	1,39E+09	7,89E-03	2,53E-07	4,42E-02	9,86E-07					
6 sample measurements (DacBS-4B9, P6-1, P6-1, Mir 1700-1-1, 1700-2 and 1700-1-2)											
08/12/2017	Galice@10	1,39E+09	7,89E-03	2,23E-07	4,42E-02	7,57E-07	-0,16	0,03	-0,30	0,02	0,00
08/12/2017	Galice@11	1,35E+09	7,89E-03	2,66E-07	4,42E-02	1,48E-06	-0,11	0,03	-0,47	0,03	0,13
08/12/2017	StdInside ring3@21	1,37E+09	7,88E-03	2,84E-07	4,42E-02	9,67E-07					
5 sample measurements (Mir 1607-a, 1607-b-1, 1607-b-rep, 1607-c and 1584R-a)											
08/12/2017	CpNorilsk@11	1,11E+09	7,94E-03	4,66E-07	4,48E-02	2,96E-06	8,02	0,06	14,80	0,07	0,42
08/12/2017	CpNorilsk@12	1,09E+09	7,94E-03	5,70E-07	4,48E-02	5,82E-06	7,49	0,07	13,91	0,13	0,35
08/12/2017	CpNorilsk@13	1,12E+09	7,94E-03	3,29E-07	4,48E-02	2,38E-06	8,11	0,04	14,88	0,05	0,47
08/12/2017	CpNorilsk@14	1,12E+09	7,93E-03	5,12E-07	4,47E-02	4,83E-06	7,04	0,06	12,94	0,11	0,40
08/12/2017	PnNorilsk@12	1,09E+09	7,95E-03	3,94E-07	4,48E-02	3,48E-06	9,89	0,05	18,03	0,08	0,64
08/12/2017	PnNorilsk@13	1,40E+08	7,93E-03	1,84E-06	4,46E-02	4,53E-06	7,93	0,23	13,79	0,10	0,85
08/12/2017	PnNorilsk@14	1,01E+08	7,95E-03	1,86E-06	4,48E-02	2,85E-06	10,01	0,23	17,92	0,06	0,82
08/12/2017	PnNorilsk@15	2,47E+08	7,93E-03	9,28E-07	4,47E-02	3,43E-06	8,35	0,12	15,95	0,08	0,17
08/12/2017	Mif-Po@10	8,48E+08	7,92E-03	2,98E-07	4,44E-02	1,89E-06	5,47	0,04	6,61	0,04	2,07
08/12/2017	Mif-Po@11	8,44E+08	7,92E-03	4,07E-07	4,44E-02	2,20E-06	5,59	0,05	6,86	0,05	2,06
08/12/2017	Mif-Po@12	8,41E+08	7,92E-03	4,65E-07	4,44E-02	1,82E-06	5,35	0,06	6,59	0,04	1,96
08/12/2017	Mif-Po@13	8,44E+08	7,92E-03	4,31E-07	4,44E-02	1,55E-06	5,46	0,05	6,63	0,04	2,05
08/12/2017	GaleneEtienne@10	1,20E+09	7,75E-03	3,97E-07	4,27E-02	3,96E-06					
08/12/2017	GaleneEtienne@11	1,06E+09	7,75E-03	3,51E-07	4,27E-02	2,16E-06					
08/12/2017	GaleneEtienne@12	1,04E+09	7,75E-03	3,98E-07	4,27E-02	3,34E-06					
08/12/2017	GaleneEtienne@13	1,07E+09	7,74E-03	3,77E-07	4,27E-02	2,41E-06					
08/12/2017	PyriteEmerald@10	1,08E+09	8,06E-03	3,52E-07	4,61E-02	1,29E-06					
08/12/2017	PyriteEmerald@11	1,09E+09	8,06E-03	3,59E-07	4,61E-02	1,22E-06					
08/12/2017	PyriteEmerald@12	1,08E+09	8,06E-03	2,90E-07	4,61E-02	1,10E-06					
08/12/2017	PyriteEmerald@13	1,08E+09	8,06E-03	3,82E-07	4,61E-02	1,08E-06					

Raw and IMF-corrected stable sulphur isotope data of standard reference materials analysed before and during the sample measurement sessions. The reference materials define the correlation: y = 0.51136 (±0.003016) x + 0.69825 (±0.23947). The timing of sample measurements is noted in bold. Data for GaleneEtienne (PbS) and PyriteEmerald standards have not been corrected, because their true compositions are unknown at this time.

Figure B1. Electron microprobe EDS maps at 20 kV showing the major element distribution (Fe, Ni, Cu, S) of exposed sulphide inclusions in four of the five analysed Dachine diamonds; The white points and dashed circles show the location of the SIMS analyses and the estimated analysed volume area respectively (scales = 10 µm)

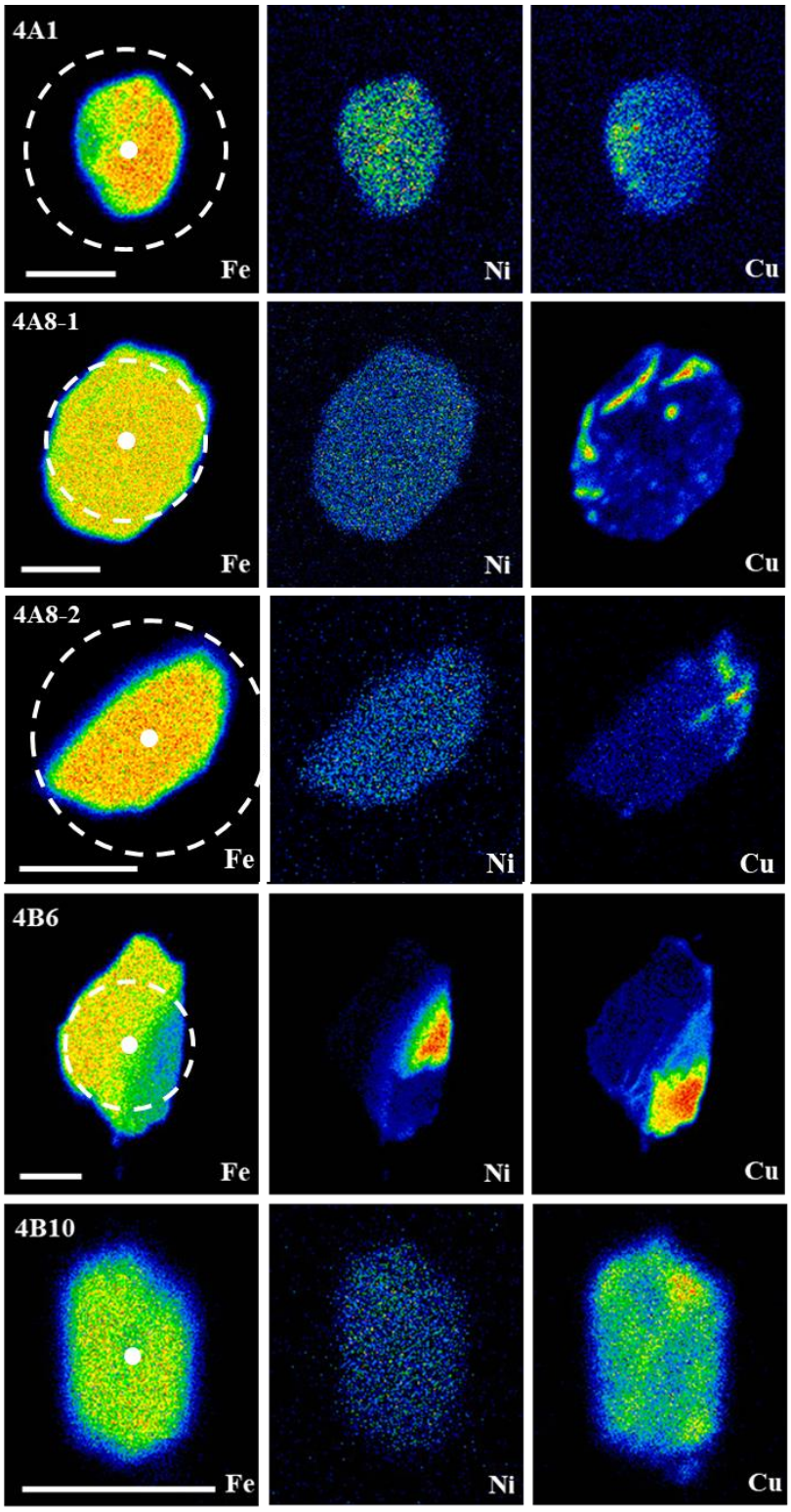

Figure B2. Backscattered electron image of the exposed pyrite inclusion in diamond Ju5-54 and electron microprobe EDS maps at 20 kV showing the major element distribution (Fe, Ni, Cu, S) of exposed sulphide inclusions in the remaining three Juina-5 diamonds and Collier-4 diamond J6. The white points and dashed circles show the location of the SIMS analyses and the estimated analysed volume area respectively (scales = 10 µm)

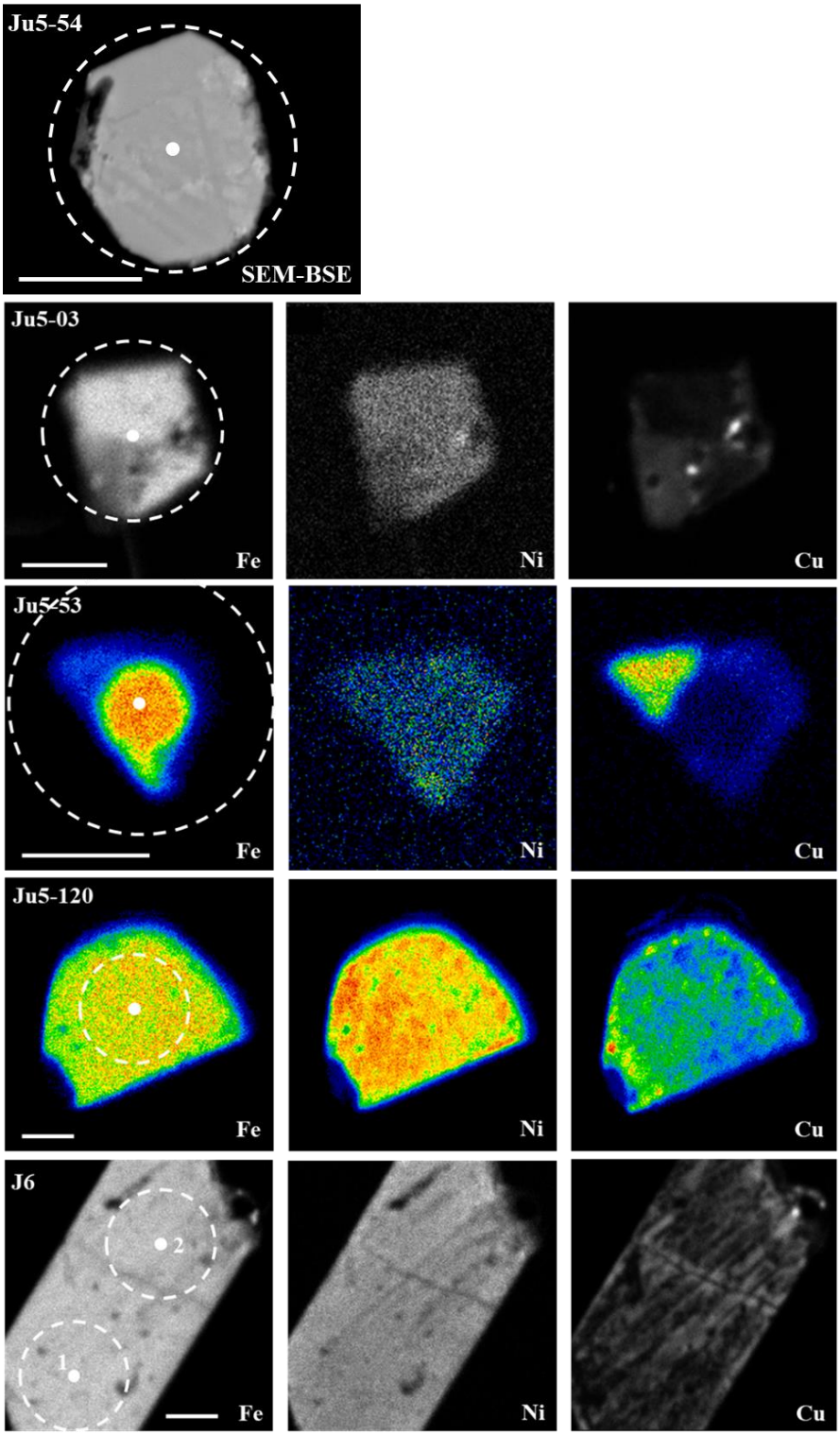

Figure B3. Optical micrographs paired with recent cathodoluminescence images of Mir diamonds 1584r, 1607 and 1700 showing the location of the inclusions in which sulphur isotope measurements were performed by SIMS (red boxes). Scales = 1 mm